1985

Synthesis and characterization of compounds containing discrete tetranuclear clusters and extended arrays of molybdenum atoms

Brent Allen Aufdembrink
Iowa State University

INFORMATION TO USERS

This reproduction was made from a copy of a manuscript sent to us for publication and microfilming. While the most advanced technology has been used to photograph and reproduce this manuscript, the quality of the reproduction is heavily dependent upon the quality of the material submitted. Pages in any manuscript may have indistinct print. In all cases the best available copy has been filmed.

The following explanation of techniques is provided to help clarify notations which may appear on this reproduction.

1. Manuscripts may not always be complete. When it is not possible to obtain missing pages, a note appears to indicate this.

2. When copyrighted materials are removed from the manuscript, a note appears to indicate this.

3. Oversize materials (maps, drawings, and charts) are photographed by sectioning the original, beginning at the upper left hand corner and continuing from left to right in equal sections with small overlaps. Each oversize page is also filmed as one exposure and is available, for an additional charge, as a standard 35mm slide or in black and white paper format.*

4. Most photographs reproduce acceptably on positive microfilm or microfiche but lack clarity on xerographic copies made from the microfilm. For an additional charge, all photographs are available in black and white standard 35mm slide format.*

***For more information about black and white slides or enlarged paper reproductions, please contact the Dissertations Customer Services Department.**

Aufdembrink, Brent Allen

SYNTHESIS AND CHARACTERIZATION OF COMPOUNDS CONTAINING DISCRETE TETRANUCLEAR CLUSTERS AND EXTENDED ARRAYS OF MOLYBDENUM ATOMS

Iowa State University PH.D. 1985

Synthesis and characterization of compounds containing discrete tetranuclear clusters and extended arrays of molybdenum atoms

by

Brent Allen Aufdembrink

A Dissertation Submitted to the
Graduate Faculty in Partial Fulfillment of the
Requirements for the Degree of
DOCTOR OF PHILOSOPHY

Department: Chemistry
Major: Inorganic Chemistry

Approved:

Signature was redacted for privacy.

In Charge of Major Work

Signature was redacted for privacy.

For the Major Department

Signature was redacted for privacy.

For the Graduate College

Iowa State University
Ames, Iowa
1985

TABLE OF CONTENTS

LIST OF TABLES

LIST OF FIGURES

GENERAL INTRODUCTION

The chemistry of metal clusters, both molecular and in the solid state, has enjoyed an astonishing growth in the two decades following the recognition of the quadruple bond (1). This remarkable expansion has been stimulated by a variety of reasons, one of the most important being their implications in deciphering the role of heterogeneous catalysts in chemical reactions (2, 3). The superconducting properties of clusters, their use as models for biological species, and their similarity to bulk metals have provided further technological impetus for the study of metal cluster systems.

The most important reason for studying cluster systems may be in the science itself and the extraction of the vast amount of basic chemical knowledge which exists in these systems. Metal clusters provide the arena for understanding the metal-metal bond. Scrutiny of the structural, electronic, and chemical properties of cluster compounds can provide insight to the nature of metal-metal bonds (4).

The dramatic increase in cluster chemistry has been most prolific for molybdenum (5). Molybdenum cluster compounds where the nuclearity of the cluster varies from one through six are known. Unfortunately, pathways whereby the cluster unit is systematically expanded are rare.

Unlike organic chemistry, where large molecules are routinely fabricated from smaller building blocks, a rational synthetic pathway where one begins with a unimolecular transition metal compound and in a stepwise fashion increases the nuclearity to a hexanuclear cluster is yet to be found. Some insight to this problem is beginning to be shown, especially for lower valent molybdenum compounds. A vast number of di- and trinuclear clusters are known to exist (6,7). In contrast, the number of clusters with four and five metal atoms in the cluster unit is relatively small.

Synthetic cluster chemistry can be initiated with the multiply bonded dinuclear molybdenum compounds. A vast number of these compounds have been isolated and can be divided into two main classifications. The first of these is the quadruply bonded molybdenum dimers in which the molybdenum atoms are in the +2 oxidation state (8). Each metal contributes four electrons to the metal-metal bond. The eight electrons comprise a sigma, two pi and one delta bonds. The second classification, the triply bonded Mo_2X_6 compounds possess a metal-metal triple bond (9). These two systems have been the subject of numerous theoretical and synthetic studies which will not be detailed here (6).

The utility of the dinuclear compounds in the context

of cluster expansion is that of precursors for larger cluster species (10). Triply and quadruply bonded dimeric compounds are ideal precursors because they possess low coordination numbers and sources of electrons with which additional bonds can be made. Compounds with labile ligands increase this reactivity even more because these ligands can easily dissociate from the dimers. Examples of this chemistry have recently begun to emerge.

Chisholm and co-workers have shown that a single metal atom can be added to a metal-metal triple bond to form a trinuclear cluster species as shown in reaction 1 (11).

$$Mo_2(OR)_6 + MoO(OR)_4 \longrightarrow Mo_3(\mu_3\text{-}O)(OR)_{10}$$

1

$$R = -Pr^i, -CH_2Bu^t$$

In reaction 1, the six electrons in the metal-metal triple bond are redistributed to form three metal-metal single bonds. While this reaction is not general (if the R group is too bulky the reaction does not occur), it does show that rational syntheses of larger cluster units from smaller precursors are possible.

Earlier work in the same laboratory had proven the usefulness of the triply bonded dinuclear units as precursors in the formation of tetranuclear cluster

compounds (reaction 2) (12).

$$2\ Mo_2(OR)_6 + 4\ CH_3COX \xrightarrow{X = Cl,Br} Mo_4(OPr^i)_8X_4 + CH_3COOR \quad 2$$

The important factor with regard to this discussion is the fact that the dimeric units undergo addition to produce a tetrameric cluster. The reaction is remarkable because the two clusters, $Mo_4(OPr^i)_8Cl_4$ and $Mo_4(OPr^i)_8Br_4$, exist in square planar and butterfly configurations, respectively. Both geometries can be considered as fragments of the larger $Mo_6Cl_{14}^{2-}$ cluster unit. These clusters indicate that subtle factors may cause structural differences in cluster synthesis.

In these compounds, there are 12 electrons for metal-metal bonding. The planar compound, $Mo_4(OPr^i)_8Cl_4$ adopts a delocalized bonding scheme with an average bond order of 1.5. The single metal-metal distance of 2.378 Å corresponds to a bond order greater than one. The butterfly compound differs in that five metal-metal bonds must be formed by the 12 metal cluster electrons. The bonding in this cluster has been described (13). The molybdenum orbitals form a set of six bonding and two nonbonding orbitals. The bonding orbitals are occupied by the electrons. The nonbonding orbitals which are not occupied involve interactions

between the apical metal atoms. The distances in the cluster support this analysis. There are five short bonds (2.50 Å, ave.) and one essentially non-bonding distance (3.287 Å) in the cluster unit.

The addition of quadruply bonded dimeric units rather than triply bonded dimers was the first example of dimerization to form larger cluster units from smaller precursors (14). Here, the reactive dimeric cluster unit $Mo_2Cl_4(P\emptyset 3)_2(MeOH)_2$ was found to spontaneously lose MeOH, in benzene, and condense to form $Mo_4Cl_8(P\emptyset_3)_4$ (reaction 3). In an acidic MeOH/hexane solution the dimeric units

$$2\ Mo_2Cl_4(P\emptyset_3)_2(MeOH)_2 \longrightarrow Mo_4Cl_8(P\emptyset_3)_4 \qquad 3$$

lost $P\emptyset_3$ and formed $Mo_4Cl_8(MeOH)_4$. The reaction is best described as a 2+2 cyclo-addition of quadruply bonded dimers forming an inorganic analogue of cyclobutadiyne. Structural and spectroscopic studies of these clusters have shown that the delta bonds in the quadruple bond of the dimer are recast to form two long sigma bonds in the new tetranuclear unit while leaving the remaining triple bond relatively undisturbed. An entire series of planar $Mo_4Cl_8(L)_4$ compounds have been synthesized proving the stability of the cluster unit and generality of the reaction (15). The chemistry has also been developed to produce W_4 clusters

(15) and more recently, pathways to mixed Mo_2-W_2 cluster units have been elucidated (16).

This condensation chemistry has been extended even further in more recent work (17). Addition of reagents to abstract PR_3 from $Mo_4Cl_8(PR_3)_4$ cluster compounds have caused further condensation to $[Mo_4Cl_8(PR_3)_2]_x$, where x=2. Based on experimental evidence it has been postulated that the 'dimer of tetrameric units' exists in one of the structures shown in Figure 1.

Not all reactions produce easily foreseen products. However, these unusual reactions are enlightening and interesting; they expand the knowledge new cluster types that are possible. The unpredictability of cluster synthesis is demonstrated by the reactions of triply bonded Mo(III) dimers. The addition of $(Bu^tO)_3WN$ to $W_2(OPr^i)_6(py)_2$ proceeded with the formation of the trinuclear cluster by the reaction shown in reaction 4 (18).

$$(Bu^tO)_3W{-}N \text{ to } W_2(OPr^i)_6(py)_2 \longrightarrow W_3(\mu_3\text{-}NH)(OPr^i)_{10} \qquad 4$$

However, the analogous reactions for molybdenum gave a much different product described by reaction 5 (19). The novel

$$2\ (Bu^tO)_3Mo{-}N + Mo_2(OPr^i)_6 \longrightarrow Mo_4(\mu\text{-}N)_2(OPr^i)_{12} \qquad 5$$

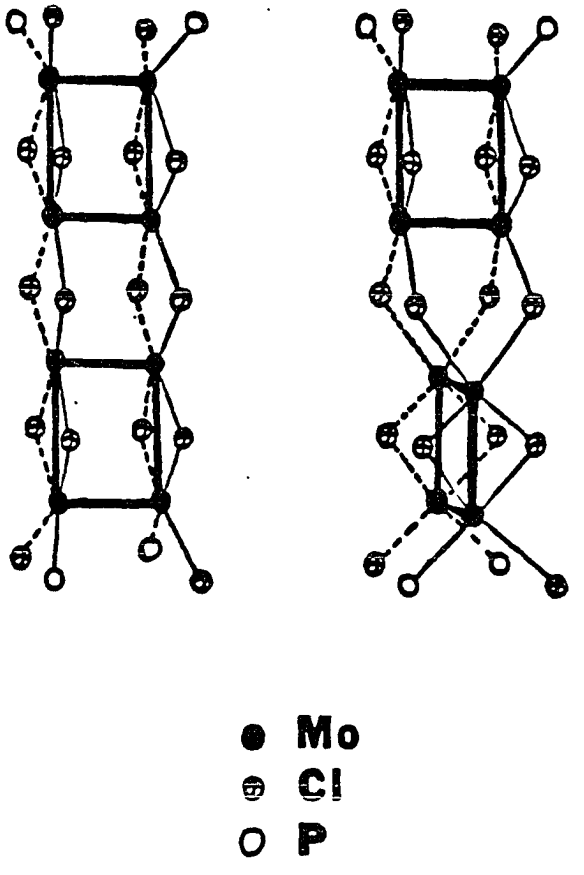

Figure 1. Coupling of tetranuclear clusters to form an octameric unit (from reference 17)

product formed has a zig-zag chain of molybdenum atoms with an unusual T coordination about the two nitrogen atoms.

In addition to the tetranuclear clusters previously described, the number of tetrameric clusters of molybdenum presently known is very small. The solid state compounds $Mo_4S_4Br_4$ (20) and MMo_4S_8 (M=Al, Ga) (21, 22) were the first tetranuclear clusters synthesized, utilizing high temperature preparations. Solid state tetranuclear clusters were also found in the oxide compounds $M_xMo_8O_{16}$ (M=K, x=2; M=Ba, x=1.14) (23). Discrete molecular clusters are also exemplified by several recent discoveries. A cluster similar to that in the $M_xMo_8O_{16}$ compounds is observed for $W_4(OR)_{16}$, synthesized when $W_2(NMe_2)_6$ was oxidized in MeOH or EtOH (24). The metal atoms in these cluster compounds form a planar 1,2,1 arrangement in which there are five metal-metal bonds. The opened tetrahedron, in addition to being observed in $Mo_4(OPr^i)_8Br_4$ is present in $Mo_4I_{11}^{2-}$, formed by thermal decomposition of $Mo(CO)_4I_3^-$ in chlorobenzene (13) and reaction between HI and $Mo_2(O_2CCH_3)_4$ in methanol (25). This 15 e cluster is distinctive in that steric constraints in the cluster unit are thought to cause the loss of an iodide from the Mo_4I_8 core and observation of an unusual bridging iodide bonded to the apical molybdenum atoms across the opened edge of the tetrahedron. Most recently, discrete regular tetrahedral clusters have been observed with the

synthesis of $Mo_4S_4(CN)_{12}^{8-}$ (26) and $Mo_4S_4(S_2CNR_2)_6$ (27).

Only one example of an Mo_5 cluster anion exists. The $Mo_5Cl_{13}^{2-}$ cluster has been synthesized in very low yield (<20%) by reaction of $MoCl_2$ with $AlCl_3$, KCl, $BiCl_3$, and Bi in a melt at 300^{o} C (28). Redox chemistry has shown that several oxidation states are attainable (29). The compound is interesting because it represents the stepping stone from the tetranuclear clusters to the larger, well-known hexanuclear clusters. Indeed, it has already been shown that the Mo_6 species can by obtained from the Mo_5 cluster compound (30). The $Mo_5Cl_{13}^{2-}$ cluster has 19 e to form the eight metal-metal bonds in the square pyramidal cluster. More convenient preparations are desired which will enable further study of these compounds and more information on the nature of metal-metal bonding in these and other cluster compounds.

The research described in the first two sections of this dissertation are the results of investigations of the reactivity of previously synthesized $Mo_4Cl_8(L)_4$ compounds with regard to their use as a convenient precursor to new and different cluster species which could be utilized to enlarge the cluster unit.

In recent years, low valent ternary and quaternary molybdenum oxides, whose structures are dominated by metal-metal bonding manifested in infinite chains of metal atoms

throughout the crystal lattice, have been the focus of a growing amount of research. One such compound is the ternary molybdenum oxide, $Sn_{0.9}Mo_4O_6$, which initially appeared to be a simple analogue of the previously observed $NaMo_4O_6$ (31). Investigations of this compound proved that it was an interesting and thought-provoking member of the growing family of molybdenum oxides with the stoichiometry, MMo_4O_6 (M = Na, $Ba_{0.62}$ (32), $Pb_{0.75}$ (33), In (33), and Cs (34)). The synthesis and characterization of this compound are presented in the final section of this dissertation.

Explanation of Dissertation Format

This dissertation consists of three sections, each of which is formatted for publication in a technical journal. While the references cited in the general introduction may be found at the end of the dissertation, each section contains an independent listing of references cited in that section.

SECTION I. IMPROVED SYNTHESES OF 'REACTIVE' $Mo_4Cl_8(L)_4$ CLUSTER COMPOUNDS AND THEIR REACTION TO PRODUCE COMPOUNDS WITH THE $Mo_4Cl_{12}^{4-}$ CLUSTER ANION

INTRODUCTION

The synthesis of tetrameric clusters by coupling of dimeric fragments was initiated by the discovery of the reaction where the reactive quadruply bonded dinuclear molybdenum compound, $Mo_2Cl_4(P\emptyset_3)_2(MeOH)_2$, spontaneously lost MeOH in benzene solution to form $Mo_4Cl_8(P\emptyset_3)_4$, eq. 1

$$2\ Mo_2Cl_4(P\emptyset_3)_2(MeOH)_2 \xrightarrow[-4\ MeOH]{} Mo_4Cl_8(P\emptyset_3)_4 \qquad 1$$

The analogous reaction in an acidic methanol/hexane solution caused loss of $P\emptyset_3$ and isolation of $Mo_4Cl_8(MeOH)_4$ (1). The reaction is explicitly described as a 2 + 2 cycloaddition of quadruply molybdenum dimers to form a tetranuclear cluster, where the metal orbitals comprising the δ bond of the dimeric unit are recast to form two sigma bonds across the long edges of the new tetrameric unit, leaving the remaining triple bond in the former dimeric unit relatively undisturbed (Figure I-1).

Subsequent research showed that a variety of the tetrameric clusters, $Mo_4X_8(L)_4$ (X=Cl, Br, I; L=PEt_3, PBu_3^n, THF, MeOH, RCN, $P\emptyset_3$), could be synthesized using appropriate conditions (2). The clusters can be divided into two classifications depending on the ability of the

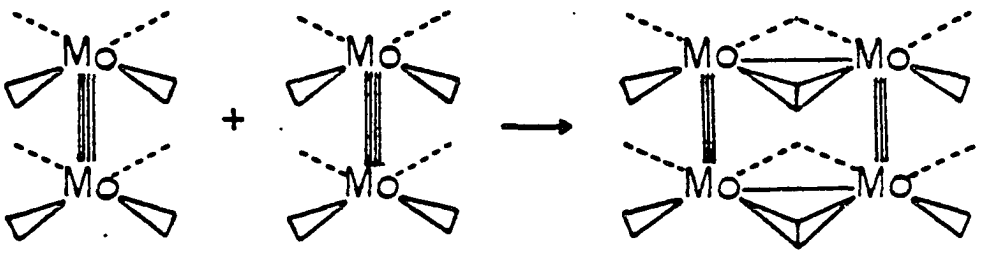

Figure I-1. Formation of a tetranuclear cluster from quadruply bonded dimeric compounds (reference 1)

ligand, L, to coordinate to the Mo_4 cluster unit (Table I-1). If L is a weakly coordinating ligand, the cluster is termed reactive because of the propensity for the cluster to lose the ligand and undergo further reaction. Conversely, if the ligand is more strongly coordinating the cluster is termed unreactive because of the strongly bound nature of the ligand to the cluster frame.

Table I-1. Classification of $Mo_4Cl_8(L)_4$ cluster compounds

Reactive	Unreactive
L = MeOH	L = PEt_3
CH_3CH_2CN	PBu_3^n
CH_3CN	
$P\emptyset_3$	
THF	

Two remarkable reactions allow the synthesis of the tetrameric cluster compounds with L=PR_3 (R=Et, Bu^n), via a one step reaction from $Mo_2(O_2CCH_3)_4$, eqs. 2,3 (2).

$$2\ Mo_2(O_2CCH_3)_4 + 8\ AlCl_3 + 4\ PR_3 \longrightarrow Mo_4Cl_8(PR_3)_4 + 8\ AlCl_2(O_2CCH_3) \qquad 2$$

$$2\ Mo_2(O_2CCH_3)_4 + 8\ (CH_3)_3SiCl + 4\ PR_3 \longrightarrow Mo_4Cl_8(PR_3)_4 + 8\ (CH_3)_3Si(O_2CCH_3) \qquad 3$$

These reactions are completed in 80-90% yields and have proven to be very efficient methods for obtaining these tetrameric clusters. The reactive tetrameric clusters cannot be synthesized using this method.

One objective of the work described in this dissertation was to investigate the reactivity of the reactive clusters. This was hindered by the fact that the very property that made them desirable for study (the ability of the ligand, L, to act as a leaving group) also made them more difficult to prepare.

The reaction scheme for preparing the reactive tetramers (Figure I-2) begins from $Mo_2(O_2CCH_3)_4$ and proceeds via the synthesis of $(NH_4)_5Mo_2Cl_9 \cdot 2\ H_2O$ (3). This salt is converted to the reactive dimeric compound, $Mo_2Cl_4(PO_3)_2(MeOH)_2$, by a two step reaction. The reactive tetramer, $Mo_4Cl_8(MeOH)_4$, is obtained as previously described and can be easily converted to $Mo_4Cl_8(CH_3CH_2CN)_4$ by extraction with propionitrile.

This procedure is time consuming and inefficient. The low yields in preparation encumbered the new chemistry which we wished to study. Clearly, a more efficient synthetic pathway to the reactive $Mo_4Cl_8(L)_4$ clusters would facilitate

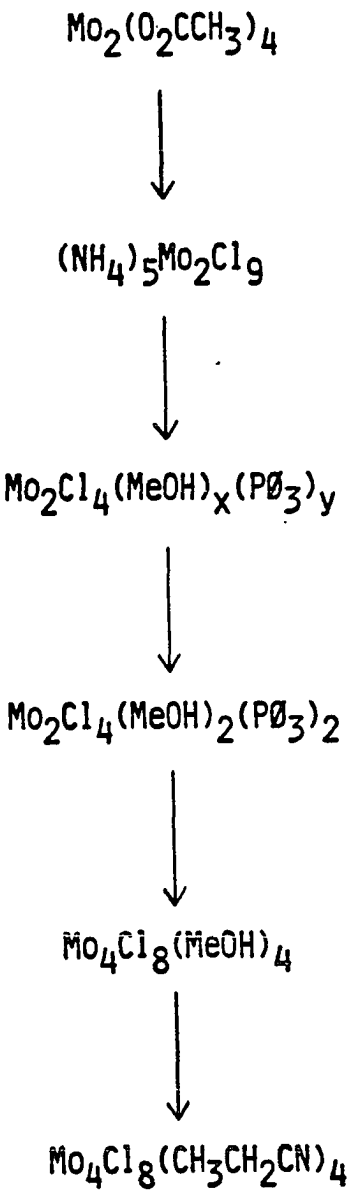

Figure I-2. Synthetic route to reactive tetrameric clusters

the study of their chemistry. One such pathway is the subject of the first part of this section.

The isolation of a pentanuclear cluster $Mo_5Cl_{13}^{2-}$, via an extremely difficult, low yield preparation (4) and its subsequent reaction to form a hexanuclear cluster compound (5) provided insight that rational expansion of the cluster could be effected if suitable precursors could be found.

The reactivity of the $Mo_4Cl_8(L)_4$ clusters led us to believe that these clusters might prove to be just such precursors.

This section describes the synthesis of $Mo_4Cl_{12}^{4-}$ cluster compounds. These compounds have an interesting chemistry and are likely to possess properties which would allow synthesis of the pentanuclear cluster in an efficient manner.

EXPERIMENTAL

Methods and Materials

The compounds reported in this section are extremely air and moisture sensitive. Thus, caution was required with regard to preparation and handling of reagents and solvents. All reactions were carried out under inert atmospheres, as were manipulations such as filtering, weighing, and preparation of samples for physical measurements, by use of standard drybox, vacuum, and Schlenk techniques.

Precautions were taken to insure that solvents were pure and dry. Dichloromethane (DCM), 1,2-dichloroethane (DCE), acetonitrile and propionitrile were refluxed over P_2O_5 for a minimum of 2-4 hours, then degassed by triple freeze-evacuate-thaw cycles before vacuum distilling onto 3 Å molecular sieves for storage until use. Subsequent transfers were made by vacuum distillation or Schlenk techniques. Chlorobenzene was refluxed with P_2O_5 and distilled under N_2, later transfers being made by syringe under a flow of N_2. Diethyl ether and tetrahydrofuran were dried and treated for peroxides simultaneously by refluxing with sodium metal and benzophenone, before vacuum transfer onto 3 Å molecular sieves for storage. Methanol was purified by refluxing with a large excess of sodium methoxide and distilling onto 3 Å molecular sieves. Hexane and cyclohexane were dried by refluxing with CaH_2 and

distilling onto sieves in solvent bulbs.

The tetraalkylammonium halides used were extremely hygroscopic. Purification of commercially available salts was effected by recrystallizing three times from acetone (tetrapropylammonium chloride, Pr_4NCl), chloroform (tetraethylammonium chloride, Et_4NCl), or methanol (tetramethylammonium chloride, Me_4NCl) with diethyl ether, followed by vacuum drying and heating before storing in the drybox (6). Tetraphenylphosphonium chloride ($\emptyset_4PCl$) was purchased from Aldrich Chemical Co. and used without further purification, but was opened and stored in the drybox. Tetraphenylarsonium chloride hydrochloride ($\emptyset_4AsCl$, Hach) was used without further purification.

Trifluoromethane sulfonic acid was transferred quickly from the commercially obtained vials under a flow of N_2 to a storage tube equipped with a sidearm. Subsequent transfers were made under a vigorous flow of nitrogen. The storage tube was stored at 3° C.

Aluminum trichloride was purified by sublimation as previously described (7).

Analytical Methods

Molybdenum analyses, for samples not containing phosphorus, were obtained by direct ignition of the samples to MoO_3. Samples were weighed into tared porcelain

crucibles, initially oxidized by addition of dilute HNO_3 and heated. Oxidation was completed by addition of concentrated HNO_3 followed by evaporation of the sample to dryness. If this method was unsuccessful in affecting complete oxidation the samples were subjected to an oxidation with NH_4OH/H_2O_2. The analyses were then completed by firing to MoO_3 at 550° C.

Samples containing phosphorus required the use of a precipitation method for the determination of molybdenum (8). Here, after the samples had been decomposed in a basic solution and neutralized to methyl red using an acetic acid/sodium acetate buffer, quantitative precipitation of $MoO_2(ONC_9H_6)_2$ was effected by addition of a solution of 8-hydroxyquinoline. The precipitate was filtered into previously tared fritted crucibles and fired at 140° C for 6-8 hours.

In cases where information on the oxidation state of the molybdenum atoms was desired, an oxidation state titration was completed. The samples were oxidized by a known excess of standardized Ce(IV) and the solution was back titrated to a ferroin (1,10-phenanthroline) endpoint with a freshly standardized Fe(II) solution. From these data, the oxidation state of the molybdenum was calculated.

Chlorine content was determined by potentiometric titrations. Samples were decomposed by dissolution in a

$NaOH/H_2O_2$ solution and brought to a pH of ~4 with dilute HNO_3 before being titrated with a previously standardized $AgNO_3$ solution.

Carbon, hydrogen, and nitrogen analyses were completed by the Ames Laboratory analytical services group.

Syntheses

Starting materials

$Mo_2(O_2CCH_3)_4$ (9), $Mo_4Cl_8(CH_3CH_2CN)_4$ (2), $Mo_4Cl_8(MeOH)_4$ (1), $Mo_4Cl_8(PBu_3^n)_4$ (2), $(NH_4)_5Mo_2Cl_9 \cdot H_2O$ (3), and reactive β-$MoCl_2$ (10) were prepared by methods previously reported in the literature.

$Mo_4Cl_8(CH_3CH_2CN)_4$

$Mo_4Cl_8(PBu_3^n)_4$ (3.00 g, 2.03 mmole) was placed in a 100 ml round bottom reaction flask. The flask was evacuated and approximately 20 ml of CH_3CH_2CN was distilled onto the solid. CF_3SO_3H (1.22 g, 8.13 mmole, 0.72 ml) was syringed into the flask under a flow of N_2. The mixture was gently heated and stirred for six hours during which time the color of the solution changed from orange-brown to lime-green. Caution must be taken to insure that the reaction temperature does not exeed 45° C or the reaction will proceed past the formation of the desired tetrameric product to form the extremely soluble green dimeric species, assumed

to be $Mo_2Cl_4(CH_3CH_2CN)_4$ analogous to the previously reported $Mo_2Cl_4(CH_3CN)_4$ (11). However, experience has shown that the reaction temperature must be above 40^{o} C or the reaction will not occur.

The reaction products were a yellow solid and deep green solution. The yellow solid was filtered, and extracted with the reaction solution until the washings were changed from green to a pale yellow. The solid was then dried in vacuo, weighed, and stored in the drybox. The yield was 1.60 g (88.7%). Analyses: Calc. for $Mo_4Cl_8(CH_3CH_2CN)_4$; Mo, 43.23; Cl, 31.95; Found; Mo, 42.22; Cl, 31.76 (Cl/Mo, 2.036/1).

$Mo_4Cl_8(MeOH)_4$

$(NH_4)_5Mo_2Cl_9 \cdot H_2O$ (1.00 g, 1.62 mmole) was placed in a 100 ml round bottom flask equipped with a sidearm. MeOH (70 ml) was distilled into the flask and the flask was allowed to stir at room temperature for three days. The bright purple dimeric solid gradually disappeared and a yellow brown solid was seen at the bottom of the green solution in the flask. The product was isolated by filtration, washed with several 2 ml washes of methanol and dried in vacuo. The yields were 25-30%. Analyses: Calc. for $Mo_4Cl_8(MeOH)_4$; Mo, 48.24; Cl, 35.65; C, 6.03; H, 2.01; Found; Mo, 47.49; Cl, 33.28; C, 6.34; H, 2.24 (Cl/Mo 1.90/1). The infrared

spectrum for this compound was identical to that of $Mo_4Cl_8(MeOH)_4$ prepared by previously described methods (1). $[Et_4N]_4Mo_4Cl_{12}$ was successfully prepared using $Mo_4Cl_8(MeOH)_4$ obtained by this method.

$\underline{[Et_4N]_4Mo_4Cl_{12}}$

Two different syntheses have been developed. Method (b) might be of greater synthetic utility since it circumvents the isolation of $Mo_4Cl_8(CH_3CH_2CN)_4$ however, since both the reactants and products of method (b) are extremely insoluble, a somewhat purer product is obtained by method (a).

a) $Mo_4Cl_8(CH_3CH_2CN)_4$ (0.7 g, 0.789 mmole) and Et_4NCl (0.5 g, 3.15 mmole) were placed in a reaction flask. The flask was evacuated and 20 ml of DCE were distilled onto the solid. The mixture was warmed to room temperature and the reaction began to occur as seen by the change in the color of the solution from yellow to purple. The reaction was pushed to completion by heating the reaction mixture to reflux for four hours. The insoluble purple product was separated from the essentially clear solution by filtration, extracted extensively with the reaction solution and dried <u>in vacuo</u>. The product was weighed and stored under N_2 in the drybox. This compound is unstable towards oxygen and H_2O, decomposing in one to three hours in laboratory air.

The yield was 0.98 g (93.5%). Analyses: Calc. for $[Et_4N]_4Mo_4Cl_{12}$; Mo, 28.87; Cl, 32.00; C, 28.91; H, 6.02; N, 4.21; Found; Mo, 28.67; Cl, 32.00; C, 28.32; H, 6.08; N, 4.03 (Cl/Mo, 3.02/1). An oxidation state titration confirmed that the molybdenum in this compound was in the 2+ oxidation state.

b) β-$MoCl_2$ (1.00 g, 5.99 mmole) and Et_4NCl (1.00 g, 5.99 mmole) were placed in a 100 ml reaction flask. DCE (20 ml) was distilled onto the solids. The reaction mixture was stirred while refluxing for 40 hours during which time the contents changed from brown to purple. The solid was filtered, extracted with solvent from the reaction solution and dried in vacuo. The yield was 1.93 g (96.5%). Confirmation of the identity of the product was made by comparison of its far infrared spectrum and x-ray powder pattern with those from a sample prepared by method (a). Anal.: Found; Mo, 28.53; Calculated; 28.87.

$[Pr_4N]_4Mo_4Cl_{12}$

$Mo_4Cl_8(CH_3CH_2CN)_4$ (0.50 g, 0.563 mmole) and Pr_4NCl (0.50 g, 2.25 mmole) were added to a 100 ml round bottom flask with a sidearm using the drybox. The flask was evacuated and 20 ml of DCE were distilled onto the solids. The solvent was allowed to warm to -20° C and the temperature was maintained in the range of -25 to -10° C for

four hours with an ice/MeOH/NaCl slush bath. As the reaction mixture was stirred, the solution turned bright purple and a purple solid precipitated. The solid was filtered quickly to assure that the temperature of the product did not rise above -5° C. Working quickly, the solid was washed by syringing three 5 ml portions of DCM which had been cooled to -20° C. Immediately after each, a vacuum was drawn on the solid to dry it as quickly as possible. The product was thoroughly dried, weighed, and stored in the drybox. The dry solid is stable indefinitely under inert atmospheres. In air, the compound will decompose in less than 1/2 hr. Solutions of the compound are unstable above -10° C. The yield was 0.53 g (60.1%). Analyses: Calculated for $[Pr_4N]_4Mo_4Cl_{12}\cdot C_2H_4Cl_2$; Mo, 24.70; Cl, 27.38; C, 37.10; H, 7.21; N, 3.61; Found; Mo, 24.38; Cl, 27.56; C, 33.36; H, 6.98; N, 3.61.

$[\emptyset_4P]_4Mo_4Cl_{12}$

$Mo_4Cl_8(CH_3CH_2CN)_4$ (0.50 g, 0.563 mmole) and $\emptyset_4PCl$ (0.84 g, 2.25 mmole) were placed in a 100 ml round bottom flask. The flask was evacuated and 20 ml of DCE was distilled onto the solids. The frozen solvent was allowed to warm to -20° C where it was maintained for three hours, while mechanically stirring the reaction solution. When $Mo_4Cl_8(CH_3CH_2CN)_4$ was no longer evident in the purple

solution the solvent was stripped by drawing a vacuum on the solution while maintaining the low temperature. The stripping procedure took approximately 24 hours to insure complete dryness of the solid. If not completely dry the solid decomposed when warmed. Once dry, the reaction flask was taken into the drybox and the solid purple product was scraped from the walls of the reaction flask, weighed, and stored. The yield was 0.89 g (69.9%). Analyses: Calculated for $[\emptyset_4P]_4Mo_4Cl_{12}\cdot C_2H_4Cl_2$; Mo, 16.96; Cl, 18.80; C, 52.01; H, 3.71; Found; Mo, 16.41; Cl, 18.52; C, 51.98; H, 3.70 (Cl/Mo, 3.05/1).

$[Bu_4N]_4Mo_4Cl_{12}$

$Mo_4Cl_8(CH_3CH_2CN)_4$ (0.66 g, 0.743 mmole) and Bu_4NCl (0.830 g, 2.99 mmole) were placed in a 100 ml round bottom flask equipped with a sidearm. The flask was evacuated and 20 ml of DCE was distilled into the flask. The reaction was held at -20° C for four hours. Solid was isolated by stripping the solvent from the reaction. The product was dried in vacuo, weighed, and stored in the drybox. The yield was 0.99 g (74.8%). Confirmation of the identity of the product was made by comparison of the far-infrared spectrum and visible spectrum of the product with those of $[Et_4N]_4Mo_4Cl_{12}$.

Physical Measurements

Infrared spectroscopy

Infrared spectra were recorded using an IBM Instruments, Inc. IR 90 Fourier transform infrared spectrometer. Samples were prepared as Nujol mulls and pressed between CsI plates. Separate spectra were recorded for the mid-infrared (4000-600 cm^{-1}) and far-infrared (600-200 cm^{-1}) regions. The spectra were recorded against blank CsI plates as references.

Visible spectroscopy

Visible spectra were recorded on a Cary 14 UV-visible recording spectrophotometer. Spectra were obtained on Nujol mulls of finely ground powder pressed between 1 in^2 quartz plates. The spectra were recorded from 700-300 nm using a scan rate of 25 Å/sec.

X-ray photoelectron spectroscopy

X-ray photoelectron spectra were obtained on freshly ground powders using an AEI ES 200 B photoelectron spectrometer. Nonmonochromatic Al Kα radiation (1486.6 eV) was used to irradiate the sample. Charging of the smaple surface, due to the insulating nature of the compounds, was kept to a minimum with the use of an electron flood gun. A 4 x 4 slit width was used. Data were referenced to the C 1s

peak of adventitious carbon at 285.0 eV. The data were resolved using the APES program developed in this group (12). With this program, the data are smoothed and corrected for inelastic electron scattering. The program allows for input of atoms with different chemical environments (modes of bonding) and variation of several parameters to provide the best fit to the observed data (13).

X-ray powder patterns

Powder patterns were obtained as a method of finger-printing the compounds which were synthesized. An Enraf Nonius Delft FR552 focusing Gunier camera maintained in this group was used to obtain the patterns. X-rays were generated by a General Electric XRD-5 generator equipped with a Phillips normal focus tube with a Cu target. A current of 20 mA and 40 kV produced the radiation. $K\alpha_1$ and $K\alpha_2$ radiation were separated by means of a graphite monochromating crystal.

Air sensitive samples were thoroughly ground and mounted on cellophane tape. The sample was covered and sealed with a second piece of tape before mounting on the sample holder to prevent decomposition from occurring upon transfer from the drybox to the camera.

RESULTS AND DISCUSSION

Syntheses

Improved routes to $Mo_4Cl_8(L)_4$ cluster compounds

The study of tetrameric molybdenum clusters, $Mo_4Cl_8(L)_4$, was hindered by the fact that their synthesis required time consuming preparations which produced low yields. During the course of our investigations into the reactivity of these cluster compounds, we serendipitously discovered routes which would circumvent the tedious preparative processes required.

In an attempt to oxidize the compound, $Mo_4Cl_8(PBu_3^n)_4$,

$$Mo_4Cl_8(PBu_3^n)_4 + CF_3SO_3H \longrightarrow [Mo_4Cl_8(PBu_3^n)_4]CF_3SO_3 + 1/2\ H_2 \quad (4)$$

with the strong organic acid CF_3SO_3H in methanol, eq. 4, an alternative reaction, eq. 5, occurred.

$$Mo_4Cl_8(PBu_3^n)_4 + 4\ CF_3SO_3H \xrightarrow[MeOH]{} Mo_4Cl_8(MeOH)_4 + 4\ (PBu_3^nH)CF_3SO_3 \quad (5)$$

The driving force for this reaction is the protonation of the tri-n-butyl phosphine group which then becomes a good leaving group; the vacant coordination sites on the cluster subsequently filled by the solvent methanol molecules present in abundance.

The propionitrile tetramer, $Mo_4Cl_8(CH_3CH_2CN)_4$, could be synthesized in a similar manner by substituting propionitrile for methanol. The reaction with propionitrile consistently produced higher yields.

The reaction could also be effected using dichloromethane as the solvent. In these reactions, methanol or propionitrile was added to $Mo_4Cl_8(PBu_3^n)_4$ in the stoichiometry of eq. 6.

$$Mo_4Cl_8(PBu_3^n)_4 + 4\ MeOH + 4\ CF_3SO_3H \xrightarrow[CH_2Cl_2]{[CH_3CH_2CN]} Mo_4Cl_8(MeOH)_4 + 4\ (PBu_3^n)CF_3SO_3 \quad (6)$$

$$[Mo_4Cl_8(CH_3CH_2CN)_4]$$

The bulk solid isolated from this reaction gives the same infrared spectra as that prepared by the first method but it behaves peculiarly when dried, forming a black coating on the surface which disappears when re-wetted with the solvent. The reason for this behavior is unknown, but it occurs when either $Mo_4Cl_8(CH_3CH_2CN)_4$ or $Mo_4Cl_8(MeOH)_4$ is synthesized in DCM.

The reactions in MeOH and propionitrile are completed in 75-85% yields, representing an efficient high yield synthesis of the reactive tetrameric clusters. These methods eliminate the need for synthesizing the reactive dimeric compound, $Mo_2Cl_4(P\emptyset_3)_2(MeOH)_2$.

The reaction temperature is crucial in obtaining the

desired products from these reactions. Under too vigorous conditions, the reaction proceeds past the simple substitution products to fragment the cluster into its dimeric components, the products being $Mo_2Cl_4(CH_3CH_2CN)_4$ (identified by comparison of its visible spectrum with that reported for $Mo_2Cl_4(CH_3N)_4$ in the literature (11)) and presumably $Mo_2Cl_4(MeOH)_4$, in the case where methanol is the solvent. Reaction conditions which are too mild are not sufficient for removal of the phosphine ligands. A temperature window of ~40-45° C has been found to produce the cluster in the highest yields.

These reactions are also convenient because these clusters are not attainable from β-$MoCl_2$. In similar reactions, where β-$MoCl_2$ is refluxed in propionitrile or methanol, the majority of the brown β-$MoCl_2$ is recovered and the green solution which is also produced contains only dimeric compounds (10).

$Mo_4Cl_8(MeOH)_4$ can be obtained directly from dimeric $(NH_4)_5Mo_2Cl_9 \cdot H_2O$ by stirring for extended periods of time in large excesses of methanol, eq. 7.

$$2\ (NH_4)_5Mo_2Cl_9 + 4\ MeOH \longrightarrow Mo_4Cl_8(MeOH)_4 + 10\ NH_4Cl \qquad 7$$

The products of this reaction are the dull yellow-brown methanol tetramer and a green solution. $Mo_4Cl_8(MeOH)_4$ was

identified by its infrared spectrum and by analysis (Cl:Mo = 1.89:1). The chemical reactivity of the product also identified it as $Mo_4Cl_8(MeOH)_4$; reacting with Et_4NCl to produce $[Et_4N]_4Mo_4Cl_{12}$ (vide infra).

The reaction requires a large excess of methanol before proceeding to completion. If only 20-30 ml of methanol are used in a reaction with 1.0 g of $(NH_4)_5Mo_2Cl_9 \cdot H_2O$, the purple dimeric species will remain indefinitely. Only when 80-100 ml of methanol are reacted with the same amount of $(NH_4)_5Mo_2Cl_9 \cdot H_2O$ is the dimeric compound completely consumed.

Yields of the product are extremely low. The reason for this is not clear but is one of several reasons. First, the presence of H_2O in the reactant dimer causes some concern about oxidation of the tetramer produced. Addition of 2,2-dimethoxypropane to the reaction (known to react with H_2O to produce acetone and methanol) failed to increase the yield. An oxidation state determination on the green solution determined the oxidation state of the molybdenum to be 2.4, suggesting that the green color of the solution might be due to an oxidized molybdenum species. No reaction was observed when $K_4Mo_2Cl_8$ was substituted for $(NH_4)_5Mo_2Cl_9 \cdot H_2O$ to eliminate this problem.

Second, the reaction probably proceeds past the formation of the tetranuclear cluster to form a dimeric

species. The green solution is most likely comprised of a series of anions of the formula $(NH_4)_{4-x}Mo_2Cl_{8-x}(MeOH)_x$.

The reaction to produce the methanol tetramer is interesting. It was not noted by previous workers in this laboratory during investigations which led to the synthesis of the reactive dimeric species $Mo_2Cl_4(P\emptyset_3)_2(MeOH)_2$. Similar reactions in nitriles or phosphines have been shown to produce dimeric $Mo_2Cl_4(CH_3CH_2CN)_4$ or $Mo_2Cl_4(PR_3)_4$ compounds (11).

The success of this reaction might be attributed to two factors. The first is the slight solubility of $(NH_4)_5Mo_2Cl_9 \cdot H_2O$ in methanol. This solubility factor also explains why such large amounts of MeOH are necessary for the reaction to occur and why the apparently less soluble $K_4Mo_2Cl_8$ does not react in a similar fashion. For the reaction to proceed in methanol, Cl^- must be lost from the dimeric unit to enable MeOH to fill the vacant coordination site. If $(NH_4)_5Mo_2Cl_9 \cdot H_2O$ was not soluble in MeOH, then the Cl^- ligands would not dissociate from the dimeric unit as easily. Visual examination of methanol solutions of $K_4Mo_2Cl_8$ suggest that it is much less soluble than $(NH_4)_5Mo_2Cl_9 \cdot H_2O$ in methanol and therefore, it does not react as readily under similar conditions.

The second factor allowing formation of the tetrameric

species, is the ability of a second metal dimer to rival MeOH in performing as a ligand in filling the vacated coordination sites. The failure of this reaction in nitrile solvents can be seen in this context. Strongly ligating species favor the preservation of the dimer, since they are better ligands than a second dinuclear unit. If an excess of ligands (L) is present, the equilibrium of eq. 8 is pushed to the right. When the ligand species are weakly ligating, the formation of the tetranuclear species is favored.

$$Mo_4Cl_8(L)_4 + 4\ L \longrightarrow 2\ Mo_2Cl_4(L)_4 \qquad 8$$

New $R_4Mo_4Cl_{12}$ cluster compounds

The synthesis of the $Mo_4Cl_{12}^{4-}$ anion was stimulated by the desire to form a tetranuclear cluster that was completely ligated by chlorine atoms for, among several reasons, the possibility that it might be a precursor to $Mo_5Cl_{13}^{n-}$ cluster compounds. The reactive tetranuclear clusters which had been studied appeared to be ideal starting materials for such reactions.

The initial choice of chlorinating agent was tetraethylammonium chloride. When four equivalents of Et_4NCl were reacted with one mole of $Mo_4Cl_8(MeOH)_4$ in refluxing dichloromethane, eq. 9, the product was a bright

$$Mo_4Cl_8(MeOH)_4 + 4\ Et_4NCl \longrightarrow [Et_4N]_4Mo_4Cl_{12} + 4\ MeOH \quad 9$$

purple solid whose analytical composition indicated a Cl:Mo ratio of 2.9:1. Addition of excess Et_4NCl and slightly longer reaction times allowed isolation of the completely substituted product, $[Et_4N]_4Mo_4Cl_{12}$. Substitution of $Mo_4Cl_8(CH_3CH_2CN)_4$ for $Mo_4Cl_8(MeOH)_4$ produced the compound equally well.

The air and moisture sensitive solid was completely insoluble in the reaction solution. It was also insoluble in all ordinary organic solvents with which it did not react (ØH, C_6H_{12}, C_6H_{14}, ØCl, and $ØCl_2$).

Initially, the color of the product led us to believe that it was dimeric, since a variety of red-purple salts of the $Mo_2Cl_8^{4-}$ anion were known (14). However, the observed compound underwent reaction, during extraction with MeOH, to regenerate $Mo_4Cl_8(MeOH)_4$, convincing us of the integrity of the cluster unit. If $[Et_4N]_4Mo_4Cl_{12}$ was allowed to stand in a solution of CH_3CN, the dimeric species $Mo_2Cl_4(CH_3CN)_4$ was produced, a reaction similar to those previously noted for the rectangular $Mo_4Cl_8(L)_4$ compounds (2).

The reaction to form the purple tetra-anion is an extremely facile reaction. After distilling the solvent onto the reactants at liquid nitrogen temperatures, the reaction begins while the reactants are still well below

room temperature, evidenced by the appearance of the characteristic purple color. Reaction times are extended to insure complete reaction and pure product.

The analogous reaction to form $[Pr_4N]_4Mo_4Cl_{12}$ did not produce the same results. A brown solid was isolated. When repeating the reaction a purple color was noted while the reaction mixture warmed from liquid nitrogen temperatures but disappeared as the reaction was warmed to reflux temperatures. Subsequent experiments showed that $[Pr_4N]_4Mo_4Cl_{12}$ could be isolated by maintaining the reaction temperature below -15^{o} C.

The preparation entails quickly filtering the solid at low temperatures and washing the product with cold DCM before drying. Once isolated in dry form the product is stable indefinitely in inert atmospheres, but solutions decompose rapidly if allowed to warm. In air, solid $[Pr_4N]_4Mo_4Cl_{12}$ decomposes in less than 60 seconds.

The tetrabutylammonium and tetraphenylphosphonium analogues were similarly synthesized by keeping the reaction temperature below -10^{o} C. These compounds were much more soluble in the solvent than were the $(Pr_4N)^{+}$ or the $(Et_4N)^{+}$ salts. Precipitates were not observed, but bright purple solids were isolated by stripping the solvent from the purple solutions obtained by reacting $\emptyset_4PCl$ or Bu_4NCl with $Mo_4Cl_8(CH_3CH_2CN)_4$ in a 4:1 mole ratio. The solubility of

these clusters led to the hope that crystals suitable for a single crystal structure determination would be found. Crystals suitable for such work have remained elusive even though a number of different attempts to grow crystals have been made.

This problem is quite troublesome because the structure of the $Mo_4Cl_{12}^{4-}$ anion is unknown. The structure of the anion is essential in understanding its properties and reactivity.

One difficulty in obtaining crystals of the $Mo_4Cl_{12}^{4-}$ compounds lies in the sensitivity of these compounds towards oxidation. Their behavior when exposed to laboratory air is testament to this. Sensitivity towards oxidation is also indicated by the methods needed to isolate the compounds. $[Et_4N]_4Mo_4Cl_{12}$ is insoluble in DCE or DCM. The remaining salts thus far synthesized exhibit solubility in the chlorinated hydrocarbons and are much more susceptible to oxidation by the solvents than is $[Et_4N]_4Mo_4Cl_{12}$. Reactions, such as 10, are believed to occur.

$$[R]_4Mo_4Cl_{12} + 1,2\text{-}C_2H_4Cl_2 \longrightarrow [R]_3Mo_4Cl_{12} + RCl + C_2H_4Cl^{\cdot} \qquad 10$$

The insolubility of the tetraethylammonium salt insulates it from the oxidizing nature of the solvent and it

is possible to isolate the compound at reflux temperatures in the solvents used. Reaction 10 is apparently sufficiently slowed kinetically to allow isolation of the soluble compounds at low temperatures. At higher temperatures, this (or similar) reactions become kinetically more favorable and isolation of the purple 4- anions is unsuccessful.

The choice of solvent was changed from DCM to DCE in these reactions because DCE seemed to have less of an oxidizing effect on the prepared clusters, making the preparation somewhat easier. Thus, in DCM, a typical reaction would have to be held at -15 to -20° C while in DCE the same reaction could be carried out at -5 to -10° C.

$[Et_4N]_4Mo_4Cl_{12}$ can also be prepared from reactive β-$MoCl_2$, eq. 11.

$$4\ \beta\text{-}MoCl_2 + 4\ Et_4NCl \longrightarrow [Et_4N]_4Mo_4Cl_{12} \qquad 11$$

The reaction is completed in 100% yield, based on Guinier x-ray powder patterns of the product, when refluxed in DCE for 2 days. When DCM is used, the lower temperature does not push the reaction to completion and an inseparable mixture of β-$MoCl_2$ and $[Et_4N]_4Mo_4Cl_{12}$ result (if excess Et_4NCl is used the reaction is pushed farther than the tetranuclear species to a compound or mixture of compounds where the Cl

content is consistent with a formula of $[Et_4N]_4Mo_2Cl_8$).

This reaction, starting with β-$MoCl_2$, provides an efficient high yield synthesis of $[Et_4N]_4Mo_4Cl_{12}$. Preparation of the purple solid from molybdenum acetate can be completed in two steps, providing a facile entrance to this chemistry. However, β-$MoCl_2$ cannot be used to obtain the $(\emptyset_4P)^+$, $(Pr_4N)^+$, or $(Bu_4N)^+$ salts of $Mo_4Cl_{12}^{4-}$ because the reaction requires elevated temperatures not possible with these compounds.

$[Et_4N]_4Mo_4Cl_{12}$ isolated by this method does not appear to be as brightly colored as that obtained by reacting $Mo_4Cl_8(CH_3CH_2CN)_4$ with Et_4NCl, however, its infrared spectrum, powder pattern, and analysis, as well as its reactivity confirm its identity.

Physical Measurements

The physical measurements on the $R_4Mo_4Cl_{12}$ cluster compounds provide data which allow postulations concerning the structure even though this has not been elucidated from a structure determination.

Infrared spectroscopy

The far-infrared spectra of the different $Mo_4Cl_{12}^{4-}$ compounds are essentially identical and remarkably simple. The infrared data are shown in Table I-2. Representative

spectra of $[Et_4N]_4Mo_4Cl_{12}$ and $[Pr_4N]_4Mo_4Cl_{12}$ are shown in Figure I-3. The spectrum of $[Et_4N]_4Mo_4Cl_{12}$ is compared to that of $K_4Mo_2Cl_8$ in Figure I-4.

The far-infrared spectra of both $Mo_4Cl_{12}^{4-}$ and $Mo_2Cl_8^{4-}$ are dominated by the large band at ~300 cm^{-1}. In both cases, there is an additional smaller band at ~275 cm^{-1}. The difference between the spectra is seen in the band that occurs at 347 cm^{-1} in the spectrum of $[Et_4N]_4Mo_4Cl_{12}$, but which is absent in the spectrum of $K_4Mo_2Cl_8$.

It is most reasonable to assume that this band is caused by Mo-Cl stretching vibrations however, it is interesting to note that the Raman frequency of the Mo-Mo stretch of quadruply bonded $Mo_2Cl_8^{4-}$ compounds is reported at 347 cm^{-1} (15). This stretching mode is absent in the infrared spectra of the dinuclear compound because it is totally symmetric.

At first approximation, one should not attribute the band at 347 cm^{-1} to a quadruply bonded metal-metal stretch. One would expect that the interaction of two dimers to form a tetranuclear species would lower the energy of this band. One possibility would permit its observation here. If $[Et_4N]_4Mo_4Cl_{12}$ is actually two dinuclear species coupled in a manner that doesn't significantly effect the interaction of the metal atoms this vibration would most likely become infrared active due to the lowering of the symmetry from D_{4h}

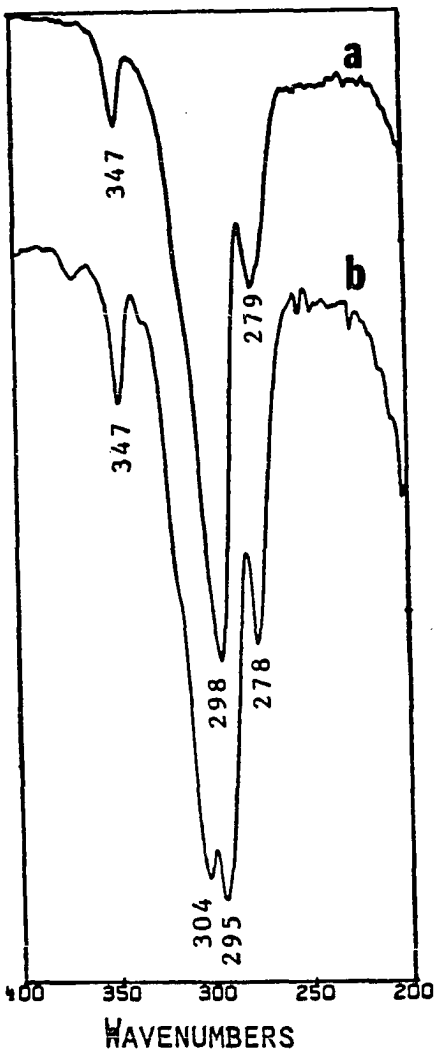

Figure I-3. Far-infrared spectra (cm^{-1}) of a) $[Et_4N]_4Mo_4Cl_{12}$ and b) $[Pr_4N]_4Mo_4Cl_{12}$ from 400-200 cm^{-1}

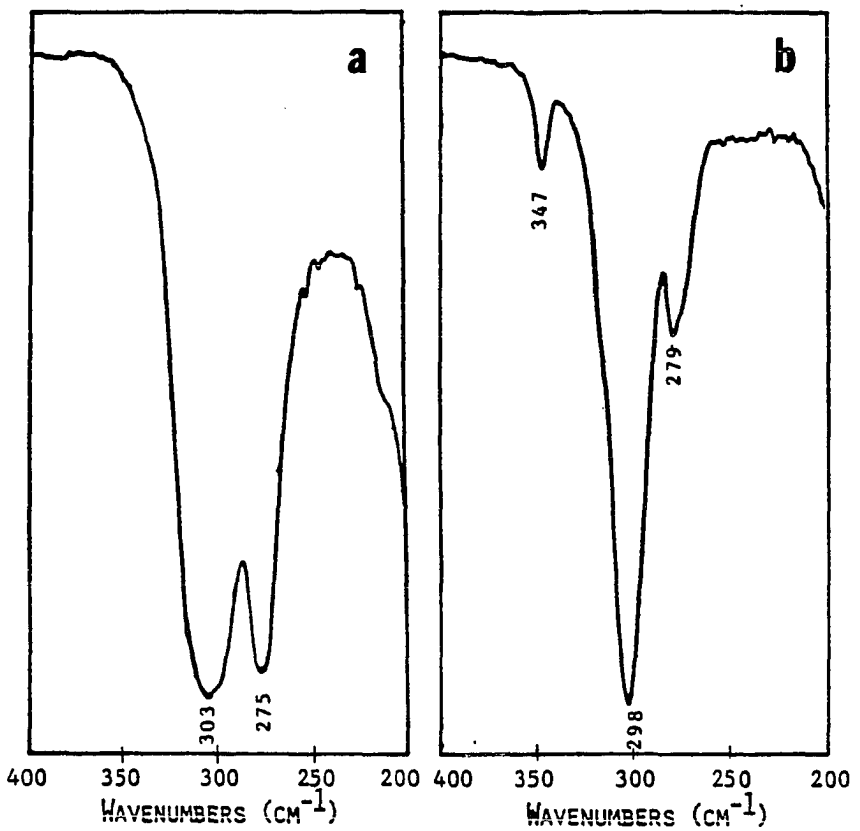

Figure I-4. Comparison of far-infrared spectra (cm^{-1}) of a) $K_4Mo_2Cl_8$ and b) $[Et_4N]_4Mo_4Cl_{12}$

to whatever the symmetry of new species happens to be. Two possibilities for such coupling are shown Figure I-5.

The simplicity of the infrared spectra of the $Mo_4Cl_{12}^{4-}$ compounds is worth remark. Based on a rectangular cluster of D_{2h} symmetry, simple group theory would predict that 8 Mo-Cl stretching bands are infrared active along with 2 infrared active Mo-Mo stretches. Lower cluster geometries would predict more. Only three bands are observed which means that either the cluster is of higher symmetry than D_{2h} or, more likely, a number of bands overlap and are present in the large band at 300 cm^{-1}. The latter is supported by the additional splitting of this band observed in the far-infrared spectrum of $[Pr_4N]_4Mo_4Cl_{12}$.

Visible spectroscopy

The visible spectra of three $Mo_4Cl_{12}^{4-}$ salts are shown in Figure I-6. The insolubility and air sensitivity of these compounds required that the spectra be obtained on Nujol mulls. Concentration and hence, molar absorptivity are unknown. Nevertheless, the energy at which the bands appear could be determined. The spectrum of $[Et_4N]_4Mo_4Cl_{12}$ is most resolved showing three bands at 563, 454, and 378 nm. The spectra of $[\emptyset_4P]_4Mo_4Cl_{12}$ and $[Pr_4N]_4Mo_4Cl_{12}$ do not show the higher energy bands as clearly but the band at 563 nm is evident.

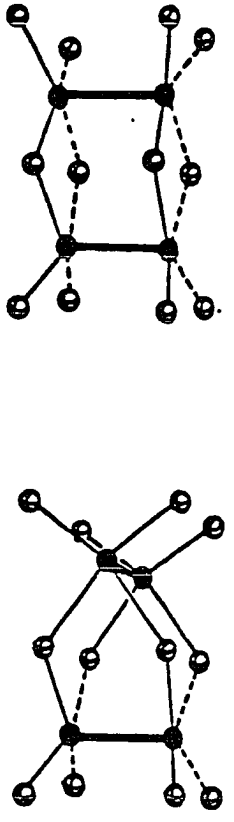

Figure I-5. Possible structures for a coupled 'dimer' of dimeric units forming a tetranuclear Mo_4Cl_{12} cluster

Table I-2. Far-infrared absorption bands of $Mo_4Cl_{12}^{4-}$ compounds[a,b]

$[Et_4N]_4Mo_4Cl_{12}$	$[Pr_4N]_4Mo_4Cl_{12}$	$[\emptyset_4P]_4Mo_4Cl_{12}$	$[Bu_4N]_4Mo_4Cl_{12}$
347 w	347 w	345 w	347 w
			330 sh
325 sh	325 sh	326 sh	326 sh
	304 vs	308 sh	305 sh
298 v vs	295 vs	296 v vs	293 vs
279 m	278 vs	278 m	275 m
		254 vw	252 vw
		248 vw	243 vw

[a]Absorptions given in cm^{-1}.

[b]Intensity abbreviations, s-strong, m-medium, w-weak, sh-shoulder, v-very.

These spectra also reveal an interesting relation between the $Mo_4Cl_{12}^{4-}$ salts and the dinuclear $Mo_2Cl_8^{4-}$ compounds. The electronic structure of the dinuclear species has been the subject of numerous investigations due to the relevance it has to understanding the quadruple bond (16). Germane to this discussion is the fact that the relatively low enery δ-δ^* transition in $Mo_2Cl_8^{4-}$ occurs at a wavelength of 532 nm. If the tetranuclear species is actually a dimer of dimeric species, one would expect to see this band (this absorption disappears when dinuclear species couple to form the tetranuclear $Mo_4Cl_8(L)_4$ clusters (2)).

The increase of wavelength, upon formation of the $Mo_4Cl_{12}^{4-}$ salts, by ~30 nanometers might not be unexpected since a small interaction might occur between metal atoms in separate dinuclear units of the proposed tetrameric compound. Any such interaction would decrease interaction between metal atoms forming the quadruple bond, thus decreasing the δ-δ^* separation.

One notes the contradiction of the structural interpretation based on the similarity of infrared and visible spectra to those of $Mo_2Cl_8^{4-}$ compounds. It is unlikely that the metal-metal stretch in a quadruply bonded species would remain at 347 cm^{-1} if the strength of the delta bond is altered as is suggested by the visible spectra.

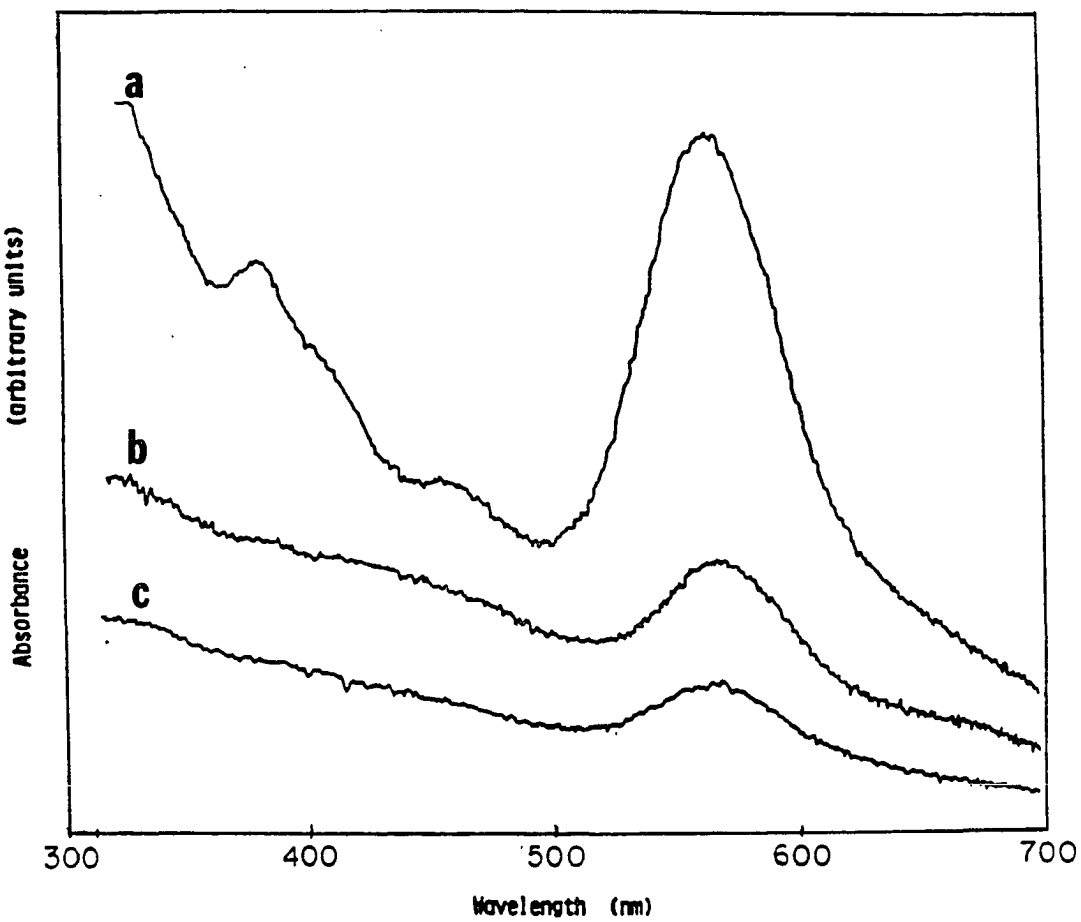

Figure I-6. Electronic absorption spectra (nm) of Nujol mulls of a) $[Et_4N]_4Mo_4Cl_{12}$, b) $[Pr_4N]_4Mo_4Cl_{12}$, and c) $[\emptyset_4P]_4Mo_4Cl_{12}$

Photoelectron spectroscopy

The chlorine 2 p x-ray photoelectron spectra, obtained for $[\emptyset_4P]_4Mo_4Cl_{12}$ and $[Et_4N]_4Mo_4Cl_{12}$, allow a different strutural prediction. Both consisted of a broad peak with a smaller pronounced shoulder on the low energy side of the peak, indicating the presence of more than one type of chlorine atom in the cluster unit. Utilizing the APES fitting algorithm (12) the observed peaks were resolved into their components. Relevant data to the interpretations are summarized in Table I-3, pointing out the similarity of the two spectra.

The observed data for $[Et_4N]_4Mo_4Cl_{12}$ were initially resolved into peaks attributable to two chlorine atoms present in equal amounts. The sum of the chlorine peaks in this interpretation provided a curve that agreed very well with the observed data, as seen in Figure I-7a. The full width at half maximum (FWHM), however, was somewhat large for the high energy peak, suggesting that an additional chlorine atom was present in the cluster anion.

Figure I-7b shows that a three chlorine interpretation produced an equally good fit to the observed data and gave more reasonable FWHMs. The best fit was obtained by holding the chlorines in fixed ratio of 3 terminal : 2 doubly bridging : 1 terminal, as would be found if the compound adopted a butterfly structure like that of $[Et_4N]_3Mo_4Cl_{12}$.

Table I-3. Cl 2p x-ray photoelectron spectra of $R_4Mo_4Cl_{12}$ cluster compounds

	Cl Type[a]	Energy[b]	FWHM[b,c]	Rel. Area	ΔE[b]
2 Cl fit					
$[Et_4N]_4Mo_4Cl_{12}$	T	197.55	1.33	1.0	1.23
	2b	198.78	1.53	1.1	
3 Cl fit					
$[Et_4N]_4Mo_4Cl_{12}$	T	197.54	1.39	3.0	1.11
	2b	198.65	1.39	2.0	0.97
	3b	199.62	1.39	1.0	
$[\emptyset_4P]_4Mo_4Cl_{12}$	T	197.66	1.33	2.9	0.98
	2b	198.64	1.33	2.0	0.77
	3b	199.41	1.33	1.0	

[a] T, terminal; 2b, doubly bridging; 3b, triply bridging.

[b] Energy in eV.

[c] Full width at half maximum.

The FWHMs are reasonable and similar to those observed for other types of molybdenum clusters containing chlorine ligands (17). The binding energies associated with the peaks are also indicative of the presence of terminal, doubly bridging, and triply bridging chlorines.

Three chlorine peaks can also be resolved from the observed data for $[\emptyset_4P]_4Mo_4Cl_{12}$ as observed in Figure I-8. The small peak on the low energy side of the observed data is not as pronounced as it is in the photoelectron spectrum of $[Et_4N]_4Mo_4Cl_{12}$ data, but the similarity of the fitted curve to the observed data is easily seen. The agreement between the fitted curve and the observed curve is not as good for the $[Et_4N]_4Mo_4Cl_{12}$ sample. The best fit was obtained when the relative ratio of terminal : double bridge : triple bridge was held at 2.9 : 2.0 : 1. This suggests that the terminal chlorine ligands are easily lost from the cluster unit, possibly due to decomposition in the x-ray beam. Samples often appear brown after removal from the sample chamber.

Electron paramagnetic resonance and magnetic susceptibility

Electron paramagnetic resonance and magnetic susceptibility measurements of compounds with the $Mo_4Cl_{12}^{4-}$ anion indicated that the samples were diamagnetic.

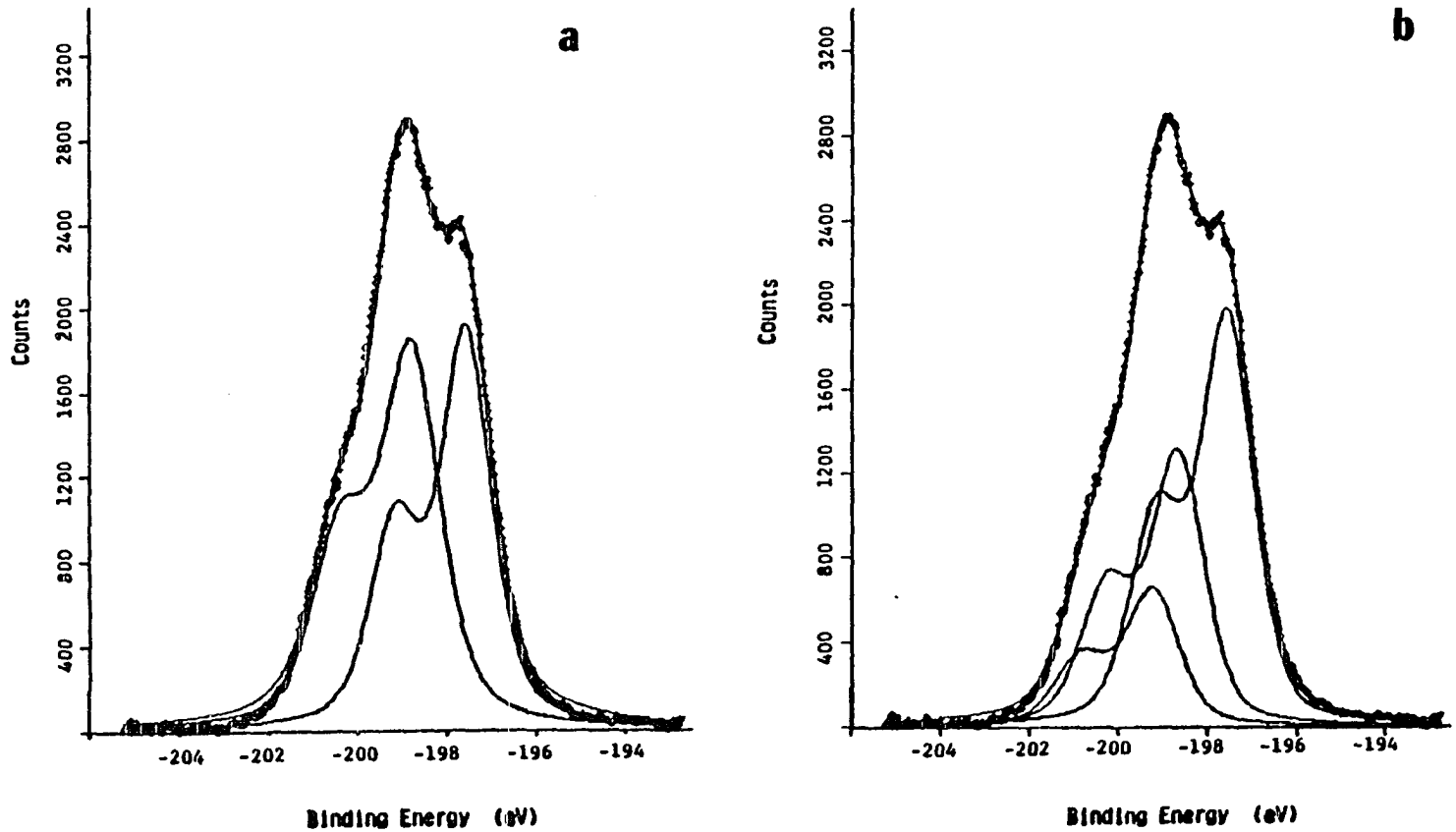

Figure I-7. Cl 2p x-ray photoelectron spectra of $[Et_4N]_4Mo_4Cl_{12}$ showing fits for a) two and b) three types of chlorine atoms. The sum of the components is given by the solid line through the experimental data points (+)

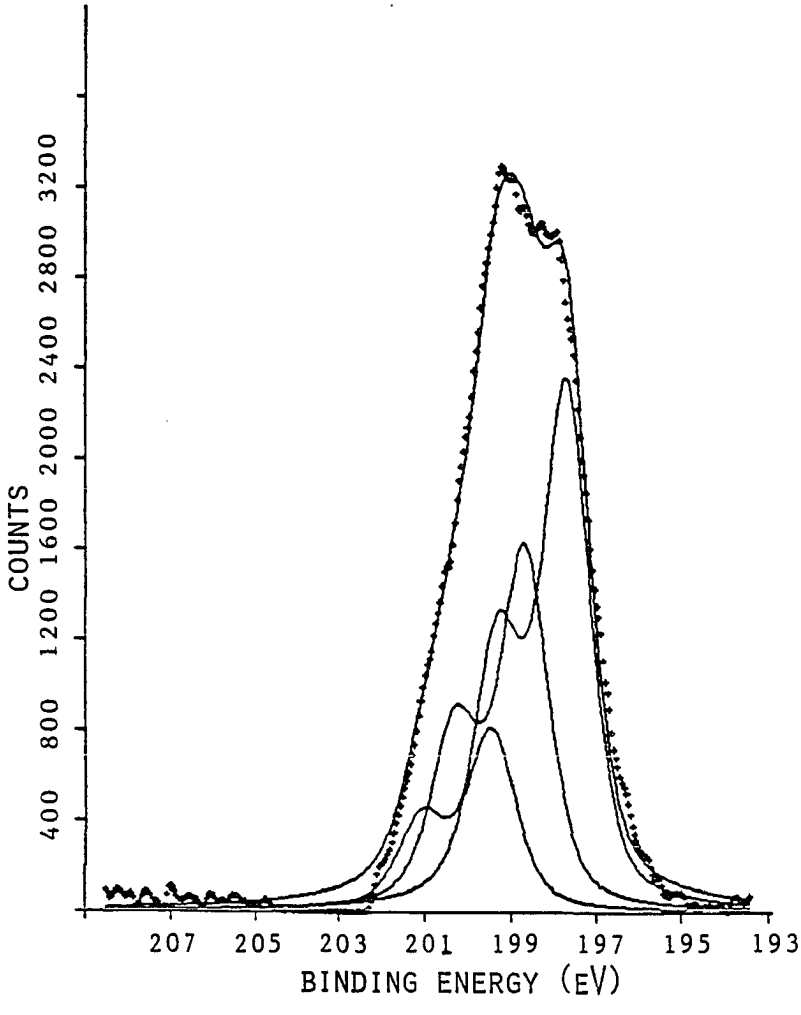

Figure I-8. Cl 2p x-ray photoelectron spectrum of $[\emptyset_4P]_4Mo_4Cl_{12}$. The sum of the components is given by the solid line through the experimental data points (+)

CONCLUSION

Compounds with the stoichiometry $R_4Mo_4Cl_{12}$ have been isolated from reactions of the 'reactive' tetranuclear clusters previously synthesized in this group. Our research has indicated that the cluster anion in these compounds is tetranuclear and is thus, the first tetranuclear molybdenum chloride cluster isolated.

The bright purple color of these compounds is intriguing since most other tetrameric cluster compounds isolated by this group are yellow or brown in color. The color is possibly due to the existence of a δ bond in a coupled quadruply bonded dimer in the cluster unit but, more likely, formation of a different structure type with an alternative electronic structure is responsible for the observed color. X-ray photoelectron spectroscopy has shown that different types of chlorine atoms are present which would agree with the adoption of an opened tetrahedral geometry for the cluster atoms. Crystals suitable for a structure determination have not yet been obtained.

The reactivity of these clusters suggests that they may be suitable precursors for other cluster compounds. For example, the $R_4Mo_4Cl_{12}$ clusters have an interesting chemistry which leads to the isolation of oxidized tetranuclear clusters which have been structurally characterized. These compounds are discussed in Section II.

REFERENCES AND NOTES

1. McGinnis, R. N.; Ryan, T. R.; McCarley, R. E. J. Am. Chem. Soc. 1978, 100, 7900.

2. Ryan, T. R.; McCarley, R. E. Inorg. Chem. 1982, 21, 2072.

3. Brencic, J. V.; Cotton, F. A. Inorg. Chem. 1970, 9, 346.

4. Jödden, K.; von Schnering, H. G.; Schäfer, H. Angew. Chem., 1975, 87, 595.

5. Jödden, K.; Schäfer, H. Z. Anorg. Allg. Chem. 1977, 430, 5.

6. Mann, C. K. In "Electroanalytical Chemistry"; Bard, A., Ed.; Marcel Dekker Inc.: New York, 1969; Vol. 3, page 132.

7. Beers, W. W. Ph.D. Dissertation, Iowa State University, Ames, Iowa, 1983; Section I.

8. Erdey, L. In "International Series of Monographs on Analytical Chemistry: Gravimetric Analysis, Part II", Buzar, I., Ed.; Macmillan: New York, 1965; Vol. 7, page 535.

9. McCarley, R. E.; Templeton, J. L.; Colburn, T. J.; Katovic, V.; Hoxmier, R. J. Adv. Chem. Ser. 1976, 150, 318.

10. Beers, W. W.; McCarley, R. E. Inorg. Chem. 1985, 24, 472.

11. San Filippo, J. S.; Sniadoch, H. J.; Grayson, R. L. Inorg. Chem. 1974, 13, 2121.

12. Luly, M. H. "APES, A Fortran Program to Analyze Photoelectron Spectra", U.S.D.O.E. Report IS-4694, 1979.

13. Michel, J. B.; McCarley, R. E. Inorg. Chem. 1982, 21, 1864.

14. Brencic, J. V.; Cotton, F. A. Inorg. Chem. 1970, 9, 351.

15. Clark, R. J. H.; Franks, M. L. J. Am. Chem. Soc. 1975, 97, 2691.

16. Norman, J. G. Jr.; Kolari, H. J. J. Am. Chem. Soc. 1975, 97, 33.

17. Beers, W. W. Ph.D. Dissertation, Iowa State University, Ames, Iowa, 1983; Section V.

SECTION II. SYNTHESES AND CHARACTERIZATION OF CLUSTER COMPOUNDS CONTAINING THE $Mo_4Cl_{12}^{3-}$ CLUSTER ANION. ISOMERIC FRAGMENTS OF THE $Mo_6Cl_{14}^{2-}$ CLUSTER ANION

INTRODUCTION

In our continuing studies on the synthesis and properties of molybdenum cluster compounds, we desired to investigate the possibilities of expanding the cluster size through a logical progression of synthetic steps. The synthesis of the tetranuclear cluster $R_4Mo_4Cl_{12}$ ($R = Et_4N^+$, Pr_4N^+, $\emptyset_4P^+$, Bu_4N^+) which we believed would be a logical precursor to the larger $Mo_5Cl_{13}^{n-}$ and $Mo_6Cl_{14}^{2-}$ cluster compounds was the initial step (1). During our attempts to derive a homologue of this cluster anion which we could structurally characterize, we serendipitously discovered the oxidized cluster compound $[\emptyset_4As]_2[Et_4N]Mo_4Cl_{12}$. Further investigation of the chemistry of the $Mo_4Cl_{12}^{3-}$ cluster anion revealed that it could adopt two different geometric configurations. In addition, a variety of interesting properties and characteristics were exhibited by the various salts of the oxidized $Mo_4Cl_{12}^{3-}$ cluster anion. The isolation of this anion and the investigation of its properties and structures are described in this section.

EXPERIMENTAL

Methods and Materials

Compounds whose preparations are described in this section are stable in air for short periods of time. However, to insure their integrity, all preparations, manipulations, and subsequent characterizations were carried out under inert atmospheres by using vacuum and Schlenk techniques.

Chlorobenzene, dichloromethane (DCM), and 1,2-dichloroethane (DCE) were dried by literature methods and distilled under N_2 or by vacuum distillation and stored over 3 Å molecular sieves prior to use. Cl_2 was passed through a series of two bubblers filled with H_2SO_4 to dry the reagent. Dichlorophenyliodine (DCPI) was prepared by literature methods (2). The DCPI was stored in a covered weighing bottle wrapped in aluminum foil at 3° C. Iodine (Fischer Scientific) was used as received without further purification. Solutions of a known I_2 titer were prepared by syringing previously dried and distilled DCE or DCM onto a carefully weighed sample of solid I_2 to give the desired concentration. These solutions were stored away from light at 3° C.

Chemical Analyses

Chemical analysis of synthesized compounds was performed as previously described (1).

Syntheses

Starting materials

$[\emptyset_4P]_4Mo_4Cl_{12}$, $[Et_4N]_4Mo_4Cl_{12}$, $[Pr_4N]_4Mo_4Cl_{12}$ and $Mo_4Cl_8(CH_3CH_2CN)_4$ were prepared as previously described (1).

$[Pr_4N]_3Mo_4Cl_{12} \cdot 0.7\ C_2H_4Cl_2$

$Mo_4Cl_8(CH_3CH_2CN)_4$ (0.5 g, 0.56 mmole) and of tetrapropylammonium chloride (0.5 g, 2.25 mmole) were placed in a 100 ml round bottom flask equipped with a sidearm. DCE (20 ml) was distilled onto the solids at liquid N_2 temperature and the reaction mixture was warmed to -10 to -20 ^{o} C where it was stirred until the formation of $[Pr_4N]_4Mo_4Cl_{12}$ was complete, as determined when visual examination of the mixture showed no $Mo_4Cl_8(CH_3CH_2CN)_4$ remained. A dropping funnel was placed on the reaction flask and purged with N_2, taking precaution to insure that the reaction mixture remained below -10^{o} C. A solution of iodine in DCM (5.63 ml of 0.05 M I_2/DCM, 0.282 mmole) was allowed to drip into the reaction mixture at a rate of one drop per second. The purple solid disappeared and formation of a densely colored brown solution occurred. The reaction

was allowed to warm to room temperature once the addition of I_2 was complete. Brown crystals were grown from the solution by stripping the solvent to one half volume and then layering several milliliters of dry chlorobenzene on top of the reaction mixture.

The compound could also be prepared from previously isolated $[Pr_4N]_4Mo_4Cl_{12}$. In this reaction, $[Pr_4N]_4Mo_4Cl_{12}$ (0.85 g .547 mmole) was placed in a reaction flask and 20 ml of DCE were distilled onto the solid. Solid I_2 (0.069 g) was added to the reaction solution which was warmed to room temperature and stirred for two days. Precipitation of a brown solid from a dense brown solution occurred during this period. The product was filtered and washed with two three ml portions of DCE. The yield was 0.37 g (49.5%). Analysis: Calc. for $[(C_3H_7)_4N]_3Mo_4Cl_{12}\cdot 0.7C_2H_4Cl_2$; Mo, 26.71; Cl, 29.62; Found; Mo, 26.72; Cl, 29.71.

When ground for infrared spectra and x-ray powder patterns the brown material became olive-green.

$\underline{[\emptyset_4P]_3Mo_4Cl_{12}\cdot 0.5\ \emptyset_4PI}$

$Mo_4Cl_8(CH_3CH_2CN)_4$ (0.5 g, 0.56 mmole) and tetraphenylphosphonium chloride (0.84 g, 2.25 mmole) were placed in a reaction flask. DCE (20 ml) was distilled onto the solids. The reaction was warmed to -5° C and stirred for 1 1/2 hours, after which 5.6 ml of 0.05 M I_2 in DCE

(0.281 mmole I_2) was syringed into the reaction mixture. A change from purple to brown was noted in the color of the reaction mixture. After several hours, the reaction solution was filtered but no solid was isolated at this point. After several days, a brown solid was noted on the bottom of the flask. Chlorobenzene was then layered onto the solution to facilitate precipitation. The mixture was filtered and dried.

The product was a mixture of brown blade-like crystals of $[\emptyset_4P]_3Mo_4Cl_{12}\cdot 0.5\ \emptyset_4PI$ and white solid, presumably $\emptyset_4PCl$. These solids were extracted with DCE and washed with DCM but separation of them was not successful because of the similar solubilities of the two solids. Thus, the product was not obtained in pure form and analytical data were not obtained. The yield of the mixture was 0.25 g, 49% based on pure $[\emptyset_4P]_3Mo_4Cl_{12}\cdot 0.5 \emptyset_4PI$. The brown crystals, when ground, turned olive green.

$\underline{[Et_4N]_3Mo_4Cl_{12}}$

Several methods for preparing the solid with the nominal composition $[Et_4N]_3Mo_4Cl_{12}$ have been found.

a) $[Et_4N]_4Mo_4Cl_{12}$ (1.0 g, 0.752 mmole) was placed in a 100 ml round bottom flask with side-arm. DCE (20 ml) was distilled onto the solid. While stirring the mixture, a solution of I_2 in DCE (0.095 g I_2 in 20 ml of DCE) was added

dropwise at a rate of 1 drop every 1-2 seconds. During this addition, the color of the reaction mixture changed from bright purple to olive green. The insoluble green product was filtered, extracted with the reaction solution and dried in vacuo.

b) A product that was identical to that in (a) could be prepared by use of Cl_2 as the oxidizing agent. $[Et_4N]_4Mo_4Cl_{12}$ (1.0 g, 0.75 mmole) was placed in a reaction flask and 20 ml of DCM were distilled onto the solid. A glass tube was placed in the reaction flask such that the opening of the tube was approximately 2 cm from the surface of the solution. For two minutes, chlorine gas was allowed to pass over the surface of the solution while stirring, after which N_2 was passed through the solution to flush excess Cl_2 from the system. When the Cl_2 was passed over the system, the reaction mixture immediately turned dark and produced an olive green solid and a relatively clear solution. The mixture was filtered, washed with DCM and dried in vacuo. The yield was 0.80 g (89%).

If Cl_2 is passed over the solution for a longer period of time, a product with a Cl:Mo ratio of 3.92 may be obtained. Guinier x-ray powder patterns of this product showed that the product is a mixture of the product formed in (a) and another unidentified product.

c) Difficulties controlling the stoichiometry using

chlorine gas as an oxidant led to the use of the somewhat novel chlorinating oxidant, dichlorophenyl-iodine (DCPI). The yellow crystalline compound, formed by the reaction of Cl_2 with iodobenzene at 0^{o} C, can be handled in air and permits convenient addition of stoichiometric quantities of chlorine to a reaction mixture. The solid slowly loses Cl_2 and cannot be stored for extended periods of time or subjected to vacuum drying without undergoing decomposition.

$[Et_4N]_4Mo_4Cl_{12}$ (0.75 g,0.56 mmole) and DCPI (0.15 g, 0.56 mmole) were placed in a reaction flask. DCM (20 ml) was syringed into the reaction flask. A reaction occurred immediately, turning the solid olive-green. The reaction was stirred for 20 minutes, filtered, and washed with three 5 ml washes of DCM. After drying <u>in vacuo</u> 0.5 g of product was obtained. The yield was 75%.

<u>$[\emptyset_4As]_2[Et_4N]Mo_4Cl_{12}$</u>

This compound was prepared by the additon of a large excess of $\emptyset_4AsCl$ to a small amount of $[Et_4N]_4Mo_4Cl_{12}$ in DCE. (ØAs:Mo = 8:1). The reaction was allowed to stand, undisturbed, for three weeks. During this time, a number of small crystals of two morphologies had formed. Plates and daggers were separated from the reaction mixture by decantation of the supernatant solution under a flow of N_2 and the solid was dried in vacuo. [Indexing of the needles

failed, but a structure determination was carried out on the platelet crystals (vide infra).] The structure determination confirmed the composition as $[\emptyset_4As]_2[Et_4N]Mo_4Cl_{12}\cdot 2\ CH_2Cl_2$. Numerous attempts to repeat the preparation failed to yield the platelet crystals, however the crystals of the needle morphology were produced. These crystals exhibited a composition intermediate between that of $[\emptyset_4As]_2[Et_4N]Mo_4Cl_{12}$ and $[\emptyset_4As][Et_4N]Mo_4Cl_{12}$, due to a mixture of compounds containing different amounts of cations.

Analysis: Calc. for $[\emptyset_4As]_2[Et_4N]Mo_4Cl_{12}$; Mo, 22.50; Cl 24.94. Calc. for $[\emptyset_4As][Et_4N]Mo_4Cl_{12}$; Mo, 29.01; Cl 32.16. Found; Mo, 27.00; Cl, 30.70.

$\underline{[Et_4N]_x[\emptyset_4As]_yMo_4Cl_{12}}$

A number of reactions were attempted where the $[\emptyset_4As]_2[Et_4N]Mo_4Cl_{12}$ crystals could be prepared. These reactions took one of two forms: 1) duplications of the reaction from which $[\emptyset_4As]_2[Et_4N]Mo_4Cl_{12}$ crystals were obtained where $[Et_4N]_4Mo_4Cl_{12}$ was stirred or allowed to set for extended periods of time with $\emptyset_4AsCl$, and 2) reactions where $\emptyset_4AsCl$ and Et_4NCl were mixed with $Mo_4Cl_8(CH_3CH_2CN)_4$. The reactions gave needle-like crystals and a yellow-green powdery solid.

$[Pr_4N]_4Mo_6Cl_{17}$

$Mo_4Cl_8(CH_3CH_2CN)_4$ (0.75 g, 0.845 mmole) and Pr_4NCl (0.75 g, 3.38 mmole) were placed in a reaction flask. DCM (20 ml) was distilled onto the solids. The reaction was allowed to come to room temperature and stirred 10 hours. The green-black crystals which appeared during this time were filtered, washed with DCM until the washings were colorless, and dried in vacuo. The yield was 0.60 g (55.4%). Analysis: Calc. for $[(C_3H_7)_4N]_4Mo_6Cl_{17}$; Mo, 29.92; Cl, 31.32; C, 29.26; H, 5.82; N, 2.91; Found; Mo, 29.60, 29.92; Cl, 31.19, 31.09; C, 29.88, 29.26; H, 6.41, 6.39; N, 2.90, 2.82.

$[\emptyset_4P]_{4.5}Mo_6Cl_{17}$

$Mo_4Cl_8(CH_3CH_2CN)_4$ (0.5 g, 0.563 mmole) and $\emptyset_4PCl$ (0.84 g, 2.24 mmole) were placed in a reaction flask. DCM (20 ml) were distilled onto the solid. The reaction was heated to approximately 40° C and stirred for twelve hours. The reaction mixture produced a green-black solid from a dark red-brown solution. The solid product was separated by filtration and extracted for three hours with the reaction solution, before being dried in vacuo and stored in the drybox. The yield was 0.69 g (67.9%). Analysis: Calc. for $[(C_6H_5)_4P]_{4.5}Mo_6Cl_{17}$; Mo, 21.28; Cl, 22.27; Found; Mo, 21.28; Cl, 22.15.

Physical Measurements

Physical measurements (Fourier transform infrared spectra, UV-visible spectra, X-ray photoelectron spectra, and Guinier powder patterns) were obtained using instruments and procedures previously described (1). Powder patterns were calculated from known structural parameters for $[\emptyset_4P]_3Mo_4Cl_{12}\cdot 0.5\ \emptyset_4PI$ and $[Pr_4N]_3Mo_4Cl_{12}\cdot 0.7\ C_2H_4Cl_2$ using the program POWDER (3). The diffraction lines on the calculated pattern were then compared to lines obtained from powder patterns of these materials.

Magnetic susceptibility

Magnetic susceptibilities were measured using a Quantum Design SQUID (superconducting quantum interference device) susceptometer maintained in Dr. Robert Shelton's group. Samples were thoroughly ground and placed in quartz tubes (2 mm o.d., 1 mm i.d.) which had been designed for use with the susceptometer. The gram susceptibilities were measured over the temperature range 4-300^{o} K. Magnetic fields of 5000 and 10,000 gauss were used.

The initial raw data indicated paramagnetic samples at low temperatures, and at higher temperatures showed a discontinuity in the chi vs. T curve where a jump from positive (paramagnetic) to negative (diamagnetic) chi values

was observed. This jump was due to a combination of factors. The small and decreasing paramagnetic signal of the sample itself is gradually overpowered by the diamagnetism of the quartz sample holder as the temperature is raised. At sufficiently high temperature, the jump occurs because of the manner in which the signal is measured. At each temperature the sample is pulled through a magnetic field and the change in the induced field is monitored at 128 points. These points graph a curve, the area under which is proportional to the magnetic susceptibility of the sample. Compounds which are diamagnetic exhibit a curve opposite in sign to those which are paramagnetic. If there is a mixture of two types of magnetic behavior in the sample, the type with the larger magnitude is dominant. The area under the curve and the sign of signal is then determined by the dominant susceptibility. Normally, the magnetic susceptibility for a sample is an order of magnitude greater than that of the sample holder and these difficulties are not encountered. For these compounds however, the susceptibility of the quartz sample holder is on the same order of magnitude (10^{-7} emu/gram) as the sample. At lower temperatures, the paramagnetism of the sample is dominant but as this signal decreases with increasing temperature the diamagnetic signal due to the quartz sample holder begins to have increasing

significance until it dominates the susceptibility at temperatures around 200° K causing a break, due to the change in sign of the observed magnetism, in what would otherwise be a smooth curve.

Corrections for this problem required measuring the susceptibility of the sample holder separately and subtracting this signal from the total signal for each of the 128 points at each temperature to give a signal corresponding to sample alone, which were then used to calculate chi(apparent). The corrected chi vs. T curves for $[\emptyset_4P]_3Mo_4Cl_{12}$ and $[Pr_4N]_3Mo_4Cl_{12}$ are shown in Figure II-1.

Electron paramagnetic resonance

X-band electron paramagnetic resonance experiments were performed using a Bruker ER 200D-SRC electron spin resonance spectrometer. The spectrometer was equipped with an Oxford ESR-900 flow through cryostat and a DTC-2 digital temperature controller. A Hewlett-Packard 5342 A microwave frequency counter was used to accurately measure the frequency of the spectrometer. Spectra were obtained on powders which were finely ground and placed in quartz tubes (4 mm o.d., 2 mm i.d.) before being evacuated and sealed. The spectra were obtained at various temperatures (4°, 77°, and 300° C).

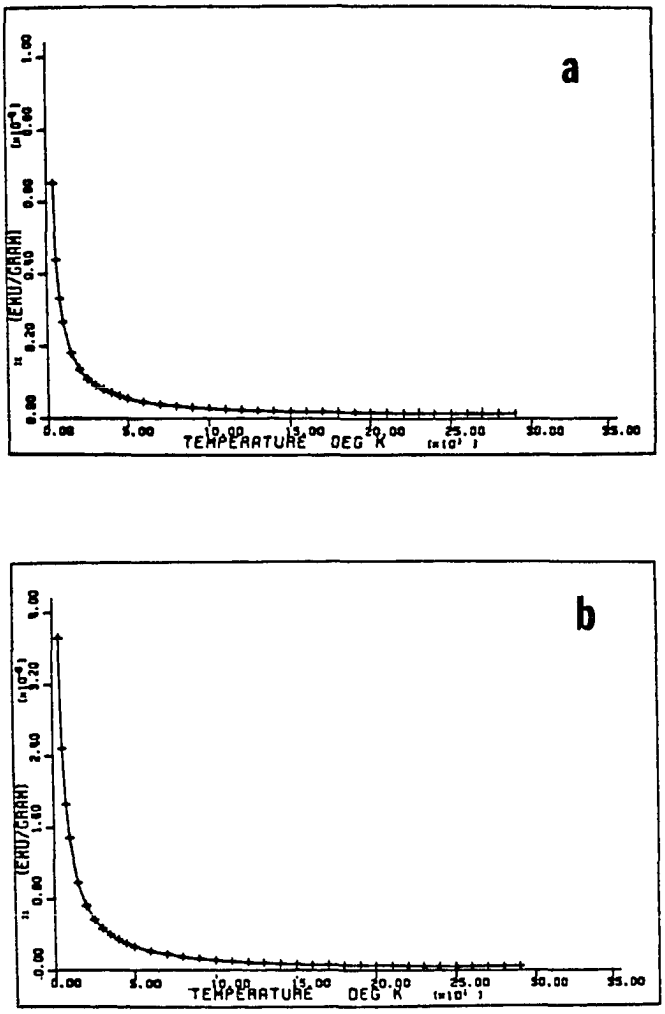

Figure II-1. Chi (emu/g) vs temperature for
a) $[Pr_4N]_3Mo_4Cl_{12}\cdot 0.7\ C_2H_4Cl_2$ and
b) $[\emptyset_4P]_3Mo_4Cl_{12}\cdot 0.5\ \emptyset_4PI$

Cyclic voltammetry

Cyclic voltammetry experiments were carried out using a PAR 173/179 potentiostat/coulometer and a PAR 175 voltage sweep programmer. The spectra were recorded using a Houston Instruments Model 2200 x-y recorder. An electrochemical cell was used which allowed measurement requiring only small amounts of sample and also allowed for protection of the sample from the atmosphere. A platinum disc served as the working electrode and a platinum wire was the auxiliary electrode. The voltammograms were referenced to a Ag/AgCl reference electrode in contact with the sample solution via a 0.1 M Bu_4NBF_4/CH_2Cl_2 electrolyte solution. The recorded potentials were uncorrected for junction potential effects.

The 0.1 M Bu_4NBF_4/CH_2Cl_2 solution also served as the solvent and the support electrolyte for the sample solution. Potential limits (0.8 to -1.8 V) for the solvent/electrolyte solution were found by increasing the potential scan experimentally until the oxidation and reduction waves went off scale on the recorder using a large tolerance limit for the current.

For a sample measurement, the electrochemical cell was loaded in the drybox (samples sizes were calculated to give concentrations of 0.005 M solutions for 10 ml of solvent). A flow of Ar or N_2 was kept over the sample at all times during the experiment to prevent oxidation of the sample by

adventitious oxygen.

In order to prevent decomposition observed for these compounds in solution, the electrochemical cell was maintained at -10° C by use of an ice/MeOH/NaCl slush bath. Electrolyte solutions were similarly cooled and syringed through septa to prevent 0_2 contamination. The sample solution was thoroughly stirred before measurements to insure complete dissolution and also stirred between runs to insure fresh samples were measured at the electrode.

Voltammograms were recorded at the stationary platinum disc as the system came to steady state and recorded after the steady state had been reached. Various scan rates were recorded so that the reversibility/irreversibility of the system could be determined.

X-ray Data Collection and Structure Solution for

$[Et_4N]_3Mo_4Cl_{12}$, $[\emptyset_4P]_3Mo_4Cl_{12}\cdot 0.5\ \emptyset_4PI$,

$[Pr_4N]_3Mo_4Cl_{12}\cdot 0.7\ C_2H_4Cl_2$, and

$[\emptyset_4As]_2[Et_4N]Mo_4Cl_{12}\cdot 2\ CH_2Cl_2$

X-ray data collection for $[Et_4N]_3Mo_4Cl_{12}$

Several small crystals of $[Et_4N]_3Mo_4Cl_{12}$ were isolated by extensive extraction of a reaction product obtained when a solution of I_2 was added dropwise to a stirred suspension of $[Et_4N]_4Mo_4Cl_{12}$ in DCM. These crystals were separated by

decanting the solution from them under a flow of N_2 and drying *in vacuo*. Crystals from this batch were mounted in thin walled capillaries using the microscope and drybox facilities in Dr. J.D. Corbett's group. The crystals were of two types, platelets and octahedra. Several of each type were mounted using silicone grease to attach them to the walls of the capillary.

Oscillation and Weissenberg photographs were taken of both types of crystals. The platelet crystals were disordered, as evidenced by lines in the Weissenberg photograph; however, approximate cell constants could be obtained from the photograph. A cell which measured 13.77 x 7.63 x 12.18 Å, $\alpha = \beta = \gamma = 90.0^{\circ}$ was calculated from the photograph. Due to the poor diffracting nature of the crystals, indicated by the Weissenberg photography, collection of a data set was not attempted.

The octahedral crystals diffracted x-rays clearly and distinctly. Oscillation and Weissenberg photography indicated a cell of dimensions 23.90 x 7.66 x 6.28 Å, $\alpha = \beta = \gamma = 90^{\circ}$. One crystal was selected and indexed on the DATEX (4) single crystal diffractometer in Dr. Jacobson's group. Fourteen reflections randomly obtained from oscillation photographs at $\chi = 0.0^{\circ}$ and $\phi = 0.0, 45.0, 90.0^{\circ}$ were used as input to the Ames Laboratory automatic indexing algorithm, ALICE (5). Based on these reflections, a

triclinic cell (a = 23.02, b = 23.06, c= 22.99 Å, α = 116.92, β = 116.25, γ = 96.03) was predicted. The cell scalars ($R_{11} = R_{22} = R_{33}$, $(R_{11}-R_{12})/2$, $(R_{11}-R_{12})/2$, R_{12}) indicated that this cell could be transformed to a body-centered tetragonal cell. The transformation produced a cell with dimensions a = 24.08, b = 24.29, c = 30.83 Å, $\alpha = \beta = \gamma = 90.0$. Axial oscillation photographs were taken and insured the correct choice of unit cell had been made. Three standards were selected (0,0,20; 0,20,0; 0,0,24) with $2\theta > 30.0^{\circ}$. Calculation of cell parameters based on these standards gave a = 24.21, b = 24.22, c = 30.85 Å.

All data from 2.0-50.0° in 2θ were collected in the hkl octant using an omega scan mode. The intensities of the three standards were checked every 75 reflections to insure that the crystal had not become disoriented due to mechanical vibration or had started to decay due to the prolonged exposure to x-rays. No significant loss of intensity was observed. The data set consisted of 8954 reflections.

Two phi scans were made, using reflections 2,16,0, and 0,0,12, with chi approximately equal to 90.0°. Intensity measurements were made at ten degree intervals in phi from 0 to 360 degrees. The intensities from these reflections varied less than 5 percent. Because the absorption coefficient was so small and the phi scan showed little

deviation in intensity an absorption correction was deemed unnecessary.

The final lattice parameters were calculated from least squares refinement of the two theta values for twenty one reflections and their Friedel related pairs by use of the program LATT (6). Final cell parameters were a = b = 24.181(7), c = 30.826(18) $\mathring{A}$; $\alpha = \beta = \gamma = 90.0$; V = 18,024(13) $\mathring{A}^3$. Information pertaining to data collection and structure refinement is shown in Table II-1.

Structure solution and refinement of $[Et_4N]_3Mo_4Cl_{12}$

The raw data were corrected for Lorentz and polarization effects. Two data sets were then obtained, one for use with MULTAN80 (7) algorithms which contained all reflections and a smaller set for use with the ALLS (8) refinement algorithms where reflections with $I < 3\sigma(I)$ or $F < 3\sigma(F)$ had been eliminated. Evaluation of the data sets showed that the systematic extinction conditions were present: h,k,l h+k+l≠2n; h,k,0 h(k)≠2n; 0,k,l k(l)≠2n; h,h,l 2h+l≠2n. These conditions unambiguously determined the space group as $I4_1/acd$, the highest symmetry tetragonal space group. The HPR plot obtained also inferred that the space group should be centrosymmetric (9).

The data were subsequently averaged in 4/mmm Laue symmetry yielding 4028 and 1231 reflections for the MULTAN80

Table II-1. Crystallographic data for $[Et_4N]_3Mo_4Cl_{12}$

formula	$[Et_4N]_3Mo_4Cl_{12}$
molecular weight	1369.85
space group	$I4_1/acd$
systematic absences	hkl, h+k+l≠2n; hk0, h(k)≠2n; okl, k(l)≠2n; hhl, 2h+l≠2n
a, Å	24.181(7)
b, Å	24.181(7)
c, Å	30.826(18)
α, β, γ, deg	90.00
V, $Å^3$	18024(13)
Z	16
d, calc g/cm^3	1.768
crystal size	0.08 x 0.08 x 0.08
shape	octahedral
instrument	Datex diffractometer
radiation	Mo Kα monochromated wavelength =0.71069
# orientation refl.	14
# parameter refl.	21
scan method	ω
data collection range	2.0-50.0° in 2 theta
octants collected	HKL
standard reflections	20,0,0; 0,20,0; 0,0,24
# reflections	8954
$F_o > 3\sigma(F_o)$	2174
# averaged data	1231, R=2.45
# parameters refined	204
refl/parameter	6.0
R^a	5.4
$R_w{}^b$	5.8
Quality of fit, Q^c	2.169

[a] $R=\Sigma||F_o|-|F_c||/\Sigma|F_o|$.

[b] $R_w=[\Sigma w(|F_o|-|F_c|)^2/\Sigma|w|F_o|^2]^{1/2}$, $w=1/\sigma(F_o)^2$.

[c] $Q=[\Sigma w(|F_o|-|F_c|)^2/N(\text{observations})-N(\text{parameters})]^{1/2}$.

and ALLS data sets, respectively. The scattering factors used were those of Hansen et al. (10), with those for molybdenum and chlorine corrected for the real and imaginary parts of anomalous dispersion (11).

The structure was solved by using MULTAN80. A randomly oriented planar Mo_4Cl_{12} moiety was used as input for the normalization section of the program. Based on this input, sixteen possible solution sets were generated. The set with the highest combined figure of merit was selected as the correct solution and from it the positions of the two unique molybdenum atoms in the asymmetric unit were obtained. Refinement on these positions using the space group setting where the center of inversion is located at the origin gave a residual $[R=\Sigma||F_o|-|F_c||/\Sigma|F_o|]$ of 0.380.

The cluster unit adopted the butterfly geometry. Subsequent identification and location of chlorine atoms was determined by visual inspection of electron density maps although retrospective analysis of the MULTAN80 output showed that five of the six chlorine atoms were identified in that peak list. Once the six chlorine and two molybdenum atoms were identified and refined isotropically the R value dropped to 0.139.

The refinement of the nitrogen and carbon atoms of the tetraethylammonium cations proceeded with great difficulty. $(Et_4N)^+$ cations are situated at four different sites in the

asymmetric unit.

Two of the cations (identified by their nitrogen atoms as N(1) and N(4)) are located on sites of $\bar{4}$ symmetry. The nitrogen atom is located at the symmetry site with a multiplier of 0.25. Two unique carbon atoms form the ethyl branches of the cation and have atom multipliers of 1.0. The $\bar{4}$ symmetry operations of the space group generate the additional carbon sites and the remaining density at the nitrogen site thus creating a full tetraethylammonium cation.

A third cation is located with the nitrogen, N(2), located on a site of 2-fold symmetry. There are four unique carbons associated with this molecule (C(21), C(22), C(23), and C(24)). The four carbons comprise two ethyl branches, the remaining two ethyl branches of the tetraethylammonium cation being generated by the 2-fold axis.

This site is also fully occupied. When the multiplier for the nitrogen atom was allowed to vary it refined to a value of 0.5364 and was subsequently restrained to 0.5. Refinement of the carbon atom positions was very difficult. Although four distinct sites are observed, they refine with a multiplier less than one as required by the full occupancy of the site. The positional parameters resisted refinement even during late stages of refinement, causing extremely high standard deviations in positional and thermal

parameters. This type of behavior is most likely due to disorder of the cation around the center of the site. This would explain the observed normal behavior for N(2) while the carbons associated with it would be smeared over space around the site, manifested in low occupancies of the defined sites and unusually large thermal parameters. Due to this problem, these carbon atoms were not refined anisotropically.

The fourth tetraethylammonium cation is located with the nitrogen, N(3), on an inversion center. This site is also fully occupied. Tetraethylammonium cations do not have a center of inversion so disorder at the site is required. There are six carbon atoms associated with this cation. Four of them [C(31), C(31A), C(32), C(32A)] are in alpha positions with respect to the nitrogen atom. These four carbons and their inversion related partners form a cube around N(3) shown in Figure II-2. Each of these carbons has a multiplier of 0.5. The remaining two carbons [C(33) and C(34)] are in beta positions with respect to N(3) and have a multiplier of 1.0. The cation has two different orientations in this site, each occupied 50% of the time. One orientation includes N(3), C(31), C(32'), C(31A), C(32A'), C(33) and C(34). [C(31A') and C(32A') are the inversion generated partners of C(31A) and C(32A), respectively]. The other orientation is the inversion of

the first, and consists of N(3), C(31'), C(32), C(31A'), (C32A), C(33), and C(34).

Positional and thermal parameters for the compound are listed in Tables II-2, II-3, II-4, and II-5.

During the latter stages of refinement it was noted that most of the very intense reflections exhibited calculated structure factors which were greater than the observed structure factors, suggesting that a secondary extinction correction should be made. This was applied in the latter stages of refinement (12). The final R values were R=0.054 and R_w=0.059. A final electron difference map showed no peaks greater than 0.5 e/$\AA^3$.

The stoichiometry of the molecule is realized as follows. The two unique molybdenum atoms at general positions define 64 molybdenum atoms in the unit cell, comprising 16 Mo_4 butterfly cluster units. All of the cations reside on special positions. Two of the cations, containing nitrogen atoms N(1) and N(4), reside on the eight $\bar{4}$ sites in the cell. There are 16 2-fold sites of the type occupied by N(2) and 16 centers of inversion where the N(3) cation are located. Thus, there are 48 cations per cell to balance the charge of the 16 anions giving the stoichiometry $[Et_4N]_3Mo_4Cl_{12}$.

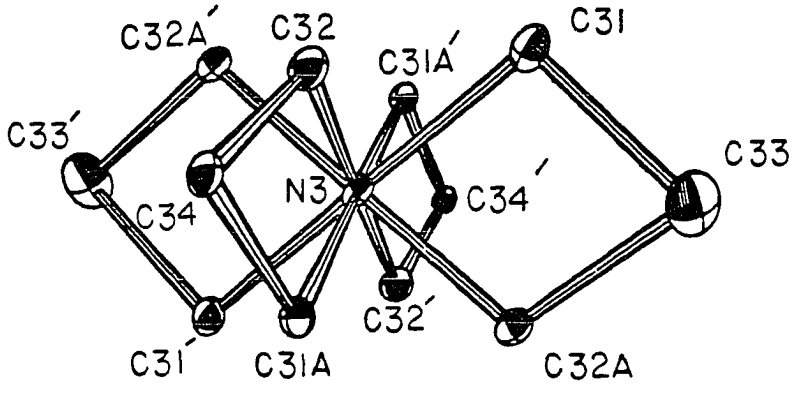

Figure II-2. Tetraethylammonium cation in $[Et_4N]_3Mo_4Cl_{12}$ showing disordered alpha carbons which form a cube around the nitrogen atom. Atoms marked with (') are inversion related to unmarked atoms with same number. Ten percent probablility isotropic thermal ellipsoids are shown

X-ray data collection for $[\emptyset_4As]_2[Et_4N]Mo_4Cl_{12}$

The reaction mixture yielded two types of crystals, plates and needles. Several crystals of each type were chosen from the reaction mixture and mounted in thin walled capillaries. Attempts to index reflections from the needles failed due to the poor diffracting quality of the crystals but one platelet was indexed to a monoclinic cell with the dimensions 17.01 x 17.68 x 13.07 Å. Collection of a data set using the Ames Laboratory diffractometer (13) was carried out as previously described for $[Et_4N]_3Mo_4Cl_{12}$ using the DATEX diffractometer. Lattice parameters were also determined in a similar manner. All data in the octants hkl and $\bar{h}\bar{k}l$ were collected. Details of the data collection and data treatment are tabulated in Table II-6.

During data collection, the three standard reflections showed a gradual decay in intensity, indicating the data set required a correction. The decay in intensity could be approximated by fitting to the exponential equation, $A + BX + CX^2 + DX^3 = I$, where I is the intensity of a standard reflection and X is the reflection number (a rough approximation of time that the crystal was exposed to x-rays). The value for A is the intensity of the 0,12,0 reflection at X=0. B, C, and D are coefficients which are calculated. The values that were calculated are; A = 3447, B = -0.1598, C = 2.0×10^{-5} and D = -9×10^{-14}. Solving the

Table II-2. Atom coordinates (x 10^4) for $[Et_4N]_3Mo_4Cl_{12}$[a]

Atom	x	y	z	U(ave)
Mo(1)	2556.(2)	2267.(1)	4581.5(9)	47.
Mo(2)	3198.(1)	1718.(1)	5051.(1)	47.
Cl(1)	1898.(4)	1737.(4)	4153.(3)	60.
Cl(2)	3200.(4)	2782.(3)	5058.(3)	58.
Cl(3)	3308.(4)	1742.(4)	4258.(3)	61.
Cl(4)	1814.(4)	755.(3)	4954.(4)	64.
Cl(5)	4206.(4)	1775.(4)	5109.(3)	67.
Cl(6)	2648.(6)	2952.(4)	3984.(3)	89.

[a]The isotropic equivalent thermal parameter U(ave) $Å^2$ is the average of U_{11}, U_{22}, and U_{33}. Estimated standard deviations are given in parentheses for last significant digit.

Table II-3. Anisotropic thermal parameters for $[Et_4N]_3Mo_4Cl_{12}$ ($Å^2$ x 10^3)[a]

atom	U_{11}	U_{22}	U_{33}	U_{12}	U_{13}	U_{23}
Mo(1)	64.(2)	43.(2)	36.(1)	-1.(2)	-1.(2)	4.(2)
Mo(2)	56.(2)	46.(2)	41.(2)	1.(2)	-1.(2)	-1.(2)
Cl(1)	62.(7)	76.(7)	42.(5)	-3.(6)	-13.(5)	-7.(5)
Cl(2)	70.(6)	47.(5)	57.(6)	-12.(5)	1.(5)	-6.(5)
Cl(3)	71.(7)	66.(7)	46.(5)	2.(6)	8.(5)	1.(5)
Cl(4)	72.(6)	46.(5)	74.(7)	-10.(5)	12.(7)	-8.(6)
Cl(5)	56.(6)	80.(7)	66.(6)	-6.(6)	-3.(5)	-10.(6)
Cl(6)	159.(12)	58.(7)	51.(6)	13.(8)	-5.(7)	11.(5)

[a]The general thermal parameter expression used is $\exp[-2\pi^2(U_{11}h^2a^{*2} + U_{22}k^2b^{*2} + U_{33}l^2c^{*2} + 2U_{12}hka^*b^* + 2U_{13}hla^*c^* + 2U_{23}klb^*c^*)]$. Estimated standard deviations are given in parentheses for last significant figure.

Table II-4. Atom coordinates (x 10^3) for cations in $[Et_4N]_3Mo_4Cl_{12}$

	x	y	z	U(ave)
N(1)	0.(0)	250.0(0)	375.0(0)	11.
C(11)	18.3(2)	198.9(2)	345.7(2)	142.
C(12)	47.4(2)	148.5(2)	368.1(1)	82.
N(2)	264.1(1)	48.588(0)	375.0(0)	90.(12)
C(21)	302.4(5)	52.2(5)	370.2(4)	448.(63)
C(22)	315.6(4)	545.8(4)	328.7(3)	217.(44)
C(23)	279.7(4)	464.3(4)	337.7(3)	179.(49)
C(24)	311.2(5)	423.7(1)	328.7(4)	203.(56)
N(3)	250.0(0)	250.0(0)	250.0(0)	70.
C(31)	204.7(3)	251.3(4)	286.1(2)	123.
C(31A)	289.8(4)	200.5(3)	261.3(2)	57.
C(32)	266.5(4)	251.4(3)	294.3(2)	153.
C(32A)	212.7(4)	188.0(3)	238.5(3)	119.
C(33)	164.8(2)	191.9(3)	274.7(2)	203.
C(34)	304.5(2)	199.6(2)	309.8(1)	80.
N(4)	500.0(0)	250.0(0)	375.0(0)	51.
C(41)	518.5(4)	294.5(4)	344.7(2)	217.
C(42)	446.5(2)	304.2(2)	318.3(2)	135.

[a]The isotropic equivalent thermal parameter U(ave) is the average of U_{11}, U_{22}, and U_{33}. Estimated standard deviations are given in parentheses for last significant digit.

Table II-5. Anisotropic temperature factors for cations in $[Et_4N]_3Mo_4Cl_{12}$ ($Å^2 \times 10^2$)[a,b]

atom	U_{11}	U_{22}	U_{33}	U_{12}	U_{13}	U_{23}
N(1)	21.2(7)	19.1(3)	1.4(3)	0.0(0)	0.0(0)	0.0(0)
C(11)	13.4(4)	18.8(4)	10.3(4)	5.9(3)	-3.7(4)	-6.5(3)
C(12)	9.2(3)	7.8(5)	7.4(3)	4.1(3)	-1.1(2)	-3.2(3)
N(2)	90.(12)	---	---	---	---	---
C(21)	448.(63)	---	---	---	---	---
C(22)	217.(44)	---	---	---	---	---
C(23)	179.(49)	---	---	---	---	---
C(24)	203.(56)	---	---	---	---	---
N(3)	8.2(3)	7.4(3)	5.3(2)	0.8(3)	1.1(3)	0.9(3)
C(31)	6.2(6)	25.2(9)	5.6(5)	6.8(6)	2.2(5)	-3.9(6)
C(31A)	8.2(8)	4.5(5)	4.4(4)	3.8(5)	-1.2(5)	1.1(4)
C(32)	19.2(5)	17.3(6)	9.4(47	-3.0(7)	0.5(6)	3.5(5)
C(32A)	9.1(8)	16.2(7)	10.5(8)	1.3(7)	-4.3(6)	-3.0(6)
C(33)	9.8(3)	20.3(6)	30.8(8)	-3.1(4)	0.1(4)	17.8(6)
C(34)	10.7(3)	6.4(7)	7.0(2)	4.7(3)	-0.2(2)	0.8(2)
N(4)	4.1(1)	4.0(1)	13.2(3)	0.0(0)	0.00()	0.0(0)
C(41)	33.6(7)	22.7(6)	8.7(3)	135.5(9)	1.6(7)	0.5(6)
C(42)	15.4(4)	14.7(4)	10.3(5)	5.7(3)	-3.4(4)	4.2(4)

[a]Cation with nitrogen N(2) not refined anisotropically. Value listed is average isotropic thermal parameter.

[b]The general thermal parameter expression used is $\exp[-2\pi^2(U_{11}h^2a^{*2} + U_{22}k^2b^{*2} + U_{33}l^2c^{*2} + 2U_{12}hka^*b^* + 2U_{13}hla^*c^* + 2U_{23}klb^*c^*)]$. Estimated standard deviations are given in parentheses for last significant figure.

Table II-6. Crystal data for $[\emptyset_4As]_2[Et_4N]Mo_4Cl_{12}\cdot 2\ CH_2Cl_2$

formula	$[\emptyset_4As]_2[Et_4N]Mo_4Cl_1\cdot 2\ CH_2Cl_2$
molecular weight	1887.69
space group	$P2_1/a$
systematic absences	0k0, k≠2n; h00 h≠2n; h01, h≠2n
a, Å	17.0182(33)
b, Å	17.6805(24)
c, Å	13.0724(27)
β, deg	113.0724(166)
V, $Å^3$	3607(1)
Z	2
d calc. g/cm^3	1.51
crystal size	0.05 x 0.05 x 0.02
μ, cm	21.22
instrument	Ames Laboratory in house designed four-circle diffractometer
octants collected	hkl, $\bar{h}k\bar{l}$
radiation	Mo Kα, λ = 0.71069
lattice refl.	21
#orientation refl.	16
temperature	22^o C
scan method	omega
data collection range	2.0-60.0 in 2 theta
# refl. collected	10630
# $F_o > 3\sigma(F_o)$	4820
# unique data	4463
# parameters refined	448
R^a	5.5
$R_w{}^b$	6.6
quality of fit, Q^c	2.034

[a] $R=\Sigma||F_o|-|F_c||/\Sigma|F_o|$.

[b] $R_w=[\Sigma w(|F_o|-|F_c|)^2/\Sigma|w|F_o|^2]^{1/2}$, $w=1/\sigma(F_o)^2$.

[c] $Q=[\Sigma w(|F_o|-|F_c|)^2/N(\text{observations})-N(\text{parameters})]^{1/2}$.

equation for the remaining two standard reflections (10,0,0; 0,0,6) gave the same values for B, C, and D. Since the terms C and D were small the decay was considered linear. The data set was treated accordingly to correct for the loss of intensity due to the crystal decay. The treated data yielded a satisfactory averaged data set (R=0.029), indicating the validity of the correction. The data exhibited systematic extinctions which defined the space group as $P2_1/a$, a nonstandard setting of $P2_1/c$.

Structure solution and refinement of $[\emptyset_4As]_2[Et_4N]Mo_4Cl_{12}$

Empirical absorption corrections (14) and corrections for Lorentz and polarization effects were applied. The structure was solved using Patterson and superposition techniques to locate the positions of the two unique molybdenum atoms in the asymmetric unit. An inversion center near these two molybdenum atoms generated two additional molybdenum atoms which altogether defined a planar tetrameric cluster unit. Positions of arsenic and chlorine atoms were found from electron density maps based on Fourier syntheses from results of the least squares refinements of the molybdenum atom positions (8). The carbon atoms of the tetraphenylarsonium cation were similarly located. Following isotropic refinement of these atoms the residual was 0.1740.

An electron density map based on the difference of observed and calculated density revealed a dichloromethane solvent molecule in the lattice. Only the carbon and two chlorine atoms of the molecule were found and their distances and angles were similar to those found for solvent dichloromethane in other structures (15).

At this point, several peaks of electron density were seen near the inversion center at 0, 0, 1/2. Examination of this density showed that it could be accounted for by a disordered tetraethylammonium cation, similar to that found in $[Et_4N]_3Mo_4Cl_{12}$ (Figure II-2). The nitrogen atom was located at the inversion center and was surrounded by four unique alpha carbons, each with a multiplier of 0.5, and two beta carbons with a multiplier of 1.0. The four alpha carbons and their inversion generated partners defined a cube with the nitrogen atom at the center. The $(Et_4N)^+$ ion was disordered over two orientations. One half of the time, the tetraethylammonium cation was constituted by the nitrogen atom, two of the alpha carbons and the inversion related partners of the two remaining alpha carbons such that these four carbons defined a tetrahedron, plus the two beta carbons and their inversion partners. The alternate orientation consists of the inversion related partners of the alpha carbons used in the first setting as well as the nitrogen atom and two beta carbon atoms. Positional and

thermal parameters for nonhydrogen atoms are listed in Tables II-7, II-8, II-9, and II-10.

Hydrogen atoms contributed a significant portion of the scattering density of the compound. Hydrogen atom positions could not be determined from the electron difference map but were calculated from the positions of the carbon atoms (8). Hydrogen atom parameters are listed in Table II-11 and were not varied in the refinement. Their inclusion did improve the residual value. Final convergence factors are listed in Table II-6. The final electron density map was flat to less than 0.5 $e^-/\text{Å}^3$.

There are eight molybdenum atoms which define two planar tetranuclear clusters per unit cell. There are four $(\emptyset_4As)^+$ cations at general positions in the unit cell. The tetraethylammonium cation is situated at an inversion center, thereby giving only two per unit cell. Thus, the stoichiometry of the molecule is $[\emptyset_4As]_2[Et_4N]Mo_4Cl_{12}\cdot 2CH_2Cl_2$.

Structure determination of $[Pr_4N]_3Mo_4Cl_{12}$

Crystals isolated from a reaction of $[Pr_4N]_4Mo_4Cl_{12}$ and an I_2/DCM solution were selected and mounted as previously described. These crystals were generally columnar in shape. They diffracted x-rays very strongly. Oscillation and Weissenberg photography indicated a monoclinic cell with approximate cell parameters of 11.2, 15.52, and 8.95 Å.

Table II-7. Atom coordinates (x 10^4) for $[\emptyset_4As]_2[Et_4N]Mo_4Cl_{12}\cdot 2\ CH_2Cl_2$[a]

atom	x	y	z	U(ave)[b]
Mo(1)	199.8(6)	675.7(6)	916.6(9)	40.
Mo(2)	-59.6(7)	9196.7(6)	940.1(9)	42.
Cl(1t)	495.(2)	1607.(2)	2477.(3)	61.
Cl(2t)	102.(2)	1796.(2)	7689.(3)	67.
Cl(3)	1249.(2)	-190.(2)	2192.(3)	51.
Cl(4)	968.(2)	-130.(2)	8697.(3)	50.
Cl(5)	1365.(2)	1298.(2)	536.(3)	56.
Cl(6)	9179.(2)	1614.(2)	9706.(3)	57.

[a]Estimated standard deviations are given in parentheses for the last significant digit.

[b]U(ave)-average isotropic temperature factor ($Å^2$, x 10^3) is average of U_{11}, U_{22}, and U_{33}.

Table II-8. Anisotropic thermal parameters (x 10^4) for $[\emptyset_4As]_2[Et_4N]Mo_4Cl_{12}\cdot 2\ CH_2Cl_2$[a]

atom	U_{11}	U_{23}	U_{33}	U_{12}	U_{13}	U_{23}
Mo(1)	34.7(6)	40.9(6)	45.1(7)	0.1(5)	8.8(5)	1.9(5)
Mo(2)	40.3(6)	40.6(6)	45.7(7)	0.8(5)	9.9(5)	-1.8(6)
Cl(1t)	70.(2)	56.(2)	57.(2)	-15.(2)	24.(2)	-16.(2)
Cl(2t)	96.(3)	39.(2)	67.(3)	5.(2)	39.(2)	9.(2)
Cl(3)	42.(2)	57.(2)	55.(2)	2.(2)	-1.(2)	4.(2)
Cl(4)	42.(2)	47.(2)	59.(2)	-1.(1)	20.(2)	0.(2)
Cl(5)	48.(2)	63.(2)	57.(2)	-17.(2)	18.(2)	-8.(2)
Cl(6)	59.(2)	49.(2)	63.(2)	16.(2)	23.(2)	8.(2)

[a]The general thermal parameter expression used is $\exp[-2\pi^2(U_{11}h^2a^{*2} + U_{22}k^2b^{*2} + U_{33}l^2c^{*2} + 2U_{12}hka^*b^* + 2U_{13}hla^*c^* + 2U_{23}klb^*c^*)]$ with U's in $Å^2$. Estimated standard deviations are given in parentheses for the last significant digit.

Table II-9. Atom coordinates (x 10^4) for cations in $[\emptyset_4As]_2[Et_4N]Mo_4Cl_{12}\cdot 2\ CH_2Cl_2$[a]

atom	x	y	z	U(ave)[b]	mult[c]
As(1)	4085.2(7)	618.8(7)	6257.(1)	42.	
N(1)	0.0(0)	0.0(0)	5000.0(0)	53.	
C(1)	5492.(18)	5233.(17)	4299.(24)	75.	0.5
C(2)	541.(18)	580.(18)	5936.(22)	74.	0.5
C(3)	1297.(10)	9163.(11)	5226.(18)	122.	
C(4)	937.(9)	1203.(9)	5433.(13)	82.	
C(1A)	406.(15)	541.(13)	4523.(22)	51.	0.5
C(2A)	781.(18)	9475.(16)	5942.(27)	71.	0.5
Cl(s1)	6769.(3)	1584.(3)	1233.(4)	99.	
Cl(s2)	5037.(4)	1044.(3)	328.(5)	124.	
C(s)	5673.(10)	1852.(9)	524.(15)	89.	
C(11)	3463.(6)	970.(7)	7100.(10)	47.	
C(12)	2764.(9)	740.(8)	8330.(13)	76.	
C(13)	3377.(7)	1747.(7)	7204.(11)	48.	
C(14)	2655.(9)	1499.(9)	8402.(12)	73.	
C(15)	2954.(8)	2005.(8)	7837.(13)	66.	
C(16)	3170.(8)	469.(8)	7662.(12)	68.	
C(21)	5278.(7)	600.(6)	7209.(10)	43.	
C(22)	5750.(8)	-60.(7)	7387.(12)	52.	
C(23)	6603.(8)	-56.(8)	8134.(12)	66.	
C(24)	6979.(8)	588.(8)	8642.(12)	67.	
C(25)	6513.(9)	1250.(8)	8439.(12)	73.	
C(26)	5640.(7)	1256.(8)	7716.(11)	55.	
C(31)	3891.(7)	1280.(6)	5046.(10)	40.	
C(32)	3038.(7)	1422.(7)	4303.(11)	49.	
C(33)	2875.(8)	1888.(7)	3371.(12)	60.	
C(34)	3540.(9)	2193.(8)	3187.(13)	72.	
C(35)	4359.(9)	2067.(7)	3902.(13)	69.	
C(36)	4544.(7)	1608.(7)	4833.(11)	52.	
C(41)	1293.(7)	4638.(6)	4314.(10)	37.	
C(42)	1708.(7)	4511.(6)	5444.(11)	49.	
C(43)	1174.(8)	4038.(7)	3581.(11)	51.	
C(44)	1989.(8)	3799.(8)	5839.(12)	62.	
C(45)	1458.(8)	3304.(6)	3998.(12)	56.	
C(46)	1874.(8)	3185.(7)	5109.(12)	56.	

[a]Estimated standard deviations are given in parentheses for last significant digits.

[b]Average temperature factor ($Å^2$ x 10^3) is average of U_{11}, U_{22}, and U_{33}.

[c]Occupancy of atom (1.0 unless otherwise noted).

Table II-10. Anisotropic thermal parameters for cations in $[\emptyset_4As]_2[Et_4N]Mo_4Cl_{12}\cdot 2\ CH_2Cl_2$[a]

atom	U_{11}	U_{22}	U_{33}	U_{12}	U_{13}	U_{23}
As(1)	34.2(7)	39.2(7)	51.3(9)	0.9(5)	10.7(6)	3.7(6)
N(1)	54.(9)	76.(11)	30.(9)	-11.(8)	12.(7)	-13.(8)
C(1)	78.(21)	91.(22)	55.(20)	-17.(17)	32.(17)	13.(17)
C(2)	80.(21)	113.(26)	30.(17)	-25.(19)	7.(15)	-13.(17)
C(3)	65.(11)	133.(16)	168.(20)	14.(11)	55.(12)	-51.(15)
C(4)	76.(11)	91.(12)	80.(12)	-38.(9)	17.(9)	14.(10)
C(1A)	47.(15)	47.(16)	60.(18)	-16.(12)	10.(14)	7.(14)
C(2A)	70.(20)	56.(19)	87.(25)	-20.(15)	-19.(18)	8.(17)
Cl(s1)	116.(4)	91.(3)	90.(4)	-7.(3)	21.(3)	0.(3)
Cl(s2)	134.(4)	123.(4)	115.(5)	-43.(4)	-15.(4)	14.(4)
C(s)	88.(12)	74.(11)	105.(14)	-16.(9)	22.(11)	-10.(10)
C(11)	17.(6)	65.(9)	58.(9)	1.(6)	10.(6)	4.(7)
C(12)	62.(9)	80.(11)	87.(12)	-3.(8)	28.(9)	22.(9)
C(13)	31.(7)	49.(8)	65.(10)	9.(6)	13.(7)	4.(7)
C(14)	68.(10)	103.(12)	48.(10)	3.(9)	21.(8)	-16.(9)
C(15)	57.(9)	58.(9)	81.(11)	1.(7)	13.(8)	-13.(8)
C(16)	49.(8)	74.(10)	81.(11)	-15.(7)	37.(8)	-16.(8)
C(21)	42.(7)	45.(7)	42.(8)	4.(6)	16.(6)	-6.(6)
C(22)	36.(7)	56.(8)	65.(10)	5.(6)	2.(7)	1.(7)
C(23)	49.(8)	84.(11)	66.(10)	27.(8)	5.(8)	28.(9)
C(24)	47.(8)	94.(11)	61.(10)	-4.(8)	16.(7)	-5.(9)
C(25)	73.(10)	82.(11)	64.(11)	-25.(8)	21.(9)	-7.(9)
C(26)	37.(7)	75.(10)	55.(9)	1.(7)	15.(7)	-7.(8)
C(31)	36.(7)	46.(7)	37.(8)	5.(6)	5.(6)	0.(6)
C(32)	45.(7)	48.(8)	56.(9)	4.(6)	17.(7)	-2.(7)
C(33)	54.(9)	60.(9)	67.(10)	26.(7)	11.(8)	3.(8)
C(34)	68.(9)	64.(9)	84.(12)	21.(8)	35.(9)	25.(9)
C(35)	76.(10)	39.(8)	91.(12)	16.(7)	46.(9)	15.(8)
C(36)	45.(7)	44.(8)	67.(10)	6.(6)	27.(7)	2.(7)
C(41)	36.(7)	28.(6)	47.(8)	0.(5)	5.(6)	-3.(6)
C(42)	50.(8)	33.(7)	65.(9)	-1.(6)	19.(7)	-2.(7)
C(43)	51.(8)	53.(8)	50.(9)	-4.(6)	12.(7)	-1.(7)
C(44)	58.(9)	63.(9)	66.(10)	-11.(7)	16.(8)	12.(8)
C(45)	62.(9)	32.(7)	76.(10)	-11.(6)	24.(8)	-18.(7)
C(46)	45.(8)	44.(8)	81.(11)	-1.(6)	11.(7)	-1.(7)

[a]The general thermal parameter expression used is $\exp[-2\pi^2(U_{11}h^2a^{*2} + U_{22}k^2b^{*2} + U_{33}l^2c^{*2} + 2U_{12}hka^*b^* + 2U_{13}hla^*c^* + 2U_{23}klb^*c^*)]$ with U's in $Å^2$. Estimated standard deviations are given in parentheses for last significant figure.

Table II-11. Atom coordinates (x 10^4) for hydrogen atoms in $[\emptyset_4As]_2[Et_4N]Mo_4Cl_{12}\cdot 2CH_2Cl_2$[a]

atom	x	y	z
H(12)	2539.6(0)	358.3(0)	8752.7(0)
H(13)	3599.1(0)	2121.3(0)	6791.2(0)
H(14)	2356.8(0)	1696.2(0)	8874.0(0)
H(15)	2885.4(0)	2575.3(0)	7889.4(0)
H(16)	3225.9(0)	-97.6(0)	7604.1(0)
H(22)	5445.4(0)	-548.2(0)	7009.5(0)
H(23)	6955.4(0)	-534.8(0)	8305.8(0)
H(24)	7619.6(0)	596.7(0)	9185.9(0)
H(25)	6803.1(0)	1749.0(0)	8833.8(0)
H(26)	5288.5(0)	1738.1(0)	7559.3(0)
H(32)	2530.2(0)	1199.2(0)	4442.9(0)
H(33)	2245.8(0)	1980.3(0)	2829.3(0)
H(34)	3398.9(0)	2521.0(0)	2497.0(0)
H(35)	4850.9(0)	2295.9(0)	3748.8(0)
H(36)	5171.5(0)	1511.8(0)	5364.0(0)
H(42)	1813.6(0)	4940.9(0)	5986.9(0)
H(43)	861.9(0)	4120.3(0)	2736.4(0)
H(44)	2297.3(0)	3699.4(0)	6686.2(0)
H(45)	1364.2(0)	2873.9(0)	3465.3(0)
H(46)	2075.7(0)	2663.5(0)	5402.1(0)

[a]U(ave) is 57.0 for all hydrogen atoms.

One crystal was chosen with dimensions 0.18 x 0.23 x 0.68 mm. The crystal was indexed to a monoclinic cell with a = 18.3, b = 31.5, c = 11.25 Å, $\beta = 105.3^{\circ}$. Data collection and treatment proceeded as with the previous two sets. A phi scan showed a 12% variance in the intensity with rotation in phi, therefore an empirical absorption correction was carried out (14). Correction for Lorentz and polarization effects were applied. Relevant crystal data are tabulated in Table II-12.

MULTAN80 (7) was used to find the position of three unique molybdenum atoms in the asymmetric unit. The fourth molybdenum atom and twelve chlorine atoms were found by inspection of electron density difference maps based on atom positions determined from least squares refinements. The positions of nitrogen and carbon atoms of the organic cations were similarly found. Additional electron density was observed in the difference map at this stage of refinement and indicated that solvent molecules were present in the unit cell. Placement of two carbons and two chlorines constituting a dichloroethane molecule in these positions cleared the residual density from the difference map. Refinement, allowing the multipliers for atoms of this molecule to vary led to an occupation of 0.7 solvent molecules per asymmetric unit.

X-ray scattering by electrons on the hydrogen atoms

Table II-12. Crystal data for $[Pr_4N]_3Mo_4Cl_{12}\cdot 0.7\ C_2H_4Cl_2$

formula	$[Pr_4N]_3Mo_4Cl_{12}\cdot 0.7\ C_2H_4Cl_2$
molecular weight	1437.69
space group	$P2_1/a$
a, Å	18.354(3)
b, Å	31.571(4)
c, Å	11.254(2)
β, deg	105.275(20)
V, $Å^3$	6291.(2)
Z	4
d calc. g/cm^3	1.444
crystal shape	columns
crystal size	0.18 x 0.23 x 0.68
μ, cm^{-1}	12.92
instrument	Syntex P1 diffractometer
radiation	Mo Kα, monochromated wavelength = 0.71069 Å
# orientation refl	14
# lattice refl.	16
scan method	omega
data collection range	2.0-50.0 in 2 theta
# refl. collected	12,248
# $F_o > 3\sigma(F_o)$	5359
# unique data	4966, R=0.0208
# parameters refined	707
R^a	0.062
R_w^b	0.081
quality of fit, Q^c	1.741

[a] $R=\Sigma||F_o|-|F_c||/\Sigma|F_o|$.

[b] $R_w=[\Sigma w(|F_o|-|F_c|)^2/\Sigma|w|F_o|^2]^{1/2}$, $w=1/\sigma(F_o)^2$.

[c] $Q=[\Sigma w(|F_o|-|F_c|)^2/N(\text{observations})-N(\text{parameters})]^{1/2}$.

represented a significant portion of the scattering density of the molecule. Therefore, positions were calculated for hydrogen atoms based on the coordinates of the carbon atoms (8). These hydrogen atoms were input with relatively large isotropic temperature factors and neither positional or temperature factors were allowed to vary.

Final convergence factors were R=0.062 and R_w=0.081. The final electron density map was featureless with no peak greater than 0.4 e/$Å^3$.

The stoichiometry of the molecule is that of the asymmetric unit since no symmetry element is associated with the planar cluster unit. The atomic positions for the atoms in $[Pr_4N]_3Mo_4Cl_{12}\cdot C_2H_4Cl_2$ are listed in Tables II-13, II-15, and II-17. The anisotropic thermal parameters for non-hydrogen atoms are listed in Tables II-14, and II-16. Hydrogen positional parameters are listed in Table II-17.

Structure refinement of $[Ø_4P]_3Mo_4Cl_{12}\cdot 0.5\ Ø_4PI$

Several suitable blade-like crystals were selected from a typical reaction mixture. The crystals were mounted as previously described for $[Et_4N]_3Mo_4Cl_{12}$. Indexing, data collection, and calculation of lattice parameters also proceeded as previously described. An empirical absorption correction was deemed necessary and performed on the data (14). Corrections for Lorentz and polarization effects were

Table II-13. Atom coordinates (x 10^4) and average temperature factors for $[Pr_4N]_3Mo_4Cl_{12}\cdot 0.7\ C_2H_4Cl_2$[a]

Atom	x	y	z	U(ave)[b]
Mo(1)	7188.7(8)	1435.0(5)	7265.(1)	38.
Mo(2)	7604.8(8)	441.4(5)	7423.(1)	38.
Mo(3)	8339.5(8)	976.0(5)	6899.(1)	41.
Mo(4)	6462.1(8)	902.8(5)	7812.(1)	38.
Cl(1)	8487.(2)	1508.(1)	8518.(4)	51.
Cl(2)	6748.(2)	1525.(1)	9154.(4)	52.
Cl(3)	7509.(3)	1397.(1)	5295.(4)	53.
Cl(4)	8027.(3)	372.(1)	5499.(4)	55.
Cl(5)	5836.(2)	1378.(1)	6122.(4)	46.
Cl(6)	8971.(2)	478.(2)	8503.(4)	54.
Cl(7)	7326.(2)	500.(1)	9426.(4)	49.
Cl(8)	6289.(2)	350.(1)	6270.(4)	45.
Cl(9)	2278.(3)	338.(1)	2398.(5)	59.
Cl(10)	5278.(3)	728.(2)	8452.(5)	69.
Cl(11)	9530.(3)	1159.(2)	6305.(5)	70.
Cl(12)	7063.(3)	2233.(1)	7072.(5)	59.

[a]Estimated standard deviations are given in parentheses for last significant digit.

[b]U(ave) is average of U11, U22, and U33 ($Å^2$ x 10^3).

Table II-14. Anisotropic thermal parameters (x 10^4) for $[Pr_4N]_3Mo_4Cl_{12}\cdot 0.7\ C_2H_4Cl_2$[a]

atom	U_{11}	U_{22}	U_{33}	U_{12}	U_{13}	U_{23}
Mo(1)	36.2(8)	38.5(9)	38.5(9)	-1.2(7)	11.9(7)	0.6(7)
Mo(2)	34.4(8)	41.5(9)	37.4(9)	0.0(7)	9.4(7)	2.4(7)
Mo(3)	39.2(8)	42.(1)	41.3(9)	1.7(7)	13.5(7)	2.7(8)
Mo(4)	37.4(8)	37.4(9)	37.9(9)	-0.9(7)	10.7(7)	0.0(7)
Cl(1)	44.(2)	56.(3)	52.(3)	-8.(2)	8.(2)	-9.(2)
Cl(2)	58.(3)	49.(3)	47.(3)	-4.(2)	28.(2)	-12.(2)
Cl(3)	62.(3)	55.(3)	44.(3)	11.(2)	23.(2)	12.(2)
Cl(4)	61.(3)	53.(3)	50.(3)	1.(2)	18.(2)	-7.(2)
Cl(5)	41.(2)	46.(3)	52.(3)	6.(2)	8.(2)	2.(2)
Cl(6)	39.(2)	58.(3)	64.(3)	6.(2)	5.(2)	10.(3)
Cl(7)	59.(3)	50.(3)	39.(3)	2.(2)	11.(2)	10.(2)
Cl(8)	44.(2)	45.(3)	45.(3)	0.(2)	6.(2)	-7.(2)
Cl(9)	53.(3)	47.(3)	77.(4)	8.(2)	21.(3)	6.(3)
Cl(10)	59.(3)	79.(4)	69.(4)	-14.(3)	29.(3)	-3.(3)
Cl(11)	51.(3)	82.(4)	76.(4)	-1.(3)	31.(3)	2.(3)
Cl(12)	63.(3)	43.(3)	72.(4)	-3.(2)	24.(3)	5.(3)

[a]The general thermal parameter expression used is $\exp[-2\pi^2(U_{11}h^2a^{*2} + U_{22}k^2b^{*2} + U_{33}l^2c^{*2} + 2U_{12}hka^*b^* + 2U_{13}hla^*c^* + 2U_{23}klb^*c^*)]$ with U's in $Å^2$. Estimated standard deviations are given in parentheses for last significant figure.

Table II-15. Atom coordinates (x 10^3) and average temperature factors for cations in $[Pr_4N]_3Mo_4Cl_{12}\cdot 0.7\ C_2H_4Cl_2$[a]

Atom	x	y	z	U(ave)[b]
N(1)	989.2(8)	7.62(5)	256.5(1)	65.
C(111)	917.0(1)	103.8(6)	202.6(2)	56.
C(112)	863.8(1)	107.2(8)	287.1(2)	89.
C(113)	798.0(1)	134.1(1)	220.8(3)	132.
C(121)	39.7(1)	102.9(7)	367.4(2)	73.
C(122)	113.2(1)	80.0(8)	424.7(2)	89.
C(123)	158.2(1)	109.6(9)	524.9(2)	107.
C(131)	970.5(1)	31.8(6)	304.2(2)	65.
C(132)	916.8(1)	8.0(7)	205.3(2)	82.
C(133)	116.8(2)	25.2(7)	715.9(3)	159.
C(141)	31.3(1)	69.8(6)	152.0(2)	69.
C(142)	60.0(1)	108.3(7)	106.8(2)	78.
C(143)	89.3(1)	97.0(7)	-2.1(2)	85.
N(2)	493.0(7)	8.18(4)	221.5(1)	45.
C(211)	532.4(1)	124.6(6)	246.7(2)	61.
C(212)	571.1(1)	138.3(7)	146.9(2)	84.
C(213)	603.77(0)	18.20(7)	180.3(2)	86.
C(221)	543.4(9)	4.68(5)	196.8(2)	46.
C(222)	615.0(1)	39.2(7)	294.7(2)	73.
C(223)	660.5(1)	4.2(8)	250.9(2)	97.
C(231)	425.5(1)	87.4(6)	107.5(2)	54.
C(232)	375.7(1)	47.8(6)	79.6(2)	61.
C(233)	300.3(1)	62.9(7)	967.2(2)	81.
C(241)	468.0(1)	69.7(6)	336.5(2)	59.
C(242)	410.3(1)	98.7(6)	368.8(2)	71.
C(243)	390.0(1)	81.3(7)	482.3(2)	77.
N(3)	935.5(8)	25.97(5)	631.9(2)	62.
C(311)	955.3(1)	229.8(6)	739.2(2)	80.
C(312)	538.3(1)	251.9(9)	831.0(2)	114.
C(313)	50.5(2)	210.0(1)	935.6(3)	202.
C(321)	495.5(1)	236.3(6)	559.3(2)	69.
C(322)	7.5(1)	220.8(7)	497.5(3)	116.
C(323)	61.2(1)	230.6(8)	415.4(2)	103.
C(331)	429.2(1)	194.9(6)	676.6(2)	80.

[a]Estimated standard deviations are given in parentheses for last significant figure.

[b]U(ave) is average of U_{11}, U_{22}, and U_{33} ($Å^2$ x 10^4).

Table II-15. (Continued)

atom	x	y	z	U(ave)
C(332)	374.5(1)	190.2(7)	753.3(2)	101.
C(333)	358.8(2)	145.0(8)	782.5(3)	139.
C(341)	860.9(1)	240.6(7)	555.4(2)	73.
C(342)	327.9(1)	230.1(7)	447.3(2)	84.
C(343)	74.81(1)	248.7(1)	368.1(3)	136.
Cl(1S)	268.5(6)	18.19(3)	101.4(1)	125.
Cl(2S)	399.7(6)	25.33(5)	130.4(1)	159.
C(S1)	310.6(2)	256.2(9)	36.1(3)	85.
C(S2)	268.1(2)	224.1(2)	7.7(3)	137.

Table II-16. Anisotropic thermal parameters (x 10^3) for cations in $[Pr_4N]_3Mo_4Cl_{12}\cdot 0.7\ C_2H_4Cl_2$[a]

atom	U_{11}	U_{22}	U_{33}	U_{12}	U_{13}	U_{23}
N(1)	58.(1)	81.(1)	56.(1)	15.(9)	27.(9)	-8.(9)
C(111)	65.(1)	55.(1)	48.(1)	19.(1)	7.(1)	8.(1)
C(112)	66.(1)	125.(2)	75.(2)	18.(1)	29.(1)	-6.(2)
C(113)	71.(1)	151.(3)	175.(4)	34.(2)	43.(2)	-18.(3)
C121)	66.(1)	105.(2)	46.(1)	-1.(1)	-3.(1)	-32.(1)
C(122)	66.(2)	137.(2)	64.(1)	25.(2)	4.(1)	-18.(2)
C(123)	70.(2)	144.(2)	108.(2)	-11.(2)	-13.(2)	0.(2)
C(131)	69.(1)	60.(1)	64.(1)	10.(1)	16.(1)	21.(1)
C(132)	119.(2)	60.(2)	68.(2)	-25.(1)	-2.(2)	17.(1)
C(133)	241.(3)	10.(1)	226.(3)	46.(2)	68.(3)	27.(2)
C(141)	65.(1)	72.(2)	69.(2)	0.(1)	37.(1)	-15.(1)
C(142)	92.(2)	72.(2)	72.(2)	3.(1)	44.(1)	16.(1)
C(143)	72.(1)	104.(2)	79.(2)	13.(1)	32.(1)	8.(2)

[a]The general thermal parameter expression used is $\exp[-2\pi^2(U_{11}h^2a^{*2} + U_{22}k^2b^{*2} + U_{33}l^2c^{*2} + 2U_{12}hka^*b^* + 2U_{13}hla^*c^* + 2U_{23}klb^*c^*)]$ with U's in $Å^2$. Estimated standard deviations are given in parentheses for last significant figure.

Table II-16. (Continued)

atom	U_{11}	U_{22}	U_{33}	U_{12}	U_{13}	U_{23}
N(2)	50.(9)	53.(1)	33.(8	-6.(8)	8.(7)	-6.(7)
C(211)	59.(1)	63.(1)	60.(1)	-25.(1)	14.(1)	-7.(1)
C(212)	103.(2)	86.(2)	63.(1)	-48.(1)	38.(1)	-25.(1)
C(213)	89.(2)	73.(2)	97.(2)	-30.(1)	54.(1)	-5.(1)
C(221)	58.(1)	42.(1)	37.(1)	-1.(9)	13.(9)	-14.(9)
C(222)	66.(1)	107.(2)	47.(1)	17.(1)	-17.(1)	-19.(1)
C(223)	68.(1)	128.(2)	94.(2)	52.(2)	5.(1)	-23.(2)
C(231)	63.(1)	48.(1)	52.(1)	-4.(1)	25.(1)	8.(1)
C(232)	71.(1)	47.(1)	66.(1)	-4.(1)	-16.(1)	8.(1)
C(233)	52.(1)	73.(2)	118.(2)	3.(1)	-18.(1)	9.(1)
C(241)	52.(1)	75.(2)	49.(1)	-17.(1)	25.(9)	-9.(1)
C(242)	77.(1)	84.(2)	51.(1)	-21.(1)	37.(1)	2.(1)
C(243)	80.(1)	90.(2)	60.(1)	-30.(1)	35.(1)	-16.(1)
N(3)	71.(1)	44.(1)	72.(1)	-5.(8)	35.(9)	11.(9)
C(311)	112.(2)	48.(1)	79.(2)	12.(1)	22.(1)	11.(1)
C(312)	109.(2)	132.(2)	102.(2)	26.(2)	10.(2)	-24.(2)
C(313)	257.(4)	219.(4)	129.(3)	-37.(3)	-11.(3)	120.(3)
C(231)	82.(1)	46.(1)	79.(2)	16.(1)	54.(1)	14.(1)
C(322)	10.(2)	50.(1)	188.(3)	-11.(1)	106.(2)	-26.(2)
C(323)	97.(2)	123.(2)	88.(2)	-9.(2)	57.(2)	-12.(2)
C(331)	106.(2)	43.(1)	90.(2)	4.(1)	70.(1)	10.(1)
C(332)	134.(2)	55.(2)	115.(2)	8.(2)	66.(2)	-11.(1)
C(333)	209.(3)	69.(2)	138.(3)	-40.(2)	81.(2)	17.(2)
C(341)	56.(1)	81.(2)	81.(2)	-30.(1)	12.(1)	-18.(1)
C(342)	86.(2)	76.(2)	89.(2)	32.(1)	-5.(2)	3.(1)
C(343)	87.(2)	212.(4)	110.(2)	-20.(2)	21.(2)	35.(2)
Cl(1S)	149.(9)	76.(7)	149.(1)	19.(6)	36.(8)	-10.(7)
Cl(2S)	75.(7	231.(1)	171.(1)	11.(8)	15.(7)	72.(1)
C(S1)	127.(3)	58.(2)	71.(2)	46.(2)	-28.(2)	8.(2)
C(S2)	73.(2)	255.(5)	84.(3)	-5.(3)	17.(2)	57.(3)

Table II-17. Hydrogen atom positions (x 10^5) in $[Pr_4N]_3Mo_4Cl_{12}\cdot 0.7\ C_2H_4Cl_2$ [a,b]

atom	x	y	z	atom	x	y	z
H111	88527	9015	11666	H133A	12076	1909	81840
H111A	93218	13472	18318	H133B	6591	1326	67040
H112	89781	11041	38227	H133C	9418	62	75015
H112A	83347	7764	28730	H133D	11930	5036	80762
H121	-702	8870	30161	H133E	6447	4426	65965
H121A	1780	12832	40899	H143	13738	11561	-406
H122	14413	7327	36215	H143A	10614	6469	223
H122A	10281	5082	46703	H143B	4791	10177	-8598
H131	94507	3597	37705	H143C	5685	7248	-5457
H131A	1932	1373	33352	H143D	14635	8622	2744
H132	93493	-2323	19908	H143E	8824	12338	-6069
H132A	90868	2307	11962	H213	55914	20424	18093
H141	1218	6987	23358	H213A	64124	18253	26930
H141A	510	4859	8858	H213B	63252	19401	11727
H142	10367	12158	17794	H213C	66278	18296	19724
H142A	1617	13098	8046	H213D	58950	19315	26116
H211	57233	12508	33472	H213E	58062	20467	10910
H211A	49088	14920	25245	H223	71535	1588	24878
H212	53291	13901	5770	H223A	66775	-2232	30653
H212A	61576	11731	14365	H223B	63237	-432	15880
H221	55785	5316	11157	H223C	62826	-2304	22715
H221A	51263	1726	18172	H223D	71123	-289	31733
H222	60412	2969	37843	H223E	67598	1516	16963
H222A	64780	6778	31298	H233	25510	8171	97562
H231	44505	9436	2853	H233A	35035	7474	3584
H231A	39065	11295	11998	H233B	29156	3163	412

[a]Hydrogen atom positions were not varied.

[b]Isotropic beta was 6.0 for all hydrogen atoms and was not varied.

Table II-17. (Continued)

atom	x	y	z	atom	x	y	z
H232	40269	1976	5897	H233C	34297	4372	3560
H232A	32392	5064	592	H233D	30635	9377	574
H241	51386	6916	41413	H233E	24770	5060	97504
H241A	44282	3884	32439	H243	33492	8929	48600
H242	35915	9921	29279	H243A	42832	9415	56394
H242A	43020	12976	38159	H243B	39591	4799	48800
H311	293	23962	81385	H243C	43789	6505	53937
H311A	97115	19809	71351	H243D	37676	10629	53721
H312	51769	27551	75908	H243E	34451	6009	46135
H312A	55452	27303	91571	H313	2075	24019	93492
H321	49908	20387	57036	H313A	5178	19532	1880
H321A	48188	24200	45781	H313B	1638	19218	86213
H322	-2355	24504	52862	H313C	3852	17827	94236
H322A	-2265	19217	49396	H313D	4289	22628	1516
H331	42206	16235	64287	H313E	749	22314	85841
H331A	39482	21341	60152	H323A	11288	21392	45127
H332	31899	20616	70646	H323B	3766	22004	32455
H332A	39332	20892	83583	H323C	7608	20167	37884
H341	87385	20821	56655	H323D	11125	24453	46941
H341A	86251	25027	46685	H323E	3603	25065	34268
H342	29083	25633	45585	H333	30195	14140	78129
H342A	29195	20274	43127	H333A	39382	13817	86810
H113	81539	16579	22075	H333B	37166	12683	71371
H113A	75471	13186	26564	H333C	40969	12954	79427
H113B	77791	12347	12957	H333D	33986	14411	86160
H113C	74992	11496	19007	H333E	31787	13275	70724
H113D	78751	15732	28101	H343	76678	28060	37181
H113E	81058	14883	14489	H343A	78877	23295	44566
H123	12374	13873	52925	H343B	75413	23445	28857
H123A	16944	9728	61612	H343C	77300	21807	36555
H123B	20812	12094	50983	H343D	78566	26422	44879
H123C	21050	9926	57411	H343E	75102	26572	29170
H123D	12613	11698	59373	H123E	16467	14071	48737

also made. Information relevant to data collection, treatment and structure solution is found in Table II-18.

The structure was solved using MULTAN80 (7). Initial positions for two unique molybdenum atoms were determined from the MULTAN80 output, as were positions of four of the six unique chlorine atoms in the cluster unit. Positions of the remaining atoms in the asymmetric unit were determined from inspection of electron density maps.

In addition to the cluster atoms, an iodine atom was found in the unit cell. This iodine atom is further than 3.5 A from its nearest neighbor and thus is considered to be an ionic iodine. This site in the lattice is occupied by iodine one half of the time.

There are two sites which are occupied by tetraphenylphosphonium cations in the unit cell. Both are fully occupied, which, when considering the symmetry of the cell is equivalent to eight cations per unit cell. Symmetry operations on the two unique molybdenum atoms generate two planar cluster units. The two tri-negatively charged clusters require six cations to balance their charge. The remaining cations provide electrical neutrality for the ionic iodine in the lattice.

Two small peaks (~3 $e/\AA^3$) of electron density remain unaccounted for in the difference map of the unit cell. To date, these remain unexplained, but are considered to be

Table II-18. Crystal data for $[\emptyset_4P]_3Mo_4Cl_{12}\cdot 0.5\ \emptyset_4PI$

formula	$[\emptyset_4P]_3Mo_4Cl_{12}\cdot 0.5\ \emptyset_4PI$
molecular weight	2292.90
space group	$P2_1/a$
a, Å	17.554(14)
b, Å	15.853(7)
c, Å	18.111(12)
β, deg	102.915(54)
V, $Å^3$	4913(6)
Z	2
d calc., g/cm	2.47
crystal shape	platelets
crystal size	0.04 x 0.08 x 0.2
μ, cm^{-1}	17.84
diffractometer	Datex
radiation	Mo Kα, wavelength = 0.71069
# orientation refl.	12
# latt refl.	15
scan method	omega
data collection range	3.0-50.0 deg in 2 theta
# refl. collected	19,995
# $F_o > 3\sigma(F_o)$	4486
# unique data	2519, R = 0.0354
# parameters refined	345
R^a	0.091
$R_w{}^b$	0.110
quality of fit, Q^c	2.91

[a] $R=\Sigma||F_o|-|F_c||/\Sigma|F_o|$.

[b] $R_w=[\Sigma w(|F_o|-|F_c|)^2/\Sigma|w|F_o|^2]^{1/2}$, $w=1/\sigma(F_o)^2$.

[c] $Q=[\Sigma w(|F_o|-|F_c|)^2/N(\text{observations})-N(\text{parameters})]^{1/2}$.

sites partially occupied by solvent molecules. They are located near the sites that are left vacant by the partial iodine occupation.

Carbon atoms were not refined anisotropically because of the poor data/parameter ratio that would result with such a refinement. For the same reason, hydrogen atoms were not included in the refinement. Final convergence factors were R=0.091 and R_w=0.110. Positional and thermal parameters for the atoms are listed in Tables II-19, II-20, and II-21.

Extended Hückel Calculations

Extended Hückel calculations were performed on the $Mo_4Cl_{12}^{n-}$ cluster unit using a program obtained from E. R. Davidson at the University of Washington. Description and use of the program has been previously described (16). The program uses several parameters to define atomic orbitals of constituent atoms and performs iterative calculations to charge self-consistency. Up to three mirror planes of symmetry can be used to simplify input. The program output includes orbital energies, atomic orbital coefficients, and symmetry (with respect to the mirror planes) for the atomic orbitals comprising the resultant molecular orbitals. Symmetry of the resultant molecular orbitals was determined by inspection of the constituent atomic orbitals.

Valence orbital ionization energies for Mo and Cl were

Table II-19. Atom coordinates (x 10^4) and average temperature factors for $[\emptyset_4P]_3Mo_4Cl_{12}\cdot 0.5\ \emptyset_4PI$[a]

Atom	x	y	z	U(ave)[b]
Mo(1)	-761.(1)	286.(1)	-820.(1)	59.
Mo(2)	-465.(1)	286.(1)	700.(1)	54.
Cl(1)	-697.(3)	1556.(3)	-63.(3)	58.
Cl(2)	130.(3)	978.(3)	-1512.(3)	66.
Cl(3t)	-1279.(3)	810.(3)	1580.(3)	71.
Cl(4)	-645.(3)	-1020.(3)	-1517.(3)	62.
Cl(5)	-1532.(3)	-486.(3)	-94.(3)	64.
Cl(6t)	-1924.(3)	724.(4)	-1827.(3)	83.
I	5866.(3)	988.(4)	4265.(3)	178.
P(2)	5205.(3)	835.(3)	8505.(3)	53.
P(1)	8815.(3)	1284.(4)	4025.(3)	65.

[a]Estimated standard deviations are given in parentheses for last significant figure.

[b]U(ave) is average of U_{11}, U_{22}, and U_{33} ($Å^2$ x 10^3).

Table II-20. Anisotropic thermal parameters (x 10^4) for $[\emptyset_4P]_3Mo_4Cl_{12}\cdot 0.5\ \emptyset_4PI$[a]

atom	U_{11}	U_{22}	U_{33}	U_{12}	U_{13}	U_{23}
Mo(1)	62.(1)	56.(1)	60.(1)	-7.(1)	28.3(9)	-2.(1)
Mo(2)	48.(1)	56.(1)	59.(1)	-9.(1)	6.7(8)	7.(1)
Cl(1)	68.(3)	49.(3)	57.(3)	-6.(3)	22.(3)	-2.(3)
Cl(2)	74.(4)	61.(4)	62.(4)	-4.(3)	29.(3)	8.(3)
Cl(3t)	62.(4)	78.(4)	71.(4)	-11.(3)	20.(3)	3.(3)
Cl(4)	57.(3)	75.(4)	55.(4)	-4.(3)	15.(3)	-13.(3)
Cl(5)	56.(3)	83.(4)	54.(4)	-19.(3)	17.(3)	-7.(3)
Cl(6t)	70.(4)	104.(5)	74.(4)	5.(4)	19.(3)	-3.(4)
I	118.(4)	278.(7)	138.(4)	12.(4)	35.(3)	-63.(4)
P(2)	50.(3)	53.(4)	55.(4)	-1.(3)	19.(3)	-1.(3)
P(1)	61.(4)	74.(4)	60.(4)	6.(3)	15.(3)	9.(4)

[a]The general thermal parameter expression used is $\exp[-2\pi^2(U_{11}h^2a^{*2} + U_{22}k^2b^{*2} + U_{33}l^2c^{*2} + 2U_{12}hka^*b^* + 2U_{13}hla^*c^* + 2U_{23}klb^*c^*)]$ with U's in $Å^2$. Estimated standard deviations are given in parentheses for last significant figure.

Table II-21. Atom coordinates (x 10^4) and average temperature factors for isotropically refined atoms in $[\emptyset_4P]_3Mo_4Cl_{12}\cdot 0.5\ \emptyset_4PI$[a]

atom	x	y	z	U(ave)[b]
C(111)	8490.(11)	245.(14)	3636.(12)	64.(6)
C(112)	1090.(11)	278.(14)	6711.(12)	62.(6)
C(113)	1389.(14)	1061.(15)	6979.(14)	70.(8)
C(114)	2156.(12)	1276.(14)	6969.(13)	84.(7)
C(115)	2641.(13)	757.(14)	6619.(13)	101.(8)
C(116)	2303.(13)	-67.(15)	6303.(14)	115.(9)
C(121)	8370.(11)	2135.(12)	3419.(11)	50.(6)
C(122)	7675.(13)	1973.(14)	2883.(13)	79.(7)
C(123)	2323.(13)	2309.(14)	2469.(13)	86.(8)
C(124)	2691.(13)	1520.(15)	2562.(14)	79.(8)
C(125)	3335.(16)	1378.(17)	3048.(16)	109.(10)
C(126)	3709.(15)	2080.(16)	3510.(15)	102.(9)
C(131)	8589.(11)	1406.(13)	4950.(11)	52.(6)
C(132)	8819.(14)	770.(15)	5497.(14)	89.(8)
C(133)	8680.(14)	876.(15)	6254.(13)	66.(8)
C(134)	8245.(13)	1563.(14)	6383.(13)	71.(7)
C(135)	7970.(14)	2142.(15)	5799.(14)	92.(8)
C(136)	8154.(14)	2091.(15)	5086.(14)	72.(8)
C(141)	9850.(11)	1347.(12)	4095.(11)	54.(6)
C(142)	129.(11)	1350.(12)	3399.(11)	52.(6)
C(143)	925.(12)	1403.(14)	3477.(12)	55.(7)
C(144)	1449.(12)	1481.(13)	4176.(12)	59.(6)
C(145)	1174.(12)	1495.(14)	4845.(12)	76.(7)
C(146)	367.(11)	1435.(12)	4814.(11)	64.(6)
C(211)	4215.(10)	1017.(11)	8598.(10)	38.(5)
C(212)	3942.(10)	1865.(11)	8587.(10)	52.(5)
C(213)	3177.(12)	1996.(13)	8699.(12)	59.(6)
C(214)	2734.(12)	1315.(14)	8857.(12)	56.(7)
C(215)	2996.(12)	506.(12)	8851.(11)	50.(6)
C(216)	3774.(11)	318.(14)	8731.(11)	67.(6)
C(221)	5361.(10)	1257.(11)	7627.(10)	31.(5)
C(222)	6018.(12)	942.(13)	7395.(12)	78.(7)
C(223)	6182.(13)	1276.(15)	6685.(14)	96.(8)

[a]Estimated standard deviations are given in parentheses for last significant figure.

[b]U(ave) is average of U_{11}, U_{22}, and U_{33} ($\AA^2$ x 10^3).

Table II-21. (Continued)

atom	x	y	z	U(ave)
C(224)	5677.(14)	1791.(15)	6266.(14)	89.(8)
C(225)	5002.(15)	2075.(16)	6469.(15)	86.(9)
C(226)	4837.(15)	1750.(15)	7155.(14)	88.(9)
C(231)	5838.(11)	1323.(12)	9257.(11)	57.(6)
C(232)	6664.(13)	1280.(14)	9293.(13)	107.(8)
C(233)	7216.(13)	1641.(15)	9945.(14)	110.(9)
C(234)	6915.(13)	2040.(14)	512.(13)	67.(8)
C(235)	6153.(13)	2041.(14)	488.(13)	67.(7)
C(236)	5594.(13)	1697.(14)	9879.(13)	85.(8)
C(241)	4629.(10)	283.(13)	1508.(10)	52.(5)
C(242)	5019.(12)	739.(13)	2123.(12)	69.(7)
C(243)	4884.(14)	1664.(15)	2138.(14)	83.(8)
C(244)	4369.(13)	1999.(14)	1559.(13)	77.(7)
C(245)	3944.(13)	1558.(15)	922.(13)	100.(8)
C(246)	4061.(11)	641.(12)	886.(12)	83.(7)

calculated from spectral data (17). Zeta exponents (z) for the Slater type orbitals ($\Psi = R(r)e^{-zr}\psi(\theta,\phi)$) were calculated by the method of Cusachs and Corrington (18). The parameters used are listed in Table II-22.

Several calculations were performed on $Mo_4Cl_{12}^{n-}$ of differing geometries for comparative purposes. Initially, a calculation to determine the energy levels of an ideal square cluster was completed. For this cluster, a metal-metal distance of 2.504 Å was used, calculated from Pauling's bond length-bond order equation for a bond order of 1.5 based on a Mo-Mo single bond distance (from the hexanuclear cluster $Mo_6Cl_{14}^{2-}$) of 2.61 Å (19). Different Mo-Cl distances were used for terminal and bridging chlorines; however, all distances of a particular type in a calculation were identical.

A series of calculations were then carried out where the square cluster was distorted in a stepwise fashion, lengthening one side of the cluster while shortening the adjacent edge until a cluster with the Mo-Mo distances observed for $[\emptyset_4As]_2[Et_4N]Mo_4Cl_{12}\cdot 2\ CH_2Cl_2$ was used. In these calculations, the same Mo-Cl distances were used. A final calculation was carried out on a cluster where the Mo-Cl bond distances used were those actually observed from the structure refinement. The cluster distances and final electronic charges are listed in Table II-23.

Table II-22. Parameters for extended Hückel calculations[a]

Atom	Orbital	VOIE (eV)[b]	Zeta[c]
Mo	5s (0)	-7.00	1.46
	(+1)	-12.4	
	5p (0)	-4.26	1.46
	(+1)	-8.21	
	4d (0)	-7.99	2.53
	(+1)	-13.35	
Cl	3s (0)	-25.28	2.23
	(-1)	-17.00	
	3p (0)	-13.72	1.86
	(-1)	-3.74	

[a]Wolfsberg-Helmholtz interaction constant was 1.89 for all calculations.

[b]Valence orbital ionization energy.

[c]Calculated from data in Table 4 of reference 18.

Table II-23. Cluster geometries for extended Hückel calculations

Bond distances[a]	square	1st perturb	2nd perturb	3rd perturb	real distances
d(Mo-Mo)	2.504	2.454 2.554	2.404 2.604	2.354 2.654	2.354 2.656
$d(Mo-Cl)_{bdg}$	2.430	2.430	2.430	2.430	2.464[b] 2.436[c]
$d(Mo-Cl)_{term}$	2.518	2.518	2.518	2.518	2.518
Δ[d]	0.0	0.05	0.10	0.15	0.15
Calculated electronic charges					
Mo	0.257	0.259	0.260	0.260	0.265
Cl[b]	-0.198	-0.194	-0.196	-0.197	-0.208
Cl[c]	-0.183	-0.185	-0.183	-0.183	-0.176
Cl[e]	-0.376	-0.379	-0.382	-0.381	-0.381
$-E_{tot}$[f]	1533.27	1533.29	1533.27	1533.20	1532.43

[a]Bond distances in angstroms.

[b]Cl bridging short edge.

[c]Cl bridging long edge.

[d]Difference between metal-metal bond lengths when square and when rectangularly distorted.

[e]Cl terminal

[f]eV.

RESULTS AND DISCUSSION

Syntheses

The oxidation/reduction chemistry of cluster compounds and multiply bonded metal complexes has proven to be an interesting and informative area of study. Much has been learned about bonding and effects on the structure of clusters by addition and removal of electrons from orbitals located primarily on the metal atoms (20). Our initiation into this chemistry with the $Mo_4Cl_{12}^{4-}$ cluster compounds was by the reaction shown in eq. 1.

$$2\ \emptyset_4AsCl + [Et_4N]_4Mo_4Cl_{12} + HCl \longrightarrow \qquad 1$$

$$[\emptyset_4As]_2[Et_4N]Mo_4Cl_{12} + 3\ Et_4NCl + 1/2\ H_2$$

In attempting to provide the cluster with more solubility by exchanging cations, an unforeseen one electron oxidation of the cluster occurred, caused by the hydrogen chloride in the lattice of the solid tetraphenylarsonium chloride. The stoichiometry of the compound was determined by X-ray structure analysis on the plate-like crystals from the reaction mixture. However, so far it has not been possible to duplicate the results. The main products of subsequent reactions were the needle-like crystals which were also found in the initial reaction mixture and which

did not diffract X-rays. Analytical data on these reaction products showed that the composition was intermediate between $[\emptyset_4As]_2[Et_4N]Mo_4Cl_{12}$ and $[\emptyset_4As][Et_4N]Mo_4Cl_{12}$ indicating that the degree of oxidation and cation substitution may be variable in these clusters compounds.

The actual amount of HCl in the starting material also posed difficulties in reproducing the initial results. Attempts to completely remove the HCl from the tetraphenylarsonium chloride were unsuccessful, although it was found that approximately half of the HCl could be removed.

In light of these difficulties we attempted the oxidation of the cluster compounds under conditions where control of the reaction stoichiometry was permitted using molecular iodine, eq. 2.

$$[Et_4N]_4Mo_4Cl_{12} + 1/2\ I_2 \longrightarrow [Et_4N]_3Mo_4Cl_{12} + Et_4NI \qquad 2$$

The product of these reactions was an insoluble green powder. It can be conveniently prepared by slowly dripping a solution of known I_2 titer into a suspension of the purple $[Et_4N]_4Mo_4Cl_{12}$ in DCE. The compound is sufficiently insoluble in DCE that a solution of $[Et_4N]_3Mo_4Cl_{12}$ is essentially colorless. However, the extended extraction of a reaction mixture, where a slightly insufficient amount of

I_2 had been added to cause complete oxidation of the $[Et_4N]_4Mo_4Cl_{12}$, produced a number of small crystals of two types. The first type, in the shape of octahedra, was identified as crystals of $[Et_4N]_3Mo_4Cl_{12}$, where the structure determination showed that the metal atoms form a cluster unit with a 'butterfly geometry' (Figure II-3).

The remaining crystals were plates with cell constants of a = 13.7, b = 7.63, c = 12.18 Å in an orthorhombic space group, although crystals of sufficient quality for an x-ray structure determination were not found. These crystals are the same as those isolated from an extended extraction of $[Et_4N]_4Mo_4Cl_{12}$ using DCM, based on comparison of their lattice constants.

The one electron oxidation could also be affected by alternative oxidizing agents. The same product was obtained (based on comparison of their far-infrared spectra) when Cl_2 or dichlorophenyliodine (DCPI) was used as the oxidant, eqs. 3, 4.

$$[Et_4N]_4Mo_4Cl_{12} + 1/2\ Cl_2 \longrightarrow [Et_4N]_3Mo_4Cl_{12} + Et_4NCl \qquad 3$$

$$[Et_4N]_4Mo_4Cl_{12} + 1/2\ DCPI \longrightarrow [Et_4N]_3Mo_4Cl_{12} + Et_4NCl + \emptyset I \qquad 4$$

These reactions are useful because difficulties in

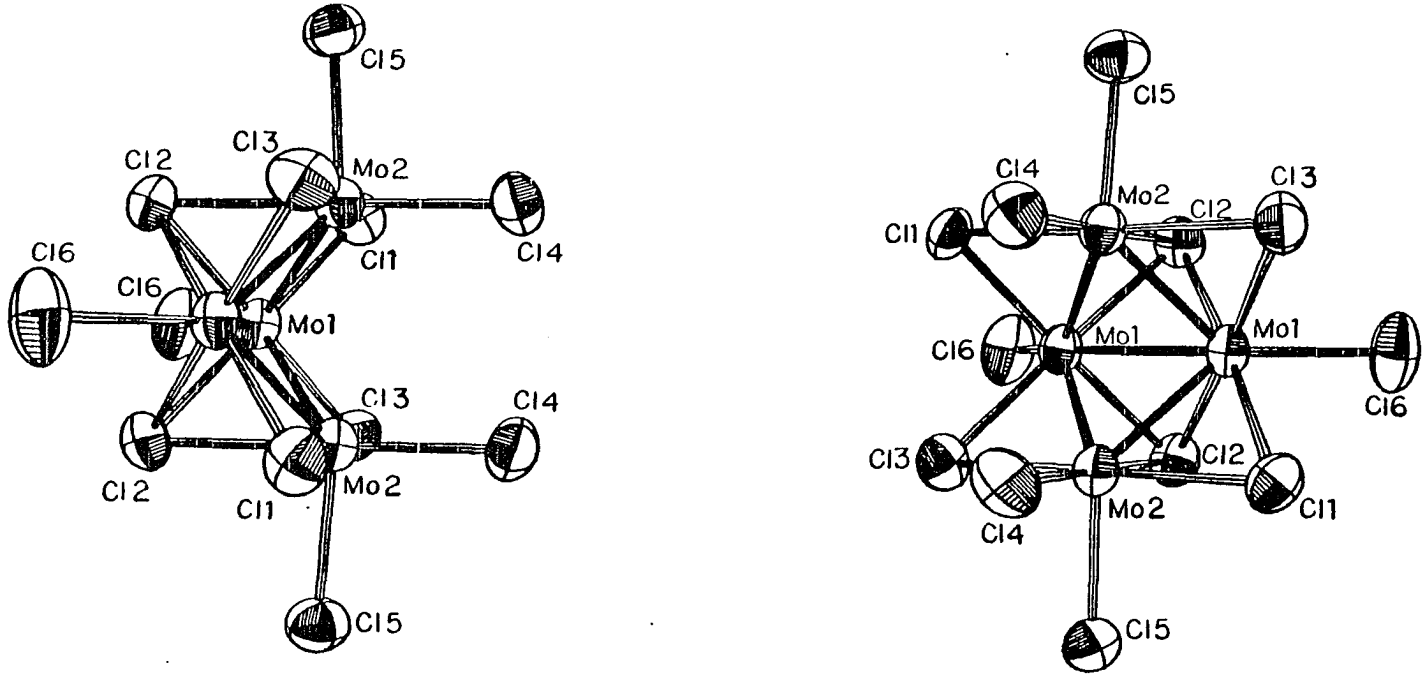

Figure II-3. Two views of 'butterfly' cluster anion in $[Et_4N]_3Mo_4Cl_{12}$. Fifty percent probability anisotropic thermal ellipsoids are shown

separation of Et_4NI, which has a relatively low solubility in DCE and DCM, are eliminated.

The procurement of reproducible analytical data on the $[Et_4N]_3Mo_4Cl_{12}$ cluster compound remains elusive. Chlorine to molybdenum ratios are approximately 3:1 for all of the analyses, however agreement between calculated and observed percentages for most of the samples is poor. Moreover, the observed compositions vary from preparation to preparation. These results suggest that the $[Et_4N]_3Mo_4Cl_{12}$ may be difficult to obtain in a pure form, for several reasons. One is that the insolubility of both the reactants and products may make separation and purification difficult. Solvents in which one species is soluble and the other is insoluble, making separation possible, have not yet been found. Solvents such as MeOH or nitriles are unsuitable because they react with the cluster.

Alternatively, the actual oxidized species may exist in a range of oxidation states (e.g., $(R)_xMo_4Cl_{12}$ $2 < x < 4$). This might be a very difficult variable to control, although experimental evidence, from attempts to vary the amount of oxidation over the range 0 to 1 electron in steps of 0.25, show no observable differences in the x-ray powder patterns which would indicate that a variable amount of oxidation is possible. In the products of these reactions, one sees the lines attributable to the 4- cluster compound disappearing

as the amount of oxidant is increased, while the lines of another compound appear.

One disconcerting fact is that the lines of the powder pattern calculated from the structure solution of $[Et_4N]_3Mo_4Cl_{12}$ do not agree with those of the observed powder pattern. Failure to easily reproduce the synthesis of octahedral crystals, which contain the butterfly cluster anion, suggests that the predominate product may contain a cluster with an alternative geometry, possibly a planar isomer.

Compounds of the $Mo_4Cl_{12}^{3-}$ were also easily prepared as the tetrapropylammonium and tetraphenylphosphonium salts, eqs. 5, 6. These salts and the previously mentioned compound, $[\emptyset_4As]_2[Et_4N]Mo_4Cl_{12}\cdot 2\ CH_2Cl_2$ contain the planar isomer of the $Mo_4Cl_{12}^{3-}$ cluster (Figure II-4).

$$[\emptyset_4P]_4Mo_4Cl_{12} + 1/2\ I_2 \longrightarrow [\emptyset_4P]_3Mo_4Cl_{12} + \emptyset_4PI \qquad 5$$

$$[Pr_4N]_4Mo_4Cl_{12} + 1/2\ I_2 \longrightarrow [Pr_4N]_3Mo_4Cl_{12} + Pr_4NI \qquad 6$$

These compounds could also be synthesized with a one pot method starting from the propionitrile tetramers, using a two step technique where the purple $Mo_4Cl_{12}^{4-}$ salt is generated <u>in situ</u> and subsequently oxidized, eq. 7. The

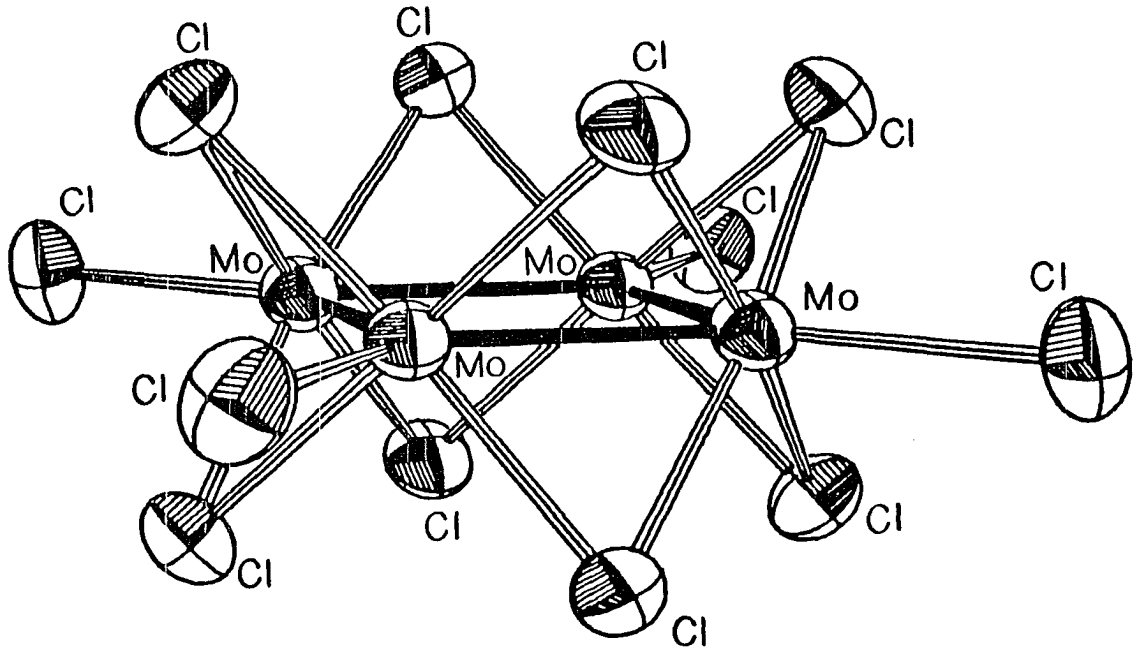

Figure II-4. Planar geometry of $Mo_4Cl_{12}^{3-}$ cluster anion found in $[\emptyset_4P]_3Mo_4Cl_{12}\cdot 0.5\ \emptyset_4PI$. The same cluster geometry is observed for $[Pr_4N]_3Mo_4Cl_{12}\cdot 0.7\ C_2H_4Cl_2$ and $[\emptyset_4As]_2[Et_4N]Mo_4Cl_{12}\cdot 2\ CH_2Cl_2$. Fifty percent probability anisotropic thermal ellipsoids are shown

reaction mixture must be kept cold during the addition of I_2 to insure that oxidation is effected by the iodine and not by solvent

$$Mo_4Cl_8(CH_3CH_2CN)_4 + 4\ R_4XCl \xrightarrow{T<0^{o}\ C} [R_4X]_4Mo_4Cl_{12} + 4\ CH_3CH_2CN \quad 7$$

$$\downarrow\ 1/2\ I_2$$

$$[R_4X]_3Mo_4Cl_{12} + [R_4X]I$$

The $Mo_4Cl_{12}^{3-}$ salts of the $(\emptyset_4P)^+$ and $(Pr_4N)^+$ cations form brown crystalline products, which are very soluble in DCE. In both cases, addition of chlorobenzene induced crystallization of the product. $[Pr_4N]_3Mo_4Cl_{12}$ was obtained in pure form and satisfactory analyses were obtained which agree with the stoichiometry observed in the structure determination.

Different oxidized products were also found when the tetrapropyl- and tetraphenylphosphonium salts of the 4- cluster were allowed to warm above 0 ^{o} C in DCM or DCE without the addition of an oxidizing agent. The product in each of these cases has a Cl:Mo ratio of 2.82:1, but the ratio of cation to anion in the salts is different. The compositions of the two salts, based on elemental analyses, are represented by the formulas $[Pr_4N]_4Mo_6Cl_{17}$ and $[\emptyset_4P]_{4.5}Mo_6Cl_{17}$. These formulas represent oxidation of 0.66 and 0.33 e per Mo_4 cluster, respectively. In the

absence of an alternative source, the solvent itself acted as the oxidant, eq. 8. Such behavior is not unexpected in halocarbon solutions of such strongly reducing species. The reduced species in these reactions is assumed to be the radical of the organic halide which would then most likely dimerize, although no attempt has been made to characterize this product.

$$3/2\ R_4Mo_4Cl_{12} + CH_2Cl_2 \longrightarrow R_4Mo_6Cl_{17} + CH_2Cl^{\cdot} + 2\ RCl \qquad 8$$

The reactions are reproducible, in each case yielding a green-black crystalline product, single crystals of which do not diffract x-rays. This fact is puzzling since the geometrical plates are grown under conditions generally favorable to crystal growth. The shiny platelets formed upon allowing the solution to set for 2-3 days are very reflective when illuminated with a flashlight. One explanation for the poor x-ray diffraction by the crystals is that solvent incorporated in the lattice causes disruption of the initial crystalline structure when it is removed under vacuum drying.

The actual cluster units which exist in these $Mo_6Cl_{17}^{n-}$ compounds are unknown. One possibility is that a mixture of $Mo_4Cl_{12}^{n-}$ and $Mo_4Cl_{11}^{n-}$ (a species which is hypothesized to be structurally similar to $Mo_4I_{11}^{2-}$ (21)) is produced in the

proper ratio to give the observed analytical data. For example, the compound with the empirical formula $[Pr_4N]_4Mo_6Cl_{17}$ would be composed of two Mo_4Cl_{11} clusters and one Mo_4Cl_{12} cluster, $[Pr_4N]_4Mo_4Cl_{12} \cdot 2\ [Pr_4N]_2Mo_4Cl_{11}$. Steric constraints may favor the loss of chloride and formation of the clusters with eleven chlorine ligands, analogous to $Mo_4I_{11}^{2-}$.

Oxidation by the solvent does not occur for $[Et_4N]_4Mo_4Cl_{12}$, eq. 9.

$$[Et_4N]_4Mo_4Cl_{12} + 1,2\text{-}C_2H_4Cl_2 \longrightarrow \text{No reaction} \qquad 9$$

Reactions 8 and 9 demonstrate the difference in the behavior of $[Et_4N]_4Mo_4Cl_{12}$ and that of $[\emptyset_4P]_4Mo_4Cl_{12}$ and $[Pr_4N]_4Mo_4Cl_{12}$ in chlorinated hydrocarbon solvents. $[\emptyset_4P]_4Mo_4Cl_{12}$ and $[Pr_4N]_4Mo_4Cl_{12}$ are both soluble in DCE and DCM. The soluble species are much more susceptible to oxidation by the solvent. These solutions are stable only when held at temperatures below -10 ^{o} C. At this temperature they appear to be stable for long periods of time. (No observable change has been noted when these solutions have been stored at -8^{o} C for 4-5 days during attempts to grow crystals.) Above this temperature, the solutions are slowly oxidized to produce the solid, having the net composition $R_xMo_6Cl_{17}$, where R is $(Pr_4N)^+$ or $(\emptyset_4P)^+$.

$[Et_4N]_4Mo_4Cl_{12}$ is essentially insoluble in DCE or DCM. In these solvents, the solid has been heated to reflux with no evidence of decomposition. Apparently, the insolubility of the $[Et_4N]_4Mo_4Cl_{12}$ protects it from the oxidizing nature of the solvent.

Structures

The square planar and butterfly clusters initially appear to be structurally quite different, however, they both may be considered as fragments of the larger hexanuclear cluster anion, $Mo_6Cl_{14}^{2-}$, and thus, structurally related (Figure II-5). The $Mo_6Cl_{14}^{2-}$ cluster anion is an octahedral cluster of molybdenum atoms where each molybdenum atom is inscribed in the center of a face of a cube defined by eight chlorine atoms. In addition, a chlorine is bound to each molybdenum in a terminal fashion with the bond extending perpendicular to the face of the cube.

The $Mo_4Cl_{12}^{3-}$ clusters are structurally derived from the hexanuclear unit by removal of two molybdenum atoms, along with their terminally bound chlorine atoms. In the planar cluster units, molybdenum atoms are removed from <u>trans</u> faces. In the butterfly cluster, removal of the molybdenum atoms occurs in <u>cis</u> or adjacent faces. Figure II-6 shows the two cluster units observed experimentally and the cubic arrangement of the chlorine atoms in which they

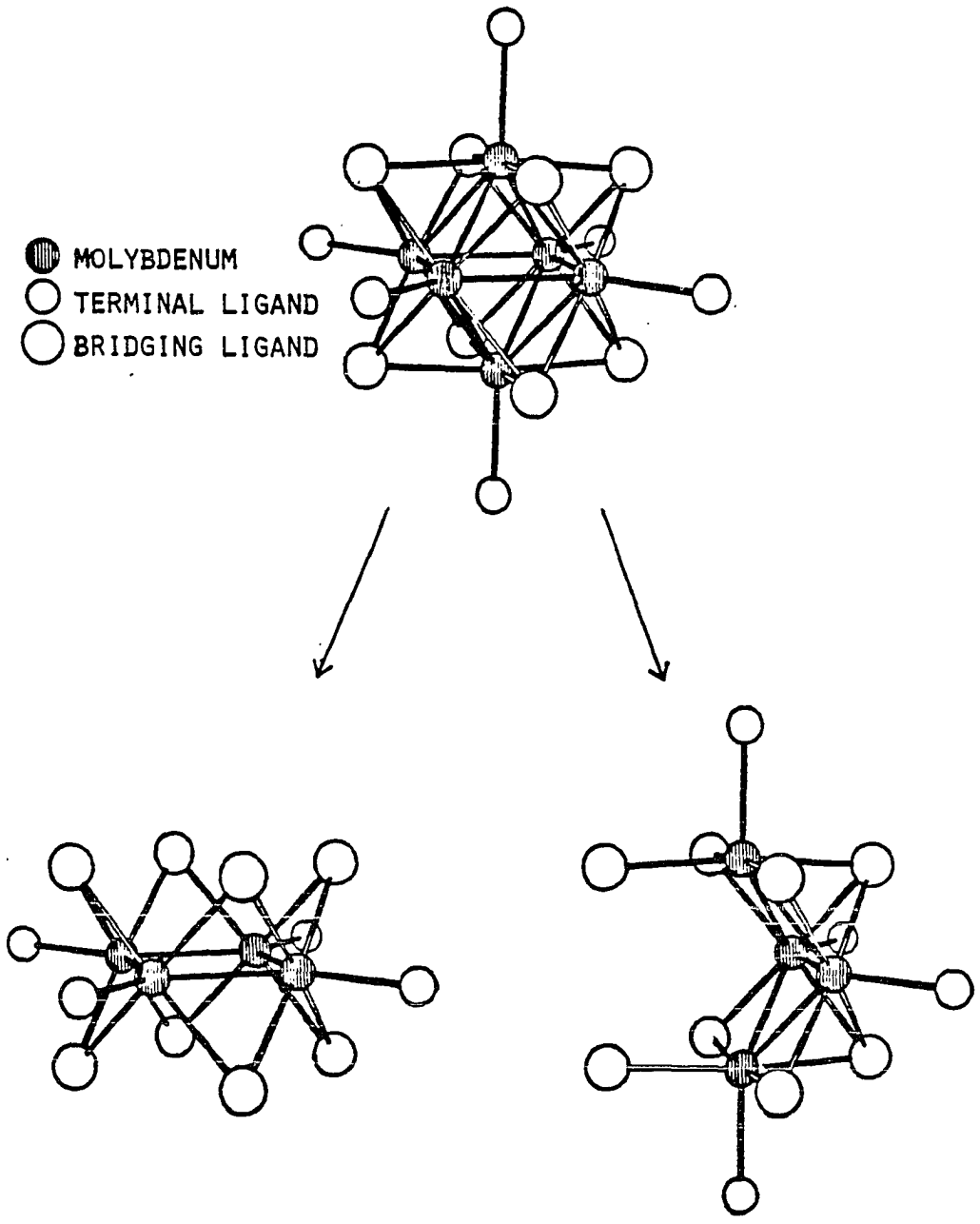

Figure II-5. Tetranuclear butterfly and planar cluster derived from hexanuclear Mo_6X_8 cluster unit by loss of two molybdenum atoms and their terminal halide ligands

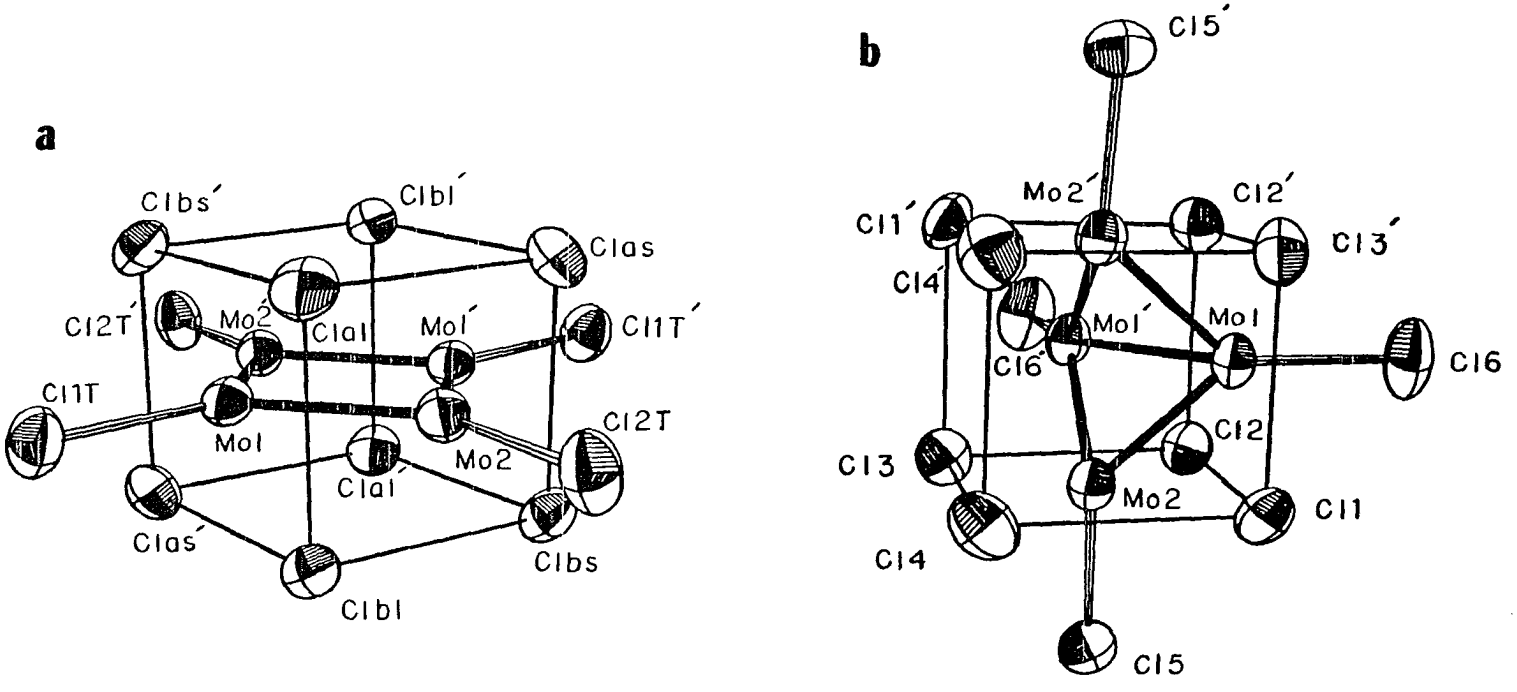

Figure II-6. Comparison of planar and butterfly geometries in a) $[\emptyset_4As]_2[Et_4N]Mo_4Cl_{12}\cdot 2\ CH_2Cl_2$ and b) $[Et_4N]_3Mo_4Cl_{12}$ cluster anions, emphasizing the cubic arrangement of chlorine atoms. Fifty percent probability anisotropic thermal ellipsoids are shown

reside.

The size of the chlorine cube is determined by the van der Waals contacts of the chlorine atoms. These nonbonded distances occur in a range of 3.35-3.45 Å for both the planar and butterfly cluster units. This is in agreement with van der Waals radii of approximately 1.7 Å for chlorine.

Planar clusters

The structures of three compounds in which the cluster anion adopts the planar rhomboidal geometry have been solved. The cluster anions in $[\emptyset_4P]_3Mo_4Cl_{12}\cdot 0.5\ \emptyset_4PI$ (I), $[Pr_4N]_3Mo_4Cl_{12}\cdot 0.7\ C_2H_4Cl_2$ (II), and $[\emptyset_4As]_2[Et_4N]Mo_4Cl_{12}$ (III) are very similar, yet small differences make each of them unique. Bond distances for I, II, and III are given in Tables II-24, II-25, II-28, II-30, II-32, and II-33 while bond angles for these compounds are listed in Tables II-26, II-27, II-29, II-31, II-34, and II-35. Atoms are designated as shown in Figure II-7.

Each cluster unit has four metal atoms in a planar arrangement. I and III have two unique molybdenum atoms in the asymmetric unit, the remaining two metal atoms in the cluster being generated by an inversion at the center of the cluster unit. No symmetry elements are present in the cluster anion of II and four distinct molybdenum atoms are

Table II-24. Interatomic distances (Å) for cluster atoms in $[\emptyset_4P]_3Mo_4Cl_{12}\cdot 0.5\ \emptyset_4PI$[a,b]

bonding distances		nonbonding contacts	
Mo(1)-Mo(2)	2.300(3)	Cl(1)-Cl(4)	3.383(8)
Mo(1)-Mo(2)	2.685(3)	Cl(1)-Cl(2)	3.397(8)
Mo(2)-Mo(2)	3.429(4)	Cl(1)-Cl(5)	3.550(7)
Mo(1)-Cl(1)	2.424(5)	Cl(1)-Cl(3t)	3.557(8)
Mo(1)-Cl(2)	2.469(6)	Cl(2)-Cl(4)	3.444(7)
Mo(1)-Cl(4)	2.457(6)	Cl(2)-Cl(5)	3.456(6)
Mo(1)-Cl(5)	2.420(3)	Cl(2)-Cl(3t)	3.495(6)
Mo(1)-Cl(6t)	2.512(6)	Cl(2)-Cl(6t)	3.545(8)
Mo(2)-Cl(1)	2.423(3)	Cl(3t)-Cl(4)	3.419(8)
Mo(2)-Cl(2)	2.478(6)	Cl(4)-Cl(5)	3.404(8)
Mo(2)-Cl(4)	2.459(6)	Cl(4)-Cl(6t)	3.526(8)
Mo(2)-Cl(5)	2.425(5)		
Mo(2)-Cl(3t)	2.507(6)		

cation-anion interactions

Cl(1) -C(212)	3.45(2)
Cl(1) -C(213)	3.49(2)
Cl(1) -C(236)	3.59(2)
Cl(3t)-C(112)	3.50(2)
Cl(4) -C(143)	3.52(2)
Cl(6t)-C(134)	3.57(2)
Cl(6t)-C(222)	3.58(2)

[a]Estimated standard deviations are given in parentheses for last significant figures.

[b]Atom labels refer to Figure II-7.

Table II-25. Bond angles (deg) for cluster atoms in $[\emptyset_4P]_3Mo_4Cl_{12}\cdot 0.5\ [\emptyset_4P]I$[a,b]

Mo(2)-Mo(1)-Mo(2)	86.6(1)	Cl(4)-Cl(2)-Cl(5)	90.1(2)
Mo(1)-Mo(2)-Mo(1)	93.4(1)	Cl(1)-Cl(4)-Cl(2)	91.7(2)
Mo(1)-Cl(1)-Mo(2)	67.3(1)	Cl(1)-Cl(4)-Cl(5)	76.8(2)
Mo(1)-Cl(5)-Mo(2)	67.3(1)	Cl(2)-Cl(4)-Cl(5)	91.0(2)
Mo(1)-Cl(2)-Mo(2)	55.4(1)	Cl(1)-Cl(5)-Cl(2)	88.7(2)
Mo(1)-Cl(4)-Mo(2)	55.8(1)	Cl(1)-Cl(5)-Cl(4)	88.9(2)
		Cl(2)-Cl(5)-Cl(4)	102.8(2)
		Cl(1)-Cl(2)-Cl(5)	75.9(2)
		Cl(1)-Cl(2)-Cl(4)	90.8(2)
		Cl(2)-Cl(1)-Cl(4)	104.4(2)
		Cl(2)-Cl(1)-Cl(5)	89.3(2)
		Cl(4)-Cl(1)-Cl(5)	89.5(2)
Mo(2)-Mo(1)-Cl(1)	56.3(2)	Mo(1)-Mo(2)-Mo(2)	42.0(1)
Mo(2)-Mo(1)-Cl(2)	121.4(2)	Mo(1)-Mo(2)-Cl(1)	56.4(1)
Mo(2)-Mo(1)-Cl(4)	120.5(2)	Mo(1)-Mo(2)-Cl(2)	125.1(2)
Mo(2)-Mo(1)-Cl(5)	56.5(1)	Mo(1)-Mo(2)-Cl(3t)	130.1(2)
Mo(2)-Mo(1)-Cl(6t)	133.1(2)	Mo(1)-Mo(2)-Cl(4)	124.3(2)
Mo(2)-Mo(1)-Cl(1)	110.5(2)	Mo(1)-Mo(2)-Cl(5)	56.3(1)
Mo(2)-Mo(1)-Cl(2)	62.5(1)	Mo(1)-Mo(2)-Mo(2)	51.4(1)
Mo(2)-Mo(1)-Cl(4)	62.1(1)	Mo(1)-Mo(2)-Cl(1)	114.6(2)
Mo(2)-Mo(1)-Cl(5)	112.0(2)	Mo(1)-Mo(2)-Cl(2)	62.1(1)
Mo(2)-Mo(1)-Cl(6t)	140.3(2)	Mo(1)-Mo(2)-Cl(3t)	136.4(2)
Cl(1)-Mo(1)-Cl(2)	87.9(2)	Mo(1)-Mo(2)-Cl(4)	62.1(1)
Cl(1)-Mo(1)-Cl(4)	172.6(2)	Mo(1)-Mo(2)-Cl(5)	116.1(2)
Cl(1)-Mo(1)-Cl(5)	94.3(2)	Mo(2)-Mo(2)-Cl(1)	81.1(1)
Cl(1)-Mo(1)-Cl(6t)	96.3(2)	Mo(2)-Mo(2)-Cl(2)	97.8(2)
Cl(2)-Mo(1)-Cl(4)	88.7(2)	Mo(2)-Mo(2)-Cl(3t)	172.0(2)
Cl(2)-Mo(1)-Cl(5)	174.5(2)	Mo(2)-Mo(2)-Cl(4)	97.3(2)
Cl(2)-Mo(1)-Cl(6t)	90.8(2)	Mo(2)-Mo(2)-Cl(5)	82.0(2)
Cl(4)-Mo(1)-Cl(5)	88.5(2)	Cl(1)-Mo(2)-Cl(2)	175.9(2)
Cl(4)-Mo(1)-Cl(6t)	90.4(2)	Cl(1)-Mo(2)-Cl(3t)	92.4(2)
Cl(5)-Mo(1)-Cl(6t)	94.1(2)	Cl(1)-Mo(2)-Cl(4)	87.7(2)
		Cl(1)-Mo(2)-Cl(5)	94.2(2)
		Cl(2)-Mo(2)-Cl(3t)	89.1(2)
		Cl(2)-Mo(2)-Cl(4)	88.5(2)
		Cl(2)-Mo(2)-Cl(5)	89.6(2)
		Cl(3t)Mo(2)-Cl(4)	87.0(2)
		Cl(3t)Mo(2)-Cl(5)	94.0(2)
		Cl(4)-Mo(2)-Cl(5)	177.9(2)

[a]Estimated standard deviations are given in parentheses for last significant figures.

[b]Atom labels refer to Figure II-7.

Table II-26. Interatomic distances (Å) for cations in $[\emptyset_4P]_3Mo_4Cl_{12}\cdot 0.5\ \emptyset_4PI$[a]

P(1)-C(111)	1.83(2)	P(2)-C(231)	1.74(2)
P(1)-C(121)	1.80(2)	P(2)-C(211)	1.80(2)
P(1)-C(131)	1.81(2)	P(2)-C(221)	1.80(2)
P(1)-C(141)	1.79(2)	P(2)-C(241)	1.80(2)
C(111)-C(112)	1.34(3)	C(211)-C(216)	1.40(3)
C(111)-C(116)	1.45(3)	C(211)-C(212)	1.45(3)
C(112)-C(113)	1.41(3)	C(212)-C(213)	1.41(3)
C(113)-C(114)	1.39(3)	C(213)-C(214)	1.42(3)
C(114)-C(115)	1.42(3)	C(214)-C(215)	1.37(3)
C(115)-C(116)	1.48(3)	C(215)-C(216)	1.46(3)
C(121)-C(122)	1.38(3)	C(221)-C(226)	1.34(3)
C(121)-C(126)	1.40(3)	C(221)-C(222)	1.42(3)
C(122)-C(123)	1.44(3)	C(222)-C(223)	1.48(3)
C(123)-C(124)	1.39(3)	C(223)-C(224)	1.33(3)
C(124)-C(125)	1.31(4)	C(224)-C(225)	1.38(3)
C(125)-C(126)	1.45(4)	C(225)-C(226)	1.46(4)
C(131)-C(132)	1.39(3)	C(231)-C(232)	1.43(3)
C(131)-C(136)	1.40(3)	C(231)-C(236)	1.44(3)
C(132)-C(133)	1.48(3)	C(232)-C(233)	1.50(3)
C(133)-C(134)	1.39(3)	C(233)-C(234)	1.37(3)
C(134)-C(135)	1.41(3)	C(234)-C(235)	1.39(3)
C(135)-C(136)	1.40(4)	C(235)-C(236)	1.38(3)
C(141)-C(146)	1.44(3)	C(241)-C(242)	1.39(3)
C(141)-C(142)	1.44(3)	C(241)-C(246)	1.42(3)
C(142)-C(143)	1.39(3)	C(242)-C(243)	1.45(3)
C(143)-C(144)	1.39(3)	C(243)-C(244)	1.34(3)
C(144)-C(145)	1.41(3)	C(244)-C(245)	1.40(3)
C(145)-C(146)	1.42(3)	C(245)-C(246)	1.50(3)

[a]Estimated standard deviations are given in parentheses for last significant figures.

Table II-27. Bond angles (deg) for cations in $[\emptyset_4P]_3Mo_4Cl_{12}\cdot 0.5\ \emptyset_4PI$[a]

C(111)-P(1)-C(121)	112.(1)	C(211)-P(2)-C(221)	111.(1)
C(111)-P(1)-C(141)	107.(1)	C(211)-P(2)-C(231)	109.(1)
C(121)-P(1)-C(131)	109.(1)	C(211)-P(2)-C(241)	108.(1)
C(121)-P(1)-C(141)	107.(1)	C(221)-P(2)-C(231)	109.(1)
C(131)-P(1)-C(141)	111.(1)	C(221)-P(2)-C(241)	108.(1)
P(1)-C(111)-C(112)	125.(1)	C(231)-P(2)-C(241)	111.(1)
P(1)-C(111)-C(116)	112.(1)	P(2)-C(211)-C(212)	118.(1)
C(111)-C(112)-C(113)	121.(2)	P(2)-C(211)-C(216)	118.(1)
C(112)-C(113)-C(114)	120.(2)	C(211)-C(212)-C(213)	118.(1)
C(113)-C(114)-C(115)	123.(2)	C(212)-C(213)-C(214)	121.(2)
C(114)-C(115)-C(116)	117.(2)	C(213)-C(214)-C(215)	120.(2)
C(111)-C(116)-C(115)	117.(2)	C(214)-C(215)-C(216)	122.(2)
P(1)-C(121)-C(122)	119.(1)	C(211)-C(216)-C(215)	116.(2)
P(1)-C(121)-C(126)	119.(2)	P(2)-C(221)-C(222)	115.(1)
C(121)-C(122)-C(123)	115.(2)	P(2)-C(221)-C(226)	124.(2)
C(122)-C(123)-C(124)	121.(2)	C(221)-C(222)-C(223)	117.(2)
C(123)-C(124)-C(125)	124.(2)	C(222)-C(223)-C(224)	119.(2)
C(124)-C(125)-C(126)	118.(2)	C(223)-C(224)-C(225)	124.(2)
C(121)-C(126)-C(125)	119.(2)	C(224)-C(225)-C(226)	117.(2)
P(1)-C(131)-C(132)	119.(2)	C(221)-C(226)-C(225)	121.(2)
P(1)-C(131)-C(136)	119.(2)	P(2)-C(231)-C(232)	118.(1)
C(131)-C(132)-C(133)	120.(2)	P(2)-C(231)-C(236)	124.(1)
C(132)-C(133)-C(134)	118.(2)	C(231)-C(232)-C(233)	119.(2)
C(133)-C(134)-C(135)	120.(2)	C(232)-C(233)-C(234)	119.(2)
C(134)-C(135)-C(136)	123.(2)	C(233)-C(234)-C(235)	121.(2)
C(131)-C(136)-C(135)	117.(2)	C(234)-C(235)-C(236)	122.(2)
P(1)-C(141)-C(142)	119.(1)	C(231)-C(236)-C(235)	121.(2)
P(1)-C(141)-C(146)	129.(1)	P(2)-C(241)-C(242)	118.(1)
C(141)-C(142)-C(143)	117.(2)	P(2)-C(241)-C(246)	118.(1)
C(142)-C(143)-C(144)	123.(2)	C(241)-C(242)-C(243)	119.(2)
C(143)-C(144)-C(145)	120.(2)	C(242)-C(243)-C(244)	118.(2)
C(144)-C(145)-C(146)	120.(2)	C(243)-C(244)-C(245)	126.(2)
C(141)-C(146)-C(145)	118.(2)	C(244)-C(245)-C(246)	118.(2)
		C(241)-C(246)-C(245)	115.(2)

[a]Estimated standard deviations are given in parentheses for last significant figures.

Table II-28. Interatomic distances (Å) for cluster atoms in $[Pr_4N]_3Mo_4Cl_{12}\cdot 0.7\ C_2H_4Cl_2$[a,b]

Mo(1)-Mo(2)	3.222(2)	Cl(1)-Cl(6)	3.372(4)
Mo(1)-Mo(3)	2.682(2)	Cl(1)-Cl(2)	3.451(5)
Mo(1)-Mo(4)	2.327(2)	Cl(1)-Cl(12)	3.532(7)
Mo(2)-Mo(3)	2.331(2)	Cl(1)-Cl(3)	3.615(6)
Mo(2)-Mo(4)	2.682(2)	Cl(1)-Cl(11)	3.688(7)
Mo(3)-Mo(4)	3.853(2)	Cl(2)-Cl(7)	3.395(6)
		Cl(2)-Cl(12)	3.398(7)
		Cl(2)-Cl(5)	3.413(6)
		Cl(2)-Cl(1)	3.451(6)
Mo(1)-Cl(1)	2.439(4)	Cl(2)-Cl(10)	3.621(7)
Mo(1)-Cl(3)	2.442(5)	Cl(3)-Cl(4)	3.364(7)
Mo(1)-Cl(2)	2.482(5)	Cl(3)-Cl(5)	3.436(6)
Mo(1)-Cl(5)	2.484(4)	Cl(3)-Cl(12)	3.536(7)
Mo(1)-Cl(12)	2.535(5)	Cl(3)-Cl(1)	3.615(6)
Mo(2)-Cl(8)	2.439(4)	Cl(3)-Cl11)	3.661(6)
Mo(2)-Cl(7)	2.446(4)	Cl(4)-Cl(6)	3.385(7)
Mo(2)-Cl(9)	2.473(5)	Cl(4)-Cl(9)	3.411(7)
Mo(2)-Cl(6)	2.484(4)	Cl(4)-Cl(8)	3.519(6)
Mo(2)-Cl(4)	2.494(5)	Cl(4)-Cl(11)	3.646(7)
Mo(3)-Cl(3)	2.429(5)	Cl(5)-Cl(8)	3.346(6)
Mo(3)-Cl(1)	2.441(5)	Cl(5)-Cl(12)	3.498(6)
Mo(3)-Cl(6)	2.443(5)	Cl(5)-Cl(10)	3.682(7)
Mo(3)-Cl(4)	2.444(5)	Cl(6)-Cl(9)	3.420(6)
Mo(3)-Cl(11)	2.515(5)	Cl(6)-Cl(7)	3.442(6)
Mo(4)-Cl(8)	2.423(5)	Cl(6)-Cl(11)	3.624(7)
Mo(4)-Cl(7)	2.432(5)	Cl(7)-Cl(9)	3.539(6)
Mo(4)-Cl(2)	2.449(5)	Cl(7)-Cl(8)	3.592(6)
Mo(4)-Cl(5)	2.458(5)	Cl(7)-Cl(10)	3.699(7)
Mo(4)-Cl(10)	2.525(5)	Cl(8)-Cl(9)	3.434(6)
		Cl(8)-Cl(7)	3.592(6)
		Cl(8)-Cl(10)	3.649(7)

[a]Estimated standard deviations are given in parentheses for last significant figures.

[b]Atom labels refer to Figure II-7.

Table II-29. Cation interatomic distances (Å) in $[Pr_4N]_3Mo_4Cl_{12}\cdot 0.7\ C_2H_4Cl_2$[a]

cation distances		anion-cation contacts	
N(1)-C(111)	1.57(2)	Cl(1)-C(311)	3.60(6)
N(1)-C(131)	1.57(3)	Cl(2)-C(113)	3.63(3)
N(1)-C(141)	1.58(2)	Cl(2)-C(212)	3.64(2)
N(1)-C(121)	1.59(3)	Cl(2)-C(213)	3.67(2)
C(111)-C(112)	1.54(3)	Cl(5)-C(321)	3.48(2)
C(112)-C(113)	1.50(3)	Cl(5)-C(331)	3.59(2)
C(121)-C(122)	1.52(3)	Cl(6)-C(141)	3.70(2)
C(122)-C(123)	1.53(4)	Cl(9)-C(122)	3.63(2)
C(131)-C(132)	1.48(3)	Cl(9)-C(232)	3.60(2)
C(132)-C(133)	1.60(4)	Cl(9)-C(141)	3.66(2)
C(141)-C(142)	1.47(3)	Cl(11)-C(121)	3.74(2)
C(142)-C(143)	1.51(3)	Cl(8)-C(222)	3.68(2)
N(2)-C(221)	1.51(2)	Cl(12)-CS(2)	3.67(4)
N(2)-C(211)	1.53(2)	Cl(12)-CS(1)	3.75(3)
N(2)-C(241)	1.53(2)		
N(2)-C(231)	1.54(2)	solvent molecule	
C(211)-C(212)	1.54(3)		
C(212)-C(213)	1.51(3)	Cl(S1)-C(S2)	1.70(5)
C(221)-C(222)	1.50(3)	Cl(S2)-C(S1)	1.70(4)
C(222)-C(223)	1.54(3)	C(S1)-C(S2)	1.27(5)
C(231)-C(232)	1.53(3)		
C(232)-C(233)	1.68(3)		
C(241)-C(242)	1.51(3)		
C(242)-C(243)	1.53(3)		
N(3)-C(311)	1.50(3)		
N(3)-C(331)	1.53(2)		
N(3)-C(341)	1.54(2)		
N(3)-C(321)	1.54(3)		
C(311)-C(312)	1.70(3)		
C(312)-C(313)	1.66(5)		
C(321)-C(322)	1.56(3)		
C(322)-C(323)	1.55(3)		
C(331)-C(332)	1.49(3)		
C(332)-C(333)	1.51(3)		
C(341)-C(342)	1.52(3)		
C(342)-C(343)	1.64(4)		

[a]Estimated standard deviations are given in parentheses for last significant figures.

Table II-30. Bond angles (deg) for cluster atoms in $[Pr_4N]_3Mo_4Cl_{12}\cdot 0.7\ C_2H_4Cl_2$[a,b]

Mo(3)-Mo(1)-Mo(4)	100.37(7)	Mo(1)-Cl(1)-Mo(3)	66.67(12)
Mo(3)-Mo(2)-Mo(4)	100.22(7)	Mo(1)-Cl(2)-Mo(4)	56.30(11)
Mo(1)-Mo(3)-Mo(2)	79.67(7)	Mo(1)-Cl(3)-Mo(3)	66.81(12)
Mo(1)-Mo(4)-Mo(2)	79.74(7)	Mo(2)-Cl(4)-Mo(3)	56.33(11)
		Mo(1)-Cl(5)-Mo(4)	56.17(1)
		Mo(2)-Cl(6)-Mo(3)	56.48(1)
		Mo(2)-Cl(7)-Mo(4)	66.71(1)
		Mo(2)-Cl(8)-Mo(4)	66.97(1)
Mo(3)-Mo(1)-Cl(1)	56.7(1)	Mo(1)-Mo(3)-Cl(1)	56.6(1)
Mo(3)-Mo(1)-Cl(2)	129.9(1)	Mo(1)-Mo(3)-Cl(3)	56.8(1)
Mo(3)-Mo(1)-Cl(3)	56.4(1)	Mo(1)-Mo(3)-Cl(4)	117.4(1)
Mo(3)-Mo(1)-Cl(5)	127.0(1)	Mo(1)-Mo(3)-Cl(6)	118.2(1)
Mo(3)-Mo(1)-Cl(12)	125.6(1)	Mo(1)-Mo(3)-Cl(11)	133.8(1)
Mo(4)-Mo(1)-Cl(1)	117.2(1)	Mo(2)-Mo(3)-Cl(1)	105.5(1)
Mo(4)-Mo(1)-Cl(2)	61.1(1)	Mo(2)-Mo(3)-Cl(3)	107.3(1)
Mo(4)-Mo(1)-Cl(3)	119.8(1)	Mo(2)-Mo(3)-Cl(4)	62.9(1)
Mo(4)-Mo(1)-Cl(5)	61.3(1)	Mo(2)-Mo(3)-Cl(6)	62.7(1)
Mo(4)-Mo(1)-Cl(12)	134.1(1)	Mo(2)-Mo(3)-Cl(11)	146.6(1)
Cl(1)-Mo(1)-Cl(2)	89.1(2)	Cl(1)-Mo(3)-Cl(3)	95.9(2)
Cl(1)-Mo(1)-Cl(3)	95.6(2)	Cl(1)-Mo(3)-Cl(4)	168.4(2)
Cl(1)-Mo(1)-Cl(5)	175.8(2)	Cl(1)-Mo(3)-Cl(6)	87.3(2)
Cl(1)-Mo(1)-Cl(12)	90.5(2)	Cl(1)-Mo(3)-Cl(11)	96.2(2)
Cl(2)-Mo(1)-Cl(3)	173.7(2)	Cl(3)-Mo(3)-Cl(4)	87.3(2)
Cl(2)-Mo(1)-Cl(5)	86.8(2)	Cl(3)-Mo(3)-Cl(6)	169.7(2)
Cl(2)-Mo(1)-Cl(12)	85.2(2)	Cl(3)-Mo(3)-Cl(11)	95.5(2)
Cl(3)-Mo(1)-Cl(5)	88.5(2)	Cl(4)-Mo(3)-Cl(6)	87.7(2)
Cl(3)-Mo(1)-Cl(12)	90.5(2)	Cl(4)-Mo(3)-Cl(11)	94.7(2)
Cl(5)-Mo(1)-Cl(12)	88.4(2)	Cl(6)-Mo(3)-Cl(11)	93.9(2)
Mo(3)-Mo(2)-Cl(4)	60.3(1)	Mo(1)-Mo(4)-Cl(2)	62.6(1)
Mo(3)-Mo(2)-Cl(6)	60.9(1)	Mo(1)-Mo(4)-Cl(5)	62.5(1)
Mo(3)-Mo(2)-Cl(7)	117.0(1)	Mo(1)-Mo(4)-Cl(7)	105.6(1)
Mo(3)-Mo(2)-Cl(8)	120.6(1)	Mo(1)-Mo(4)-Cl(8)	107.9(1)
Mo(3)-Mo(2)-Cl(9)	134.2(1)	Mo(1)-Mo(4)-Cl(10)	146.1(1)
Mo(4)-Mo(2)-Cl(4)	128.6(1)	Mo(2)-Mo(4)-Cl(2)	119.1(1)
Mo(4)-Mo(2)-Cl(6)	128.8(1)	Mo(2)-Mo(4)-Cl(5)	115.6(1)
Mo(4)-Mo(2)-Cl(7)	56.4(1)	Mo(2)-Mo(4)-Cl(7)	56.9(1)
Mo(4)-Mo(2)-Cl(8)	56.2(1)	Mo(2)-Mo(4)-Cl(8)	56.8(1)
Mo(4)-Mo(2)-Cl(9)	125.6(1)	Mo(2)-Mo(4)-Cl(10)	134.2(1)
Cl(4)-Mo(2)-Cl(6)	85.7(1)	Cl(2)-Mo(4)-Cl(5)	88.1(2)

[a]Estimated standard deviations given in parentheses for last significant figures.

[b]Atom labels refer to Figure II-7.

Table II-30. (Continued)

Cl(4)-Mo(2)-Cl(7)	174.2(2)	Cl(2)-Mo(4)-Cl(7)	88.1(2)
Cl(4)-Mo(2)-Cl(8)	91.0(2)	Cl(2)-Mo(4)-Cl(8)	170.4(2)
Cl(4)-Mo(2)-Cl(9)	86.7(2)	Cl(2)-Mo(4)-Cl(10)	93.4(2)
Cl(6)-Mo(2)-Cl(7)	88.6(2)	Cl(5)-Mo(4)-Cl(7)	167.8(2)
Cl(6)-Mo(2)-Cl(8)	174.9(2)	Cl(5)-Mo(4)-Cl(8)	86.5(2)
Cl(6)-Mo(2)-Cl(9)	87.3(2)	Cl(5)-Mo(4)-Cl(10)	95.3(2)
Cl(7)-Mo(2)-Cl(8)	94.7(2)	Cl(7)-Mo(4)-Cl(8)	95.4(2)
Cl(7)-Mo(2)-Cl(9)	92.0(2)	Cl(7)-Mo(4)-Cl(10)	96.5(2)
Cl(8)-Mo(2)-Cl(9)	88.7(2)	Cl(8)-Mo(4)-Cl(10)	95.0(2)

Table II-31. Bond angles (deg) for cations in $[Pr_4N]_3Mo_4Cl_{12}\cdot 0.7\ C_2H_4Cl_2$[a]

C(111)-N(1)-C(121)	106.(1)	C(311)-N(3)-C(321)	115.(1)
C(111)-N(1)-C(131)	113.(1)	C(311)-N(3)-C(331)	110.(1)
C(111)-N(1)-C(141)	108.(1)	C(311)-N(3)-C(341)	101.(1)
C(131)-N(1)-C(141)	110.(1)	C(321)-N(3)-C(331)	103.(1)
N(1) -C(111)-C(112)	114.(2)	C(321)-N(3)-C(341)	113.(1)
C(111)-C(112)-C(113	107.(2)	C(331)-N(3)-C(341)	115.(1)
N(1) -C(121)-C(122)	111.(2)	N(3) -C(311)-C(312)	105.(2)
C(121)-C(122)-C(123)	106.(2)	C(311)-C(312)-C(313)	97.(2)
N(1) -C(131)-C(132)	111.(1)	N(3) -C(321)-C(322)	112.(2)
C(131)-C(132)-C(133)	101.(2)	C(321)-C(322)-C(323)	106.(2)
N(1) -C(141)-C(142)	116.(2)	N(3) -C(331)-C(332)	114.(2)
C(141)-C(142)-C(143)	109.(2)	C(331)-C(332)-C(333)	115.(2)
C(211)-N(2)-C(221)	113.(1)	N(3) -C(341)-C(342)	109.(2)
C(211)-N(2)-C(231)	107.(1)	C(341)-C(342)-C(343)	107.(2)
C(211)-N(2)-C(241)	107.(1)	ClS(2)-CS(1)-CS(2)	123.(3)
C(221)-N(2)-C(231)	109.(1)	ClS(1)-CS(2)-CS(1)	124.(3)
C(221)-N(2)-C(241)	108.(1)		
C(231)-N(2)-C(241)	112.(1)		
N(2) -C(211)-C(212)	114.(2)		
C(211)-C(212)-C(213)	108.(2)		
N(2) -C(221)-C(222)	116.(2)		
C(221)-C(222)-C(223)	109.(2)		
N(2) -C(231)-C(232)	112.(1)		
C(231)-C(232)-C(233)	104.(1)		
N(2) -C(241)-C(242)	116.(1)		
C(241)-C(242)-C(243)	109.(2)		

[a]Estimated standard deviations are given in parentheses for last significant figures.

Table II-32. Interatomic distances (Å) for cluster atoms in $[\emptyset_4As]_2[Et_4N]Mo_4Cl_{12}\cdot 2\ CH_2Cl_2$[a,b,c]

cluster distances		Cl-Cl nonbonding contacts	
Mo(1)-Mo(1)	3.258(2)	Cl(AL)-Cl(BS)	3.404(5)
Mo(2)-Mo(1)	2.653(2)	Cl(AL)-Cl(AS)	3.463(5)
Mo(2)-Mo(1)	2.353(2)	Cl(AL)-Cl(BL)	3.523(4)
Cl(1T)-Mo(1)	2.511(4)	Cl(BL)-CL(AS)	3.364(5)
Cl(AL)-Mo(1)	2.436(3)	Cl(BL)-Cl(BS)	3.425(4)
Cl(BL)-Mo(1)	2.437(3)	Cl(AS)-Cl(BS)	3.480(4)
Cl(AS)-Mo(1)	2.485(3)		
Cl(BS)-Mo(1)	2.466(3)		
Cl(2T)-Mo(2)	2.530(4)		
Cl(AL)-Mo(2)	2.431(3)		
Cl(BL)-Mo(2)	2.433(3)		
Cl(AS)-Mo(2)	2.450(3)		
Cl(BS)-Mo(2)	2.453(3)		

[a]Estimated standard deviations are given in parentheses for last significant figures.

[b]Abbreviations- AL, above long edge; BL, below long edge; AS, above short edge; BS, below short edge.

[c]Atom labels refer to Figure II-7.

Table II-33. Interatomic distances (Å) for cations in $[\emptyset_4As]_2[Et_4N]Mo_4Cl_{12}\cdot 2\ CH_2Cl_2$[a]

$(Et_4N)^+$ cation		$(\emptyset_4As)^+$ cation	
C(1)-N(1)	1.52(3)	C(11)-As(1)	1.91(1)
C(2)-N(1)	1.58(3)	C(21)-As(1)	1.91(1)
C(1A)-N(1)	1.45(3)	C(31)-As(1)	1.88(1)
C(2A)-N(1)	1.68(3)	C(41)-As(1)	1.89(1)
C(3)-C(1)	1.77(3)	C(13)-C(11)	1.39(2)
C(4)-C(2)	1.56(3)	C(16)-C(11)	1.36(2)
C(2A)-C(3)	1.61(4)	C(14)-C(12)	1.36(2)
C(1A)-C(4)	1.65(3)	C(16)-C(12)	1.39(2)
		C(15)-C(13)	1.37(2)
solvent CH_2Cl_2		C(15)-C(14)	1.37(2)
		C(22)-C(21)	1.38(2)
Cl(S1)-Cl(S2)	2.86(1)	C(26)-C(21)	1.35(2)
C(S)-Cl(S2)	1.78(2)	C(23)-C(22)	1.38(2)
C(S)-Cl(S1)	1.74(2)	C(24)-C(23)	1.34(2)
		C(25)-C(24)	1.37(2)
		C(26)-C(25)	1.40(2)
		C(32)-C(31)	1.41(2)
		C(36)-C(31)	1.37(2)
		C(33)-C(32)	1.40(2)
		C(34)-C(33)	1.35(2)
		C(35)-C(34)	1.35(2)
		C(36)-C(35)	1.39(2)
		C(42)-C(41)	1.37(2)
		C(46)-C(41)	2.80(2)
		C(44)-C(42)	1.37(2)
		C(41)-C(43)	1.38(2)
		C(45)-C(43)	1.41(2)
		C(46)-C(44)	1.40(2)

[a]Estimated standard deviations are given in parentheses for last significant figures.

Table II-34. Bond angles (deg) for cluster atoms in $[\emptyset_4As]_2[Et_4N]Mo_4Cl_{12}\cdot 2\ CH_2Cl_2$[a,b,c]

Angles in the cluster unit			
Mo(2)-Mo(1)-Mo(2)	99.1(5)	Mo(1)-Cl(BS)-Mo(2)	61.1(1)
Mo(1)-Mo(2)-Mo(1)	80.9(5)	Mo(1)-Cl(AS)-Mo(2)	66.0(1)
Cl(1T)-Mo(1)-Cl(AL)	90.1(1)	Mo(1)-Cl(BL)-Mo(2)	57.0(1)
Cl(1T)-Mo(1)-Cl(BL)	90.4(1)	Mo(1)-Cl(AL)-Mo(2)	55.1(1)
Cl(1T)-Mo(1)-Cl(AS)	87.4(1)		
Cl(1T)-Mo(1)-Cl(BS)	86.7(1)		
Cl(AL)-Mo(1)-Cl(BL)	92.6(1)	Cl-Cl contacts in halogen cube	
Cl(AL)-Mo(1)-Cl(AS)	89.4(1)	Cl(BL)-Cl(AL)-Cl(AS)	89.5(1)
Cl(AL)-Mo(1)-Cl(BS)	176.5(1)	Cl(BL)-Cl(AL)-Cl(BS)	89.3(1)
Cl(BL)-Mo(1)-Cl(AS)	177.0(1)	Cl(AS)-Cl(AL)-Cl(BS)	98.9(1)
Cl(BL)-Mo(1)-Cl(BS)	88.6(1)	Cl(AL)-Cl(BL)-Cl(AS)	89.9(1)
Cl(AS)-Mo(1)-Cl(BS)	89.3(1)	Cl(AL)-Cl(BL)-Cl(BS)	89.7(1)
Cl(2T)-Mo(2)-Cl(AL)	96.3(1)	Cl(AS)-Cl(BL)-Cl(BS)	100.(1)
Cl(2T)-Mo(2)-Cl(BL)	97.6(1)	Cl(AL)-Cl(AS)-Cl(BL)	80.3(1)
Cl(2T)-Mo(2)-Cl(AS)	92.1(1)	Cl(AL)-Cl(AS)-Cl(BS)	89.8(1)
Cl(2T)-Mo(2)-Cl(BS)	91.9(1)	Cl(BL)-Cl(AS)-Cl(BS)	90.7(1)
Cl(AL)-Mo(2)-Cl(BL)	92.8(1)	Cl(AL)-Cl(BS)-Cl(BL)	80.3(1)
Cl(AL)-Mo(2)-Cl(AS)	171.5(1)	Cl(AL)-Cl(BS)-Cl(AS)	90.0(1)
Cl(AL)-Mo(2)-Cl(BS)	88.3(1)	Cl(BL)-Cl(BS)-Cl(AS)	90.9(1)
Cl(BL)-Mo(2)-Cl(AS)	87.1(1)		
Cl(BL)-Mo(2)-Cl(BS)	170.3(1)		
Cl(AS)-Mo(2)-Cl(BS)	90.4(1)		

[a]Estimated standard deviations are given in parentheses for last significant figures.

[b]Abbreviations; AL, above long edge; BL, below long edge; AS, above short edge; BS, below short edge.

[c]Atom labels refer to Figure II-7.

Table II-35. Bond angles (deg) for cations in $[\emptyset_4As]_2[Et_4N]Mo_4Cl_{12}\cdot 2\ CH_2Cl_2$[a]

C(11)-As(1)-C(21)	108.5(5)	As(1)-C(41)-C(42)	121.3(8)
C(11)-As(1)-C(31)	109.3(5)	As(1)-C(41)-C(43)	119.5(9)
C(11)-As(1)-C(41)	110.2(5)	C(41)-C(42)-C(44)	120.3(11)
C(21)-As(1)-C(31)	110.0(5)	C(41)-C(43)-C(45)	120.0(12)
C(21)-As(1)-C(41)	110.2(5)	C(42)-C(44)-C(46)	121.3(13)
C(31)-As(1)-C(41)	108.4(5)	C(43)-C(45)-C(46)	120.5(12)
As(1)-C(11)-C(13)	118.7(9)	C(44)-C(46)-C(45)	118.6(12)
As(1)-C(11)-C(16)	120.3(10)		
C(14)-C(12)-C(16)	119.7(13)		
C(12)-C(14)-C(15)	120.7(13)		
C(13)-C(15)-C(14)	120.0(13)	C(1)-N(1)-C(1A)	123.2(15)
C(11)-C(16)-C(12)	119.4(13)	C(1)-N(1)-C(2A)	99.9(15)
As(1)-C(21)-C(22)	121.2(9)	C(1)-N(1)-C(2)	110.5(15)
As(1)-C(21)-C(26)	117.4(9)	C(2)-N(1)-C(1A)	108.9(14)
C(21)-C(22)-C(23)	119.2(12)	C(2)-N(1)-C(2A)	104.8(15)
C(22)-C(23)-C(24)	120.6(13)	C(1A)-N(1)-C(2A)	107.7(14)
C(23)-C(24)-C(25)	120.0(13)	N(1)-C(1)-C(3)	102.2(17)
C(24)-C(25)-C(26)	120.5(13)	N(1)-C(2)-C(4)	100.3(17)
C(21)-C(26)-C(25)	118.3(12)	N(1)-C(1A)-C(4)	111.9(17)
As(1)-C(31)-C(32)	118.4(8)	N(1)-C(2A)-C(3)	102.5(19)
As(1)-C(31)-C(36)	123.0(9)	Cl(S2)-C(S)-Cl(S1)	108.5(9)
C(31)-C(32)-C(33)	119.7(11)		
C(32)-C(33)-C(34)	119.6(12)		
C(33)-C(34)-C(35)	120.9(13)		
C(34)-C(35)-C(36)	120.7(13)		
C(31)-C(36)-C(35)	120.2(11)		

[a]Estimated standard deviations are given in parentheses for last significant figures.

required to define the asymmetric unit.

The cluster anions are not rectangular. The angles in each of the planar clusters deviate from 90° by different amounts. The distortion in I is the smallest, where the angles are $93.4(1)^{\circ}$ and $86.6(1)^{\circ}$ (The inversion symmetry requires that the sum be 180°.). A larger distortion is observed in II and III, the deviation from 90° being approximately ten degrees. III has cluster angles of $99.08(5)^{\circ}$ and $80.92(5)^{\circ}$, whereas in II there are four unique angles because of the lower symmetry of the cluster, $100.37(7)^{\circ}$, $100.22(7)^{\circ}$, $79.74(7)^{\circ}$, and $79.67(7)^{\circ}$. The three clusters are shown in Figure II-7, which illustrates the difference in the angular distortions. For comparison, the cluster distances and angles are tabulated in Table II-36.

The cause for the deviation of cluster angles from 90° is not clear. Orbital overlaps would be optimized with a rectangular cluster so some force must be driving the distortion. Crystal packing forces may be the cause, however, no nonbonding contacts appear to be unusually constrictive in analysis of the structure results. If packing forces were the cause the distortion of the cluster would alleviate steric crowding in the cluster lattice.

Conditions are suitable for a second-order Jahn-Teller effect. This possibility is discussed along with results of the extended Hückel calculations (<u>vide infra</u>).

Table II-36. Bond distance and angle comparison for planar clusters[a,b]

	$(\emptyset_4P)_3Mo_4Cl_{12}$ I	$(\emptyset_4As)_2(Et_4N)$-Mo_4Cl_{12} III	$(Pr_4N)_3Mo_4Cl_{12}$[c] II
Distances			
Mo_1-Mo_2	2.685(3)	2.654(2)	2.682(4)
Mo_1-Mo_2	2.300(3)	2.353(2)	2.327(3)
Mo_1-Cl_a	2.429(7)	2.437(3)	2.441(4)
Mo_1-Cl_{al}	2.424(7)	2.437(3)	2.443(5)
Mo_1-Cl_{bl}	2.457(8)	2.485(3)	2.483(5)
Mo_1-Cl_{as}	2.469(7)	2.471(4)	2.478(4)
Mo_1-Cl_{bs}	2.512(9)	2.512(4)	2.535(4)
Mo_1-Cl_t	2.417(8)	2.431(4)	2.435(5)
Mo_2-Cl_{al}	2.427(8)	2.434(4)	2.442(5)
Mo_2-Cl_{bl}	2.457(8)	2.450(4)	2.473(5)
Mo_2-Cl_{as}	2.482(8)	2.451(4)	2.484(4)
Mo_2-Cl_{bs}	2.507(8)	2.530(4)	2.515(4)
Mo_2-Cl_t			
Angles			
Mo_1-Mo_2-Mo_1'	93.4(1)	99.06(5)	100.31(1)
Mo_2-Mo_1-Mo_2'	86.6(1)	80.94(5)	79.71(1)
Mo_1-Cl_{al}-Mo_2	67.3(1)	67.1(1)	66.84(2)
Mo_1-Cl_{bl}-Mo_2	67.3(1)	66.0(1)	66.75(2)
Mo_1-Cl_{as}-Mo_2	55.8(1)	55.1(1)	56.32(2)
Mo_1-Cl_{bs}-Mo_2	55.4(1)	57.0(1)	56.33(2)

[a]Estimated standard deviations are given in parentheses for last significant figures.

[b]Abbreviations– al, above long edge; bl, below long edge; as, above short edge; bs, below short edge.

[c]Distances and angles are the average of two distances or lengths found in this structure.

Figure II-7. Comparison of cluster angles in
I) $[\emptyset_4P]_3Mo_4Cl_{12}\cdot 0.5\ \emptyset_4PI$,
II) $[Pr_4N]_3Mo_4Cl_{12}\cdot 0.7\ C_2H_4Cl_2$, and
III) $[\emptyset_4As]_2[Et_4N]Mo_4Cl_{12}\cdot 2\ CH_2Cl_2$

I

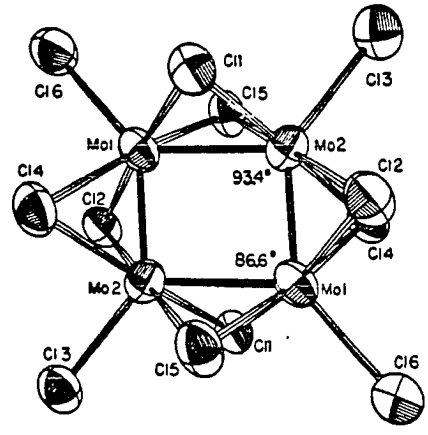
Cl1
Cl6
Cl5
Cl3
Mo1
Mo2
Cl4
93.4°
Cl2
Cl2
Cl4
86.6°
Mo2
Mo1
Cl3
Cl5
Cl1
Cl6

II

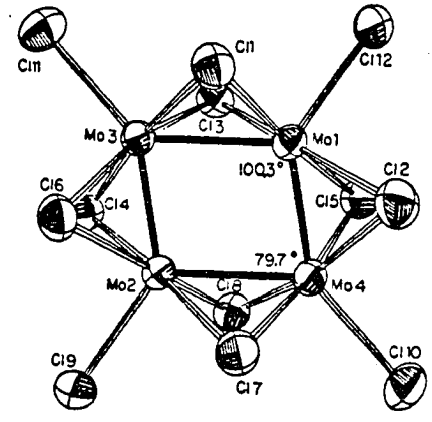
Cl11
Cl1
Cl12
Cl3
Mo3
Mo1
100.3°
Cl6
Cl4
Cl5
Cl2
79.7°
Mo2
Cl8
Mo4
Cl9
Cl7
Cl10

III

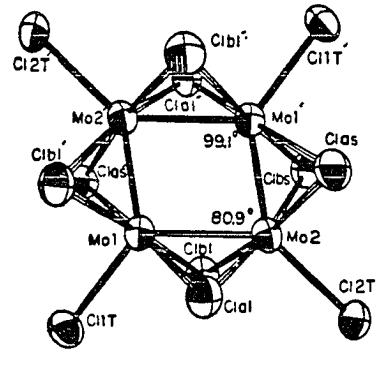
Cl2T
Cl1'
Cl1T'
Cl1'
Mo2'
Mo1'
99.1°
Cl1'
Cl3
Cl3
Cl3
80.9°
Mo1
Cl1'
Mo2
Cl2T
Cl1T
Cl1'

The Mo-Mo bond distances in the three clusters vary slightly. In III, the difference between the short Mo-Mo bond distance and the long Mo-Mo bond distance is the least, 2.654 and 2.353 Å. The difference is the greatest for I, 2.685 and 2.300 Å. The short and long Mo-Mo bond distances in II are intermediate between these two extremes. The greater difference between short and long bond distances in $[\emptyset_4P]_3Mo_4Cl_{12}\cdot 0.5\ \emptyset_4PI$ is coupled with the smallest angle deformation from 90°.

The metal-metal bond distances are indicative of multiple bond character. The distance of 2.3 Å is typical of at least a double bond length while 2.6-2.7 Å is usually considered to be typical single bond distance (20). The single bond in $Mo_6Cl_{14}^{2-}$ is 2.61 Å (19), while triple bonds found in $Mo_2(OR)_6$ compounds are of the order of 2.20 Å (22). The bond orders in the $Mo_4Cl_{12}^{3-}$ anions are not unexpected based on the chemical formulas and low valences of the molybdenum atoms. Simple electron counting rules predict that 15 electrons are available for metal-metal bonding. If all 15 electrons are distributed equally over the four bonds in bonding orbitals, one would predict an average bond order of 1.875. Considering the long and short distances found in the cluster it seems reasonable to consider that the short distances correspond to bond orders greater than two and the long distances to bond orders approximately equal to one.

The short and long Mo-Mo distances in the cluster unit are similar to those seen in $Mo_4Cl_8(PR_3)_4$ clusters (23), where the 16 cluster electrons form two short (~2.2 Å) triple bonds and two long (~2.9 Å) single bonds. In the planar $Mo_4Cl_{12}^{3-}$ clusters, the difference between the short and long bonds is not as great as it is in the $Mo_4Cl_8(P)_4$ cluster compounds suggesting that a greater degree of electron delocalization is present in the cluster unit of the former compounds. In contrast to the long and short distances observed in the $Mo_4Cl_{12}^{3-}$ system, the similar planar 12 electron cluster, $Mo_4(OPr^i)_8Cl_4$, has four equal bond distances of 2.378(2) Å (24).

The planar $Mo_4Cl_{12}^{3-}$ clusters are bridged above and below the plane on all four sides by chlorine atoms. This is the first tetranuclear cluster observed with halogen bridging of this type. The octa-bridged structure has been observed for $Mo_4(OPr^i)_8Cl_4$ where the oxygen atoms of the isopropoxy groups are in the bridging positions; however, an oxygen atom is smaller than a chlorine atom and might be expected to bridge in this manner with less steric crowding.

Some steric crowding must accompany the bridging of the short sides of the planar cluster unit. The cluster compensates by requiring that these chlorines be bound with $Mo\text{-}Cl_b\text{-}Mo$ angles approximately 10^o less than those for the chlorines bridging the long sides of the cluster unit, ~56^o

and ~67°, respectively. The difference in bond angles for these chlorines allows the chlorine-chlorine contacts in the cube to remain at the van der Waals contact distance. The Mo-Cl bond distances are similar for chlorines bridging both short and long sides, ranging from 2.42-2.48 Å.

Each molybdenum in the cluster also has a terminal chlorine bound to it at a distance of approximately 2.50-2.55 Å.

The coordination number of each molybdenum atom is seven. Each molybdenum is bound to four bridging and one terminal chlorine atom in a square pyramidal fashion. In addition, the metal-metal bonding increases the coordination of each molybdenum by two.

The manner in which the clusters of I, II, and III pack into their respective unit cells is shown in Figures II-8, II-9, and II-10. $[\emptyset_4P]_3Mo_4Cl_{12}$ and $[\emptyset_4As]_2[Et_4N]Mo_4Cl_{12}$ contain two clusters per unit cell while $[Pr_4N]_3Mo_4Cl_{12}$ contains four cluster units in the unit cell.

Butterfly cluster

The anionic cluster in $[Et_4N]_3Mo_4Cl_{12}$ has an opened tetrahedron or 'butterfly' structure. The structure is as pictured in Figure II-3. The butterfly is inscribed, as previously noted (Figure II-6), in a cube of chlorine atoms defined by Cl(1), Cl(1'), Cl(2), Cl(2'), Cl(3), Cl(3'),

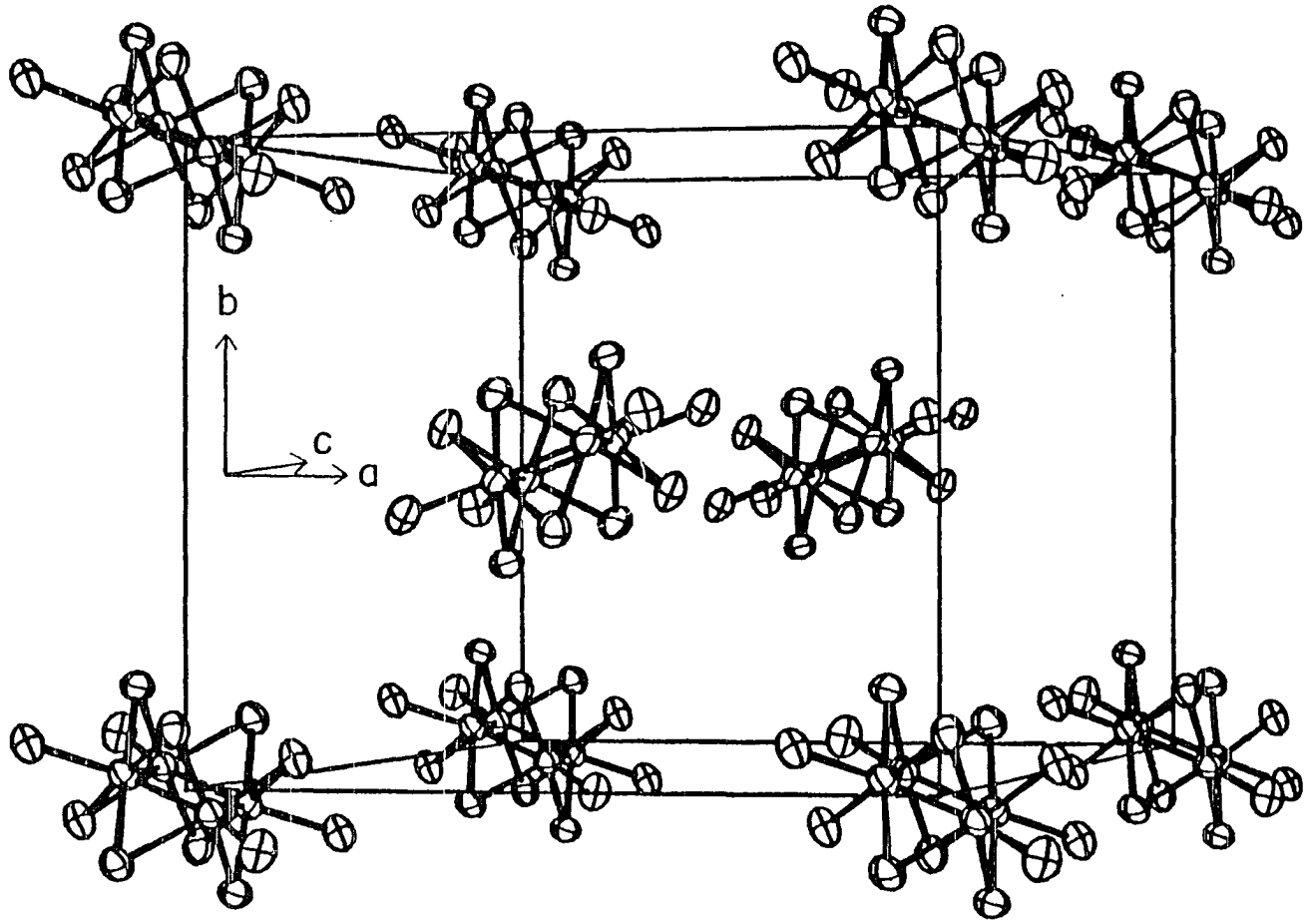

Figure II-8. Unit cell of $[\emptyset_4P]_3Mo_4Cl_{12}\cdot 0.5\ \emptyset_4PI$ showing the packing of cluster units in the cell

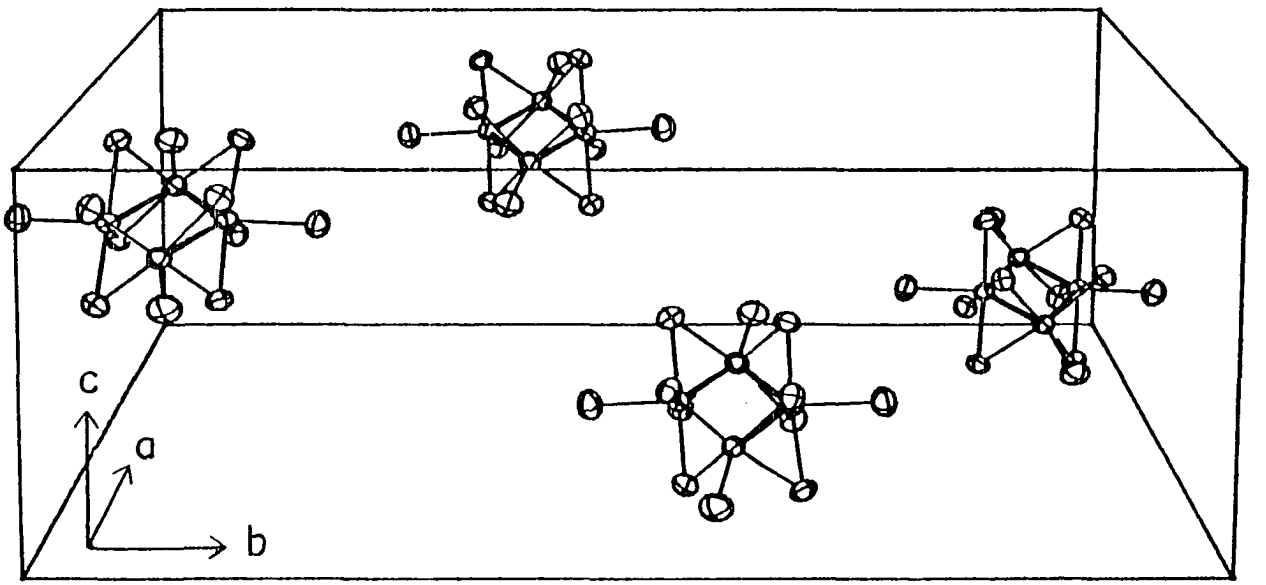

Figure II-9. Unit cell of $[Pr_4N]_3Mo_4Cl_{12}\cdot 0.7\ C_2H_4Cl_2$ showing the packing of cluster units in the cell

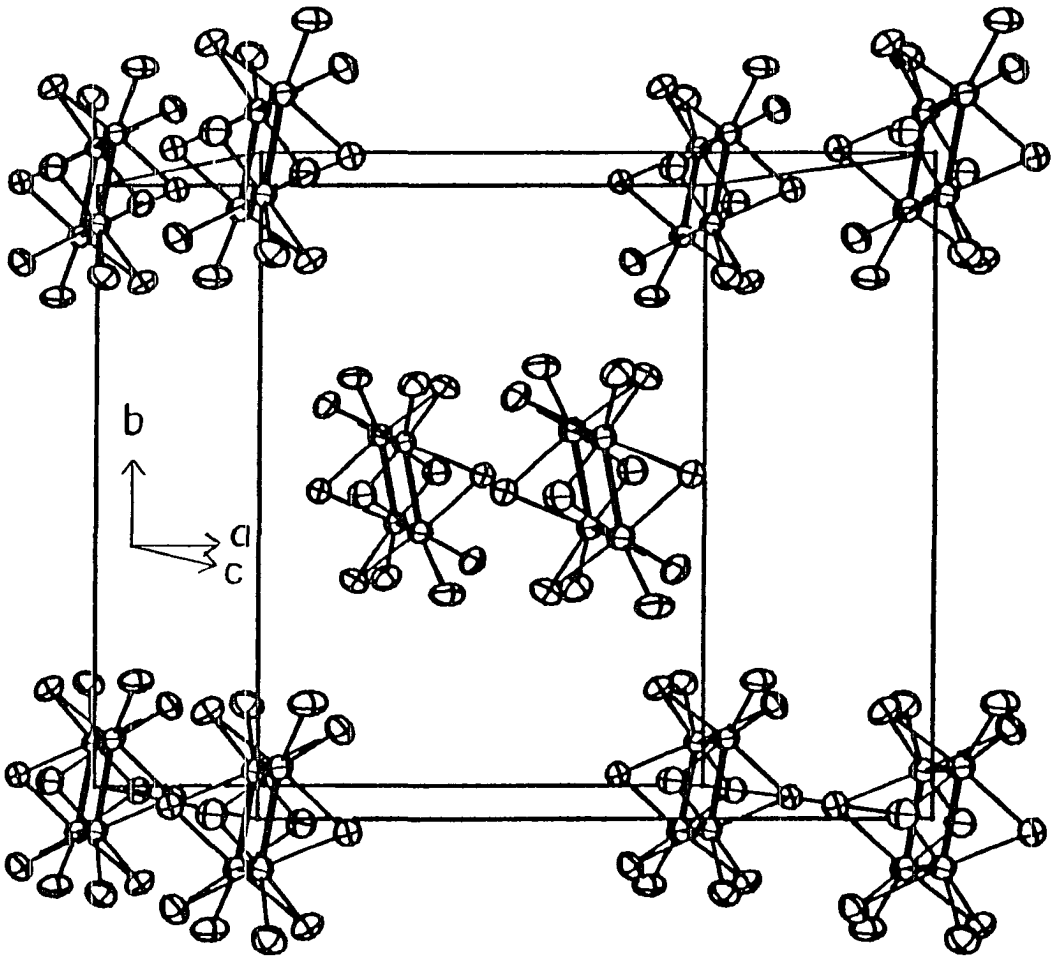

Figure II-10. Unit cell of $[\emptyset_4As]_2[Et_4N]Mo_4Cl_{12}\cdot 2\ CH_2Cl_2$ showing the packing of cluster units in the cell

Cl(4), and Cl(4'). The cluster unit has C_{2v} symmetry. A C_2 axis passes through the midpoint of the bond between the two molybdenum atoms forming the backbone of the butterfly and the midpoint of a line connecting the two wingtip molybdenum atoms. There are two unique molybdenum atoms and six unique chlorine atoms in the cluster unit, the remainder of the cluster atoms are defined by the C_2 axis. Bond distances and angles are tabulated in Tables II-37, II-38, II-39, and II-40.

The butterfly cluster has five metal-metal bonds, compared to only four in the planar cluster. Three of the bonds are unique, the other two are related by the C_2 axis.

The distance across the backbone of the butterfly (Mo(1)-Mo(1')) is 2.595(4) Å. The two distances from the backbone molybdenum to the apex molybdenum are 2.501(3) and 2.521(3) Å. In addition, the distance between the two apex molybdenum atoms is 3.388(4) Å, precluding any bonding between these atoms. This distance is greater than that found in $Mo_4(OPr^i)_8Br_4$ [3.287 Å (24)] or $(Bu_4N)_2Mo_4I_{11}$ [(3.305 Å (21)]. The average bonding distances for the remaining five bonds in the cluster unit are relatively the same (2.50 Å for $Mo_4(OPr^i)_8Br_4$, 2.57 Å for $(Bu_4N)_2Mo_4I_{11}$, and 2.53 Å for $[Et_4N]_3Mo_4Cl_{12}$).

The two triangular faces of the butterfly cluster form a dihedral angle of 104°, larger when compared to 88.9° for

$(Bu_4N)_2Mo_4I_{11}$ and 81.60° for $Mo_4(OPr^i)_8Br_4$, as might be expected from the apex-apex distance for these compounds.

There are six terminal chlorines in the cluster unit. Four of them (Cl(5), Cl(6), Cl(5'), and Cl(6')) extend perpendicular from the face of the cube where the molybdenum to which they are bound resides. In addition, a terminal chlorine (Cl(4)) is bound to each apical molybdenum atom which forms part of the cubic arrangement of chlorine atoms. There are four doubly bridging chlorine atoms (Cl(1), Cl(3), Cl(1'), and Cl(3')) which bridge each of the four waist to apex bonds in the cluster. There are also two triply bridging chlorine atoms (Cl(2) and Cl(2')) which are located above the two triangular faces formed by the molybdenum atoms.

The Mo-Cl distances are similar to those observed in other clusters for their respective mode of bonding (23), with the exception of two of the distances. The bond between the apex molybdenum (Mo(2)) and the terminal chlorine in the cube (Cl(4)) is unusually short (2.33 A) while the distance between Mo(2) and the triply bridging chlorine (which is trans to Cl(4)) is unusually long (2.56 A). This is attributed to pi bonding between the terminal Cl and the apical molybdenum; such pi bonding is not possible for the triply bridging chlorine atom because orbitals which would be required for pi bonding are already

Table II-37. Interatomic distances (Å) for cluster atoms in $[Et_4N]_3Mo_4Cl_{12}$[a,b]

cluster distances		chlorine-chlorine contacts	
Mo(1)-Mo(2)	2.501(3)	Cl(1)-Cl(2)	3.514(1)
Mo(1)-Mo(1)	2.595(4)	Cl(1)-Cl(3)	3.419(1)
Mo(2)-Mo(2)	3.388(4)	Cl(1)-Cl(4)	3.423(1)
Mo(1)-Mo(2)	2.521(3)	Cl(1)-Cl(5)	3.516(1)
Mo(1)-Cl(1)	2.428(6)	Cl(1)-Cl(6)	3.476(1)
Mo(1)-Cl(2)	2.480(6)	Cl(2)-Cl(2)	3.422(1)
Mo(1)-Cl(3)	2.430(6)	Cl(2)-Cl(5)	3.441(1)
Mo(1)-Cl(6)	2.486(6)	Cl(2)-Cl(3)	3.531(1)
Mo(1)-Cl(2)	2.487(6)	Cl(2)-Cl(6)	3.599(1)
Mo(2)-Cl(1)	2.464(5)	Cl(2)-Cl(6)	3.621(1)
Mo(2)-Cl(2)	2.535(5)	Cl(3)-Cl(5)	3.405(1)
Mo(2)-Cl(3)	2.453(6)	Cl(3)-Cl(4)	3.414(1)
Mo(2)-Cl(4)	2.330(6)	Cl(3)-Cl(6)	3.452(1)
Mo(2)-Cl(5)	2.453(6)	Cl(4)-Cl(4)	3.340(1)
		Cl(4)-Cl(5)	3.493(1)

[a]Estimated standard deviations are given in parentheses for last significant figures.

[b]Atom labels refer to Figure II-3.

Table II-38. Bond angles (deg) for cluster atoms in $[Et_4N]_3Mo_4Cl_{12}$[a,b]

Mo(1)-Mo(1)-Mo(2)	59.27(8)	Mo(1)-Cl(1)-Mo(2)	62.2(1)
Mo(1)-Mo(1)-Mo(2)	58.51(8)	Mo(1)-Cl(2)-Mo(2)	59.3(1)
Mo(2)-Mo(1)-Mo(2)	84.82(9)	Mo(1)-Cl(2)-Mo(2)	59.8(1)
Mo(1)-Mo(2)-Mo(1)	62.22(9)	Mo(1)-Cl(2)-Mo(1)	63.0(1)
Mo(1)-Mo(2)-Mo(2)	47.34(6)	Mo(1)-Cl(3)-Mo(2)	61.6(1)
Mo(1)-Mo(1)-Cl(1)	118.17(7)	Mo(1)-Mo(2)-Cl(2)	58.5(1)
Mo(1)-Mo(1)-Cl(2)	58.6(1)	Mo(1)-Mo(2)-Cl(4)	121.5(2)
Mo(1)-Mo(1)-Cl(2)	58.36(5)	Mo(1)-Mo(2)-Cl(2)	58.4(1)
Mo(1)-Mo(1)-Cl(3)	118.95(6)	Mo(1)-Mo(2)-Cl(4)	121.3(2)
Mo(1)-Mo(1)-Cl(6)	138.3(1)	Mo(2)-Mo(2)-Cl(1)	89.9(2)
Mo(2)-Mo(1)-Cl(1)	116.3(1)	Mo(2)-Mo(2)-Cl(3)	90.8(2)
Mo(2)-Mo(1)-Cl(2)	62.1(4)	Mo(2)-Mo(2)-Cl(5)	176.5(2)
Mo(2)-Mo(1)-Cl(2)	117.6(2)	Cl(1)-Mo(2)-Cl(3)	177.7(2)
Mo(2)-Mo(1)-Cl(3)	59.7(1)	Cl(1)-Mo(2)-Cl(5)	91.3(2)
Mo(2)-Mo(1)-Cl(6)	137.00(2)	Cl(2)-Mo(2)-Cl(4)	179.7(2)
Mo(2)-Mo(1)-Cl(1)	59.7(1)	Cl(2)-Mo(2)-Cl(5)	86.4(2)
Mo(2)-Mo(1)-Cl(2)	117.1(2)	Cl(3)-Mo(2)-Cl(4)	91.0(2)
Mo(2)-Mo(1)-Cl(2)	61.8(1)	Cl(3)-Mo(2)-Cl(5)	87.9(2)
Mo(2)-Mo(1)-Cl(3)	116.5(2)	Cl(4)-Mo(2)-Cl(5)	93.8(2)
Mo(2)-Mo(1)-Cl(6)	137.9(2)	Mo(1)-Cl(1)-Cl(4)	90.8(2)
Cl(1)-Mo(1)-Cl(2)	176.8(2)	Mo(1)-Cl(1)-Cl(6)	45.7(2)
Cl(1)-Mo(1)-Cl(2)	91.4(2)	Mo(2)-Cl(1)-Cl(3)	89.9(2)
Cl(1)-Mo(1)-Cl(3)	89.5(2)	Mo(1)-Cl(2)-Mo(1)	63.0(2)
Cl(1)-Mo(1)-Cl(6)	90.0(2)	Mo(1)-Cl(2)-Mo(2)	59.3(1)
Cl(2)-Mo(1)-Cl(3)	92.0(2)	Mo(1)-Cl(2)-Cl(1)	90.2(2)
Cl(2)-Mo(1)-Cl(6)	92.9(2)	Cl(1)-Cl(3)-Cl(2)	89.8(2)
Cl(2)-Mo(1)-Cl(3)	177.2(2)	Cl(1)-Cl(3)-Cl(4)	89.2(2)
Cl(2)-Mo(1)-Cl(6)	93.5(2)	Mo(2)-Cl(4)-Cl(4)	90.6(1)
Cl(3)-Mo(1)-Cl(6)	89.2(2)	Cl(1)-Cl(4)-Cl(4)	90.3(2)
Cl(1)-Cl(5)-Cl(3)	90.6(2)		
Cl(2)-Cl(6)-Cl(3)	88.0(2)		

[a]Estimated standard deviations are given in parentheses for last significant figures.

[b]Atom labels refer to Figure II-3.

Table II-39. Interatomic distances (Å) for cations in $[Et_4N]_3Mo_4Cl_{12}$[a]

N(1)-C(11)	1.51(3)
N(1)-C(12)	2.56(3)
C(11)-C(12)	1.50(4)
N(2)-C(21)	1.533(0)
N(2)-C(23)	1.641(1)
C(21)-C(22)	1.45(1)
C(23)-C(24)	1.47(0)
N(3)-C(31)	1.69(5)
N(3)-C(31A)	1.62(4)
N(3)-C(32)	1.48(4)
N(3)-C(32A)	1.78(5)
C(31)-C(33)	1.67(8)
C(31A)-C(34)	1.54(5)
C(32)-C(34)	1.54(5)
C(32A)-C(33	1.61(7)
N(4)-C(41)	1.647(1)
C(41)-C(42)	1.59(3)

[a]Estimated standard deviations are given in parentheses for last significant figures.

Table II-40. Bond angles (deg) for cations in $[Et_4N]_3Mo_4Cl_{12}$[a]

C(11)-N(1)-C(11)	105.(2)	N(3)-C(31)-C(33)	104.(4)
C(11)-N(1)-C(11)	112.(1)	N(3)-C(31A)-C(34)	110.(3)
N(1)-C(11)-C(12)	117.(2)	N(3)-C(32)-C(34)	119.(3)
C(21)-N(2)-C(23)	101.(1)	N(3)-C(32A)-C(33)	102.(3)
C(21)-N(2)-C(23)	83.(0)	C(41)-N(4)-C(41)	97.(4)
N(2)-C(21)-C(22)	107.(1)	C(41)-N(4)-C(41)	118.(2)
N(2)-C(23)-C(24)	116.(1)	C(41)-N(4)-C(41)	113.(2)
C(31)-N(3)-C(31A)	106.(2)	N(4)-C(41)-C(42)	106.(1)
C(31)-N(3)-C(32)	112.(2)		
C(31)-N(3)-C(32A)	105.(3)		
C(31A-N(3)-C(32A)	103.(2)		
C(31A)-N(3)-C(32)	115.(2)		
C(32)-N(3)-C(32A)	113.(3)		

[a]Estimated standard deviations are given in parentheses for last significant figures.

involved in bonding to the waist molybdenum atoms.

The coordination number of the wingtip molybdenum atoms is seven and is eight for the backbone molybdenum atoms. Both types of molybdenum are square pyramidal with respect to chlorine coordination. Each of the wingtip molybdenum atoms are bound to both backbone molybdenum atoms. The backbone molybdenum atoms are bound to each other as well as to both apical molybdenum atoms which increases their coordination by one.

$[Et_4N]_3Mo_4Cl_{12}$ is structurally related to both $Mo_4(OPr^i)_8Br_4$ (24) and $(Bu_4N)_2Mo_4I_{11}$ (21). $Mo_4(OPr^i)_8Br_4$ is isostructural except that the isopropoxide groups form the cubic arrangement of ligands in which the cluster atoms are found. The four bromine atoms are terminally coordinated perpendicular to the cube faces in a similar fashion to that observed for the <u>exo</u> terminal chlorines in $[Et_4N]_3Mo_4Cl_{12}$.

$Mo_4I_{11}^{2-}$ has the same butterfly geometry for the metal atoms in the cluster but the cubic arrangement of ligands has been altered. Considering both as haloanions, $Mo_4X_{12}^{3-}$, and $Mo_4X_{11}^{2-}$, the latter is derived from the former by loss of X^- from the inner positions of the Mo_4X_{12} cluster $[(Mo_4X_8)X_4^{3-} \longrightarrow (Mo_4X_7)X_4^{2-} + X^-]$. The net result is that two halides on adjacent corners of the cube are displaced by a single halide at the midpoint of one edge such that this halide then bridges the molybdenum atoms

forming the wingtips of the butterfly. Presumably, alleviation of steric strain in the hypothetical $Mo_4I_{12}^{3-}$ causes loss of iodine and stabilization of the $Mo_4I_{11}^{2-}$ unit. The steric strain is not as critical when the cube is comprised of chlorine atoms because their steric requirements are much less than that of iodine atoms.

The packing of the butterfly clusters into the unit cell is shown in Figure II-11. Evident is the $\bar{4}$ axis of the crystal lattice.

Physical Measurements

Infrared spectra

The infrared spectra of compounds containing the planar clusters, I and II, are essentially identical in the region 200-400 cm^{-1} (Table II-41). The spectra are characterized by two sets of bands split above and below 300 cm^{-1} (illustrated by the far-infrared spectrum of II, Figure II-12). These spectra are also identical to the infrared spectrum of the mixed salt, $[\emptyset_4As]_x[Et_4N]_yMo_4Cl_{12}$, which was oxidized by addition of one mole of DCPI. Infrared spectra which have these bands are therefore indicative of the planar $Mo_4Cl_{12}^{3-}$ cluster anion.

Interpretation of the spectra of the different oxidations of $[Et_4N]_4Mo_4Cl_{12}$ are more complicated. One

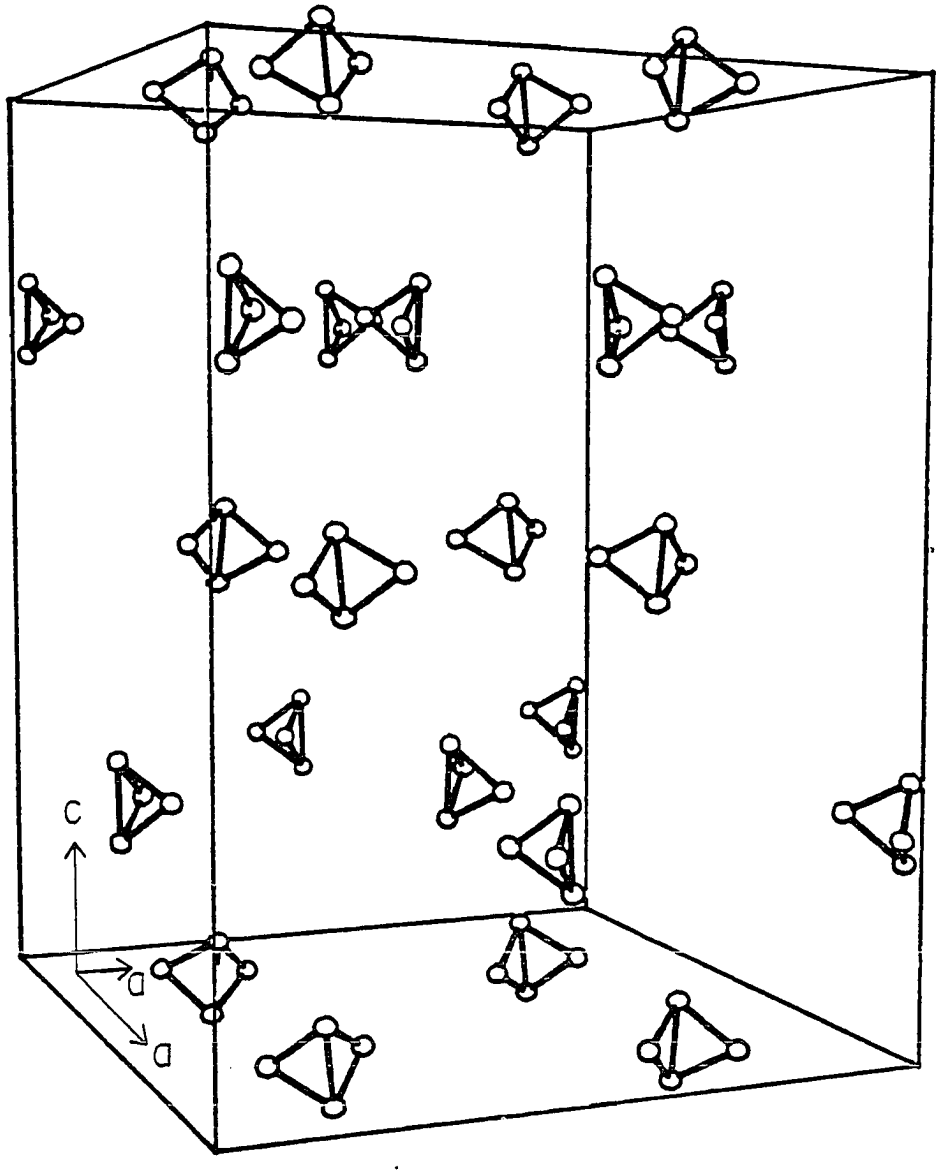

Figure II-11. Unit cell of $[Et_4N]_3Mo_4Cl_{12}$ showing the packing of cluster units in the cell

hindrance is that separation of the oxidized product from starting material is difficult because both are very insoluble in the solvents used. Thus, one is never quite sure that a pure product is obtained.

These compounds can be divided into two types based upon their infrared spectra (Table II-42). The differences in the spectra are shown in Figure II-13.

The spectra of the type A compounds are those of the planar 3- clusters whose data are listed in Table II-41, indicating that they adopt the same structure. These spectra were obtained on products of reaction 10 where x=1/2.

$$[Et_4N]_4Mo_4Cl_{12} + x/2\ I_2 \xrightarrow[Cl_2,\ DCPI]{} [Et_4N]_{4-x}Mo_4Cl_{12} \qquad 10$$

If x is greater than 1 the spectra of the type B clusters are obtained, typified by the strong bands at 366 cm^{-1} and 300 cm^{-1}, which are conspicuously absent in the spectra of type A compounds.

The largest problem associated with analysis of the infrared spectra obtained for these compounds is that most of the spectra appear to contain bands of both types. One possibility for the appearance of the two types of infrared spectra could be that two different geometric isomers are

Table II-41. Far-infrared spectra (400-200 cm^{-1}) of planar cluster compounds[a]

$[\emptyset_4P]_3Mo_4Cl_{12}$	$[Pr_4N]_3Mo_4Cl_{12}$	$[\emptyset_4As]_x[Et_4N]_xMo_4Cl_{12}$
349(s)	349(s)	346(s)
332(w)	335(w)	331(w)
328(w)		
324(w)	321(w)	321(w)
271(s)	273(s)	272(s)
254(m)	250(sh)	
245(s)	246(s)	248(s)
228(w)	223(sh)	
208(m)	215(m)	214(m)
203(m)	202(sh)	

[a] s-short, m-medium, w-weak, sh-shoulder.

Table II-42. Infrared spectra of type A and B clusters[a,b]

type A	type B
	366(s)
349-345(s)	347(m)
331-335(w)	
321-324(w)	
	300(s)
273(s)	272(m)
245-254(s)	251(w)
208-215(m)	

[a] Absorbtion in cm^{-1}.

[b] s,strong; m, medium; w,weak.

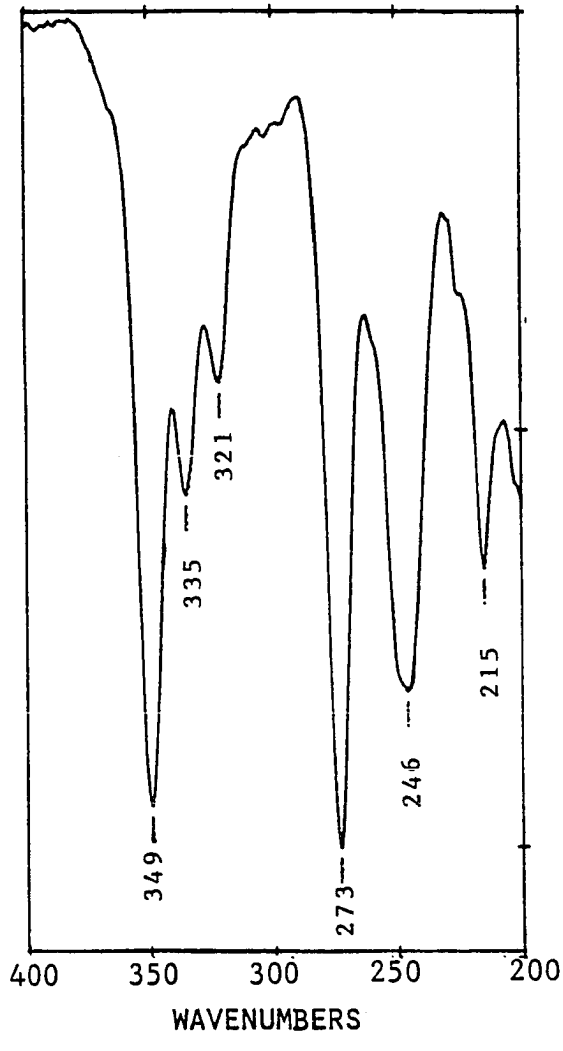

Figure II-12. Far-infrared spectrum of $[Pr_4N]_3Mo_4Cl_{12}\cdot 0.7\ C_2H_4Cl_2$ from 400-200 cm^{-1}

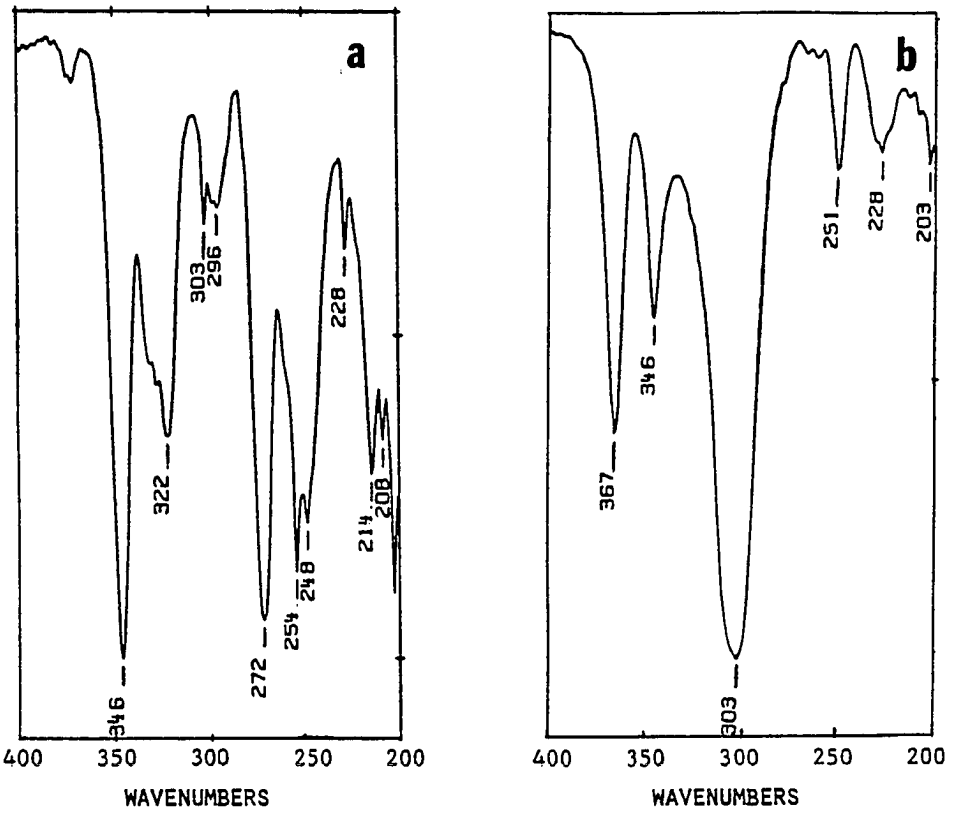

Figure II-13. Far-infrared spectra (cm^{-1}) of a) type A and b) type B cluster compounds of $[Et_4N]_3Mo_4Cl_{12}$

present. Alternatively, the differences in the spectra could be due to a mixture of clusters in different oxidation states. Formation of an insoluble tetraethylammonium salt of the compound with the Mo_6Cl_{17} stoichiometry could also be responsible for the difficulties in obtaining clean spectra. These data corroborate the fact that $[Et_4N]_3Mo_4Cl_{12}$ is extremely difficult to synthesize in pure form, as evidenced also by difficulties in obtaining satisfactory analytical data for this material. Since the compound containing the butterfly cluster has probably never been prepared in pure form it is not possible to differentiate between these possibilities.

The compounds with the composition $R_xMo_6Cl_{17}$ further confuse the interpretation. The stoichiometry suggests that the anions of $(\emptyset_4P)^+$ and $(Pr_4N)^+$ salts are similar. The far-infrared spectra for the two salts are very different. $[\emptyset_4P]_{4.5}Mo_6Cl_{17}$ gives an infrared spectrum with a large band at 304 cm^{-1} with shoulders on both sides. Additional bands are seen at 365 cm^{-1} and 338 cm^{-1}. The spectrum is very similar to that of the type B compounds of $[Et_4N]_3Mo_4Cl_{12}$, although the bands in this spectrum have different relative intensities (Figure II-14a).

In contrast, the spectrum of $[Pr_4N]_4Mo_6Cl_{17}$, shown in Figure II-14b, is identical to that of the planar clusters of $Mo_4Cl_{12}^{3-}$ with absorptions at 349, 333, 320, 280, 273,

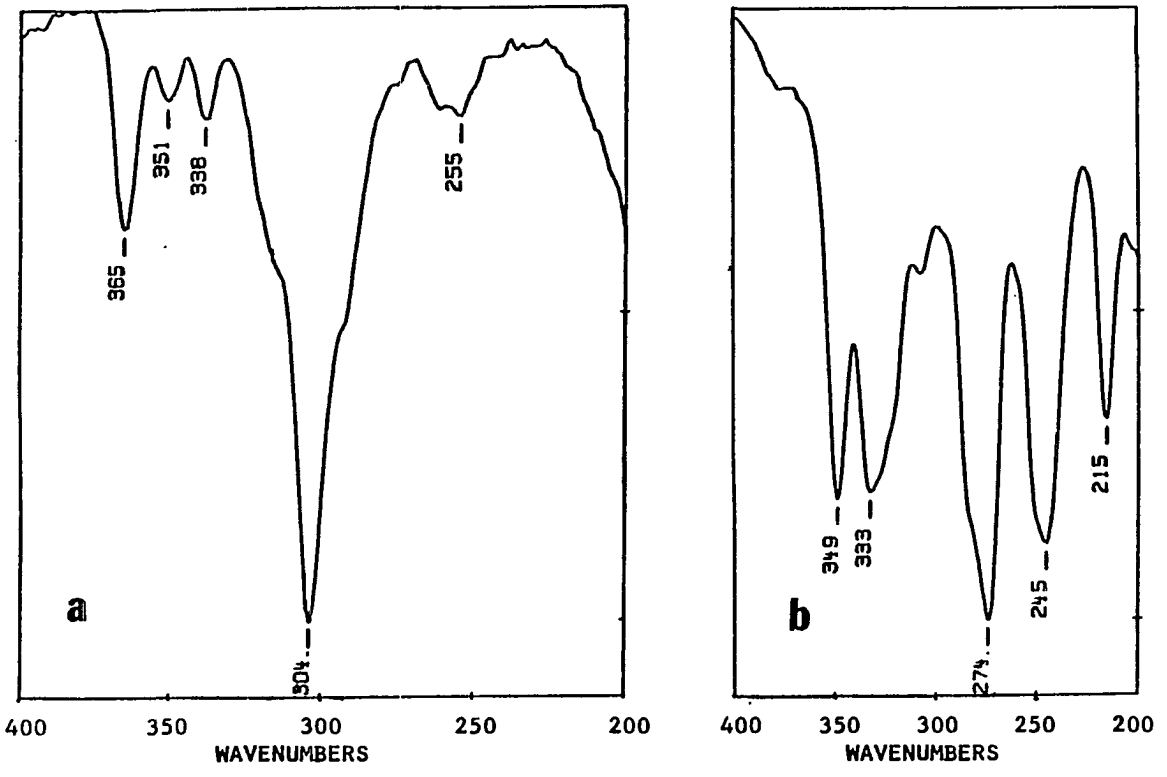

Figure II-14. Far-infrared spectra (cm^{-1}) of
a) $[\emptyset_4P]_{4.5}Mo_6Cl_{17}$ and b) $[Pr_4N]_4Mo_6Cl_{17}$

245, and 215 cm^{-1}.

X-ray photoelectron spectroscopy

Chlorine 2p x-ray photoelectron spectra were obtained for I and II. Broad peaks indicated that more than one type of chlorine atom was present in each compound. These spectra were resolved into their components using the APES (analyzed photoelectron spectra) algorithm (25). Spectral parameters for the compounds are listed in Table II-43 and the spectra, showing the resolved components, the sum of the resolved components and the fit to the observed data are given in Figures II-15 and II-16.

A number of fits were attempted varying the ratios of bridging to terminal chlorines, full widths at half maximums (FWHM), energy of spin orbit splitting, and the fraction of the curve which was Gaussian versus that which was Lorentzian.

While the shape of the curves for the observed data differs for the two compounds, both curves can be fit to clusters with a ratio of two bridging to one terminal chlorine. Differences in the observed data arise because of other components in the sample.

There is free $\emptyset_4PCl$ contaminating the sample of $[\emptyset_4P]_3Mo_4Cl_{12}\cdot 0.5\ \emptyset_4PI$ which we have been unable to separate due to the similar solubility of the two compounds.

Table II-43. X-ray photoelectron spectral data for $Mo_4Cl_{12}^{3-}$ compounds

Compound	type of Cl[a]	energy[b]	FWHM[b]	Rel. Area	ΔE[b]
$[\emptyset_4P]_3Mo_4Cl_{12}$[c]	2b	199.18	1.35	2	0.92
	terminal	198.26	1.35	1	0.69
	ionic	197.57	1.35	1.2	
$[Pr_4N]_3Mo_4Cl_{12}$	covalent	200.19	1.30	1	1.12
	2b	199.07	1.30	4	0.75
	terminal	198.32	1.30	2	

[a] 2b-doubly bridging.
[b] eV.
[c] Fraction Gaussian was fixed at 0.65.

The additional ionic chloride accounts for remaining area under the peak not accounted for by the cluster. The data are in agreement with a fitted ratio of 2 doubly bridging : 1 terminal : 1.2 ionic chlorine atoms. This amount of ionic chloride is not possible since only one mole of $\emptyset_4PCl$ can be present from the reaction stoichiometry. The unusually high values obtained from this fitting are probably due to the insensitivy of the curve fitting routines for the amount of ionic chlorine in the sample.

The values for the binding energy of the bridging chlorides are approximately 0.5 eV lower than that of similar molybdenum chloride compounds which have been measured, however the binding energy of the terminal chlorides is in excellent agreement (Table II-44).

In addition to the doubly bridging and terminal chloride listed in Table II-43, $[Pr_4N]_3Mo_4Cl_{12}\cdot 0.7\ C_2H_4Cl_2$ also has an additional type of chloride. The organic solvent molecule has chlorine atoms covalently bonded to carbon atoms. The binding energy of the 2p core electrons for this chlorine is higher than that for either of the cluster chloride ligands. The slightly higher binding energy of 200.2 eV is in agreement with that found for other chlorine atoms covalently bonded to carbon atoms (the binding energy for chlorine in polyvinyl chloride is 200. eV

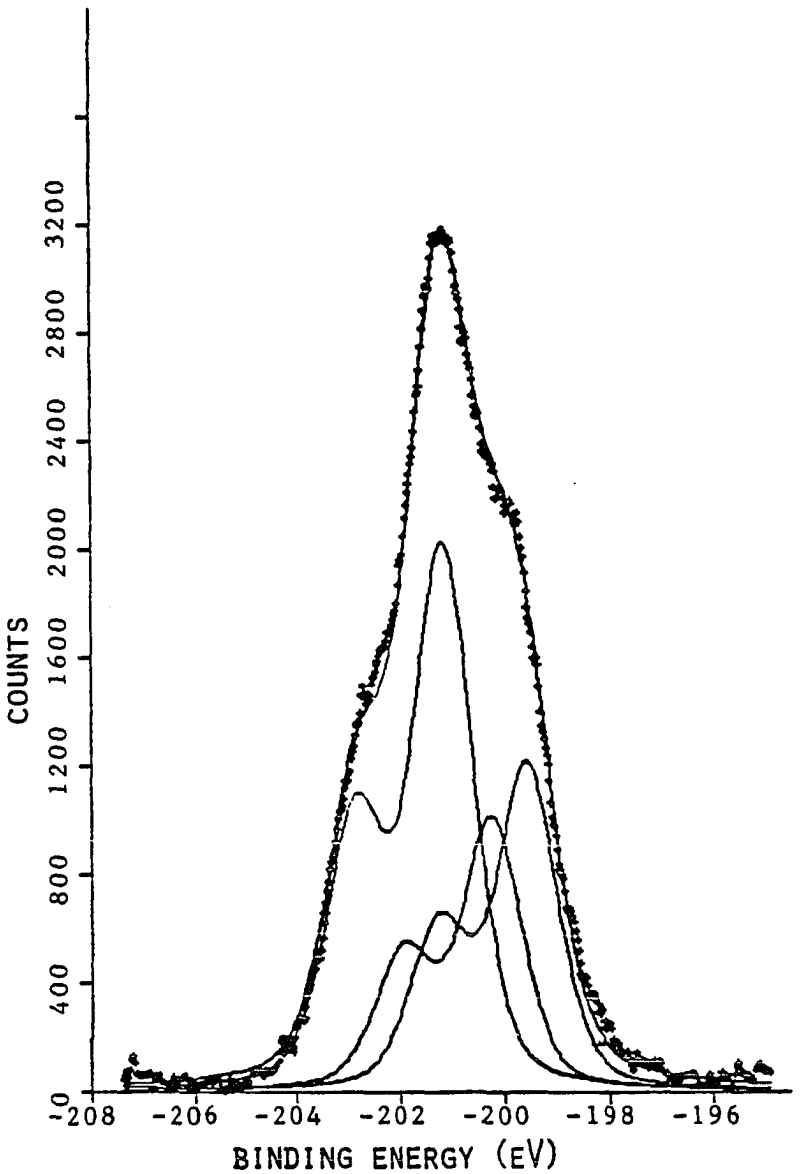

Figure II-15. Cl 2p x-ray photoelectron spectrum of $[\emptyset_4P]_3Mo_4Cl_{12}\cdot 0.5\ \emptyset_4PI$. The sum of the resolved components is given by the line through the experimental data points (+)

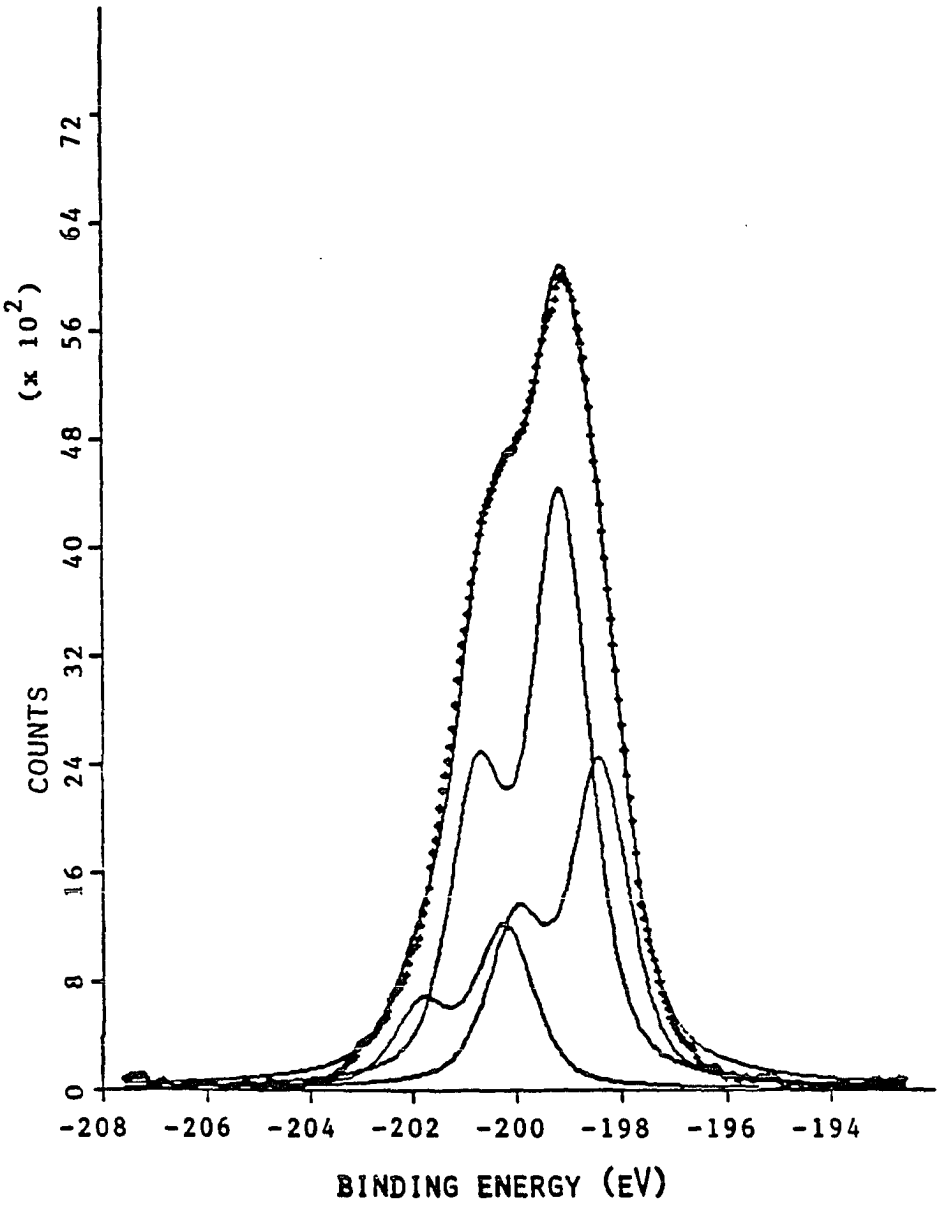

Figure II-16. Cl 2p x-ray photoelectron spectrum of $[Pr_4N]_3Mo_4Cl_{12}\cdot 0.7\ C_2H_4Cl_2$. The sum of the resolved components is given by the line through the experimental data points (+)

Table II-44. Comparison of Cl 2p binding energies for several cluster compounds

compound	binding energy[a]		
	double bridge	terminal	FWHM[b]
β-$MoCl_2$[c]	199.7	--	1.44
$Mo_4Cl_8[P\text{-}n\text{-}bu_3]_4$[d]	199.6	198.3	1.20[e]
$[Bu_4N]Mo_5Cl_{13}$[c]	199.8	198.3	1.03[e]
$[\emptyset_4P]_3Mo_4Cl_{12}\cdot 0.5\ \emptyset_4PI$[f]	199.2	198.3	1.35
$[Pr_4N]_3Mo_4Cl_{12}.0.7C_2H_4Cl_2$[f]	199.1	198.3	1.30
$[Et_4N]_4Mo_4Cl_{12}$[g]	198.6	197.7	1.33

[a]Energy given in eV for 3/2 spin orbit peak.
[b]Full width at half maximum (eV).
[c]Reference 26.
[d]Reference 15.
[e]Monochromatic radiation used.
[f]This work.
[g]Reference 1.

while that for chlorobenzene is 201. eV) (27).

The best fit to the observed data for II occurs when the ratios of the component chlorines are held in a fixed ratio of 4 double bridging : 2 terminal : 1 covalent organic. This is in very good agreement with the chemical

formula from the structural and analytical data, although the amount of chlorine due to the solvent molecule is slightly high in this fit.

Magnetic susceptibility

Electron spin resonance experiments have shown I and III to be paramagnetic. The magnetic susceptibility data, collected for these compounds from 4^{o} to 380^{o} K, supported this fact and demonstrated an inverse temperature dependence.

The apparent susceptibility per gram was converted to molar susceptibility. Simple Curie law states that

$$\chi_M = C/T + \chi_D + \chi_{TIP} \qquad 11$$

where χ_D is the diamagnetic contribution of the paired core electrons and χ_{TIP} is a temperature independent contribution due to a mixing of excited states into the ground state.

Corrections were made for the core diamagnetism of atoms in the compound by summing the core contribution for each atom and subtracting this quantity from the apparent molar susceptibility to give the corrected molar susceptibility (χ_{MC}) and eq. 12. Values for the core diamagnetism of the nonmetal substituent atoms were those of Figgis and Lewis (28) and for molybdenum the value for Mo^{2+} were those of Selwood (29).

$$\chi_{MC} = C/T + \chi_{TIP} \qquad 12$$

The plot of χ_{MC} versus 1/T was linear for these compounds showing that the Curie law was obeyed, eq. 12 (Figure II-17). The slope of the graphed line (C) is related to the effective magnetic moment, μ, of the cluster by the relation

$$C = N \beta^2 \mu_{eff}^2 / 3k \qquad 13$$

where N is Avagadro's number (6.02×10^{23}), β is the Bohr magneton (9.27×10^{-21} erg/gauss) and k is the Boltzmann constant (1.381×10^{-16} erg/deg). The y intercept of this graph is the value of the temperature independent paramagnetic susceptibility. The values for the data are shown in Table II-45.

These values for the effective magnetic moment agree very well with the assessment of one unpaired electron per cluster unit. The spin only value for the magnetic moment, $\mu=S(S+1)$, is calculated to be 1.73 BM for one unpaired electron. The value for II is in exact agreement, and the value for I is slightly low but still in very good agreement. One might expect the latter value to be somewhat low because this compound is contaminated with a small amount of $\emptyset_4PCl$.

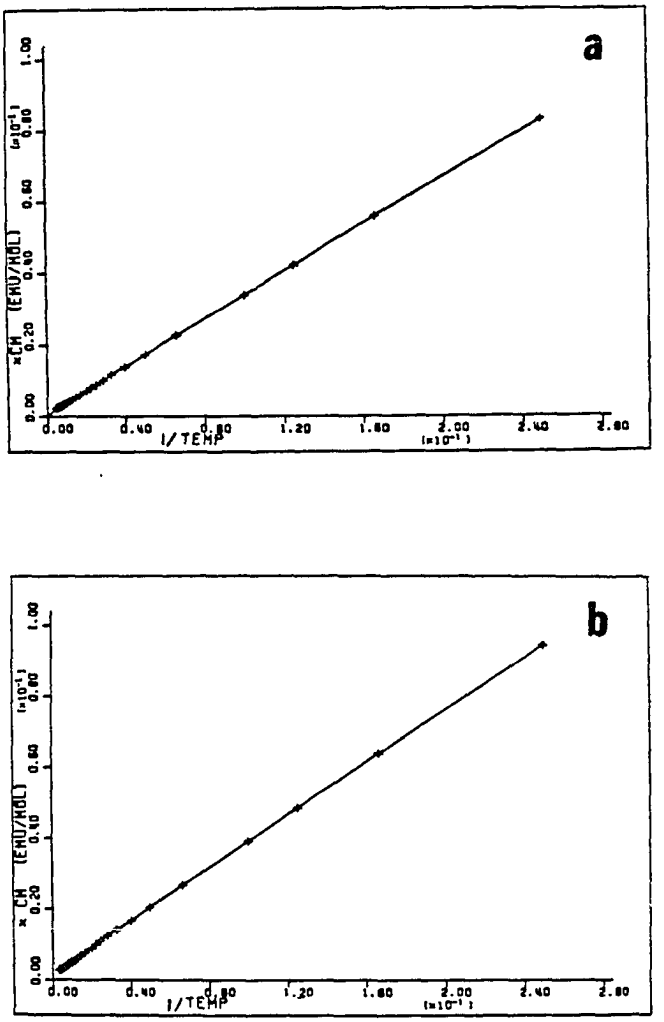

Figure II-17. Magnetic susceptibility [chi(emu/mol) vs 1/T] of a) $[\emptyset_4P]_3Mo_4Cl_{12}\cdot 0.5\ \emptyset_4PI$ and b) $[Pr_4N]_3Mo_4Cl_{12}\cdot 0.7\ C_2H_4Cl_2$

Table II-45. Magnetic susceptibility data for $[\emptyset_4P]_3Mo_4Cl_{12}\cdot 0.5\ \emptyset_4PI$ and $[Pr_4N]_3Mo_4Cl_{12}\cdot 0.7\ C_2H_4Cl_2$

Compound	R[a]	C[b]	μ_{eff}(B.M)	χ_{TIP} emu/mol
$[\emptyset_4P]_3Mo_4Cl_{12}$	0.99996	0.3301	1.63	760 x 10^{-6}
$[Pr_4N]_3Mo_4Cl_{12}$	0.99994	0.3744	1.73	1390 x 10^{-6}

[a]Correlation coefficient from least squares fit of equation 12 to a straight line.

[b]From equations 12 and 13.

The values for the temperature independent paramagnetism (TIP) are large. In studies of hexanuclear niobium and tantalum systems these values are on the order of 300-700 x 10^{-6} emu/mole (30, 31). Here, they are larger in magnitude than that. The reasons for the unusually large temperature independent paramagnetism are not known, however they arise from coupling of excited paramagnetic states into the ground state. The magnitude of the TIP is inversely dependent on the energy difference between the coupled ground and excited states (30), thus this suggests that excited states exist which are energetically very close to the ground state for these cluster compounds.

Electron paramagnetic resonance

The electron paramagnetic resonance spectra were obtained for several of the salts of the $Mo_4Cl_{12}^{3-}$ cluster anion. It was hoped that these spectra would aid in distinguishing between the planar and butterfly forms of the cluster anion. Table II-46 summarizes the paramagnetic resonance data for the various samples.

Spectra were obtained on finely ground powders of I and II known to be the planar anions, at room temperature. The spectra were identical, showing a broad nearly isotropic signal at room temperature. At 77 K, the signal showed more resolution, exhibiting an axial signal (Figure II-18). Since an axial signal is not required by the symmetry known for these compounds, the observed signal is probably anisotropic with two of the g values nearly equivalent resulting in a spectrum that appears axial.

The spectrum of bulk $[Et_4N]_3Mo_4Cl_{12}$ was identical to the spectra of the planar cluster anions, suggesting that it can adopt the planar configuration as well (Figure II-18).

The g values for these signals (~1.99-2.00) are very close to the value for a free electron indicating, not unexpectedly, that the unpaired electron is delocalized over the cluster unit. This is also in support of the magnetic susceptibility data where the g value calculated from the magnetic moment is also ~2.

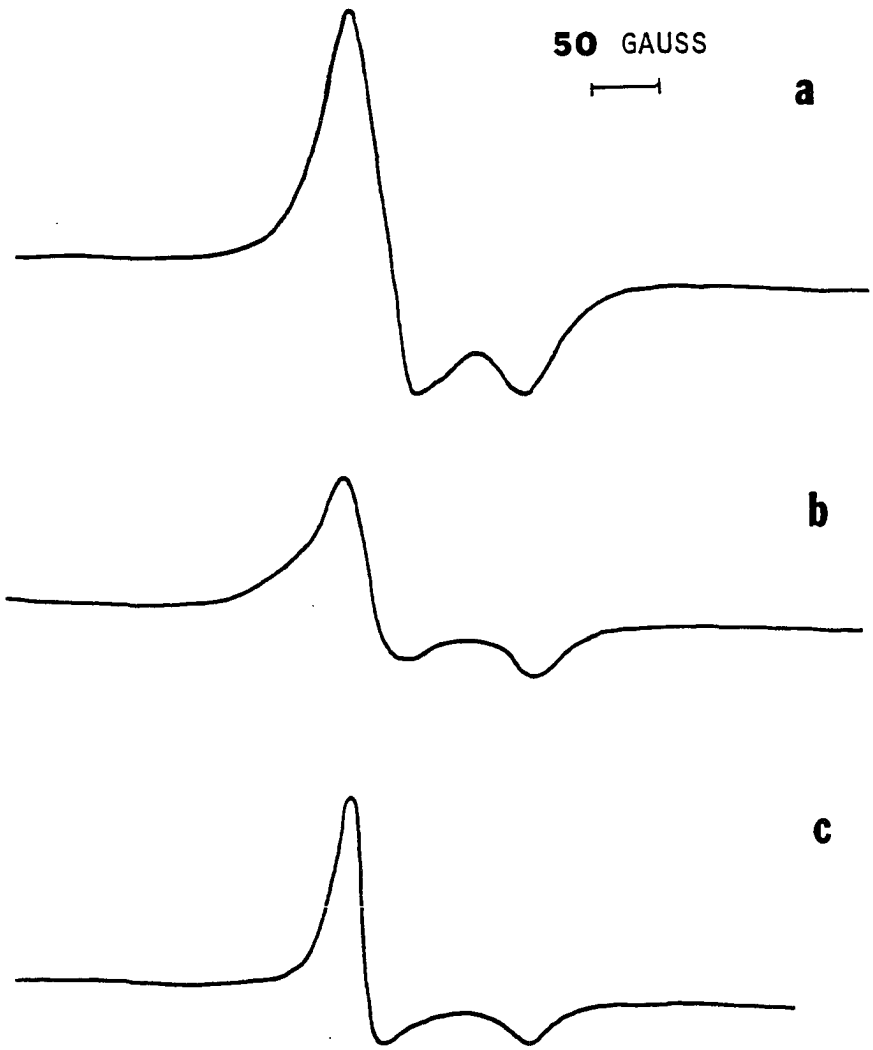

Figure II-18. Electron paramagnetic resonance spectra of
a) $[Pr_4N]_3Mo_4Cl_{12}\cdot 0.7\ C_2H_4Cl_2$
b) $[\emptyset_4P]_3Mo_4Cl_{12}\cdot 0.5\ \emptyset_4PI$ and
c) $[Et_4N]_3Mo_4Cl_{12}$

Table II-46. Electron paramagnetic resonance of $[\emptyset_4P]_3Mo_4Cl_{12}\cdot 0.5\ \emptyset_4PI$ and $[Pr_4N]_3Mo_4Cl_{12}\cdot 0.7\ C_2H_4Cl_2$[a]

Compound	Temperature (K)	g[b]
$[\emptyset_4P]_3Mo_4Cl_{12}$	293	1.99
$[\emptyset_4P]_3Mo_4Cl_{12}$	100	2.002 1.935
$[Pr_4N]_3Mo_4Cl_{12}$	293	1.92
$[Pr_4N]_3Mo_4Cl_{12}$	100	1.993 1.935
$[Et_4N]_3Mo_4Cl_{12}$	4	2.004 1.935
$[\emptyset_4As]_2[Et_4N]Mo_4Cl_{12}$	4	2.005 1.932

[a]Spectra were obtained on ground powder samples.

[b]Where one g value is listed it is the g value for the psuedo-isotropic spectrum. When two are listed, the first is g perpendicular and the second is g parallel.

No hyperfine splitting was observed for any of the spectra, nor were any new signals observed when a magnetic field from 100-6900 gauss was scanned.

Attempted preparations of frozen glasses via addition of toluene to DCM and DCE solutions of the planar clusters were unsuccessful due to oiling and precipitation of the cluster compounds.

Cyclic voltammetry

The oxidation of $(R)_4Mo_4Cl_{12}$ compounds to $(R)_3Mo_4Cl_{12}$ piqued our curiosity concerning the possibility of oxidizing these clusters even further. Cyclic voltammetry experiments were performed, therefore, to investigate the nature of the oxidation and reduction of the $Mo_4Cl_{12}^{3-}$ clusters.

Due to its insolubility, $[Et_4N]_3Mo_4Cl_{12}$ was not an acceptable compound for these experiments. The use of $[\emptyset_4P]_3Mo_4Cl_{12}$ and $[Pr_4N]_3Mo_4Cl_{12}$ circumvented this problem. The experiments were carried out using apparatus previously described. The sample was placed in the electrochemical cell in the drybox and the cell openings were stoppered. The remaining operations were carried out under an argon flow to prevent oxygen from entering the cell.

Voltammograms were obtained varying the sweep width and scan rate. Steady state cyclic voltammograms were obtained after two or three cycles. Voltammograms were recorded both before and after the steady state was attained.

The cyclic voltammetry was illuminating for these two samples. Pertinent halfwave potentials and data are in Table II-47. Cyclic voltammograms, where the scan rate was varied from 20-500 mV/sec, were essentially identical for I and II.

Two reduction peaks were observed on the cathodic sweep. One, occurring at ~0.0 V corresponds to the reduction of a $Mo_4Cl_{12}^{2-}$ species to $Mo_4Cl_{12}^{3-}$. The other occurs at a more negative potential, appearing near -1.0 V during the cathodic sweep. This has been attributed to the reduction of $Mo_4Cl_{12}^{3-}$ to $Mo_4Cl_{12}^{4-}$.

The behavior during the anodic sweep is not clear. An oxidation occurs at ~0.2 V corresponding to a 2-/3- couple. A number of poorly defined oxidative peaks are seen from 0.0 to -1.5 V. This type of behavior is indicative of coupled chemical reactions or decomposition of the reduced species. These might be due to the presence of an undetermined impurity in the samples. It is also possible that these peaks are caused by the formation of the compound with the $R_xMo_6Cl_{17}$ stoichiometry observed with these salts.

The cyclic voltammogram for the 2-/3- couple of $[Pr_4N]_3Mo_4Cl_{12}$ at a scan rate of 20 mV/sec is shown in Figure II-19. For a completely reversible electrochemical reaction, the peak to peak (E_a-E_c) separation is 0.058/n eV (32). Here, the separation is 0.06 eV, identifying this as a one electron reaction. This couple is quasi-reversible as indicated by experiments which displayed increasing peak separation with increasing scan rate. The ratio of the current peaks is approximately equal to one, indicating the absence of concurrent reactions associated with this couple.

Closer examination of this voltammogram is instructive. Steady state is reached in two cycles. The voltammogram is initialized at E=0.0, I=0.0 and the potential is initially scanned in the negative direction. No cathodic peak is seen on the initial sweep because oxidized species which can be reduced at these potentials are not present. The anodic sweep generates the oxidized 2- species at the electrode which is then reduced on the subsequent cathodic sweep producing the observed cathodic peak.

The fact that the 2-/3- couple exists suggests that an $Mo_4Cl_{12}^{2-}$ cluster is synthetically possible, although these results do not give any indication of its stability. This has not yet been realized although work on this possibility is continuing.

The irreversibility of the 3-/4- couple is suggestive that some significant structural rearrangement occurs prior to oxidation of the $Mo_4Cl_{12}^{4-}$ cluster anion.

Visible Spectra

Visible spectra were obtained on DCE solutions of $[Pr_4N]_3Mo_4Cl_{12}$ and $[\emptyset_4P]_3Mo_4Cl_{12}$. The spectra are shown in Figure II-20. Relevant parameters are shown in Table II-48.

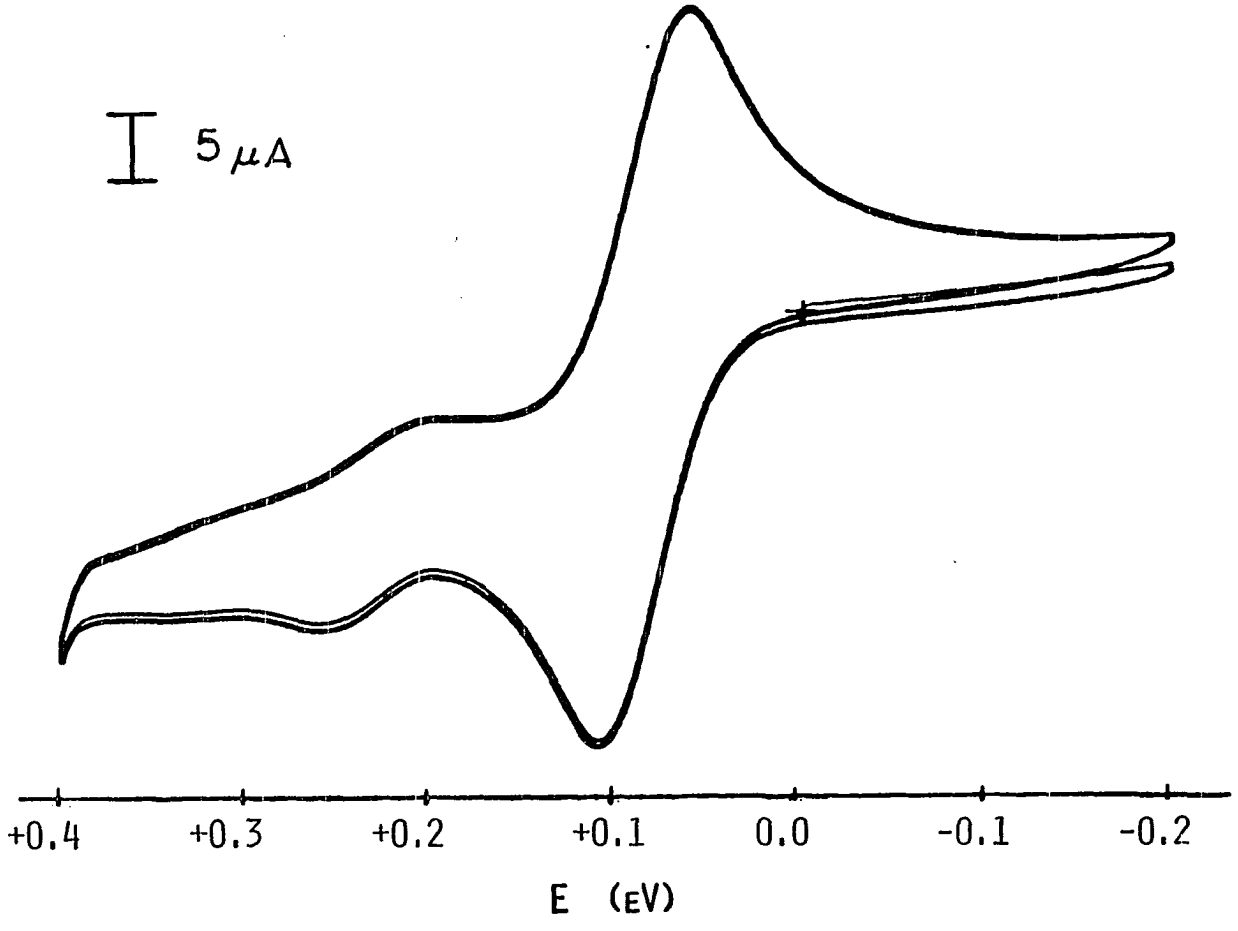

Figure II-19. Cyclic voltammogram of $2^-/3^-$ couple in $[Pr_4N]_3Mo_4Cl_{12}\cdot 0.7\ C_2H_4Cl_2$. Potentials are referenced to Ag/AgCl electrode

Table II-47. Cyclic voltammetry of $Mo_4Cl_{12}^{3-}$ clusters[a]

Compound	E_c 3-/4-[b,c]	$E_{1/2}$ 2-/3-[c]
$[\emptyset_4P]_3Mo_4Cl_{12}$	-0.82	+0.082
$[Pr_4N]_3Mo_4Cl_{12}$	-0.86	+0.085

[a]Potentials were measured in DCE and referenced to a Ag/AgCl reference electrode.

[b]Cathodic sweep peak potential, measured at 500 mV/sec scan rate.

[c]Volts.

Table II-48. Visible spectra of planar cluster compounds[a]

Compound	wavelength (nm)	$\varepsilon(M^{-1}cm^{-1})$
$[Pr_4N]_3Mo_4Cl_{12}$	390	2×10^2
	567	2×10
$[\emptyset_4P]_3Mo_4Cl_{12}$	394	3×10^2
	566	2×10

[a]Spectra were obtained for DCE solutions.

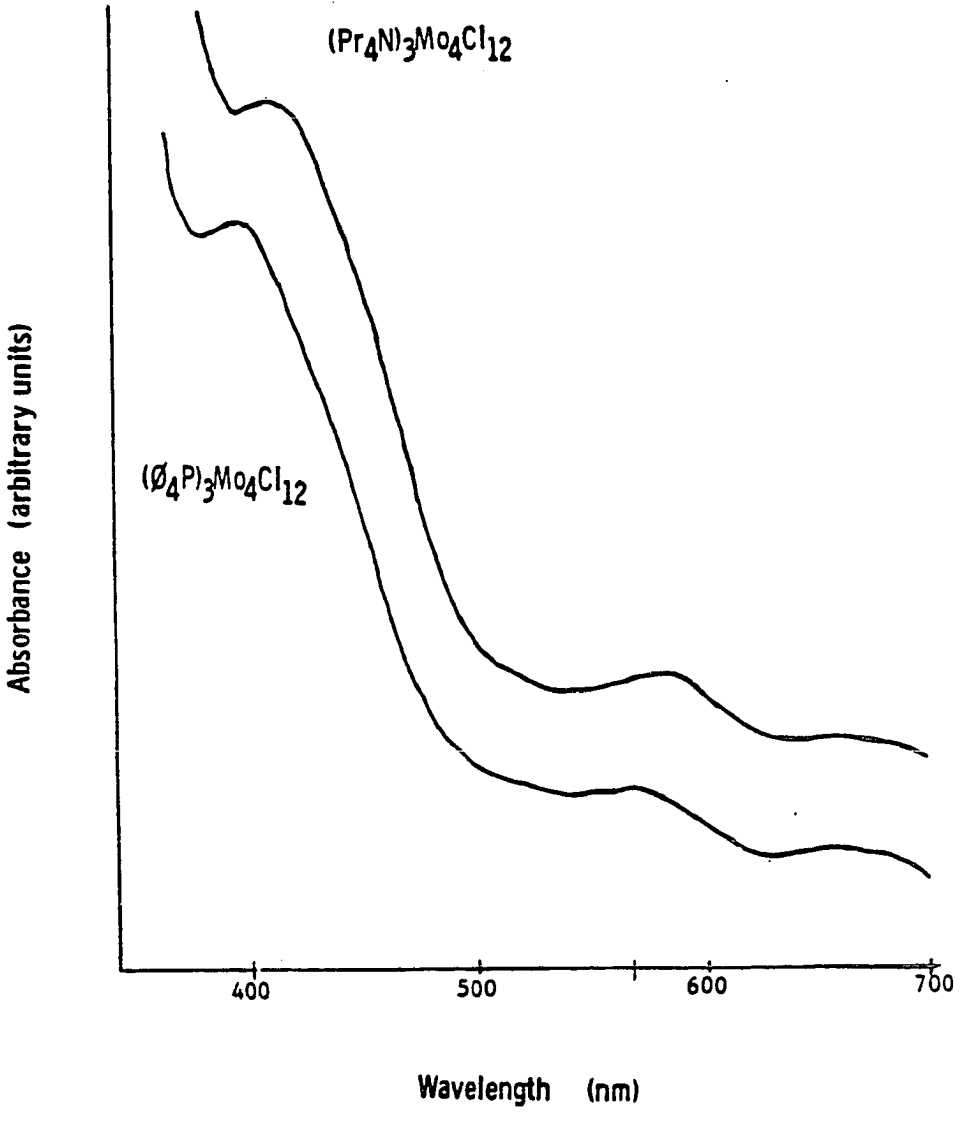

Figure II-20. Visible spectra (nm) of $[Ø_4P]_3Mo_4Cl_{12}\cdot 0.5$ $Ø_4PI$ and $[Pr_4N]_3Mo_4Cl_{12}\cdot 0.7\ C_2H_4Cl_2$ in DCE

Guinier powder photography

Guinier powder patterns were obtained for the planar clusters. The indexed powder patterns were compared to powder patterns calculated from the positional parameters and lattice constants from the single crystal structure determinations. For $[\emptyset_4P]_3Mo_4Cl_{12}\cdot 0.5\ \emptyset_4PI$ and $[Pr_4N]_3Mo_4Cl_{12}\cdot 0.7\ C_2H_4Cl_2$, good agreement was observed between the observed and calculated powder patterns. This confirms that the solid prepared in bulk is structurally identical to that found in the structure results.

When the same procedure was carried out for $[Et_4N]_3Mo_4Cl_{12}$, the compound did not match the calculated powder pattern. It is not known if the bulk preparation has the butterfly cluster, observed in the single crystal structure determination.

Extended Hückel Calculations

Extended Hückel calculations were carried out on the $Mo_4Cl_{12}^{n-}$ cluster compounds for two reasons. One reason was to examine the nature of the bonding to understand why the cluster was rectangular suggesting a somewhat localized bonding scheme rather than a delocalized square bonding arrangement that had been observed for $Mo_4(OPr^i)_8Cl_4$. The second reason was to examine if cause for the deviation of the cluster angle from 90^o could be found.

Figure II-21 shows the molecular orbital energy levels obtained from the extended Hückel calculation which are constituted primarily by molybdenum d atomic orbitals. Figure II-21 also shows the effect that a distortion from a square D_{4h} structure to a rectangular D_{2h} structure has on these orbitals. Particularly noticeable are the splittings of the e levels into bonding and antibonding components. Also shown in this diagram is the correlation of these results with results obtained from nonempirical Fenske-Hall calculations performed by Chisholm and co-workers (33). The dependence of the energy levels on the method of calculation is seen when the extended Hückel results are compared to the Fenske-Hall results. Although most of the orbital energies in the two calculations agree quite well the b_{2g} and a_g orbitals just below the HOMO of the $Mo_4Cl_{12}^{3-}$ cluster anion are reversed.

The molecular orbital diagram obtained from the extended Hückel results contain orbitals which are difficult to conceptualize because of the large amount of mixing of atomic orbitals. This is caused by the manner in which the calculation uses mirror planes to define the basis set. A simple combination of atomic orbitals is informative when used to describe a qualitative molecular orbital diagram (34) which can then be compared to the computer derived results.

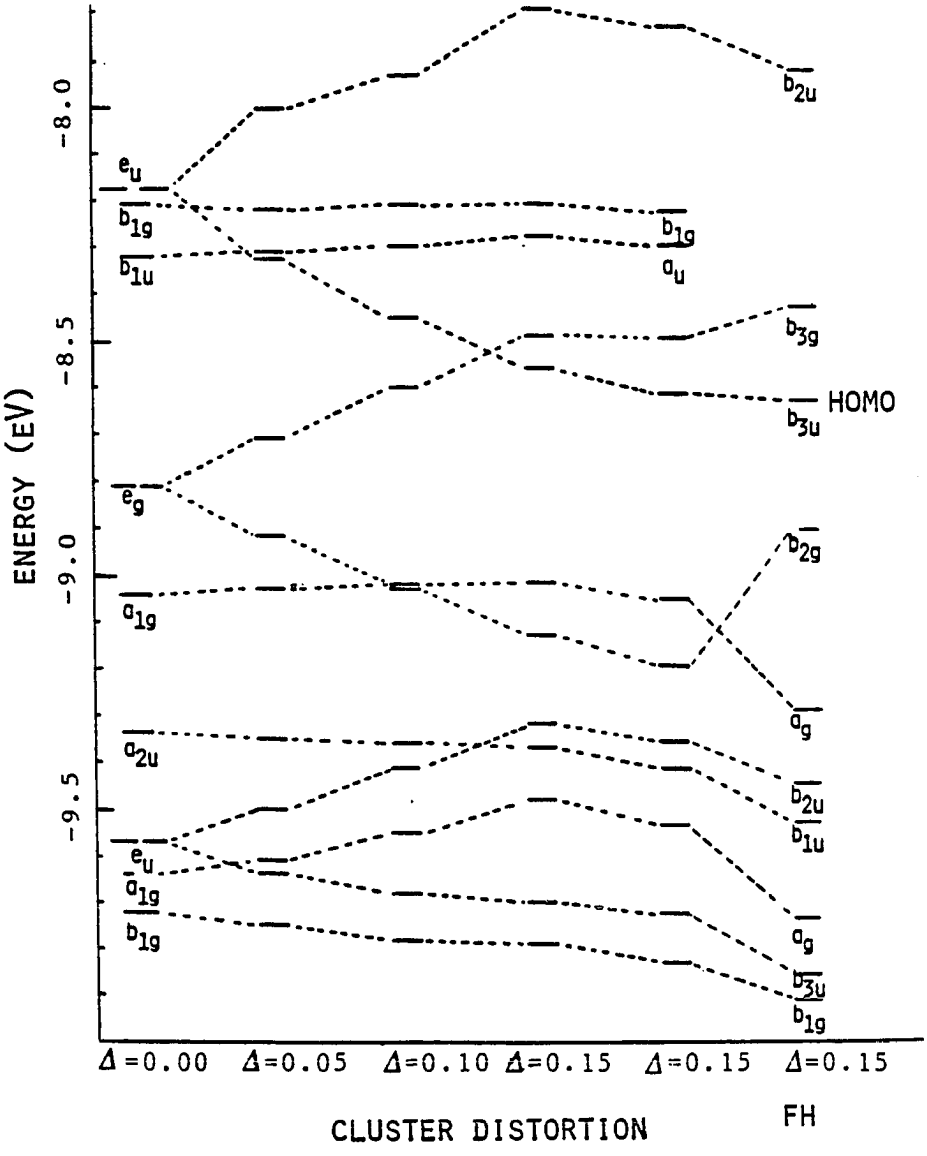

Figure II-21. Energy levels from extended Hückel calculation showing changes which occur in lowering symmetry from D_{4h} to D_{2h}. Δ labels refer to distortions in Table II-23. Calculation from reference 33 is labeled FH

The coordinate systems for a square $Mo_4Cl_{12}^{n-}$ molecule and the individual atoms are defined as shown in Figure II-22. With the axes directed in this manner, each metal atom uses its s, p_x, p_y, p_z, and $2^{1/2}(d_{xz}-d_{yz})$ (a hybrid orbital constructed from the d_{xz} and d_{yz} orbitals) orbitals to bind to the Cl ligands. The remaining orbitals ($d_{x^2-y^2}$, d_{xy}, d_{z^2}, and $2^{1/2}(d_{xz}+d_{yz})$) are involved in forming the metal-metal bonds of the cluster unit. Construction of molecular orbitals is affected by combining the four atomic orbitals of a particular type to produce four molecular orbitals with their resultant symmetry in the D_{4h} point group as shown in Figure II-22. The bonding and antibonding nature of the molecular orbitals is made by inspection of their overlap. Bonding orbitals are denoted by superscript b. Antibonding and nonbonding orbitals are designated with * and n superscripts, respectively.

Four orbitals ($3a_{1g}$+ a_{2u}) appear to be bonding on all four edges of the cluster unit. Eight orbitals possessing bonding and antibonding overlap on alternate edges of the cluster unit form four degenerate e levels ($3e_u$ + e_g). In addition, four orbitals are formally antibonding (a_{2g} + $2b_{2g}$ + b_{1u}). The molecular orbital diagram is shown in Figure II-23. When the symmetry is lowered from D_{4h} to D_{2h}, the four degenerate levels are split into their bonding and antibonding components shown in Figure II-23.

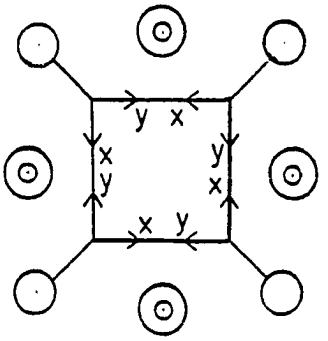

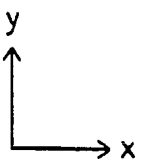

Coordinate system
z out of plane

orbitals used for bonding

metal-ligand s, p_x, p_y, p_z, $\sqrt{2}(d_{xz}-d_{yz})$

metal-metal $d_{x^2-y^2}$, d_{xy}, d_{z^2}, $\sqrt{2}(d_{xz}+d_{yz})$

molecular orbitals for metal-metal bonding as viewed down z axis

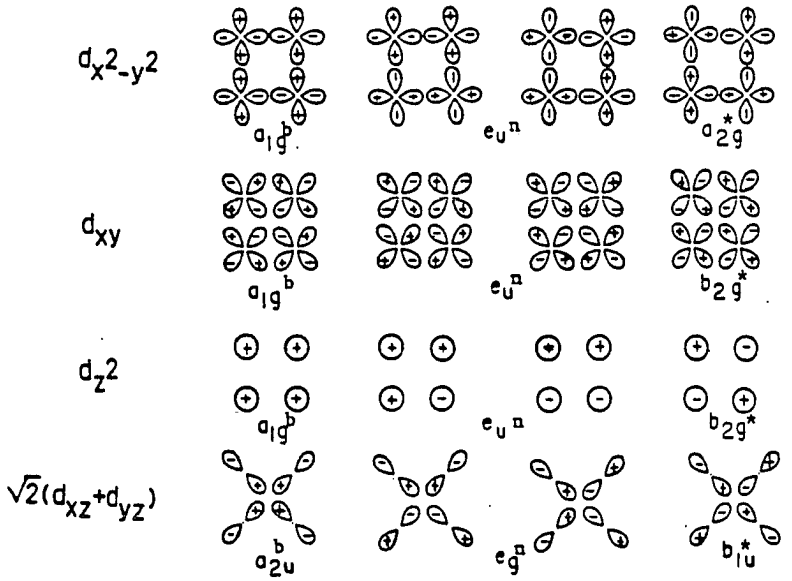

Figure II-22. Combination of atomic orbitals to produce molecular orbitals for metal bonding in a hypothetical D_{4h} $Mo_4Cl_{12}^{n-}$ cluster

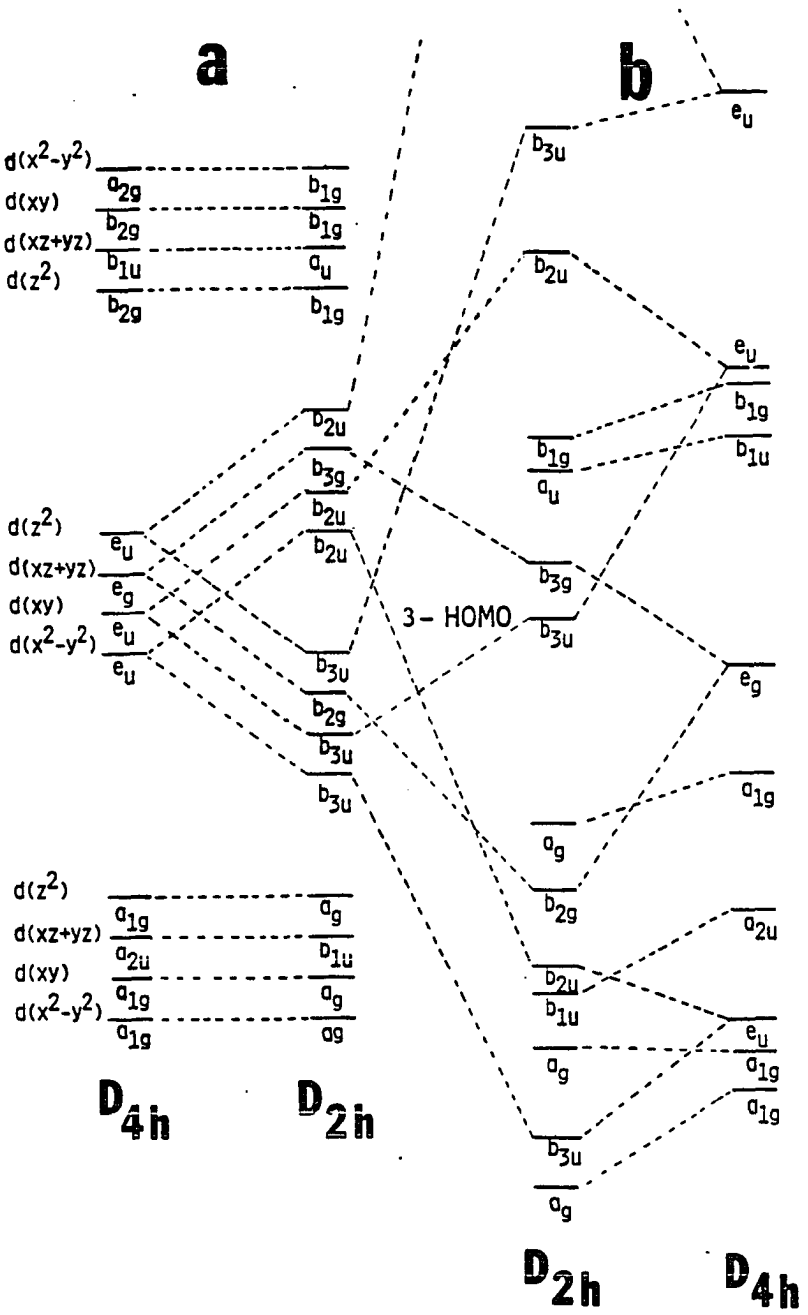

Figure II-23. Comparison of energy levels obtained from
a) qualitative approximation and
b) extended Hückel calculations

The preference for the rectangular geometry over a square geometry (observed for $Mo_4(OPr^i)_8Cl_4$) by the 15 electron $Mo_4Cl_{12}^{3-}$ clusters can be seen from Figure II-23. Twelve electrons completely fill the lower bonding orbitals and lowest of the degenerate e_u states. A stable bonding configuration is observed. If the additonal four electrons are added to a cluster with this bonding scheme they would occupy orbitals which are too high in energy and would destabilize the cluster. A more efficient mode of bonding occurs when this cluster distorts to the rectangular D_{2h} symmetry. In this symmetry, the additional three electrons occupy bonding components of the split orbitals which comprised the e states in D_{4h} resulting in more cluster bonding.

Figure II-23 also shows the correlation of the qualitative molecular orbital scheme with the extended Hückel results. Evident in this diagram is the inability of our qualitative molecular orbital scheme to determine absolute orderings of energy levels. The mixing of orbitals of similar symmetry types is also impossible to estimate by qualitative methods, thus some of the differences in observed energy levels. This diagram does show, however, the splittings of the four degenerate e levels in D_{4h} to their respective levels in D_{2h}, a satisfying result in the fact that we may be assured that we can describe the bonding

in the cluster in a manner which is understandable in terms of orbitals which we can easily envision.

The distortion of the cluster angles from 90^{o} can also be understood in terms of Jahn-Teller effects using these diagrams. The $Mo_4Cl_{12}^{3-}$ clusters should possess no degeneracies with one unpaired electron and D_{2h} symmetry, where orbital degeneracies do not exist. First order Jahn-Teller distortions require orbital degeneracies. The distortion of the angles, if electronic in nature, must be a second-order Jahn-Teller effect.

The necessary condition for the occurrence of a second-order Jahn-Teller distortion is that a low lying excited state be coupled to the ground state by one of the normal modes of vibration of the molecule (35). The two states are said to be coupled when the direct product of the irreducible representations of the excited state and the ground state are the same as the vibration. Further conditions require that the excited state and ground state be of the same symmetry in the new point group.

Disregarding the chlorine atoms, the rectangular cluster has D_{2h} symmetry. The distortion observed is pictured in Figure II-24 and is of b_{1g} symmetry. The highest occupied molecular orbital is a b_{3u} orbital producing a B_{3u} state. The direct product of $b_{3u} \times b_{1g}$ is b_{2u}. The conditions are suitable for a second-order Jahn-Teller effect if a low

lying b_{2u} orbital is present. Figure II-21 shows that the b_{2u} orbital lies approximately 0.6 eV above the HOMO in the extended Hückel calculations, confirming that a second-order Jahn-Teller effect can indeed be invoked to explain the deviation of the cluster angles.

The energy difference between the ground and excited states is small enough that a second-order Jahn-Teller effect is reasonable. Pearson has observed that orbitals as much as 4 eV apart in energy can result in large second-order Jahn-Teller distortions (35). The distorted cluster has idealized C_{2h} symmetry. In this symmetry, both the ground and excited state become ^2B_u, thus all the conditions are present for concluding that a second-order Jahn-Teller is the cause of the angular distortion.

Extended Hückel calculations were also performed on the cluster with the butterfly geometry. As with the planar case, mixing by atomic orbitals of similar symmetry made interpretation of the resultant molecular orbital diagram difficult in terms of orbitals that are easily conceptualized. Again, a simple approach is instructive.

A simple approximation of the energy levels in a butterfly molecule of this type was described for $Mo_4I_{11}^{2-}$ (36). While the approximation will not be reiterated here, the salient features are summarized by noting that the butterfly cluster has six bonding ($3a_1 + a_2 + b_1 + b_2$), two

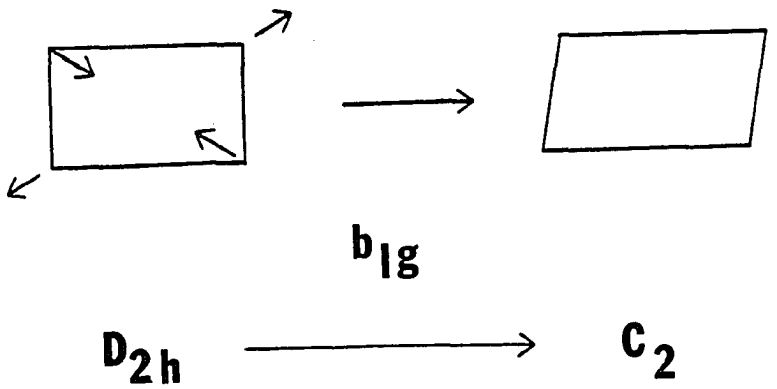

$$B_{3u} \times B_{2u} = b_{1g}$$

G. S. E. S. VIBRATION

Figure II-24. Jahn-Teller active vibration for cluster with rectangular D_{2h} symmetry. Ground state (g.s.) is coupled to excited state (e.s.) by b_{1g} vibration

nonbonding ($a_2 + b_1$), and eight antibonding ($2a_1 + a_2 + 3b_1 + b_2$) metal-metal orbitals. The nonbonding orbitals are localized on the apical molybdenum atoms. The fifteen cluster electrons fill six bonding orbitals and the remaining three electrons are placed in the nonbonding orbitals.

The molecular orbital diagram obtained by this approach is shown with the molecular orbital diagram from the extended Hückel results in Figure II-25. The close agreement extended Hückel results confirms that, neglecting the mixing by orbitals of the same symmetry, our analysis of the bonding in these cluster units is valid.

Our extended Hückel calculations have failed to show any reason for adoption of one of the observed geometries over the other.

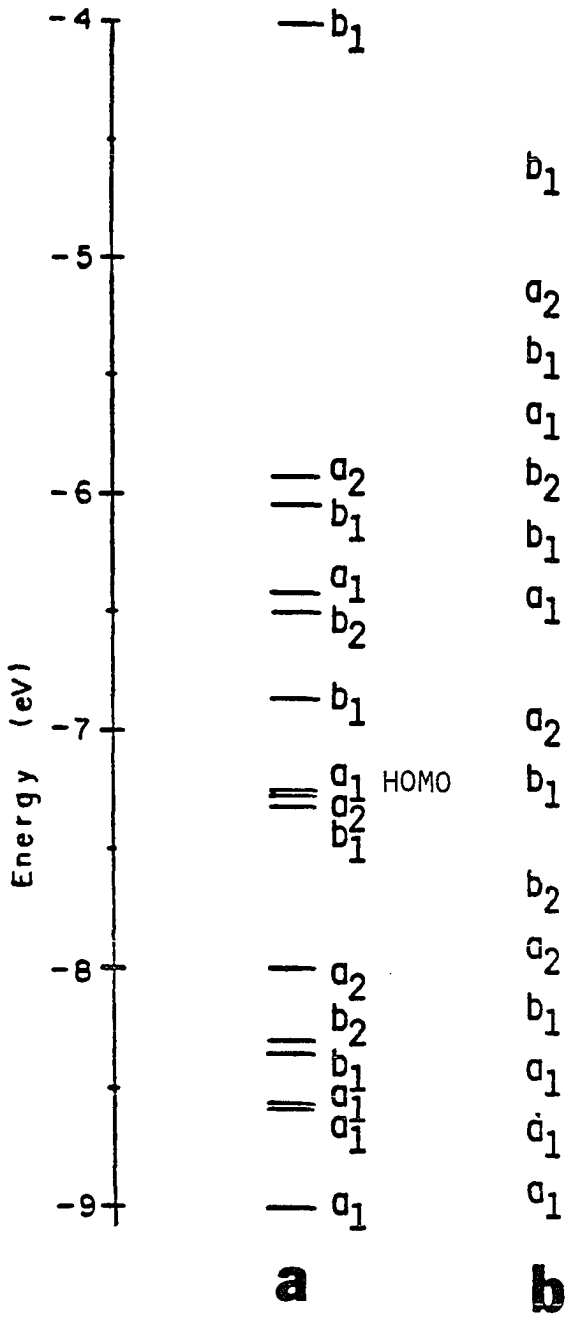

Figure II-25. Comparison of a) extended Hückel results and b) intuitive approximation for a cluster with butterfly geometry

CONCLUSION

The reaction of the purple cluster compounds, $R_4Mo_4Cl_{12}$, with various oxidants have produced new $Mo_4Cl_{12}^{3-}$ cluster compounds where the molybdenum atoms can adopt two different geometries.

The occurrence of both planar and butterfly geometries of $Mo_4Cl_{12}^{3-}$ is analogous to the situation found in $Mo_4(OPr^i)_8X_4$ compounds, where $Mo_4(OPr^i)_8Cl_4$ adopts a square planar configuration and $Mo_4(OPr^i)_8Br_4$ is found with the butterfly geometry (24). In the $Mo_4Cl_{12}^{3-}$ situation, the factors controlling the cluster geometry are even more subtle than in the alkoxide case since both the chemical composition and electronic configurations are exactly the same. At this point, the reasons responsible for the adoption of one conformation over the other are unknown. One possibility is that an equilibrium between the two forms may exist in solution, where the species of the planar geometry is the thermodynamically dominant form. The latter is isolated in the soluble salts $[Pr_4N]_3Mo_4Cl_{12}$, $[\emptyset_4P]_3Mo_4Cl_{12}$, and $[\emptyset_4As]_2[Et_4N]Mo_4Cl_{12}$, but the butterfly may be the kinetically favored product in crystallization of $[Et_4N]_3Mo_4Cl_{12}$ because of its insolubility. This is not unreasonable because photoelectron spectroscopy suggests that the $[Et_4N]_4Mo_4Cl_{12}$ compound has the butterfly

structure. Similar behavior is suspected for the $Mo_4(OPr^i)_8X_4$ compounds, except that experimental evidence indicates the butterfly is the thermodynamically favored species (24).

The difference between square and rectangular in the bond lengths of the planar clusters may be attributed to the oxidation state of the species from which they are made. Coupling of the quadruply bonded Mo(II) dimeric species creates the rectangular $Mo_4Cl_8L_4$ clusters, which retain their rectangular nature, due to the robustness of the remaining triple bond, through subsequent reactions leading to the formation of the $Mo_4Cl_{12}^{3-}$ clusters. On the other hand coupling of the triply bonded Mo(III) dimers, $Mo_2(OPr^i)_6$, forms the tetranuclear $Mo_4(OPr^i)_8Cl_4$ cluster with 12 electrons, enough for two double bonds and two single bonds. In this case the square, rather than the rectangular, geometry is adopted presumably because of the more favorable delocalized bonding.

Theoretical explanation of this difference can be found in the Jahn-Teller theorem. A hypothetical square $Mo_4Cl_{12}^{3-}$ cluster would place three electrons in a degenerate HOMO, amd the electronic ground state would be ^2E_g. The orbital degeneracy can be removed by a structural distortion, such as the lengthening and shortening of alternate sides to form a rectangular cluster having one of the HOMOs displaced to

lower energy, and one to higher energy. The energy of the system is lowered since two electrons are present to occupy the low energy orbital, but only one may occupy the orbital of higher energy. The rectangularly distorted cluster is thus more stable. The square isopropoxide cluster, $Mo_4(OPr^i)_8Cl_4$, has only 12 electrons for cluster bonding and the degenerate state is not filled so that no distortion is necessary.

Furthermore, a second order Jahn-Teller distortion can be invoked to explain the distortion of the observed angles from 90^o. A second order Jahn-Teller distortion occurs when a low lying excited state is coupled to the ground state by a normal mode of vibration. The symmetry of the vibration is said to couple the two states when the irreducible representation of the vibration is the same as that of the direct product of the ground and excited state. Examination of the orbital levels of an extended Hückel calculation of $Mo_4Cl_{12}^{3-}$ shows that it has a ground state of B_{3u}. Excitation of an electron from the b_{2g} orbital to the b_{3g} level produces an excited state of B_{2u} symmetry. The direct product of these two states is B_{1g}, corresponding to the vibration in D_{2h} symmetry which would produce the desired distortion.

These clusters are the tetranuclear members of a series of molybdenum halide compounds where the nuclearity of the

species varies from one to six. One could easily envision either the planar or butterfly clusters as precursors in the synthesis of the next larger member of the series, the $Mo_5Cl_{13}^{n-}$ cluster compounds, by simple addition of a molybdenum with a chlorine atom to the cluster unit, eq. 10.

$$Mo_4Cl_{12}^{3-} + \text{"MoCl"} \longrightarrow Mo_5Cl_{13}^{3-} \qquad 10$$

The molybdenum atom would simply fill one of the two vacant faces of the already existing chlorine cube. The additional chlorine of the incoming "MoCl" unit would serve as the terminal chlorine to the incoming molybdenum atom.

The extension of this research should yield the Mo_5 cluster and is certain to produce additional new and interesting metal cluster compounds.

REFERENCES AND NOTES

1. Aufdembrink, B. A. Ph.D. Dissertation, Iowa State University, Ames, Iowa, 1985; Section I.

2. Vogel, A. "Practical Organic Chemistry"; Longmans, Green, and Co.: London, 1975; page 541.

3. Clark, C. M.; Smith, D. K.; Johnson, G. J. "A Fortran IV Program for Calculating X-ray Powder Diffraction Patterns-Version 5", Department of Geosciences, Pennsylvania State University, University Park, PA, 1973.

4. This E&A four-circle diffractometer was modified in Dr. Jacobson's laboratory. Stepping motors and encoders were attached and interfaced to a LSI/11 computer which in turn was interfaced to a VAX 11/730 computer. It is equipped with a scintillation counter and incorporates a graphite monochromator in the detection system.

5. Jacobson, R. A. J. Appl. Crystallogr. 1976, 9, 115.

6. Lawton, S. L.; Jacobson, R. A. Inorg. Chem. 1968, 7, 2124.

7. Main, P. "MULTAN80, A System of Computer Programs for the Automatic Solution of Crystal Structure for X-ray Diffraction Data", University of York Printing Unit, York, United Kingdom, 1980.

8. Structure factor calculations and least squares refinements were done using the block matrix/full matrix program ALLS (Lapp R. L.; Jacobson, R. A. "ALLS, A Generalized Crystallographic Least Squares Program", U.S.D.O.E. Report IS-4708, 1979.), Fourier series calculations were done using the program FOUR (Powell, D. R.; Jacobson, R. A. "FOUR, A General Crystallographic Least Squares Program", U.S.D.O.E. Report IS-4737, 1980.) and for molecular drawings the program ORTEP (Johnson, C. K., "A FORTRAN thermal-ellipsoid Plot Program for Crystal Structure Illlustrations", U.S.A.E.C. Report ORNL-3794, 1965.) was used.

9. Howells, E. R.; Phillips, D. C.; Rodgers, D. Acta Crystallogr. 1950, 3, 210.

10. Hanson, H. P.; Herman, F.; Lea, J. D.; Skillman, S. Acta Crystallogr. 1964, 17, 1040.

11. Templeton, D. T. In "International Tables for X-ray Crystallography", 1st ed; Macgillavy, C. H. and Rieck, G. D., Eds.; Kynoch Press: Birmingham, England, 1962; Vol. III, page 215.

12. Cruickshank, D. W. J.; Pilling, D. I. In "Computing Methods and the Phase Problem in X-ray Crystal Analysis"; Pepsinsky, R.; Roberts, J. M.; Speakman, J. C. Eds.; Pergamon Press: New York, 1961; page 45.

13. Rohrbaugh, W. J.; Jacobson, R. A. Inorg. Chem. 1974, 13, 2435.

14. Karcher, B. A. Ph.D. Dissertation, Iowa State University, Ames, Iowa, 1981.

15. Ryan, T. R. Ph.D. Dissertation, Iowa State University, Ames, Iowa, 1981.

16. Schaffer, A. M.; Gouterman, M.; Davidson, E. R. Theoretica Chim. Acta (Berl.) 1973, 30, 9.

17. McGlynn, S. P.; Vanquickenborne, L. G.; Kinoshita, M; Carroll, D. G. "Introduction to Applied Quantum Chemistry"; Holt, Rinehart, and Winston, Inc.: New York, 1972.

18. Cusachs, L. C.; Corrington, J. H. In "Sigma Molecular Orbital Theory"; Sinanoglu, O.; Wiberg, K. B., Eds.; York University Press: New Haven, Conn. 1970, chapter VI-4.

19. Sheldon, J. C. J. Chem. Soc. 1960, 1007.

20. Cotton, F. A.; Walton, R. A. "Multiple Bonds Between Metal Atoms"; John Wiley and Sons: New York, 1982; and references cited therein.

21. Stensvad, S.; Helland, B. J.; Babich, W. W.; Jacobson, R. A.; McCarley, R. E. J. Am. Chem. Soc. 1978, 100, 6257.

22. Chisholm, M. H.; Reichert, W. W. J. Am. Chem. Soc. 1974, 96, 1249.

23. McGinnis, R. N.; Ryan, T. R.; McCarley, R. E. J. Am. Chem. Soc. 1978, 100, 7900.

24. Chisholm, M. H.; Errington, R. J.; Folting, K.; Huffman, J. C. J. Am. Chem. Soc. 1982, 104, 2025.

25. Luly, M. H. "APES, A Fortran Program to Analyze Photoelectron Spectra", U.S.D.O.E. Report IS-4694, 1979.

26. Beers, W. W. Ph.D. Dissertation, Iowa State University, Ames, Iowa, 1983, Section III.

27. Wagner, C. D.; Riggs, W. M.; Davis, L. E.; Moulder, J. F.; "Handbook of X-ray Photoelectron Spectroscopy"; Perkin Elmer Corp.: Eden Prairie, MN, 1978; page 58

28. Figgis, B. N.; Lewis, J. In "Modern Coordination Chemistry"; Lewis, J.; Wilkins, R.G., Eds.; Interscience: New York, 1960; page 403.

29. Selwood, P. W. "Magnetochemistry", 2nd ed.; Interscience: New York, 1956; page 78.

30. Converse, J. G.; McCarley, R. E. Inorg. Chem. 1970, 9, 1361.

31. O'Connor, C. J. Prog. in Inorg. Chem. 1982, 29, 203.

32. Heinz, J. Angew. Chem. Intl. Ed. Engl. 1984, 23, 831.

33. Chisholm, M. H.; Clark, D. L.; Bursten, B. E., presented at the 188th National Meeting of the American Chemical Society, Miami Beach, April, 1985.

34. McCarley, R. E. unpublished research, Department of Chemistry, Iowa State University, Ames, Iowa, 1982.

35. Pearson, R. G. Proc. Nat. Acad. Sci. USA 1975, 72, 2104.

36. Stensvad, S. Ph.D. Dissertation, Iowa State University, Ames, Iowa, 1984.

SECTION III. SYNTHESIS AND CHARACTERIZATION OF THE TERNARY MOLYBDENUM OXIDE $Sn_{0.9}Mo_4O_6$ CONTAINING CONDENSED Mo_6 OCTAHEDRA

INTRODUCTION

The discovery of the reduced molybdenum oxides, $NaMo_4O_6$ (1) and $Ba_{1.18}Mo_8O_{16}$ (2), in this laboratory sparked a vigorous interest in the study of new reduced molybdenum oxide compounds. The remarkable structures of these compounds were dominated by the metal-metal bonding manifested in discrete tetranuclear clusters and infinite extended chains of edge shared octahedra.

Attempts to modify the structural and electronic properties of these compounds has enlarged this chemistry and led to the discovery and study of a wide variety of reduced metal oxides which possess intriguing structures and interesting properties.

Reduced molybdenum oxide compounds have been isolated in which the molybdenum atoms are bound in a variety of fashions to form infinitely bonded chains of edge shared octahedra (1,3), discrete planar tetranuclear clusters (2), fused tetranuclear clusters to give extended ribbons of metal-metal bonded atoms (4), and single metal atom chains (5).

Reported here is the synthesis and structural characterization of $Sn_{0.9}Mo_4O_6$. This is one member of a class of reduced ternary molybdenum oxides, $M_xMo_4O_6$ (1). The $M_xMo_4O_6$ structure is typified by the condensed octahedral clusters of metal atoms fused on <u>trans</u> edges to

form infinite chains in the crystal lattice. $Sn_{0.9}Mo_4O_6$ is an unusual member of this class of compound because of the nonstoichiometry of the Sn atom and possibility for Sn-Sn bonding in the structure.

EXPERIMENTAL

Methods and Materials

The reduced nature of these molybdenum oxides requires that precautions be taken during preparation. Reactants were dried to minimize the amount of adventitious water in the reactions. The high temperatures required for these preparations required that reactions were carried out in sealed molybdenum or quartz tubes to insure the correct stoichiometry was maintained. Reactants were mixed together and thoroughly ground to obtain a homogenous mixture before being pressed into pellets with a pressure of approximately 7000 lb/in^2. In cases where optimum crystal growth was desired, the reactants were left as powders, which increased the size of crystals that were grown.

Molybdenum powder (99.99%) was used as obtained from Aldrich Chemical Company. Prior to use, the powder was dried at 120° C for 24 hr and stored in a desiccator. Tin powder was purchased from Fischer Scientific Company and also used after drying at 120° C. MoO_3 (Baker analyzed reagent grade; Fischer Scientific Co.) was fired at 550° C for 12 hours and stored in a desiccator. SnO was prepared by the method of Weiser and Milligan (6). The prepared solid was dried and stored in a desiccator.

Analytical Methods

Chemical analyses for the tin and molybdenum were obtained by electron microprobe analysis by Mr. Francis Laabs of the Ames Laboratory metallurgy group. The results for crystals of the chunk and needle morphology are shown in Table III-1. The nonstoichiometry of the compound was also confirmed by the single crystal structure determination where the chemical formula was found to be $Sn_{0.88}Mo_4O_6$.

Table III-1. Electron microprobe analysis of $Sn_{0.9}Mo_4O_6$

chunk	%Mo	%Sn	needles	%Mo	%Sn
1	65.7	19.4	1	66.4	19.1
2	65.5	19.5	2	66.0	19.7
3	65.6	19.5	3	65.5	19.5
4	66.2	18.9	4	65.3	19.7
5	65.6	19.4	5	66.5	18.5
			6	65.5	19.5
	65.5	19.3		65.7	19.3
Sn/Mo	0.24			0.24	
Formula	$Sn_{0.95}Mo_4O_6$			$Sn_{0.95}Mo_4O_6$	

Synthesis

$Sn_{0.9}Mo_4O_6$ was originally prepared by Dr. Larry Brough in a survey of reactions in various ternary molybdenum oxide systems. The initial reaction, eq. 1, used SnO, MoO_2 and Mo metal in stoichiometric ratio of 2 : 5 : 3 in attempting

$$2\ SnO + 5\ MoO_2 + 3\ Mo \longrightarrow 2\ SnMo_4O_6 \qquad 1$$

to prepare a tin analogue of $NaMo_4O_6$. The reactants were ground together, pressed into a pellet, and placed in a molybdenum tube which was evacuated and sealed with an electron beam welder to insure that the desired stoichiometry was maintained. The reaction was heated to 1100° C for six days. The Guinier powder pattern of the product mixture, based on its similarity to that of $NaMo_4O_6$, indicated that such a compound was indeed formed. Side products were MoO_2 and small droplets of Sn which were found on the lid of the reaction tube.

$Sn_{0.9}Mo_4O_6$ can be prepared by using several different starting materials in suitable stoichiometries. Tin metal, SnO, and SnO_2 have all been used successfully as sources of tin. Molybdenum metal, MoO_2, and MoO_3 have been used for molybdenum. The reactions have been carried out in evacuated quartz, molybdenum, or nickel tubes to insure that only the limited amount of oxygen required to produce these reduced phases is present. A variety of reaction conditions have been shown to produce $Sn_{0.9}Mo_4O_6$. Reaction temperatures have ranged from 800° to 1500° C. Reaction times have varied from 3 to 30 days. Generally, reactants have been mechanically pressed into pellets under pressure

of 7000 lb/in^2, after being thoroughly mixed and ground together with a mortar and pestle. Larger crystal growth has been observed, however, when the reactions are carried out using intimately mixed loose powders.

$Sn_{0.9}Mo_4O_6$ is formed in the bulk pellets as well as growing from the walls of the reaction vessel. The crystals obtained have two distinct morphologies. The needles obtained from these reactions are similar to the types of crystals observed in other $M_xMo_4O_6$ systems. In addition, chunky crystals were isolated with a morphology so different that they were initially thought to be another product. X-ray powder patterns, microprobe analyses, and single crystal structure determinations for the two types of crystals have proven that they are identical.

Yields of 100%, based on Guinier powder photography, have been obtained by extended reaction times at moderate temperatures (900^o C), eq. 2.

$$0.9\ SnO + 1.7\ MoO_3 + 2.3\ Mo \xrightarrow[900^o\ C]{30\ d} \underset{100\%}{Sn_{0.9}Mo_4O_6} \qquad 2$$

The fractional occupancy observed in the results of the structure determination and from electron microprobe analysis was intriguing. Reactions 4, 5, and 6 were attempts to alter the loading of tin into the structure.

$$0.50\ SnO + 1.83\ MoO_3 + 2.17\ Mo \xrightarrow[7\ d]{1100^{o}} Sn_{0.5}Mo_4O_6 \qquad 4$$

$$1.50\ SnO + 1.50\ MoO_3 + 2.50\ Mo \longrightarrow Sn_{1.5}Mo_4O_6 \qquad 5$$

$$Sn_{0.9}Mo_4O_6 + Sn \longrightarrow Sn_{1.9}Mo_4O_6 \qquad 6$$

The absence of shifts in the diffraction lines from powder patterns of the product mixtures in each case showed no indication that the occupancy of Sn had been altered. In reaction 4, MoO_2 was observed in the reaction product. The products of reactions 5 and 6 had small droplets of metallic tin on the surface of the pellet.

Physical Measurements

Resistivity

Single crystal conductivity measurements were made using a resistivity cryostat maintained in Dr. Robert Shelton's group. These measurements are based on the van der Pauw four-probe method for measuring the electrical conductivity of irregularly shaped samples (7). The method entails passage of a constant current through the sample using two contacts while measuring the concurrent potential drop with the remaining two leads.

The sample was prepared by attaching four platinum wires to a single crystal of $Sn_{0.9}Mo_4O_6$ using Epo-Tech

silver epoxy. One end of the crystal was epoxied to a small piece of fritted disk (the fritted disk was used because the absorption of the epoxy into the disk counteracted the capillary action which tended to pull the epoxy along the crystal and short-circuit the leads). Once the crystal was firmly mounted on the disk, three additional contacts were made. Platinum wires were then epoxied to these contacts. By making connections in this manner, the danger of shorting the leads by allowing the epoxy contacts to touch on the surface of the crystal was minimized. The prepared sample was then connected to the four-probe resistivity cryostat. The integrity of the leads under strain induced by contraction upon cooling was checked by plunging the cryostat into liquid N_2 and monitoring the continuity of the circuits through the crystal.

The samples were then placed in the dewar and the resistance measurements were taken from room temperature to 2 K. The temperature was monitored by means of platimum and carbon glass resistance thermometers. Periodically, the resistance across a standard resistor was measured to insure that a constant current was passed through the sample throughout the experiment.

Measurements were obtained for two different crystals whose dimensions were 1.55 x 0.30 x 0.35 mm and 1.35 x 0.05 x 0.05 mm. Measurements were taken such that the

resistivity was measured along the c axis of the crystal. In addition, experiments where the potential drop was measured perpendicular to the c axis of the crystal were performed.

The ratio of the resistance measured at temperature t, over the resistance at room temperature (ρ_t/ρ_{293}) was plotted vs temperature.

Photoelectron spectroscopy

Valence band photoelectron specta were obtained for $Sn_{0.9}Mo_4O_6$ using the same spectrometer as described in section I. Aluminum Kα (1486.6 eV) and He(I) (21.2eV) radiation were used as exciting sources. Samples remained sealed in the reaction tubes until opened in the helium drybox connected to the photoelectron spectrometer to insure quality of the sample. Sample purity was checked by obtaining a Guinier powder pattern prior to collecting sample data. Thirty-seven scans were obtained for the X-ray photoelectron spectra. Spectrometer slits were set at 4 x 4 to maintain optimum resolution, although for the XPS nonmonochromatic radiation was used.

Core spectra were obtained for the Sn 3d level using similar procedures. The core spectrum was fitted using the APES algorithms (8).

Powder photography

Guinier powder diffraction patterns were obtained on ground samples using an Enraf Nonius Delft focusing Guinier camera. Copper $K\alpha_1$ radiation (λ=1.5405 Å) was used to irradiate the sample.

A Guinier powder pattern of pure $Sn_{0.9}Mo_4O_6$ was obtained after separating a sufficient quantity of single crystals by hand. The crystals were ground prior to obtaining the powder pattern. The pattern obtained was referenced to silicon X-ray standard obtained from the National Bureau of Standards. The measured values of two theta were compared to a powder pattern calculated using parameters obtained from the single crystal x-ray structure determination (9). The data obtained are listed in Table III-2.

Data Collection and Treatment

A suitable crystal with dimensions of 0.04 x 0.04 x 0.24 mm was mounted on a glass fiber with epoxy. The crystal was placed on a goniometer head and indexed on the Ames Laboratory diffractometer (10) using the ALICE algorithms (11). Nine reflections with various chi and phi values were used as input to ALICE which subsequently showed the crystal symmetry as tetragonal. Three standards were

Table III-2. X-ray powder diffraction data for $Sn_{0.9}Mo_4O_6$

2θ [a,b]	2θ [c]	2θ (calc.) [d]	d, Å	rel I	HKL
13.00 s	13.02	13.00	6.80	40	110
18.37 m	18.43	18.43	4.81	15	200
20.56 vw	20.60	20.63	4.30	5	210
26.07 w	26.14	26.18	3.40	10	220
29.24 vs	29.30	29.33	3.04	100	310
31.33 vw	31.51	31.51	2.84	5	001
33.42 w	34.08	33.56	2.67	10	320
-----	-----	34.21	2.62	2	111
36.58 m	36.61	36.75	2.44	32.5	201
37.20 m	37.30	37.35	2.40	10	400
37.76 m	37.84	37.96	2.37	72.5	211
38.40 vw	38.40	38.55	2.33	5	410
39.55 vw	39.67	39.71	2.27	2.5	330
41.79 w	41.91	41.96	2.15	10	420
46.48 s	46.59	46.69	1.94	62.5	321
46.99 m	47.12	47.19	1.92	12.5	430
47.99 m	48.15	48.19	1.88	30	510
49.40 w	49.50	49.65	1.83	5	401
50.86 w	51.01	51.08	1.79	7.5	520
51.30 w	51.42	51.55	1.77	15	331
54.63 w	53.80	53.86	1.70	25	440
58.42	-----	57.85	1.59	5	501
58.85 vw	58.59	58.72	1.57	25	511
61.48 w	61.12	61.26	1.51	17.5	521
65.40 w	-----	65.78	1.42	12.5	002
66.70 w	-----	66.98	1.40	7.5	102
67.49 w	-----	67.77	1.38	17.5	611
----	-----	73.60	1.29	15	312

[a] Intensity abbreviations; w-weak, m-medium, s-strong, v-very.

[b] Sample appears as single phase from a reaction at 1100° C for 7 d. Cell parameters obtained from this pattern are a = 9.637 Å, c = 2.848 Å.

[c] Sample obtained from a reaction of SnO, MoO_3 and Mo at 900° C for 30 d.

[d] Calculated from single crystal data; a = 9.621 Å, c = 2.837 Å.

chosen and axial oscillation photographs were taken to insure correct choice of unit cell. Four octants of data (h,k,l; $\bar{h},\bar{k},l$; $\bar{h},k,\bar{l}$; $h,\bar{k},\bar{l}$) were collected. The intensities of three standards were monitored every 75 reflections to insure that the crystal had not become misaligned or suffered decay. Final lattice parameters were obtained by least squares refinement of eighteen reflections with two theta greater than 30^{o}. The lattice parameters thus obtained were $a = b = 9.621(1)$ Å, $c = 2.836(1)$ Å, $\alpha = \beta = \gamma = 90^{o}$.

A phi scan was performed to determine the need for an empirical absorption correction. A 34% variance in the intensity of the 0 0 2 reflection during the scan indicated that an absorption correction was necessary. The absorption coefficient was 137.8. The data were subsequently corrected for absorption effects (12).

The data were then corrected for Lorentz and polarization effects and standard deviations were calculated (13). Reflections with $I < 3\sigma(I)$ or $F < 3\sigma(F)$ were eliminated from the data set. The reduced data set consisted of 1897 reflections. One set of extinction conditions was evident, that being the condition 0 k 1, $k \neq 2n$. This extinction indicated the centric space group P4/mbm. The data were then averaged in 4/mmm Laue symmetry. The averaged data set for refinement contained 262

reflections.

Data averaging for the crystal, as well as for $InMo_4O_6$, presented difficulties. In several random instances, a wide range of intensities were included in the values averaged for a particular reflection. This led to a large residual and inclusion of several questionable data in the final averaged set. Later in the refinements, structure factors from these reflections showed poor agreement with calculated structure factors, thus inhibiting the structure refinement. (The problem was thought to arise from the crystal dimensions, which caused a large absoption problem which was not properly accounted for.) A new data set collected on a crystal with the chunk morphology did not exhibit this problem and was used in final refinements. Parameters relevant to data collection and treatment are listed in Table III-3.

Structure Solution

The positions of the molybdenum atoms in the unit cell were found by Patterson methods using superposition techniques (14). A superposition vector corresponding to a vector from apical Mo to apical Mo of one Mo_6 octahedron was used to simplify the Patterson map and allowed calculation of the positional parameters from Harker vectors. Least

Table III-3. Single crystal data for $Sn_{0.9}Mo_4O_6$

formula	$Sn_{0.9}Mo_4O_6$
molecular weight	586.581
space group	$P_{4/mbm}$
systematic absences	0,k,l; k=2n+1
a, Å	9.621(2)
b, Å	9.621(2)
c, Å	2.836(1)
V, $Å^3$	262.4(1)
Z	2
d, calc. g/cm^3	7.57
crystal size, mm	0.04 x 0.04 x 0.24
μ, cm^{-1}	137.78
instrument	Ames Laboratory in house designed diffractometer
radiation	Mo Kα, λ=0.71069
# orientation refl.	12
scan method	omega
octants collected	hkl, $\bar{h}$kl, $\bar{h}\bar{k}$l, h,$\bar{k}$,l
data collection range	2-60° in 2 theta
# data collected	1106
$F_o > 3\sigma(F_o)$	1036
# unique data, R	242, 3.96
#parameters refined	30
R^a	0.028
R_w^b	0.047
quality of fit, Q^c	2.0061

[a] $R=\Sigma||F_o|-|F_c||/\Sigma|F_o|$.

[b] $R_w=[\Sigma w(|F_o|-|F_c|)^2/\Sigma w|F_o|^2]^{1/2}$, $w=1/\sigma^2(F_o)$.

[c] $Q=[\Sigma w(|F_o|-|F_c|)^2/N(\text{observations})-N(\text{parameters})]1/2$.

square refinement on this atom produced a difference map from which the waist molybdenum atoms were found. Least squares refinement using these positional parameters resulted in a residual value ($R=\Sigma||F_o|-|F_c||/\Sigma|F_o|$) of 47%. From the resulting electron difference map, the position of a tin atom at 0,0,0 was obtained and refined to an R of 28.7%. Positional parameters for oxygen atoms were found and refined, followed by isotropic and anisotropic refinement on these atoms.

A secondary extinction was performed on the data set (14), its necessity indicated by the fact that the observed structure factors were generally smaller than the calculated structure factors. Once the correction was applied, it was observed that the correction had improved the correlation of approximately half of the structure factors but this was negated by increased differences in F_o and F_c for the remaining reflections.

At this stage of refinement, the multiplier of the Sn atom was varied. Initially, the multiplier was input to provide one tin atom per Mo_4O_6 unit. Varying the multiplier led to an occupancy of 0.76 for the site at 0,0,0. Examination of an electron density map revealed residual density located in the center of the tunnel formed by four Mo_4O_6 chains and 5/16 of the distance along the z axis. A tin atom was placed at this position and refined. Its

multiplier refined to 0.13 and the R value was lowered to 2.9% (R_w=4.9%).

Residual density remained in the tunnel and near the molybdenum atoms, however, this density was less than one $e/\AA^3$ and was considered negligible. More disturbing was the extremely large thermal parameter of the apical molybdenum atom in the octahedral chain along the c axis of the unit cell. The beta(33) was four times larger than that for beta(11) and beta(22). This behavior was also seen in $InMo_4O_6$ and to a lesser extent in $NaMo_4O_6$ (15). This behavior is indicative of the fact that the true site for this molybdenum might be off the mirror plane at z=0.5 on which it resided. Placing the apical molybdenum off the mirror and allowing it to vary, while holding the remaining atoms fixed, produced a result with an improved residual value (R=2.8, R_w=4.7).

There is some question whether this is the best refinement. When the apical molybdenum atom was removed from the refinement and the electron difference map was examined, no maximum in electron density was observed away from the mirror plane, rather there was a gradual increase in density which reached a maximum at the mirror. While this refinement did improve the relative sizes of the thermal parameters, the standard deviations of the parameters for the apical molybdenum atoms refined off the

mirror plane are very large. Positions of oxygen atoms were not varied from the mirror planes on which they were situated with this refinement. When a similar refinement was attempted for $InMo_4O_6$, the refinement did not converge (15).

The consequence of this refinement is that the repeat distance along the c axis should be doubled, doubling the volume of the unit cell. Attempts to collect a data set and solve the structure in the doubled unit cell were unsuccessful. Although, the doubled unit cell was indicated by reflections observed in many oscillation photographs obtained using a Weissenberg camera, it was not possible to obtain indexing on this unit cell with a diffractometer. The doubled cell was, therefore, artificially indexed by doubling the c axis of the indexed subcell. Collection of a data set with these cell parameters yielded only ten additional reflections to the original data set. The parameter/data ratio was satisfactory for the subcell refinement, but a much poorer ratio was found in the doubled cell because the parameters were increased with no significant increase in unique data. Therefore, a satisfactory refinement of the structure for the supercell was not possible.

The final electron density map revealed residual density of 1.0 $e/\AA^3$ at Mo(1) and 1.4 at Mo(2). In the

channels the maximum residual density was 0.8 e/$\AA^3$ observed at c = 0.0.

Positional and thermal parameters for the subcell refinements are listed in Tables III-4 and III-5.

Table III-4. Atomic positions (x 10^4) for $Sn_{0.9}Mo_4O_6$[a]

	mult	x	y	z	U(ave)[b]
Mo(2) on c = 0.5 mirror plane					
Mo(1)	2500	6020.9(5)	11020.9(0)	0.0(0)	7.
Mo(2)	2500	1444.3(5)	6444.3(0)	5000.0(0)	11.
O(1)	2500	2922.(5)	7922.5(0)	5000.0(0)	10.
Sn(1)	946	00.(0)	00.(0)	148.(2)	15.
Sn(2)	154	00.(0)	00.(0)	3018.(4)	19.
O(2)	5000	2637.(5)	5404.(5)	0.0(0)	9.
Mo(2) off mirror plane					
	mult	x	y	z	U(ave)[b]
Mo(1)	2500	6021.9(5)	11021.9(0)	0.0(0)	7.
Mo(2)	2500	1445.3(6)	6445.3(0)	4610.(85)	7.
O(1)	2500	2926.(9)	7926.3(0)	5000.0(0)	11.
Sn(1)	946	0.0(0)	0.0(0)	138.3(0)	16.
Sn(2)	154	0.0(0)	0.0(0)	3030.4(0)	19.
O(2)	5000	2635.(5)	5411.(5)	0.0(0)	11.

[a]Estimated standard deviations are given in parentheses for last significant figure.

[b]The isotropic equivalent thermal parameter, U(ave), is the average of U_{11}, U_{22}, and U_{33}.

Table III-5. Anisotropic thermal parameters (x 10^4) for $Sn_{0.9}Mo_4O_6$[a]

Refinement with Mo(2) on mirror plane

atom	U_{11}	U_{22}	U_{33}	U_{12}	U_{13}	U_{23}
Mo(1)	6.4(2)	6.4(0)	7.5(3)	0.7(2)	0.0(0)	0.0(0)
Mo(2)	5.3(2)	5.3(0)	22.8(4)	-1.1(2)	0.0(0)	0.0(0)
O(1)	10.(2)	10.1(0)	10.(3)	3.(2)	0.0(0)	0.0(0)
Sn(1)	11.3(0)	11.2(0)	23.5(0)	0.0(0)	0.0(0)	0.0(0)
Sn(2)	20.0(0)	20.0(0)	15.5(0)	0.0(0)	0.0(0)	0.0(0)
O(2)	6.(2)	14.(2)	8.(2)	-4.(2)	0.0(0)	0.0(0)

Refinement with Mo(2) off mirror plane

atom	U_{11}	U_{22}	U_{33}	U_{12}	U_{13}	U_{23}
Mo(1)	6.3(2)	6.3(0)	7.5(3)	0.9(2)	0.0(0)	0.0(0)
Mo(2)	5.4(2)	5.4(0)	10.(6)	-0.2(2)	-1.4(6)	-1.4(0)
O(1)	12.(3)	11.4(0)	9.(3)	- 5.(2)	0.0(0)	0.0(0)
Sn(1)	11.3(6)	11.4(0)	23.8(6)	0.0(0)	0.0(0)	0.0(0)
Sn(2)	20.(5)	19.8(0)	18.(4)	0.0(0)	0.0(0)	0.0(0)
O(2)	8.(2)	18.(2)	7.(2)	-6.(2)	0.0(0)	0.0(0)

[a]The general thermal parameter expression used is $\exp[-2\pi^2(U_{11}h^2a^{*2} + U_{22}k^{*2} + U_{33}l^{*2} + 2U_{12}hka^*b^* + 2U_{13}hla^*c^* + 2U_{23}klb^*c^*)]$. Estimated standard deviations are given in parentheses for last significant figure.

RESULTS AND DISCUSSION

Structure of $Sn_{0.9}Mo_4O_6$

$Sn_{0.9}Mo_4O_6$ is isostructural with $NaMo_4O_6$ (1) and $InMo_4O_6$ (15). Like these compounds the structure of $Sn_{0.9}Mo_4O_6$ is dominated by the metal-metal bonding. Extended chains of trans-edge shared Mo_6 octahedra extend through the lattice parallel to the c-axis of the structure. Figure III-1 shows a view of one molybdenum oxide chain as viewed perpendicular to the chain direction, which clearly shows the edge sharing of the octahedral cluster units. Figure III-2 shows a view of the structure looking down the c axis. Evident from this view is the manner in which the cluster chains are linked together via oxygen atoms to form a tunnel in which the tin atoms reside. The diameter of the tunnel (the linear O(2)-Sn-O(2) distance when Sn is located at z=0) is 4.6 Å. The four-fold symmetry is clearly evident from this view. There are two distinct molybdenum atoms, Mo(1) (waist) and Mo(2) (apex), in the asymmetric unit of $Sn_{0.9}Mo_4O_6$. The remaining molybdenum atoms are generated by the symmetry of the cell. Both types of Mo are situated in mirror planes at special positions in the unit cell.

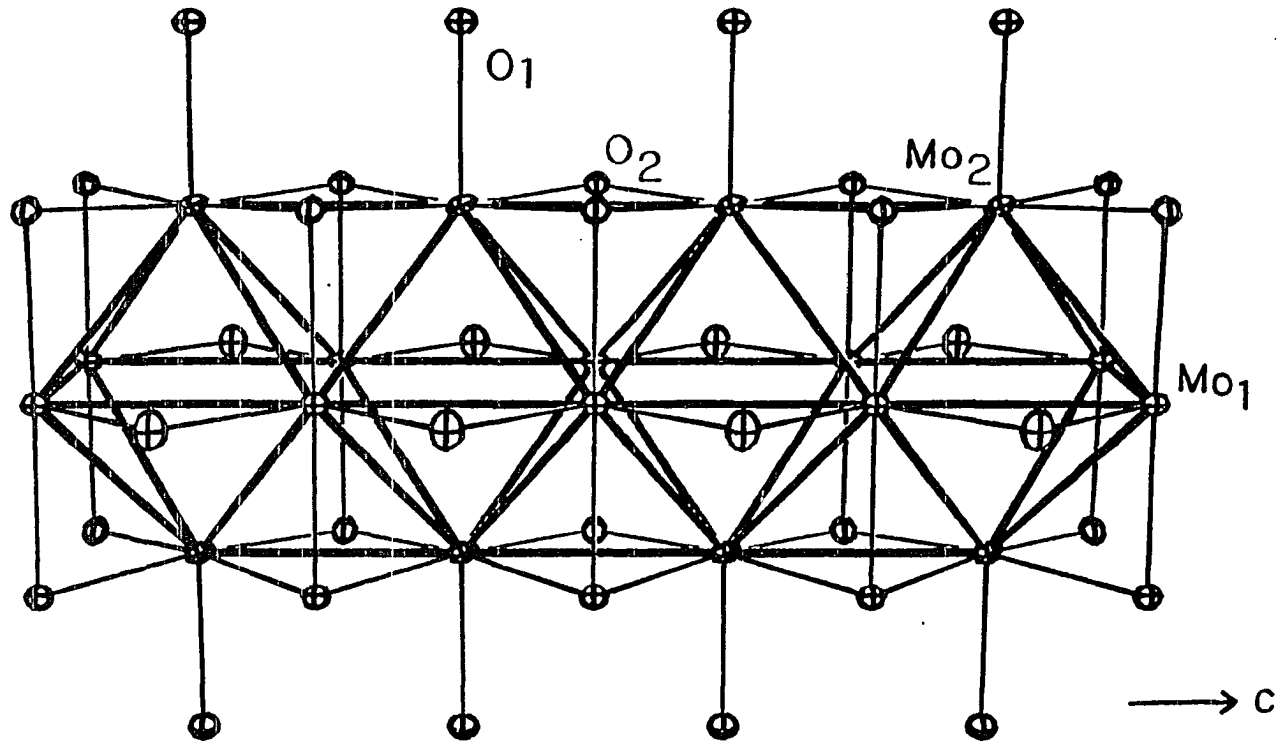

Figure III-1. View of Mo_4O_6 chain in $Sn_{0.9}Mo_4O_6$ perpendicular to chain axis showing the condensed edge-shared octahedra

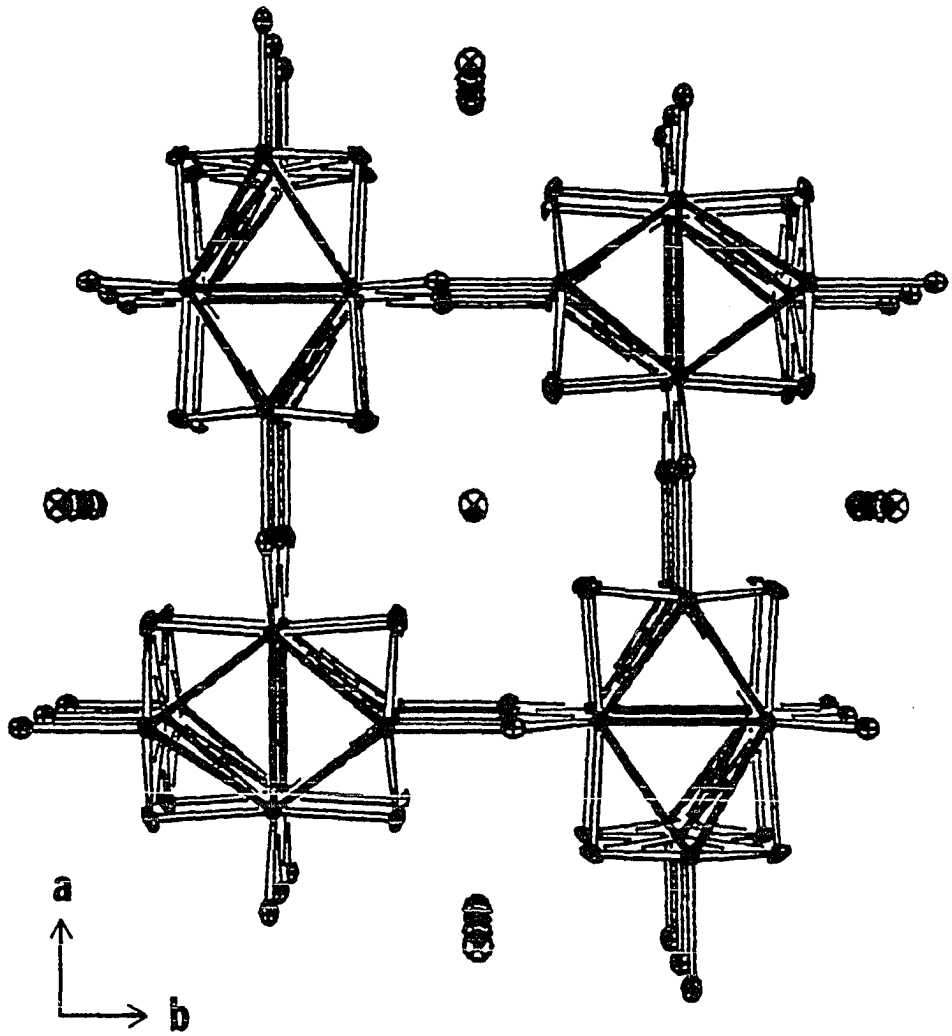

Figure III-2. View of $Sn_{0.9}Mo_4O_6$ looking down the infinite c axis and showing the manner in which four Mo_4O_6 chains are coupled to form a channel which is occupied by Sn atoms

Bond distances and angles are shown in Table III-6 and III-7. There are three distinct Mo-Mo bond distances in the compound. The distance from waist Mo(1) to waist Mo(1) along the c axis is 2.8369(6) Å, which is the repeat distance of the unit cell. This is also the apical Mo(2) to apical Mo(2) distance. The waist to waist molybdenum distance forming the shared edges of the cluster units is 2.7770(8) Å. There is only one Mo(1) to Mo(2) distance which is 2.7927(5) Å.

The coordination number of the waist molybdenum atoms is eleven. Seven bonds are to neighboring Mo atoms in the chain and four bonds are to bridging oxygen atoms. The apex molybdenum atom has a coordination number of eleven also. This atom bonds to the four metal atoms forming the waist of the octahedron as well as to the two apical molybdenum atoms in adjacent octahedra. Mo(2) also bonds to four bridging intrachain oxygen atoms (O(2)) and to one interchain oxygen bridge (O(1)).

It was possible to refine the apical molybdenum atom away from the mirror plane at z = 0.5. The atom refined to a position 0.11 Å away from the mirror. A consequence of this refinement is that alternate long and short apex-apex bonds occur along the chain, 2.62 Å and 3.06 Å, respectively. With this interpretation the c axis of the unit cell should be at least doubled, providing an

Table III-6. Interatomic distances (Å) in $Sn_{0.9}Mo_4O_6$[a]

Mo(2) on mirror plane			
Mo(1)-Mo(1)	2.8369(6)	Sn(1)-Sn(1)	2.8369(6)
Mo(1)-Mo(1)	2.7770(8)	Sn(1)-Sn(1)	2.75846(6)
Mo(2)-Mo(1)	2.7927(5)		
Mo(2)-Mo(2)	2.8369(6)	Sn(1)-O(2)	2.3059(3)
		Sn(2)-O(2)	2.4568(2)
Mo(1)-O(1)	2.019(3)		
Mo(1)-O(2)	2.072(5)	O(1)-O(2)	2.8206(6)
Mo(2)-O(1)	2.011(4)	O(1)-O(2)	2.8276(3)
Mo(2)-O(2)	2.081(4)		
Mo(2) off mirror plane			
Mo(1)-Mo(1)	2.8369(6)	Mo(1)-O(1)	2.013(1)[b]
Mo(1)-Mo(1)	2.783(4)	Mo(1)-O(2)	2.075(2)[b]
Mo(2)-Mo(1)	2.855(3)	Mo(2)-O(1)	2.015(2)[b]
Mo(2)-Mo(1)	2.742(2)	Mo(2)-O(2)	2.002(2)[b]
Mo(2)-Mo(2)	3.0583(6)	Mo(2)-O(2)	2.153(2)[b]
Mo(2)-Mo(2)	2.6156(5)		

[a]Standard deviation of last significant figure is given in parentheses.

[b]Standard deviation for this distance is based only on the uncertainty in the molybdenum atom position.

Table III-7. Bond angles (deg) in $Sn_{0.9}Mo_4O_6$[a]

Mo(2) on mirror plane							
atom	atom	atom	angle	atom	atom	atom	angle
Mo(1)-	Mo(1)-	Mo(1)	90.00(0)	O(1)-	Mo(1)-	O(2)	87.43(0)
Mo(1)-	Mo(2)-	Mo(1)	61.05(1)	O(2)-	Mo(1)-	O(2)	172.79(0)
Mo(1)-	Mo(2)-	Mo(1)	59.63(1)	O(1)-	Mo(2)-	O(2)	87.15(1)
Mo(1)-	Mo(1)-	Mo(2)	59.47(1)	O(2)-	Mo(2)-	O(2)	89.95(1)
Mo(1)-	Mo(1)-	Mo(2)	90.59(1)	O(2)-	Mo(2)-	O(2)	93.76(1)
Mo(1)-	O(2)-	Mo(1)	89.25(1)	O(2)-	Mo(2)-	O(2)	174.31(0)

[a]Standard deviation of last significant figure is given in parentheses.

explanation for the supercell reflections observed in the oscillation photographs. One possible arrangement for the molybdenum chain with short and long distances is pictured in Figure III-3, although the short and long distances may not be staggered as they are shown. Alternating short and long distances between apical molybdenum atoms in condensed octahedral chains have been previously observed in related quaternary oxides with the $M_xM'_yMo_4O_7$ stoichiometry (3,4).

There are two types of oxygen atoms in the cell. One, O(1), forms the inter-cluster linkage. This atom bridges the two waist molybdenum atoms in one chain and is also bound to the apical molybdenum atom of an adjacent chain. The atom is thus bonded in trigonal planar geometry to three Mo atoms. The second oxygen atom, O(2), bridges from waist to apex Mo atoms within a cluster chain and is thus bound to two apex and one waist molybdenum atom. Four O(2) atoms, each from different chains, provide the coordination for the tin atom in the tunnel of the structure.

The best refinement for the structure was obtained when tin atoms were placed in two separate sites in the tunnel. Both positions are located off the mirror planes at c=0. One Sn atom, with an occupancy of 0.76 Sn per Mo_4O_6 unit, occurs 0.0392 Å away from c=0. In this position, it is nearly square planar with respect to coordination by four O(2) atoms, as shown in Figure III-4a. The Sn(1)-O(2)

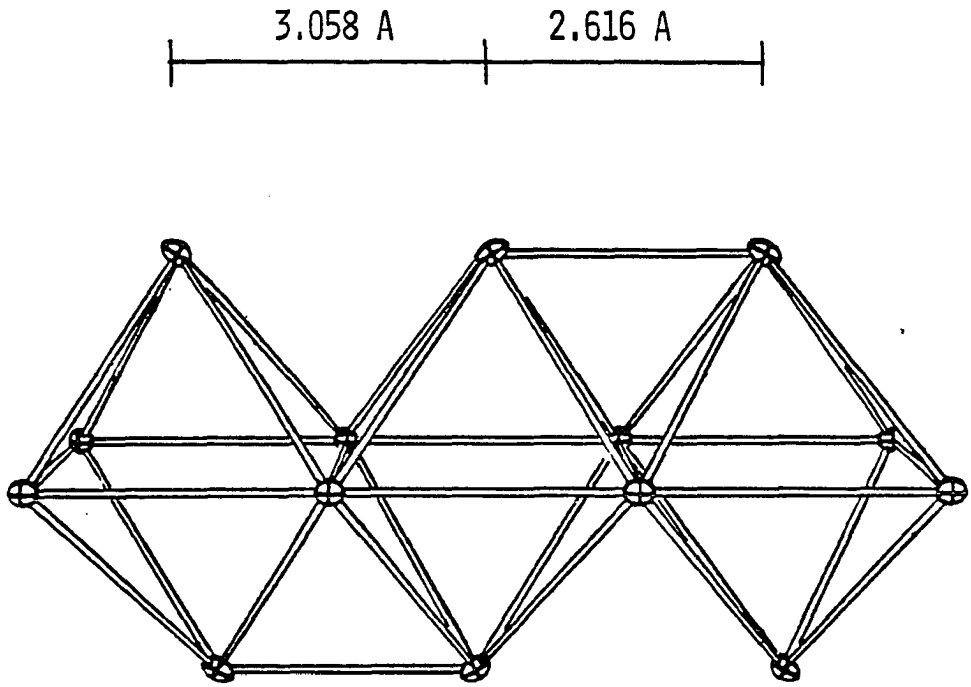

Figure III-3. View of one Mo_4O_6 chain in $Sn_{0.9}Mo_4O_6$ showing long and short distances resulting from allowing the apical molybdenum to refine away from the c=0.5 mirror plane

distance is 2.3059(3) Å, slightly longer than the 2.21 Å found for the Sn-O distance in SnO (16), where Sn is in square pyramidal coordination.

The second Sn atom, shown in Figure III-4b, is found in the center of the tunnel 0.848 Å away from the c=0 mirror plane. This atom has an occupancy of 0.12 per Mo_4O_6 unit and is coordinated by four oxygen atoms at the base of a square pyramid. The long Sn-O distance in this site, 2.457 Å, suggests that an additional factor is present in determining the location of the Sn atom in the tunnel.

The square pyramidal coordination of Sn(2) is similar to that found for In in $InMo_4O_6$ (15) but very different than the environment for Na in $NaMo_4O_6$ (1). In $NaMo_4O_6$, the Na atom occupies the center of a cube of oxygen atoms formed by the O(2) atoms in the c=0 layers of two adjacent cells. The indium atom in $InMo_4O_6$ is located approximately 0.15 Å away from the plane of four oxygen atoms. In $Sn_{0.9}Mo_4O_6$, one Sn atom is displaced from the center of the cube such that it has nearly square planar coordination while the other has the coordination discussed above.

The atom multipliers sum to give an occupancy of 0.88 Sn per Mo_4O_6. Electron microprobe analysis of the compound determined 0.95 per Mo_4O_6. The cause of the partial occupancy remains unexplained. While evidence for doubling

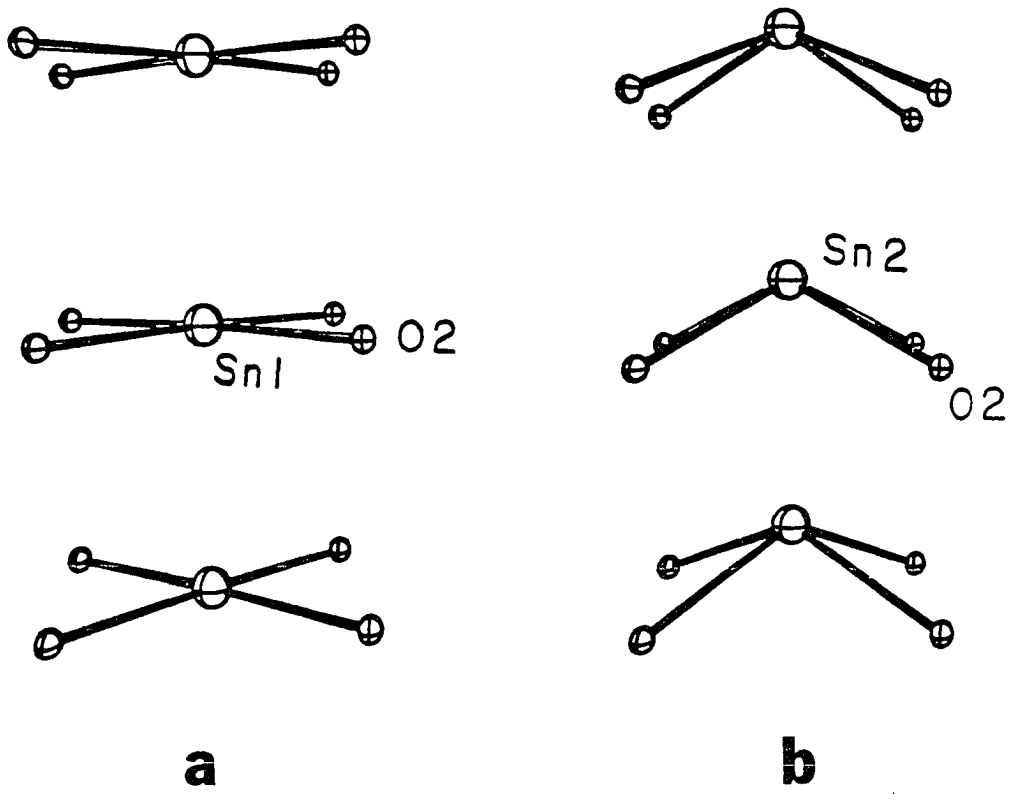

Figure III-4. View of coordination of the two types of Sn in $Sn_{0.9}Mo_4O_6$. a) Sn approximately in plane of four O(2) oxygen atoms b) Sn with square pyramidal coordination

of the c-axis has been observed no evidence of superstructure which might explain the stoichiometry and ordering of the Sn atoms in the tunnel has been found. Perhaps complete filling of the bonding and nonbonding bands by electrons occurs with this stoichiometry. If Sn is actually in a 2+ oxidation state, the stoichiometry observed here represents the maximum amount of electrons donated to the chain for the Mo_4O_6 structure type when compared to other ternary metal atoms. Similar partial occupancy is observed for other divalent cations in $Pb_{0.75}Mo_4O_6$ (15) and $Ba_{0.62}Mo_4O_6$ (2).

There is an important question about the true nature of the occupation of the Sn sites in the channels. It is possible that Sn-Sn bonding is responsible for the disordered behavior in the occupation of these sites. Consider a channel in the structure with ten Mo_4O_6 units, shown in Figure III-5. The 10 channel sites may be occupied by 9 Sn atoms, with one vacancy separating short chains of Sn atoms in the manner shown. There are two types of Sn atoms. One type is adjacent to a vacancy and forms a bond to only one other Sn atom, while the remaining Sn atoms are adjacent to two other Sn atoms on both sides. There are thus two of the first type and seven of the latter in the ten unit supercell. The total occupation corresponds to 0.9 Sn per Mo_4O_6. The occupation of the two sites in

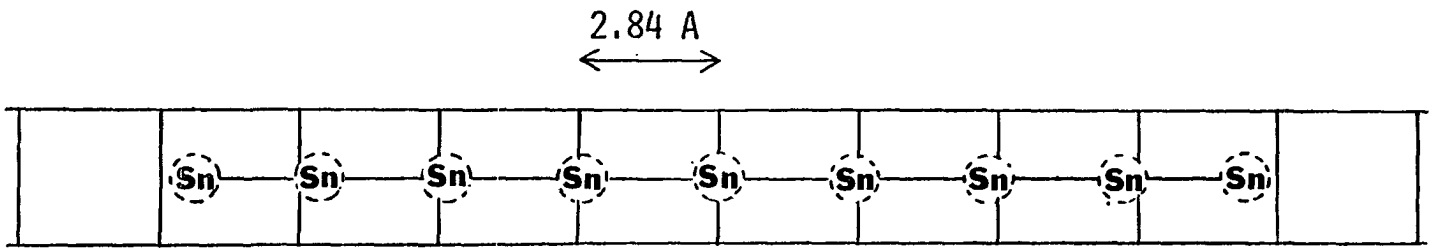

Figure III-5. Possible occupation of tin atoms in tunnel of $Sn_{0.9}Mo_4O_6$ showing the effect of Sn-Sn bonding on the position of Sn with respect to the mirror planes at c=o.

the structure solution are similar to those of the hypothesized occupancy (2/10 and 7/10). If one considers that the Sn atoms are pulled towards each other by Sn-Sn bonding, the density along the channel observed in the crystal structure is explained. The residual electron density remaining in the channel is an indication that the two site model of the crystal structure is not completely correct and that the true behavior of the Sn in these sites is more complicated.

Bond Length-Bond Order Relationships

The application of bond length-bond order (or strength) relationships has provided interesting insights into the structure and bonding of the reduced molybdenum oxides synthesized in this group (17). $Sn_{0.9}Mo_4O_6$ is no exception.

The approach involves the application of bond length-bond order equations to calculate the Mo-O and Mo-Mo bond orders for observed distances in the compound and the subsequent use of these bond orders to estimate the number of electrons available for metal-metal bonding, the anion charges, and oxidation states of metal atoms and ternary atoms in the compound.

The bond order of the metal-metal bonds is determined by use of Pauling's bond order equation eq. 1, (18) where d_1

$$d_n = d_1 - 0.6 \log n \qquad 1$$

and d_n are the bond lengths of bonds with orders 1 and n respectively. The distance used for d_1 is 2.614 Å, based on calculations of distances to nearest neighbor and next nearest neighbor in bcc molybdenum metal (17).

Bond strengths (s) of Mo-O bonds are calculated from the empirical relation (eq. 2) put forth by Brown and Wu (19) and used by Bart and Ragaini (20).

$$s(Mo\text{-}O) = [d(Mo\text{-}O)/1.882]^{-6.0} \qquad 2$$

This relation is based on an extensive examination of a number of molybdenum oxide compounds where the oxidation state of Mo ranges from +2 to +6. The value of s in these calculations is given in valence units. Thus, the sum of the bond strengths around any given Mo atom should give the valence of that particular molybdenum atom.

The numerical values for these calculations, carried out separately for the cases where Mo(2) is constrained to the c = 0.5 mirror plane and where it is refined away from the mirror plane, are tabulated in Tables III-8 and III-9.

The number of metal cluster electrons (MCE) per Mo_4O_6 repeat unit may be estimated from the sum of the metal-metal bond orders, eq. 3.

$$MCE = 2\Sigma n(Mo_4O_6) \qquad 3$$

In this way the result MCE = 12.6 was obtained.

The total valence of the Mo_4O_6 unit is 10.6, obtained from eq. 2 by summing the individual valences of the Mo atoms in the Mo_4O_6 unit. Subtracting the 10.6 from the maximum possible valence of four molybdenum atoms, 24, leaves 13.4 electrons for the metal atoms to utilize in metal-metal bonding.

The difference between 12.6 electrons calculated from metal-metal bond orders, and 13.4 electrons calculated from the Mo-O bond strengths is 0.8 electrons. This difference is an indication of electrons which reside in nonbonding or antibonding orbitals.

The number of electrons available for metal-metal bonding calculated from the chemical formula assuming the Sn atom is present in the +2 oxidation state is 13.8. The difference between the MCE of 12.6 and this value of 13.8 is also an indication that some electron density resides in non- or antibonding orbitals.

A comparison of the bond order analysis when the apical molybdenum atoms are both on and off the mirror plane shows that more efficient use of the bonding electrons is made by forming a shorter bonding distance and a longer nonbonding distance between the two apical molybdenum atoms (MCE =

Table III-8. Bond length-bond order relationships in $Sn_{0.9}Mo_4O_6$ with Mo(2) on mirror plane

Bond orders					
Metal atom	d(Mo-Mo)	n	f		nf
Mo(2) apical	2.8369(6)	0.425	2		0.85
	2.7927(5)	0.504	4		2.02
				Σnf	2.87
Mo(1) waist	2.8369(6)	0.425	2		0.85
	2.7770(8)	0.535	1		0.54
	2.7929(5)	0.504	4		2.02
				Σnf	3.41
Atom valence					
Metal atom	d(Mo-O)	s	f		sf
Mo(2) apical	2.010(4)	0.67	1		0.67
	2.081(4)	0.55	4		2.20
				Σsf	2.87
Mo(1) waist	2.019(3)	0.65	2		1.30
	2.071(5)	0.56	2		1.12
				Σsf	2.42

Metal-Metal MCE = $2(\Sigma nf_a) + 2(\Sigma nf_w)$

$2(2.87) + 2(3.41) = 12.56$

Total valence of Mo_4 unit = $2\,\Sigma sf_a + 2\,\Sigma sf_w$

$5.74 + 4.84 = 10.58$

MCE = $24 - 10.58 = 13.4\ e^-$ for M-M bonding

delta = $13.4 - 12.6 = 0.8\ e^-$ non- or antibonding

Table III-9. Bond length-bond order relationships in $Sn_{0.9}Mo_4O_6$ with Mo(2) off mirror plane

Bond orders					
Metal atom	d(Mo-Mo)	n	f		nf
Mo(2) apical	2.855(3)	0.404	2		0.81
	2.743(2)	0.617	2		1.23
	3.058(1)	0.181	1		0.18
	2.616(1)	1.01	1		1.01
				Σnf	3.23
Mo(1) waist	2.836(6)	0.425	2		0.85
	2.783(4)	0.529	1		0.53
	2.743(2)	0.617	2		1.23
	2.855(3)	0.404	2		0.81
				Σnf	3.42
Atom valence					
Metal atom	d(Mo-O)	s	f		sf
Mo(2) apical	2.002(2)	0.69	2		1.39
	2.153(2)	0.45	2		0.90
	2.015(2)	0.67	1		0.67
				Σsf	2.96
Mo(1) waist	2.013(1)	0.66	2		1.33
	2.075(2)	0.56	2		1.11
				Σsf	2.44

Metal-Metal MCE = $2(\Sigma nf_a) + 2(\Sigma nf_w)$

$2(3.23) + 2(3.42) = 13.30$

Total valence of Mo_4 unit = $2(\Sigma sf_a) + 2(\Sigma sf_w)$

$2.96 + 2.44 = 5.40 \times 2 = 10.80$

MCE = 24 - 10.58 = 13.2 e^- for M-M bonding

13.3) over two equidistant weaker bonding distances (MCE = 12.6). Because the oxygen atoms were not varied from their sites on mirror places these results should be viewed with some caution.

Extended Hückel Calculations

Extended Hückel calculations were carried out on $Sn_{0.9}Mo_4O_6$ to determine if Sn-Sn bonding could be responsible for the disorder of the Sn atoms along the tunnel of the structure. The program employed the extended Hückel method previously described (21, 22). The parameters used for molybdenum and oxygen are tabulated in Table III-10 and are the same as those used in previous calculations for the Mo-oxide chain (23). The H_{ii}'s for Sn were estimated from Herman-Skillman tables of orbital energies (24). The H_{ij} matrix elements for all atoms were calculated using the weighted Wolfsberg-Helmholtz formula (25, 26). Zeta exponents for Slater type orbitals were obtained from Clementi and Roetti (27).

The contents of an entire unit cell were input so that the interaction of the Sn atom with four Mo-oxide chains could be examined. Only six k-points were used so that computing time could be minimized. The electron count in the calculation was varied so that the effect of the partial occupancy of the Sn could be examined.

Table III-10. Parameters for extended Hückel calculations

Orbital		VOIE[a]	ζ_1[b]	ζ_2[c]
Mo	4d	-11.06	4.54	1.90
	5s	-8.77	1.96	
	5p	-5.60	1.90	
O	2s	-32.3	2.275	
	2p	-14.8	2.275	
Sn	5s	-16.0	2.13	
	5p	-8.5	1.68	

[a] H_{ii}, valence orbital ionization energy.
[b] Slater type orbital exponents.
[c] Double zeta expansion used for molybdenum.

The diagram of the total density of states (DOS) near the Fermi level is shown in Figure III-6a and is essentially the same as that observed in previous calculations for the Mo-oxide chain (23). The Mo d and Sn orbital contributions to the total DOS are shown in Figures III-6b and III-6c. The similarity of the Mo d contribution to the total DOS in the conduction band indicates that the bands at the Fermi level are primarily Mo d in character. The Sn contribution to the DOS is very small, although it is evident that some Sn bands are present. In addition to these bands, a large band occurring 4 to 6 eV below the Fermi level in the total DOS is believed to be an oxygen 2p band.

In Figure III-7, the Sn density of states for the same energy range is magnified and separated into its components. Evident is the large band at -4 to -6 eV for the Sn p_x and p_y bands which indicates that these orbitals mix with and therefore bond to the oxygen orbitals which are found at this same energy in Figure III-6. The Sn s and p_z orbitals are completely separated from the Sn p_x and p_y orbitals. The Sn s and p_z orbitals have high densities of states at similar energies which suggests a significant amount of mixing of these orbitals. In valence bond theory, one would consider this an sp hybrid. The Sn p_z orbitals exhibit significant density of states at the Fermi level. If the placement of the Fermi level is correct, then conduction of

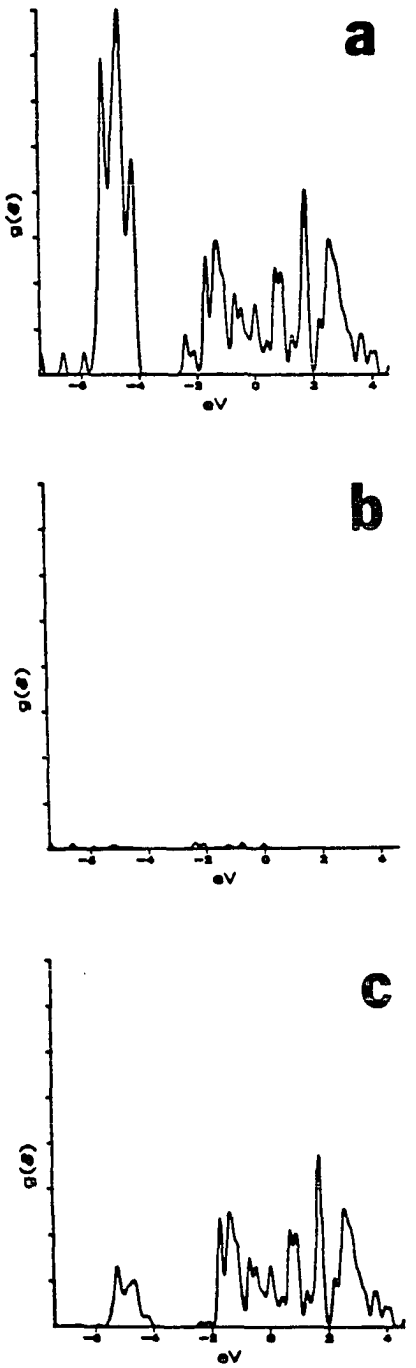

Figure III-6. Density of states (DOS) in $Sn_{0.9}Mo_4O_6$.
a) total DOS b) Sn contribution to total DOS
and c) Mo d orbital contribution to total DOS

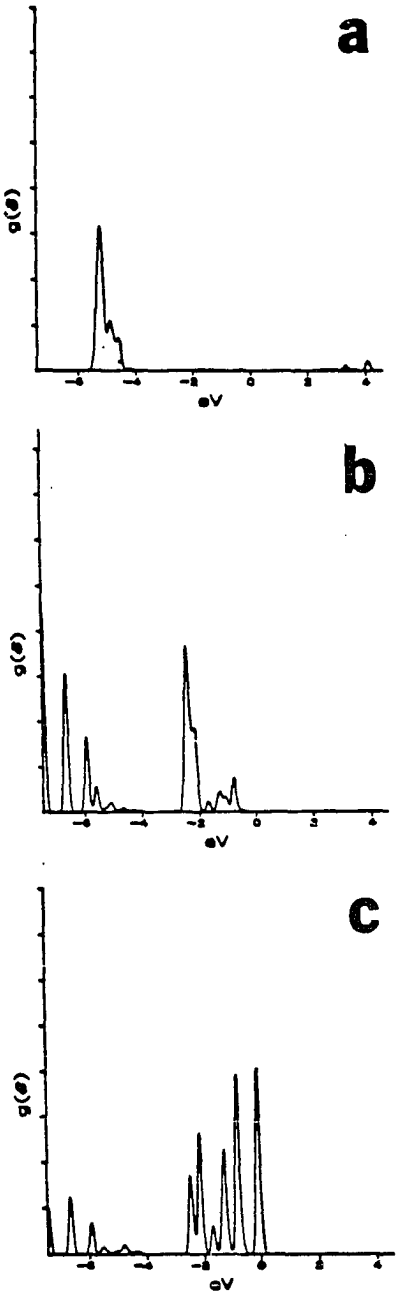

Figure III-7. Density of states for Sn orbitals in $Sn_{0.9}Mo_4O_6$. a) px, py contribution to Sn DOS
b) s contribution to Sn DOS and
c) pz contribution to Sn DOS

electrons can occur along the Sn atoms in the channel (vide infra).

The crystal orbital overlap populations for Sn-Sn and Sn-O bonding are shown in Figure III-8. The bonding character of the Sn s and p_z orbitals is clearly evident. Nearly all of the density observed below the Fermi level is bonding in character. The overlap for the Sn-O bonds is positive for the region where there is p_x and p_y character in the density of states (-4 to -6 eV) and negative for the s and p_z character. Thus, it can be concluded that Sn-Sn bonds are formed in the channel and are composed of Sn s-p_z hybrid orbitals. Bonding of the Sn atom to the Mo-oxide chain is effected by the p_x and p_y orbitals.

Physical Measurements

Resistivity

$Sn_{0.9}Mo_4O_6$ is a metallic conductor. Figure III-9 shows a plot of the normalized resistivity ratio, $\rho(T^o)/\rho(4^o)$, versus temperature for one of the crystals. The crystals exhibited this behavior regardless of the direction in which the potential drop was measured. The decreasing resistance with decreasing temperature is attributed to reduced phonon scattering of conduction electrons as the thermal motion of the lattice is decreased. Evident in Figure III-9 is the point at approximately 20 K where the thermal motion of the

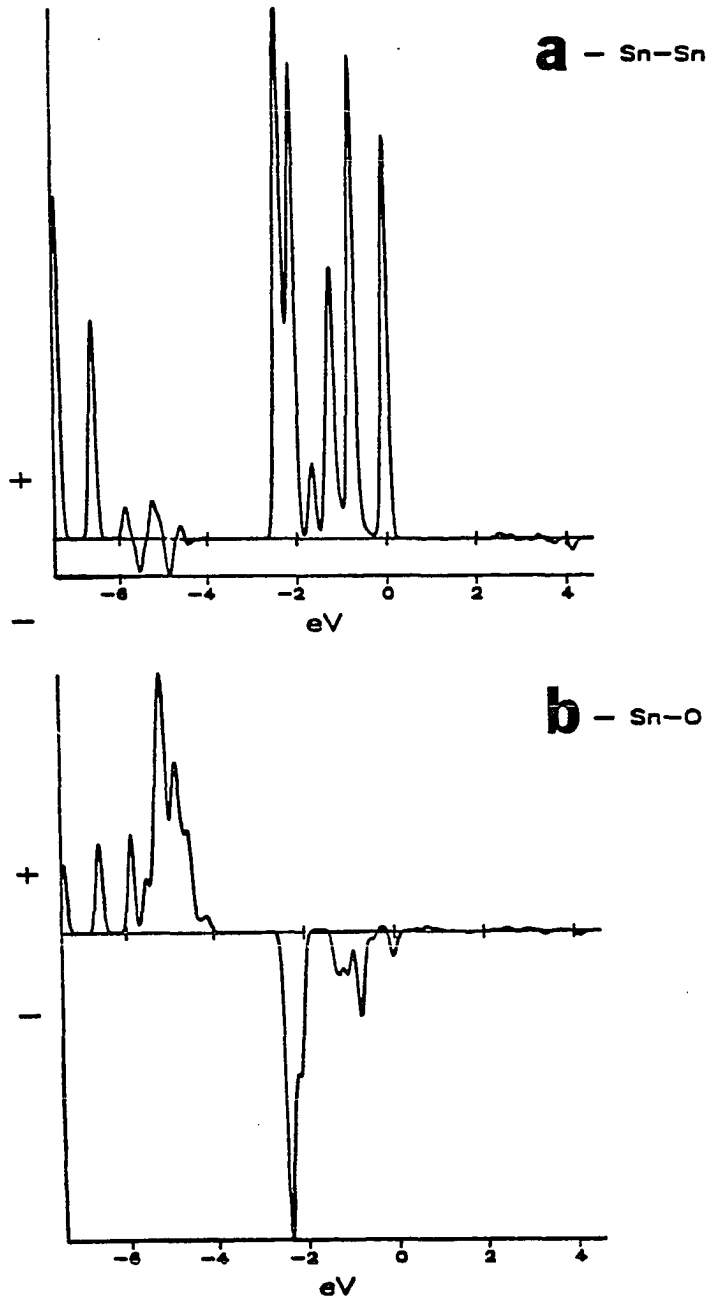

Figure III-8. Crystal orbital overlap populations for a) Sn-Sn and b) Sn-O bonding in $Sn_{0.9}Mo_4O_6$

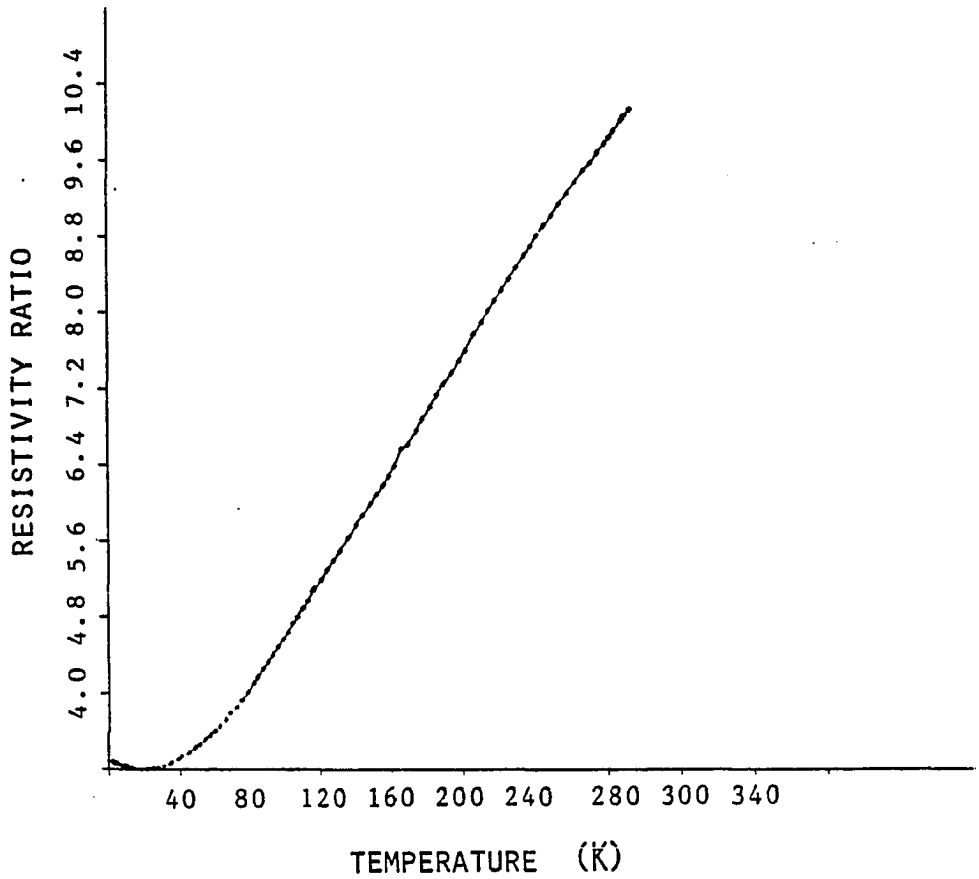

Figure III-9. Resistivity ratio vs temperature for a single crystal of $Sn_{0.9}Mo_4O_6$

lattice is essentially eliminated.

There is a slight upturn of the curve at very low temperatures. This behavior however was not observed when the measurement was made perpendicular to the c axis of the crystal. The cause for this behavior in unknown.

Table III-11 displays the calculated specific resistivites for the two crystals measured. The specific resistivities along the crystal c axis are similar for the two crystals. Even though $Sn_{0.9}Mo_4O_6$ exhibited metallic behavior the anisotropic character of the structure was evident in the information gained from the resistivity measurements. The resistivity measured across the a or b axis of the crystals was much larger than the resisitivity measured along the c axis of the crystals. The ratio of the resistivities at room temperature, $\rho_{\perp}/\rho_{\parallel}$, was 27 for the larger crystal while the same ratio for the smaller crystal was 430.

It was noted later that while our measurements of $\rho_{\parallel}$ are accurate those of $\rho_{\perp}$ are not strictly a measurement of the resistivity along the a or b axis. The resistivity can be considered a 3 x 3 tensor. The values for the resistivity along each of the axes are represented by the diagonal elements of this matrix. Our measurements of $\rho_{\perp}$ are actually a combination of several off-diagonal elements of the resistivity matrix along with the values of the

resistivity along the a and b axis. Measurement of the resistivity strictly along the a or b axis would require attachment of the leads in a manner physically impossible with the methods available to us. In spite of this difficulty, the measurements obtained do indicate the crystal is electrically anisotropic as would be predicted from the structure. As expected, the conductivity along the octahedral chains is greater than that across the chains.

Metallic behavior is also seen for $InMo_4O_6$ (15). $NaMo_4O_6$ has a very low resistivity at room temperature and appears to be metallic, but there is evidence that it undergoes a continuous transition to semiconducting behavior at low temperatures (28). Two explanations can be put forth for the different behavior observed for these materials. The first is simply the fact that the conductivity might be carried in part by the ternary atoms along the tunnels. Thus, $Sn_{0.9}Mo_4O_6$ and $InMo_4O_6$ are able to conduct at low temperatures due to the greater extension of the orbitals on the Sn and In atoms which allows direct bonding between these ternary atoms in the channel. Electron density remaining on the ternary atom is such that conduction can be carried along the tunnel in which they reside. It should be noted that this type of conduction would be more likely for the indium compound because the indium fully occupies the channel in $InMo_4O_6$ where in $Sn_{0.9}Mo_4O_6$ some vacancies must

Table III-11. Resistivity data for $Sn_{0.9}Mo_4O_6$

Crystal dimension (Å)		Vs[a]	ρ[b]	ρ293/ρ4	$\rho_\perp/\rho_\parallel$[c]
0.05 x 0.05 x 1.35	$\rho_\parallel$	757	158	2.4	
	$\rho_\perp$	570	6.8×10^3	2.4	
					430
0.30 x 0.35 x 1.55	$\rho_\parallel$	31	210	3.1	
	$\rho_\perp$	31	5.6×10^3	3.1	
					26.7

[a]Sample resistance (μΩ-cm).

[b]μΩ-cm.

[c]Ratio of the resistivity measured parallel over the resistivity measured perpendicular to the crystal c axis.

exist (which would prevent the conduction of electricity in the channels) because of the nonstoichiometry.
For conduction to be possible in $Sn_{0.9}Mo_4O_6$ the vacancies would have to be ordered such that continuous chains of Sn atoms extended through the lattice. For example, one channel might be completely vacant while nine neighboring channels are fully occupied. The Sn-Sn and In-In distances in these compounds (about 2.8 Å) are short enough to allow metal-metal bonding and conduction of electricity. The interatomic distances for In metal and Sn metal (grey Sn) are 3.25 and 2.81 Å, respectively (16). In $NaMo_4O_6$, the electropositive nature of the Na atom is such that essentially no valence electrons remain on the atom by which the conductivity can be carried.

An alternative explanation is similar to one put forth in explaining the electical and magnetic behavior of the quasi-one dimensional compounds, $M_xMo_6X_6$ (M=K, Rb, Cs, Tl, In; X=Se, Te) (29). These compounds are composed of infinite Mo_3X_3 chains extending in one direction through the lattice, separated by the ternary cations (30). Band calculations (31) on these compounds show, in the one dimensional limit, that a lattice distortion (Peierls type) (32) should occur leading to semiconducting behavior. This is observed for the alkali metal compounds, where a continuous metal-nonmetal transition is observed at low

temperatures. The Tl derivatives, however, exhibited a highly anisotropic metallic conductivity with a superconducting transition at 3.5 K. The above-mentioned band calculations neglected the interchain coupling by the ternary element in these compounds. This is a valid approximation for the compounds with the electropositive alkali metals as the ternary cation because their s and p valence levels are too high in energy to significantly interact with the occupied Mo d and chalcogenide p orbitals near the Fermi level. These compounds can thus be considered as one-dimensional. However, this is not the case for $TlMo_6Se_6$ and $InMo_6Se_6$. The Tl and In s and p valence levels are lower in energy and do mix with the occupied metal and chalcogenide orbitals comprising the conduction band. These compounds are therefore more three-dimensional in character and not subject to the Peierls distortion. At lower temperatures they retain their metallic behavior and even become superconductors.

A similar argument exists for the $M_xMo_4O_6$ compounds. The metal to semiconducting transition is thought to occur for $NaMo_4O_6$ at temperatures below 150^{O} K. $NaMo_4O_6$ may justifiably be considered a one-dimensional compound because of the inability of the Na valence orbitals to effectively interact with the valence levels of the Mo-oxide chains. It should be subject to instability towards Peierls type

distortions which it would undergo, at sufficiently low temperatures, quenching its metallic conductivity. Hoffmann and coworkers have pointed out that symmetry considerations require that this transition be of second order (23) and would thus be a continuous transition, as observed, which would drive the change in the conductivity from conducting to semiconducting behavior. $Sn_{0.9}Mo_4O_6$ and $InMo_4O_6$ are not subject to this type of distortion. The s and p valence orbitals of these ternary atoms interact to a greater extent with the Mo-oxide chain increasing the three-dimensional nature of the structure so that it is no longer subject to a Peierls type distortion. While the highly anisotropic nature of the structure is evident from these conductivity studies the compound retains its metallic nature at temperatures as low as 2 K.

Photoelectron spectroscopy

Valence band The valence and conduction band x-ray photoelectron and ultraviolet photoelectron spectra are shown in Figure III-10. Both spectra clearly exhibit occupied states at the Fermi level. This is in agreement with metallic behavior observed in the resistivity measurements. These spectra are similar to those observed for $NaMo_4O_6$ and $InMo_4O_6$ (15). The x-ray photoelectron spectrum shows a band arising from transitions out of the Mo

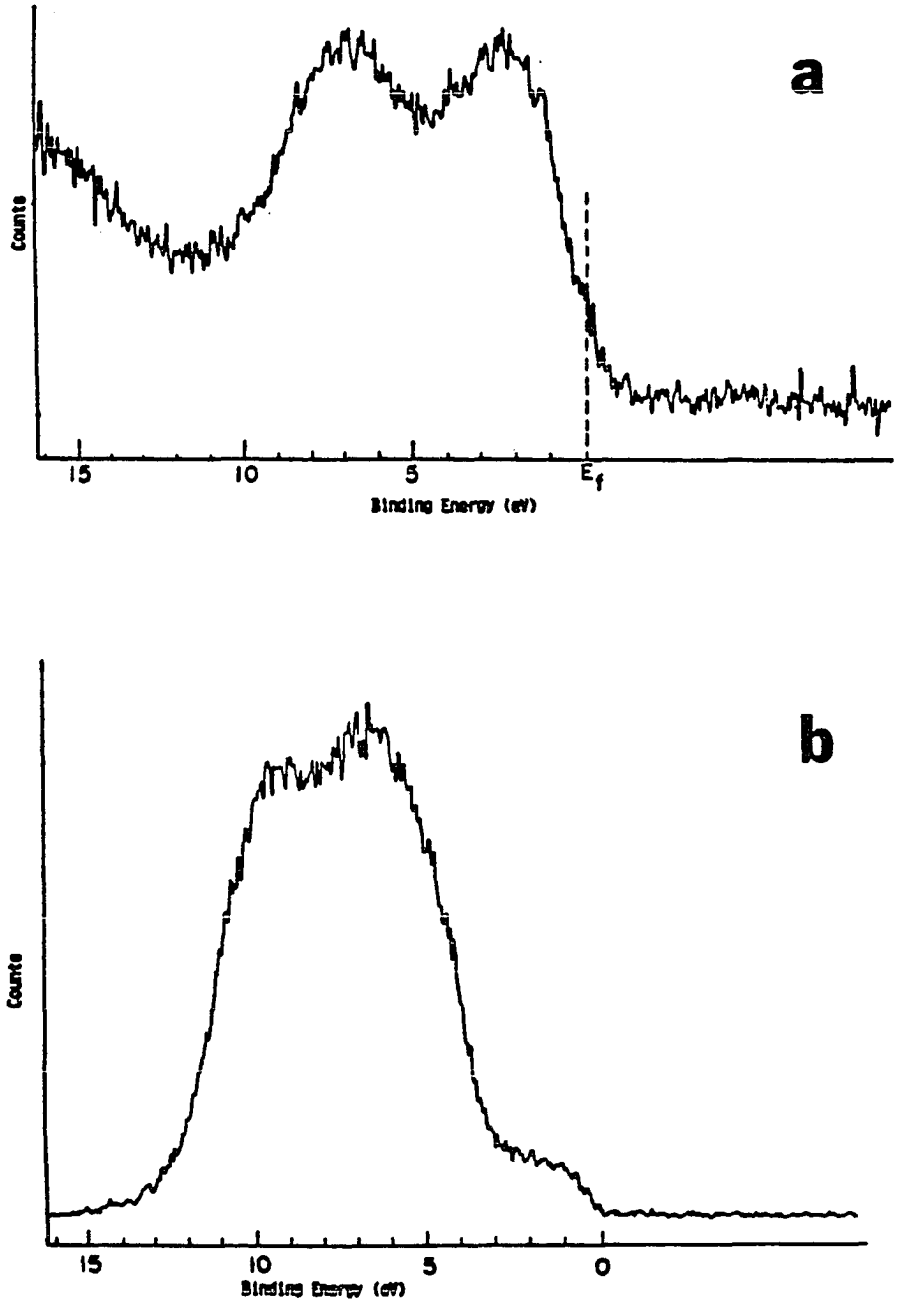

Figure III-10. Photoelectron spectra of $Sn_{0.9}Mo_4O_6$. a) X-ray and b) ultraviolet valence band photoelectron spectra of $Sn_{0.9}Mo_4O_6$

4d orbitals at a binding energy of 2-3 eV and an oxygen 2p band occurring at a binding energy of about 8 eV. The intensity arising from transitions out of the conduction band is larger, relative to the oxygen 2p band than that observed in the spectra of $InMo_4O_6$. This correlates with a greater number of conduction electrons in $Sn_{0.9}Mo_4O_6$ (Sn^{2+} can contribute 2 e to the conduction band while In^+ is thought to contribute only 1).

The helium UPS spectrum reveals a much lower intensity for the conduction band relative to that observed in the x-ray spectrum. While it is difficult to attribute this effect to one contribution, this behavior has been observed for other transition metal oxides (33).

Comparison of the valence band spectra to the density of states near the Fermi level obtained from the extended Huckel calculations is informative. The calculations predict that two bands should be observed. One should appear in the valence band spectra at the Fermi level and should end at a binding energy of 2.5 eV. In addition, a band primarily oxygen in character should occur with a binding energy of 4 to 6 eV. These two bands are clearly evident in the valence band UPS and XPS although the oxygen band has been shifted to slightly lower binding energy.

Sn core spectra The Sn 3d core photoelectron spectrum was also measured to see if any bands could be detected which might indicate more than one type of Sn atom present in the structure. This was not the case. The spectra obtained is shown in Figure III-11. The binding energy of 485.72 is similar to the 486.2 observed for SnO and SnO_2 (34). The full width at half maximum for each spin-orbit component is 1.88 eV is also similar to that observed for other these compounds. No additional peaks or asymmetry that might signal the presence of a different type of Sn were detected.

Mössbauer spectroscopy

The Mössbauer spectrum of $Sn_{0.9}Mo_4O_6$ was collected by Dr. William Reiff at Northeastern University. Spectra were recorded at liquid N_2 and room temperatures using $CaSnO_3$ as reference. The low temperature spectra are shown in Figure III-12; numerical results are listed in Table III-12. The spectrum exhibited a doublet occuring at approximately 4 mm/s with respect to $CaSnO_3$. This is consistent with Sn^{+2} oxidation state. Stannous tin usually lies in the range of 3.5-4.5 mm/s (35). Values for the isomer shift of the stannic ion in SnO_2 are much smaller (Values of 0.55 mm/s are reported) (36). The absorptions arise from a single type of Sn. The doublet is the result of quadrupolar

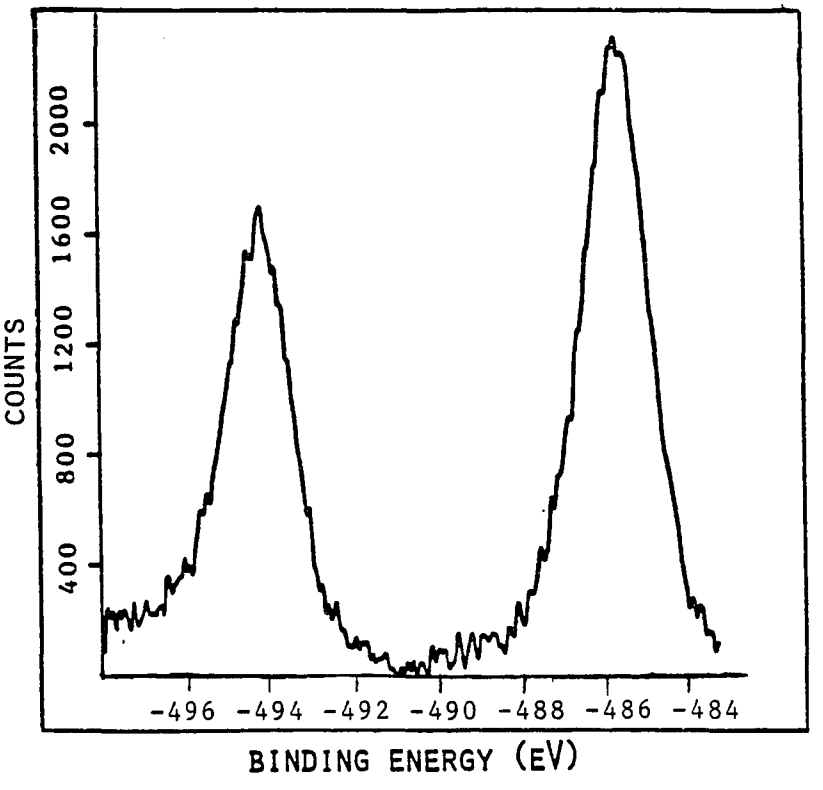

Figure III-11. Sn 3d x-ray photoelectron spectrum of $Sn_{0.9}Mo_4O_6$

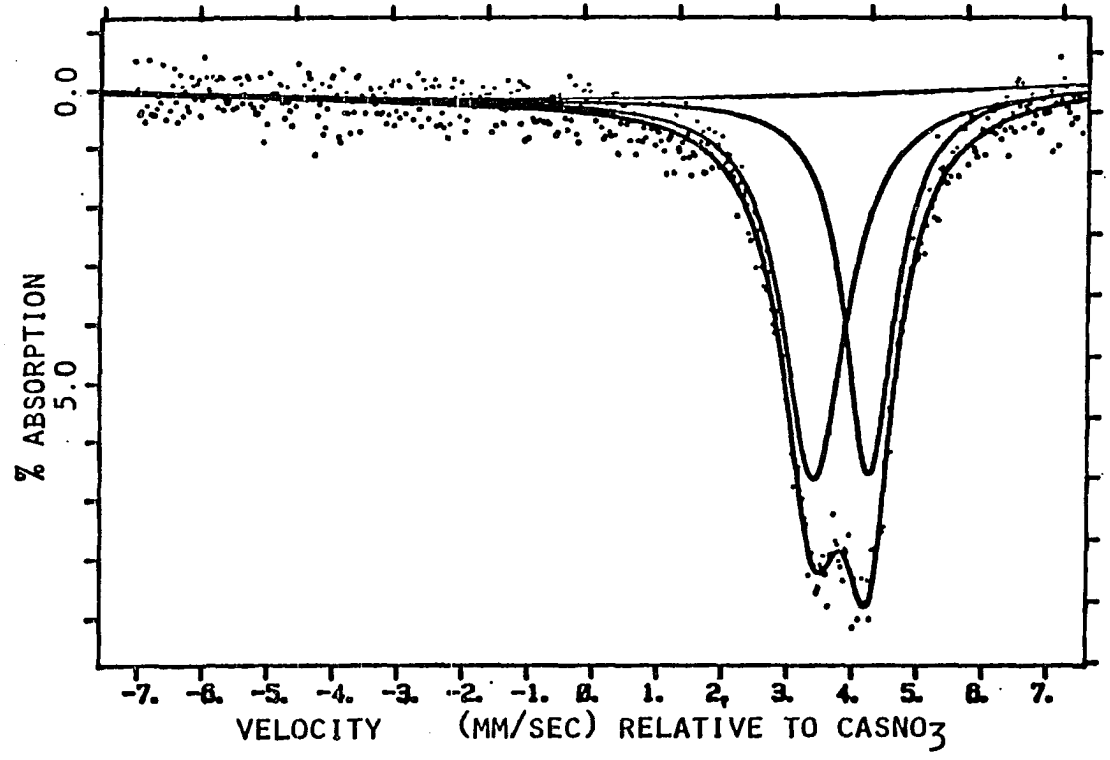

Figure III-12. ^{119}Sn Mössbauer spectrum of $Sn_{0.9}Mo_4O_6$

Table III-12. ^{119}Sn Mössbauer data for $Sn_{0.9}Mo_4O_6$

Reference Source	1/2 —> 3/2	1/2 —> 1/2	I.S.[a]	Q.S.[b]
$CaSnO_3$	3.4014	4.2505	3.8259	0.8491
	(1.1741)[c]	(0.9167)[c]		

[a]Isomer shift (mm/sec).

[b]Quadrupole splitting (mm/sec).

[c]Figures in parentheses are full widths at half maximum (mm/sec).

interaction which splits the M_I=3/2 excited state providing for two absorptions. This result further suggests that the two types of Sn atoms observed in the single crystal structure determination are actually an average of disordered Sn sites. If only two distinct sites were occupied in $Sn_{0.9}Mo_4O_6$, the Mössbauer spectrum should result in four absorptions arising from two different isomer shifts and quadrupole splitting of these peaks.

Mössbauer spectroscopy is heavily dependent on the

density of s electrons near the nucleus. Using the method of Flinn (37), a correlation between the ^{119}Sn isomer shift and the s and p density near the nucleus can be calculated, eq. 4. IS represents the isomer shift in mm/sec, n_s and n_p are the populations of s and p orbitals, respectively.

$$IS = -0.45 + 3.10\, n_s - 0.20\, n_s^2 - 0.17\, n_s n_p \qquad 4$$

If our bond strength-bond length calculations are correct, 13.4 electrons are involved in forming the metal-metal bonds of the Mo_4O_6 cluster unit. Of this number, 1.4 electrons must be transferred from the Sn atom. Considering 0.9 instead of 1 Sn atom per Mo_4O_6, 2.4 electrons remain in the valence levels of the Sn atom, available for Sn-Sn or Sn-O bonding. These electrons can be placed in the s and p orbitals in a variety of configurations described by the formula $s^{2-x}p^{0.4+x}$. Combining this condition with the isomer shift equation, the best fit is obtained with a configuration of $s^{1.6}p^{0.8}$.

Thus, by this interpretation 0.8 electrons populate the p orbitals on the Sn atoms. The Sn atom can utilize these electrons in covalent bonding with the oxygen atoms or in forming Sn-Sn bonds along the tunnels. The latter is suggested as reasonable in view of known Sn-Sn bond distances and the Sn occupation in the tunnel. If all of

the density is directed as sp hybrid orbitals along the chain direction an Sn-Sn bond order of 0.4 is possible.

Magnetic susceptibility

The magnetic susceptibility of $Sn_{0.9}Mo_4O_6$ was obtained using procedures identical to those described for $[Pr_4N]_3Mo_4Cl_{12}\cdot 0.7\ C_2H_4Cl_2$ (Section II).

The magnetic susceptibility *vs.* temperature of $Sn_{0.9}Mo_4O_6$ is plotted in Figure III-13. The susceptibility of the sample is plotted as the smooth line in Figure III-13 and exhibits a paramagnetic 'tail' at low temperatures due to the presence of small amounts of paramagnetic impurities. The data were corrected for the impurity by the method of Tarascon *et al.* (29), considering the molar susceptibility, χ_M, of the sample to be described by eq. 5, where, C_M, theta, and χ_O are constant at low temperatures. Above 50 K

$$\chi_M = C_M/(T-\theta) + \chi_O \qquad 5$$

C_M and theta are constant but χ_O may change. The molar susceptibility is gained by correcting for the paramagnetic tail at each temperature as in eq. 6.

$$\chi_T = \chi_M - C_M/(T-\theta) \qquad 6$$

The corrected molar susceptibility data are shown plotted versus temperature in Figure III-13. $Sn_{0.9}Mo_4O_6$ exhibits a small temperature independent paramagnetic susceptibility throughout the measured temperature range . A similar type of behavior was observed in $InMo_4O_6$. The value of the susceptibility is 3.41×10^{-7} emu/g.

Similar work on the alkali metal $M_xMo_4O_6$ compounds would be of interest to determine if the transition to semiconducting behavior is evident in the magnetic susceptibility of those compounds.

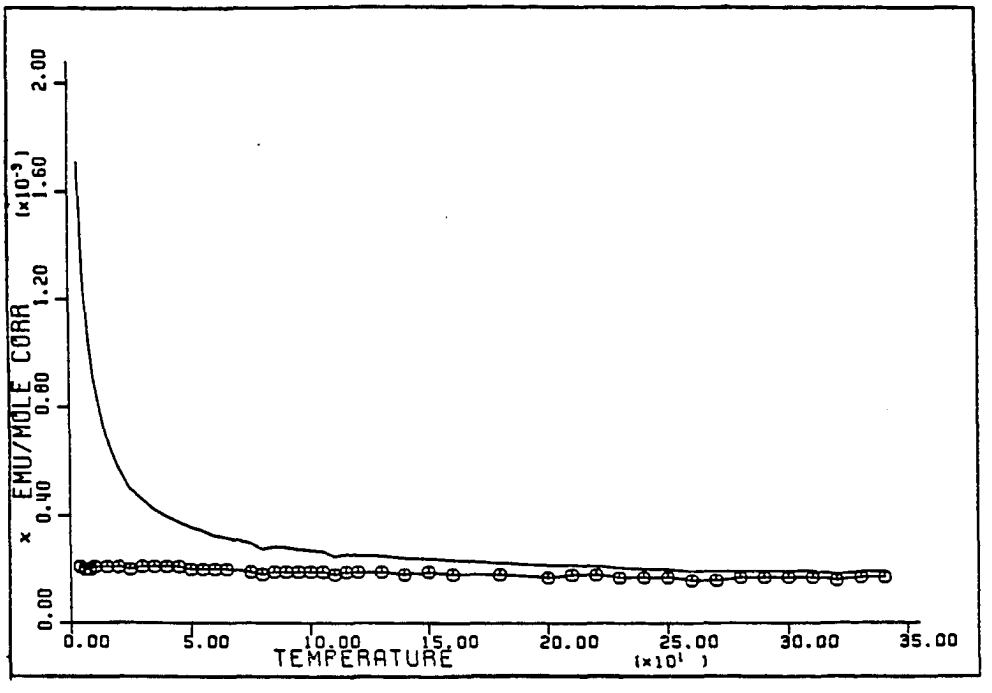

Figure III-13. Magnetic susceptibility [chi (emu/mol) vs T] of $Sn_{0.9}Mo_4O_6$ from 4-300° K. Solid line represents raw data; circles represent data corrected for paramagnetic impurity

CONCLUSION

$Sn_{0.9}Mo_4O_6$ is an interesting compound from the $M_xMo_4O_6$ family because of its nonstoichiometry and physical properties. Our investigations have shown it to be a metallic conductor which exhibits a slight temperature independent paramagnetism. The short repeat distance of 2.83 Å suggests that Sn-Sn bonding occurs in the tunnel of the structure, which has been supported by extended Hückel calculations. Furthermore, the partial occupancy suggests that small chains of approximately nine Sn atoms might be formed in the structure. Similar small chains of five and six indium atoms have been observed in $In_{11}Mo_{40}O_{62}$ (28).

Oscillation photographs have shown that some structural deformation occurs that doubles the length of the c axis observed in the structure determination. Large thermal parameters for the apical molybdenum atoms along the c axis in the structure determination of the compound indicate that these atoms of the octahedral chains are distorted such that short and long distances are the result. This effect could be the cause of the doubling of the c axis. Bond length-bond order relationships show that this corresponds to a more efficient use of bonding electrons.

Further work on these cluster systems shall produce more unforeseen structures with equally interesting properties.

REFERENCES AND NOTES

1. Torardi, C. C.; McCarley, R. E. J. Am. Chem. Soc. 1979, 101, 3963.

2. Torardi, C. C.; McCarley, R. E. J. Solid State Chem. 1981, 37, 393.

3. McCarley, R. E. Phil. Trans. R. Soc. Lond. A, 1982, 308, 141.

4. McCarley, R. E.; Lii, K.-H.; Edwards, P.A.; Brough, L. J. Solid State Chem. 1985, 57, 17.

5. Lii, K. H. Ph.D. Dissertation, Iowa State University, Ames, Iowa, 1985, Section III.

6. Weiser, H.; Milligan, O. "Inorganic Colloid Chemistry: The Hydrous Oxides and Hydroxides"; J. Wiley and Sons, Inc.: London, 1933; Vol. III, page 3039.

7. van der Pauw, L. J. Phillips Research Reports 1958, 13, 1.

8. Luly, M. H. "APES, A Fortran Program to Analyze Photoelectron Spectra", U.S.D.O.E. Report IS-4694, 1979.

9. Clark, C. M.; Smith, D. K.; Johnson, G. J. "A Fortran IV Program for Calculating X-ray Powder Diffraction Patterns-Version 5", Department of Geosciences, Pennsylvania State University, University Park, PA, 1973.

10. Rohrbaugh, W. J.; Jacobson, R. A. Inorg. Chem. 1974, 13, 2435.

11. Jacobson, R. A. J. Appl. Crystallogr. 1976, 9, 115.

12. Karcher, B. A. Ph.D. Dissertation, Iowa State University, Ames, Iowa, 1981.

13. Lawton, S. L.; Jacobson, R. A. Inorg. Chem. 1968, 7, 2124.

14. Structure factor calculations and least squares refinements were done using the block matrix/full matrix program ALLS (Lapp R. L.; Jacobson, R. A. "ALLS, A Generalized Crystallographic Least Squares Program", U.S.D.O.E. Report IS-4708, 1979.), Fourier series calculations were done using the program FOUR (Powell, D. R.; Jacobson, R. A. "FOUR, A General Crystallographic Fourier Program", U.S.D.O.E. Report IS-4737, 1980.) superposition calculations were done using the program SUPERPOSITION (Hubbard, C. R.; Babich, M. W.; Jacobson, R. A. "A PL/1 Program System for Generalized Patterson Superpositions", U.S.E.R.D.A. Report IS-4106, 1977.) and for molecular drawings the program ORTEP (Johnson, C. K., "A FORTRAN thermal-ellipsoid Plot Program for Crystal Structure Illustrations", U.S.A.E.C. Report ORNL-3794, 1965) was used.

15. Lii, K.-H. Ph.D. Dissertation, Iowa State University, Ames, IA, 1985; Section II.

16. Greenwood, N. N.; Earnshaw, A "Chemistry of the Elements"; Pergamon Press: Oxford, 1984; page 446.

17. McCarley, R. E. Department of Chemistry, Iowa State University, in press.

18. Pauling, L. "The Nature of the Chemical Bond", 3rd ed.; Cornell University Press: Ithaca, N. Y.,1960; page 400.

19. Brown, I. D.; Wu, K. K. Acta Crystallogr. 1976, B32, 1957.

20. Bart, J. C.; Ragaini, V. Inorg. Chim. Acta 1979, 36, 262.

21. Computations were carried out using a program employing the extended Huckel method (reference 22) which may be used for both molecular and crystal calculations. It has been developed to its present state by M. -H. Whangbo, S. Wijeyesekera, M. Kertesz, C. N. Wilker, C. Zheng, and T. Hughbanks.

22. Hoffmann, R. J. J. Chem. Phys. 1963, 39, 1397.

23. Hughbanks, T.; Hoffmann, R. J. Am. Chem. Soc. 1983, 195, 3537.

24. Herman, F; Skillman, S. "Atomic Structure Calculations"; Prentice Hall: Englewood Cliffs, N. J., 1963.

25. Amneter, J. H.; Burs, H. -B.; Thibeault, J.C.; Hoffmann, R. J. Am. Chem. Soc. 1978, 100, 1978, 3686.

26. Summerville, R. H.; Hoffmann, R. J. Am. Chem. Soc. 1976, 98, 7240.

27. Clementi, E.; Roetti, C. At. Nucl. Data Tables 1974, 14, 177.

28. Simon, A.; Max-Planck-Institut fur Festkorperforschung, Stuttgart, G.B.R., private communication to Dr. R. E. McCarley.

29. Tarascon, J. M.; DiSalvo, F. J.; Woszcak, J. V. Solid State Comm. 1984, 52, 227.

30. Potel, M.; Chrevel, R.; Sergent, M.; Armici, J. C. Decroux, M.; Fischer, O. J. Solid State Chem. 1980, 35, 286.

31. Hughbanks, T.; Hoffmann, R. J. Am. Chem. Soc. 1883, 105, 1150.

32. Peierls, R. E. "Quantum Theory of Solids"; University Press: London, 1955; page 108.

33. Beatham, N.; Orchard, A. F. J. Elect. Spect. and Rel. Phen. 1979, 16, 77.

34. Albert, W. C. L.; Armstrong, N. R.; Kuwana, T. Anal. Chem. 1977, 49, 1228.

35. Herber, R.H.; DiSalvo, F. J.; Frankel, R. B. Inorg. Chem., 1980, 19, 3135.

36. Berry, F. J.; Hallet, C. J. Chem. Soc., Dalton Trans. 1985, 451.

37. Flinn, P. A. In "Mössbauer Isomer Shifts"; Shenoy, G.K.; Wagner, F., Eds.; North-Holland Publishing Co.: Amsterdam, 1978; page 598.

SUMMARY

Considerable progress has been made in the synthetic chemistry of tetranuclear metal cluster compounds. The improved syntheses of $Mo_4Cl_8(CH_3CH_2CN)_4$ and $Mo_4Cl_8(MeOH)_4$ from conveniently obtained starting materials has provided a facile entrance into this chemistry. These cluster compounds can be used to synthesize the new tetranuclear cluster compounds $R_4Mo_4Cl_{12}$ (R=Et_4N, Pr_4N, Bu_4N, and $\emptyset_4P$). Investigations of these compounds show that they react similarly to previously synthesized tetranuclear clusters.

An interesting redox chemistry is associated with the $Mo_4Cl_{12}^{4-}$ clusters. One electron oxidation has resulted in the isolation of planar and butterfly clusters with the stoichiometry $R_3Mo_4Cl_{12}$. These clusters are fragments of the hexanuclear $Mo_6Cl_{14}^{2-}$ cluster anion, in which the six metal atoms occupy the faces of a cube defined by eight chlorine atoms. In addition, each metal atom has one chlorine atom terminally bound to it. The tetranuclear clusters are derived by removal of two molybdenum atoms and their terminal chlorine atoms from cis or trans faces.

Electron paramagnetic resonance spectra of the planar clusters has shown that they are paramagnetic with a g value of approximately 2.0. The effective magnetic moment has been shown to be 1.7 B.M. corresponding to one unpaired electron. Extended Hückel calculations have shown that

the planar clusters adopt a rectangular rather than a square geometry due to a Jahn-Teller distortion. Second order Jahn-Teller effects explain the deviation of the angles from 90^{o}.

The most interesting feature of these cluster compounds may be their potential for further cluster synthesis. Cyclic voltammetry experiments have shown that a one electron oxidation to $Mo_4Cl_{12}^{2-}$ is synthetically possible, at least on that time scale. The synthesis of the next larger member of the Mo_xCl_y series, $Mo_5Cl_{13}^{n-}$, should be possible by addition of a "MoCl' moiety to the $Mo_4Cl_{12}^{4-}$ cluster unit. In this research, unforeseen products are certain to be delightful surprises. Indeed, it has recently been observed that oxidation of $[\emptyset_4P]_3Mo_4Cl_{12}$ has produced the trinuclear cluster $[\emptyset_4P]_2Mo_3Cl_{11}$ (35).

The compound $Sn_{0.9}Mo_4O_6$ has provided interesting insight to an already fascinating molybdenum oxide chemistry. The chains of edge shared octahedra which are found in the structure are similar to those found in $NaMo_4O_6$. The evidence for doubling of the c axis of the unit cell indicates that additional factors are present in determining the true structure of this compound. The doubling of the c axis is likely to be caused by the apical molybdenum atoms occupying positions away from the mirrors on which they reside in the subcell refinement. Short and

long apical-apical molybdenum distances are the result.

Most interesting for this compound is the possibility of Sn-Sn bonding in the channels formed by the four interlinked Mo_4O_6 chains. The short repeat distance of the c axis (2.83 Å) is similar to the Sn-Sn distance in Sn metal. The nonstoichiometry suggests vacancies limit the length of the chains to 9 or 10 atom segments, however this is not the only possibility. The disorder observed along the tunnel chain is indicative that the two Sn atom interpretation used in the structure determination is not entirely correct. The Sn-Sn bonding model provides an explanation for the observed residual density in the channel.

ADDITIONAL LITERATURE CITED

1. Cotton, F. A.; Chisholm, M. H. Chem. and Eng. News June 28, 1982, 40.

2. Muetterties, E. L. Science 1977, 196, 839.

3. Muetterties, E. L. Angew. Chem. Intl. Ed. Engl. 1983, 22, 135.

4. Muetterties, E. L. Chem. and Eng. News August 30, 1982, 28.

5. Cotton, F. A.; Wilkinson, G. "Advanced Inorganic Chemistry", 4th ed.; John Wiley and Sons: New York, 1980; page 1094.

6. Cotton, F. A.; Walton, R. A. "Multiple Bonds Between Metal Atoms", John Wiley and Sons: New York, 1982.

7. Jang, Y.; Aoquing, T; Hoffmann, R.; Huang, J.; Lu, J.; Organometallics 1985, 4, 27.

8. Templeton, J. L. Prog. Inorg. Chem. 1979, 26, 211.

9. Chisholm, M. H. Polyhedron 1983, 2, 211.

10. McCarley, R. E.; Ryan, T. R.; Torardi, C. C. ACS Symp. Ser. 1981, 155, 41.

11. Chisholm, M. H.; Folting, K.; Huffman, J. C.; Kirkpatrick, C. C. J. Am. Chem. Soc. 1981, 103, 5967.

12. Chisholm, M. H.; Errington, R. J.; Folting, K.; Huffman, J. C. J. Am. Chem. Soc. 1982, 104, 2025.

13. Stensvad, S.; Helland, B. J.; Babich, M. W.; Jacoboson, R. A.; McCarley, R. E. J. Am. Chem. Soc. 1978, 100, 6257.

14. McGinnis, R. N.; Ryan, T. R.; McCarley, R. E. J. Am. Chem. Soc. 1978, 100, 7900.

15. Ryan, T. R.; McCarley, R. E. Inorg. Chem. 1982, 21, 2072.

16. Carlin, R. T. Ph.D. Dissertation, Iowa State University, Ames, Iowa, 1982.

17. Beers, W. W.; McCarley, R. E. Inorg. Chem. 1985, 24, 465.

18. Chisholm, M. H.; Hoffman, D. M.; Huffman, J. C. Inorg. Chem. 1985, 29, 798.

19. Chisholm, M. H.; Folting, K.; Huffman, J. C.; Leonelli, J.; Marchant, N.; Smith, C; Taylor, L. C. E. J. Am. Chem. Soc. 1985, 107, 3722.

20. Perrin, C.; Chevrel, R.; Sergent, M. C. R. Acad. Sci. Paris 1975, 281C, 23.

21. Perrin, C.; Chevrel, R.; Sergent, M. C. R. Acad. Sci. Paris 1975, 280C, 949.

22. Vandenberg, J. M.; Brasen, D. J. Solid State Chem. 1975, 14, 203.

23. Torardi, C. C.; McCarley, R. E. J. Am. Chem. Soc. 1981, 37, 393.

24. Chisholm, M. H.; Huffman, J. C.; Kirkpatrick, C. C.; Leonelli, J.; Folting, K. J. Am. Chem. Soc. 1981, 103, 6093.

25. Glicksman, H. D.; Walton, R. A. Inorg. Chem. 1978, 17, 3197.

26. Müller, A.; Eltzner, W.; Bögge, H.; Jostes, R. Angew. Chem. Intl. Ed. Engl. 1982, 21, 795.

27. Mak, T. C.; Jasim, K. S.; Chien, C. Inorg. Chem. 1985, 24, 1587.

28. Jödden, K.; von Schnering, H. G.; Schäfer, H. Angew. Chem. 1975, 87, 595.

29. Beers, W. W. Ph.D. Dissertation, Iowa State University, Ames, Iowa, 1983; Section V.

30. Jödden, K.; Schäfer, H. Z. Anorg. Allg. Chem. 1977, 430, 5.

31. Torardi, C. C.; McCarley, R. E. J. Am. Chem. Soc. 1979, 101, 3963.

32. Torardi, C. C.; McCarley, R. E. J. Solid State Chem. 1981, 37, 393.

33. Lii, K. -H. Ph.D. Dissertation, Iowa State University, Ames, Iowa, 1985; Section III.

34. Gougeoun, P. Ames Laboratory, U.S.D.O.E.,Iowa State University, Ames, IA, private communication, 1985.

35. Blatchford, T. P. Ames Laboratory, U.S.D.O.E., Iowa State University, Ames, IA, private communication, 1985.

ACKNOWLEDGEMENTS

I wish to thank Dr. McCarley for his guidance and instruction during the course of this work. His suggestions during our many discussions proved insightful and helpful. Most certainly, I would like to sincerely thank the members of this research group for their discussions and friendship. Rich Carlin and Bill Beers were especially helpful and deserve special thanks.

I wish to express my appreciation to Dr. Jacobson's group, especially Jim Richardson, Jim Benson, Barb Helland, Sang Soo Kim, and Brenda Smith for their assistance in obtaining data and solving crystal structures. The electron paramagnetic resonance spectra could not have been obtained without the help of Gudrun Lukat, for which I am grateful. Special thanks are due Peter Klavins and Dr. R. N. Shelton for their assistance in obtaining resistivity and magnetic susceptibility measurements. Robin Ziebarth and Tim Hughbanks should be credited for their help with the extended Hückel band calculations for $Sn_{0.9}Mo_4O_6$.

The largest debt of gratitude goes to my parents, whose love and support has been limitless. Their encouragement of my goals has never wavered.

Most of all, I wish to thank my wife, Wendy, for her love and support, without which I would be lost.